

# Report on the photochemical induced halogen activation of Fe-containing aerosols

Julian Wittmer, Sergej Bleicher and Cornelius Zetzsch

Atmospheric Chemistry Research Unit, University of Bayreuth, Dr.-Hans-Frisch-Str. 1-3, Bayreuth,  
Germany

## Abstract

Iron (Fe) occurs in minerals and highly saline media (e.g. sea salt aerosol, salt brines etc.) and induces photochemical processes. High salinity, low pH, and organic constituents promote the dissolution of iron, forming photosensitive complexes that are responsible for a production of gaseous Cl atoms when irradiated by sunlight.

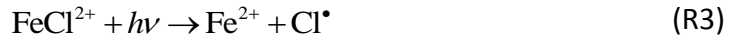
We studied the production of atomic Cl, Br and OH radicals from modeled salt pans and artificial sea-salt aerosols containing Fe(III) ions or pyrogenic  $\text{Fe}_2\text{O}_3$  particles (Sicotrans Orange, BASF) at various compositions in a Teflon smog-chamber. The samples were either spread on a Teflon sheet or they were nebulized from dilute brines (most abundant particle diameter:  $\sim 0.4 \mu\text{m}$ , initial surface area: up to  $3 \cdot 10^{-2} \text{ cm}^2 \text{ cm}^{-3}$ ) and exposed to simulated sunlight at 60-90% relative humidity. The photochemical formation of Cl, OH (and Br if possible) in the gas phase was quantified by the radical clock method resulting in time profiles of the radical-production rates and total productions.

Simultaneous monitoring of the aerosol surface area enabled us to determine the initial Cl production rate per  $\text{cm}^2$  aerosol surface. Whereas no significant Cl production was detected employing a molar  $\text{Cl}^-/\text{Fe(III)}$  ratio of 955, the rate increased to  $\sim 2.8 \cdot 10^{17} \text{ atoms cm}^{-2} \text{ s}^{-1}$  (at a ratio of 101),  $\sim 4.1 \cdot 10^{17} \text{ atoms cm}^{-2} \text{ s}^{-1}$  (at a ratio of 53) and  $\sim 1.9 \cdot 10^{18} \text{ atoms cm}^{-2} \text{ s}^{-1}$  (at a ratio of 13). The presence of  $\text{NO}_2$  ( $\sim 20 \text{ ppb}$ ) or  $\text{O}_3$  (630 ppb) in the gas phase additionally increased the Fe(III)-induced chloride activation to  $\sim 7 \cdot 10^{18} \text{ atoms cm}^{-2} \text{ s}^{-1}$  and  $\sim 9 \cdot 10^{18} \text{ atoms cm}^{-2} \text{ s}^{-1}$  (at a  $\text{Cl}^-/\text{Fe(III)}$  ratio of 13), respectively.  $\text{SO}_2$  slightly restrained the Cl formation. Artificial sea salt aerosols doped with  $\text{Fe}_2\text{O}_3$  particles ( $\text{Cl}^-/\text{Fe}_{\text{tot}} \sim 13$ ) did not result in detectable Cl concentrations. However, decreasing the pH below 2 favored the dissolution of Fe and led to Cl production rates comparable to the Fe(III) experiments ( $\sim 7 \cdot 10^{18} \text{ atoms cm}^{-2} \text{ s}^{-1}$ ) whereas accelerating the erosion of the particles by freezing and thawing did not lead to detectable results. These observations are in accord with the speciation of the photolabile, aqueous Fe(III) complexes obtained from an equilibrium model (PHREEQC).

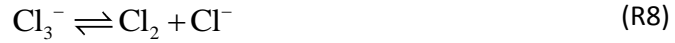
The aerosol experiments result in much higher effective Cl production rates with  $\sim 50\%$  of active Fe(III) in zero air, as compared to the previous salt-pan experiments in the same Teflon smog-chamber with a portion of 0.05-0.07% of active Fe(III)). This is caused by the larger active surface area of the homogeneously distributed aerosols.

## 1 Introduction and Background

The photolytic reduction of Fe(III) halides to Fe(II) and halide radicals has been proven and investigated by several studies (*Eder*, 1880; *Nadtochenko and Kiwi*, 1998b; *Nadtochenko and Kiwi*, 1998a; *Vione et al.*, 2005; *Lim et al.*, 2006; *Machulek et al.*, 2006; *Wittmer et al.*, 2014). If Fe(III) is present in saline media, various complexes will form (depending on salt composition, pH, and ionic strengths in the aqueous phase). At low pH, the main Fe(III)-water complexes are  $\text{Fe}(\text{H}_2\text{O})_6^{3+}$  and  $\text{Fe}(\text{H}_2\text{O})_5\text{OH}^{2+}$  (*Nadtochenko and Kiwi*, 1998b). In the presence of chloride (Cl<sup>-</sup>) anions, the more photolabile Fe(III)-Cl complexes are formed, whereof  $\text{Fe}(\text{H}_2\text{O})_5\text{Cl}^{2+}$  and  $\text{Fe}(\text{H}_2\text{O})_4\text{Cl}^{2+}$  are the most important ones (coordinated water molecules,  $(\text{H}_2\text{O})_x$ , will be omitted in the following). The photolysis of these complexes yields OH (OH<sup>·</sup>) and Cl (Cl<sup>·</sup>) radicals according to reactions (R1)-(R4).



The resulting Cl<sup>·</sup> reacts very fast with Cl<sup>-</sup> to form Cl<sub>2</sub><sup>·-</sup> (R5,  $k = 2 \times 10^{10} \text{ M}^{-1}\text{s}^{-1}$ ), which again can combine with another Cl<sup>·</sup> or Cl<sub>2</sub><sup>·-</sup> forming either directly Cl<sub>2</sub> (R6) or Cl<sub>3</sub><sup>·-</sup> (R7) that dissociates to Cl<sub>2</sub> and Cl<sup>-</sup> (R8) (*Nadtochenko and Kiwi*, 1998a). The low physical solubility of Cl<sub>2</sub> (Henry's law constant at 298 K: 6.3-9.5·10<sup>-2</sup> M/atm) (*Sander*, 1999) causes it to degas rapidly.



Alternatively the resulting OH<sup>·</sup> (R1, R2) can react with Cl<sup>-</sup> to form ClOH<sup>·-</sup> (R9) that finally dissociates to Cl<sup>·</sup> and H<sub>2</sub>O (R10), initiating again the mechanism (R5)-(R8).





The degassing of  $\text{Cl}_2$  depends on the pH in the aqueous phase, as the poorly degassing hypochlorous acid ( $\text{HOCl}$ ) is dominant between pH 4 and 7 (Henry's law constant at 298 K:  $2.6\text{-}9.3 \cdot 10^2 \text{ M atm}^{-1}$ ; *Sander*, 1999). Furthermore, the combination of two OH leads to  $\text{H}_2\text{O}_2$  that stimulates the photo-Fenton reaction and the re-oxidation of Fe(II) to Fe(III) (*Lim et al.*, 2006). However, at high salinity and low pH, the Fe(III)-Cl complexes are dominant and thus inhibit the photo-Fenton reaction cycle (additionally to the scavenging of  $\text{OH}^\bullet$  by  $\text{Cl}^\bullet$ ) by the formation of the less reactive  $\text{Cl}_2^\bullet$  radical (*Kiwi et al.*, 2000; *Machulek et al.*, 2006). Moreover, in natural environments, iron mainly forms complexes with organic ligands (e.g. in sea water) (*Rue and Bruland*, 1995), but Fe-Cl complexes become more important when salinity increases and the pH drops below 2 (*Zhu et al.*, 1992). The inhibitory effect of organic contaminants like catechol and oxalate and of sulfate on the iron induced chloride activation was investigated recently by *Wittmer et al.*, 2014.

Once released to the gas phase,  $\text{Cl}_2$  is quickly photolysed to chlorine atoms ( $\text{Cl}$ ). Besides OH, Cl is an important oxidant in the atmosphere and a strong consumer of volatile organic compounds (VOCs). E.g. Cl has a more than a magnitude faster reaction rate towards methane in comparison to hydroxyl radicals ( $k_{\text{CH}_4+\text{Cl}} = 1.1 \cdot 10^{-13} \text{ cm}^3 \text{ molecule}^{-1} \text{ s}^{-1}$  (*Bryukov et al.*, 2002)),  $k_{\text{CH}_4+\text{OH}} = 6.3 \cdot 10^{-15} \text{ cm}^3 \text{ molecule}^{-1} \text{ s}^{-1}$  (*Atkinson et al.*, 1997)) at 298 K. Recent studies by *Levine et al.*, 2011 even find hints at an enhanced depletion of methane by chlorine during the glacial periods. The depletion of methane by Cl forms HCl and methyl radicals, which are finally oxidized to  $\text{CO}_2$ . Such activations of chloride to gaseous Cl may happen where iron and halide media come into contact under the influence of sunlight. Iron-containing minerals and salts occur relatively often in the natural environment:

- Mineral aerosol, which is blown from arid continental regions and comes into contact with sea salt aerosol above oceans (*Mahowald et al.*, 2009; *Spolaor et al.*, 2013)
- Ash aerosol from volcanic eruptions as condensation nuclei for hydrogen chloride and sulfurous volcanic gases and water (*Duggen et al.*, 2007; *Langmann et al.*, 2010)
- Coastal regions, wetted by sea spray
- Brine containing soils (*Krause et al.*, 2013)
- Sediments covered with salt crusts, where biologically induced redox zones force a mobilization of iron (*Soto-Jiménez and Páez-Osuna*, 2008).
- Coastal regions of the Arctic, where mineral and sea salt aerosol are sedimented on concentrated brines (*Spolaor et al.*, 2013).

But also anthropogenic sources of iron in the marine boundary layer exist, such as the combustion of ship fuel. Fly ash and soot aerosol containing iron oxides may form iron halides if it comes into contact with sea spray (*Ito*, 2013). The amount of soluble iron emitted by ship traffic in the northern Atlantic and Pacific is predicted to contribute 30% to 60% to the total soluble iron in the atmosphere of those regions until the year 2100 (*Ito*, 2013).

In the atmospheric aerosols, iron is mainly present in form of oxides which can dissolve in the oceans (often promoted by organics, salinity and pH). Estimates of the global average aerosol solubility have a huge range of 0.001-80% (*Jickells and Spokes*, 2001; *Mahowald et al.*, 2005; *Baker and Croot*, 2010), where the solubility in remote marine aerosols is significantly higher than in mineral/soil source materials (*Zhuang et al.*, 1992).

Besides the effect of halogen activation above iron doped saline media, the sedimentation of iron to the sea water leads to algal bloom by iron fertilization. The algae again contribute to the binding of  $\text{CO}_2$  from the atmosphere (*Duggen et al.*, 2007). This is also indicated in time profiles in Antarctic and Greenlandic ice drill cores by the anti-correlation of  $\text{CO}_2$  and methane with dust concentrations. Whenever cold periods occurred and the past atmosphere carried high concentrations of dust,  $\text{CO}_2$

and methane were in their minima. This activation of the oceanic food chain is also known as the “iron -hypothesis” (*Martin et al.*, 1990; *Blain et al.*, 2007; *Pollard et al.*, 2009; *Martínez-García et al.*, 2011; *Martínez-García et al.*, 2014). The global deposition of dissolved iron is estimated to be in the range of  $\sim 0.26 \text{ Tg yr}^{-1}$  (*Johnson and Meskhidze*, 2013).

## 1.2 The aim of this investigation

The sponsor of this study suggests that at least some processes of natural greenhouse depletion by iron-(III) photolysis mentioned above can be technically optimized, so that these can be applied to force a climate cooling economically and without hazard (neither to the environment nor to the human health). One may envisage that tropospheric aerosols in the marine boundary layer with enriched iron concentrations to force the methane and  $\text{CO}_2$  depletion. The production and the activity of such aerosols have been described by *Meyer-Oeste*, 2010 under the name “ISA-Verfahren” (ISA-technique). The depletion of  $\text{CO}_2$  occurs in the first place by analogy to the environmental processes by sedimentation of the iron aerosol to the sea and fertilization of algae (*Duggen et al.*, 2007; *Langmann et al.*, 2010; *Lindenthal et al.*, 2012). Two types of aerosols are considered: (I.)  $\text{Fe}_2\text{O}_3$  aerosol and (II.) iron-(III)-chloride aerosol. While the second is already an iron halide aerosol, the first ages in the marine boundary layer and is converted under the influence of  $\text{SO}_2$ ,  $\text{NO}_x$ ,  $\text{O}_3$ , water vapor and sea spray to an iron halide aerosol. In a further case the “ISA-technique” describes (III.) an aerosol, which chloride-containing nuclei are covered with an iron compound surface, which again is able to release chlorine. All these techniques are patented or international patents are pending (*Oeste*, 2003; *Meyer-Oeste*, 2010).

The aim of this investigation is to quantify the halogen activation in the presence of iron doped sea salt aerosols in the environmental smog chamber. In relation to the chamber environment (volume and simulated irradiation) the theoretically possible maximal methane depletion shall be estimated.

## 1.3 Parameters of investigation

For the present investigations in the smog chamber, the temperature is controlled to 20 °C, and the relative humidity (RH) is adjusted to > 50%, in accord with the RH of the marine boundary layer (MBL) (*Alappattu et al.*, 2008). Two different types of iron doping are applied:

- Ultrasonically produced aerosols from a  $\text{FeCl}_3$  doped sea salt/ $\text{NaCl}$  solution
- Ultrasonically produced aerosols from a  $\text{Fe}_2\text{O}_3$  (or higher oxidation states, Sicotrans Orange, BASF) doped sea salt suspension

The inorganic sea salt composition should be comparable to the natural aerosol composition in the MBL. After *Westervelt et al.*, 2012 the mean sea salt aerosol concentrations in the North Pacific/North Atlantic are  $20\text{-}50 \mu\text{g/m}^3$ . In order to quantify the effects, the concentrations produced in the smog chamber are exaggerated by two orders of magnitude. This should not change the main mechanisms and the observed results can anyway be extrapolated to natural conditions.

Additionally, the influence of pollutants like ozone ( $\text{O}_3$ ), nitrogen oxides ( $\text{NO}_x$ ) and sulfur dioxide ( $\text{SO}_2$ ) on the halogen activation is investigated. The concentrations are chosen to represent a similar ratio to the natural ratio between the aerosol concentrations and these pollutants. Exemplary natural mixing ratios in marine areas are:

- $\text{O}_3$ : 40 ppb at Mauna Loa (Pacific) (<http://www.esrl.noaa.gov/>)
- $\text{NO}_2$ : 30 ppt at the Cape Verde Islands (*Lee et al.*, 2009)

- SO<sub>2</sub>: 20-100 ppt (*Luria et al.*, 1990; *Andreae et al.*, 2000)

In relation to the “ISA-Verfahren” elevated levels of pollutants are justified by the planned iron containing aerosol emissions out of exhaust gas emitting vehicles. Apart from the experiments with the mentioned pollutants, all investigations are conducted in a zero air environment.

The applied artificial sea salt mixture is produced according to *Kester et al.*, 1967 with a representative mixture of inorganic salts (Table 1).

**Table 1: Compositions of stock solutions obtained by adding FeCl<sub>3</sub> to the artificial seawater (prepared according to *Kester et al.*, 1967) or to a 1 g/l NaCl solution and resulting molar Cl<sup>-</sup>/Fe(III) ratios**

Solution/Suspension	Manufacturer	weighted amount [g] in 1 l H <sub>2</sub> O	Cl <sup>-</sup> /Fe <sup>3+</sup> [mol/mol]
<b>Artificial seawater</b>			
NaCl	Sigma-Aldrich, ACS, ≥ 99 %	23.9	
Na <sub>2</sub> SO <sub>4</sub> × 10 H <sub>2</sub> O	Merck, ACS, ≥ 99 %	9.09	
KCl	Roth, ACS, ≥ 99.5 %	0.68	
NaHCO <sub>3</sub>	Merck, for analysis, ≥ 99.5 %	0.20	
KBr	Merck, for analysis, ≥ 99.5 %	0.098	
H <sub>3</sub> BO <sub>3</sub>	Grüssing GmbH, 99.5 %	0.026	
NaF	Riedel de Haën, for analysis	0.003	
MgCl <sub>2</sub>	Sigma Aldrich, 98 %	5.07	
CaCl <sub>2</sub> × 2 H <sub>2</sub> O	Grüssing, 99%	1.52	
<b>Added FeCl<sub>3</sub> to art. seawater</b>			
FeCl <sub>3</sub>	Merck, for synthesis, ≥ 98 %	0.14	955
	Merck, for synthesis, ≥ 98 %	1.36	101
	Riedel-de Haën, sublimate, ≥ 99 %	2.67	53
	Riedel-de Haën, sublimate, ≥ 99 %	13.04	13
Fe <sub>2</sub> O <sub>3</sub>	Sicotrans Orange, BASF	5.044	~13
<b>Added FeCl<sub>3</sub> to 1 g/l NaCl</b>			
FeCl <sub>3</sub>	Riedel-de Haën, sublimate, ≥ 99 %	0.278	13

All in all the following experiments are conducted:

1. Iron-free NaCl aerosol
2. Iron-free artificial sea salt aerosol
3. Iron-free artificial sea salt aerosol + 20 ppb NO<sub>x</sub>
4. Iron-free artificial sea salt aerosol + 700 ppb O<sub>3</sub>
5. Iron-free artificial sea salt aerosol + 30 ppb SO<sub>2</sub>
6. Iron-doped artificial sea salt aerosol (molar Cl<sup>-</sup>/Fe(III)=955)
7. Iron-doped artificial sea salt aerosol (molar Cl<sup>-</sup>/Fe(III)=101)
8. Iron-doped artificial sea salt aerosol (molar Cl<sup>-</sup>/Fe(III)=53)
9. Iron-doped artificial sea salt aerosol (molar Cl<sup>-</sup>/Fe(III)=13)
10. Iron-doped NaCl aerosol (molar Cl<sup>-</sup>/Fe(III)=13)
11. Iron-doped artificial sea salt aerosol (molar Cl<sup>-</sup>/Fe(III)=13) + 620 ppb O<sub>3</sub>
12. Iron-doped artificial sea salt aerosol (molar Cl<sup>-</sup>/Fe(III)=13) + 20 ppb NO<sub>x</sub>

13. Iron-doped artificial sea salt aerosol (molar Cl<sup>-</sup>/Fe(III)=13) + 20 ppb SO<sub>2</sub>
14. Iron-doped artificial sea salt aerosol (molar Cl<sup>-</sup>/Fe(III)=13) + 200 ppb SO<sub>2</sub>
15. Iron-doped artificial sea salt aerosol (molar Cl<sup>-</sup>/Fe(III)=101), acidified
16. Iron-doped artificial sea salt aerosol (molar Cl<sup>-</sup>/Fe(III)=101) + 20 ppb NO<sub>x</sub>
17. Iron-doped artificial sea salt aerosol (molar Cl<sup>-</sup>/Fe(III)=101), acidified + 20 ppb NO<sub>x</sub>
18. Sicotrans Orange doped artificial sea salt aerosol (molar Cl<sup>-</sup>/Fe(III)~13)
19. Sicotrans Orange doped artificial sea salt aerosol (molar Cl<sup>-</sup>/Fe(III)~13), acidified
20. Sicotrans Orange doped artificial sea salt aerosol (molar Cl<sup>-</sup>/Fe(III)~13), 5 times frozen and unfrozen

## 2. Instrumental set-up and methods

### 2.1 Experimental set-up

The measurements are performed in a Teflon smog chamber (FEP200A, DuPont) of a cylindrical shape (diameter: 1.33 m, height: 2.5 m). The volume is approximately 3.5 m<sup>3</sup> and depends on the internal pressure that is constantly monitored (differential pressure sensor, Kalinsky Elektronik DS1) and adjusted to 0.3-1 Pa by a continuous flow of hydrocarbon-free zero air (zero-air-generator, cmc instruments, <1 ppb of O<sub>3</sub>, <0.5 ppb NO<sub>x</sub>, <100 ppb of CH<sub>4</sub>). The zero air is humidified by streaming through a three-neck bottle filled with deionized water (Seralpur pro 90 cn, <0.055 µS cm<sup>-1</sup>). Below the smog chamber, 7 medium pressure arc lamps (Osram HMI, 1.2 kW each), a UV filter and IR filter provide an actinic flux comparable to the tropospheric sun light on the 50<sup>th</sup> latitude in the tropospheric summer (Figure 2). A Teflon fan inside the chamber ensures constant mixing. The temperature and relative humidity are monitored by two sensors at different heights (Rotronic, HC2-IC102). NO, NO<sub>x</sub> and O<sub>3</sub> are monitored by chemiluminescence gas analyzers (EcoPhysics, CLD 88p coupled with a photolytic converter, PLC 860 for NO and NO<sub>x</sub>, and UPK 8001 for O<sub>3</sub>). More details of the smog chamber set-up can be found in Bleicher, 2012; Buxmann *et al.*, 2012; Bleicher *et al.*, 2014; Wittmer *et al.*, 2014.

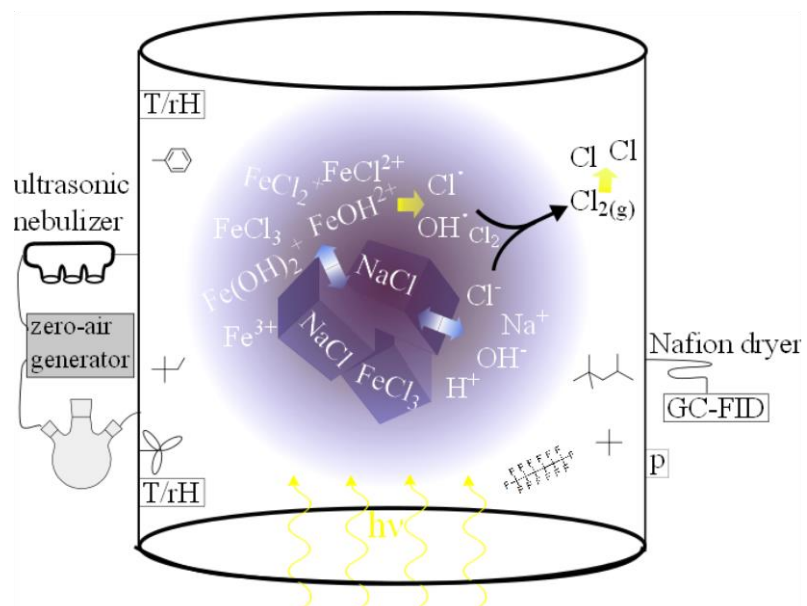


**Figure 1:** Scheme of the simulation chamber above a solar simulator including the instrumentation, measurement principle and schematic iron induced Cl production; rH / T: sensor for relative humidity and temperature; adapted and modified from Wittmer *et al.*, 2014.

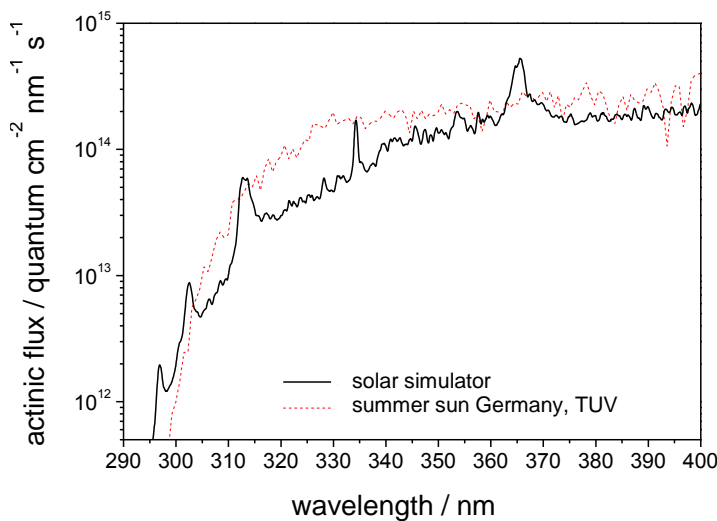


**Figure 2: The spectrum of the solar simulator in comparison to a calculation of the radiative transfer model TUV (Madronich et al., 1998) for the 50°N latitude in summer (Bleicher, 2012).**

## 2.2 Quantification of Cl, Br, and OH by the radical clock method

The direct evidence of the methane depletion is complicated due to its long life time. Even when the life time is decreased to a fraction due to high Cl concentrations, a direct experiment has to be prepared to run for many days. However, since the rate constants of the reaction of chlorine atoms and OH radicals with methane are precisely known, the proof of chlorine atom formation is sufficient. Their evidence is provided by a degradation pattern of a particular hydrocarbon (HC) mixture (Zetzsch and Behnke, 1992). Therefore, the consumption of selected hydrocarbons (2,2-dimethylpropane (DMP), 2,2-dimethylbutane (DMB), 2,2,4-trimethylpentane (TMP), toluene (Tol)) is monitored and corrected for dilution by an inert standard perfluorohexane (PFH). The measurement is performed in a time interval of 15 min by gas chromatography , GC (Siemens Sichromat 2), using an Al<sub>2</sub>O<sub>3</sub>-PLOT column with 50 m, employing a temperature gradient of 50°C/min to heat from 160°C to 200°C after 3 min runtime, using 0.25 ml/min He as carrier gas, a flame ionization detector (FID), a custom built liquid nitrogen cryo-trap enrichment for focusing the samples with a sampling flow of 100 ml/min for 3 min, and a Nafion dryer (Wittmer et al., 2014). Each peak area is integrated afterwards and is correlated to the HC<sub>i</sub> mixing ratio in the chamber. Based on the different rate constants of the HC<sub>i</sub> towards Cl, OH and Br the radicals can be quantified by fitting an appropriate analytical function to the profile of each HC<sub>i</sub> and solve the system of 4 differential equations with 3 unknown variables:

$$-\frac{d[HC_i]}{dt} = k_{Cl,i}[Cl][HC_i] + k_{Br,i}[Br][HC_i] + k_{OH,i}[OH][HC_i] \quad (1)$$

Dividing by [HC]<sub>i</sub> separates the variables (Equation (2)) and allows us to identify the contribution of each radical to the consumption of the HC<sub>i</sub> after integration:

$$-\frac{d\ln[HC_i]}{dt} = k_{Cl,i}[Cl] + k_{Br,i}[Br] + k_{OH,i}[OH] \quad (2)$$

The over-determination of the differential equation allows us to calculate a mean value of the single results and a related statistical uncertainty. In the absence of Br atoms, the statistical analysis improves accordingly. The detection limit of this method is directly related to the rate constants (Table 2) and the sensitivity of the gas chromatography system. The detection limit can be given to  $10^4 \text{ cm}^{-3}$  for Cl atoms,  $10^6 \text{ molecules cm}^{-3}$  for OH radicals and about  $10^9 \text{ atoms cm}^{-3}$  for Br.

The HC mixing ratios are constant in darkness, since the halogen activation is a photolytic reaction. Therefore, the dark mixing ratios are used as a zero point ( $t=0$ ) for fitting. The HC peak areas in the chromatogram are linearly related to the mixing ratio.

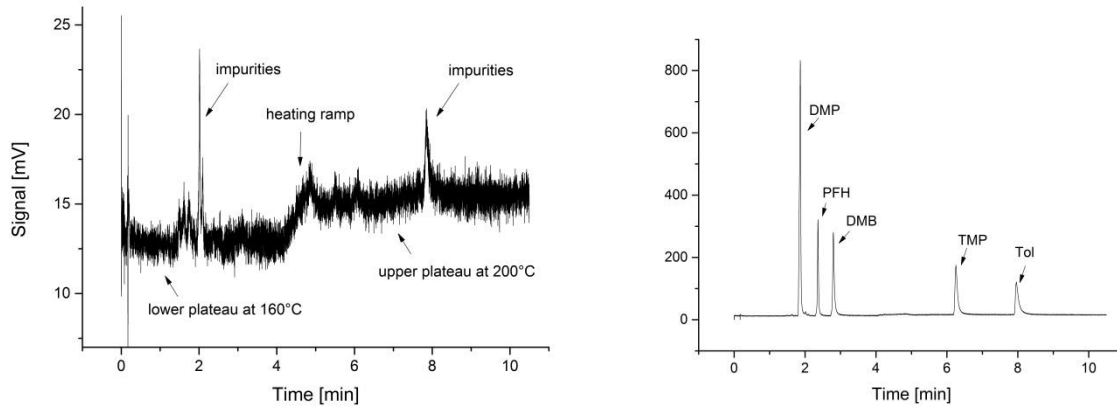


**Figure 3:** Gas chromatography measurement of zero-air (left) and a measurement with injected hydrocarbons (right). The GC oven temperature is set to 160 °C at the beginning to separate the peaks of DMP, PFH, DMB then the oven is heated to 200 °C for the rapid detection of TMP and toluene.

**Table 2:** Rate constants (in  $\text{cm}^3 \text{ molecule}^{-1} \text{ s}^{-1}$ ) of the observed hydrocarbons with the radicals at 298 K. Perfluorohexane is completely inert to OH, Cl and Br at room temperature.

Hydrocarbon	$k_{\text{OH}}$	$k_{\text{Cl}}$	$k_{\text{Br}}$
Methane ( $\text{CH}_4$ )	$6.7 \times 10^{-15}$ (Atkinson et al., 1997)	$1.07 \times 10^{-13}$ (Atkinson et al., 1997)	$4 \times 10^{-24}$ (Baulch et al., 1981)
2,2-Dimethylpropane (DMP)	$8.3 \times 10^{-13}$ (Atkinson et al., 1997)	$1.1 \times 10^{-10}$ (Atkinson and Aschmann, 1985)	$\leq 1 \times 10^{-20}$ (Amphlett and Whittle, 1968)
2,2-Dimethylbutane (DMB)	$2.2 \times 10^{-12}$ (Atkinson et al., 1997)	$1.7 \times 10^{-10}$ (Jenkin et al., 1997)	-
2,2,4-Trimethylpentane (TMP)	$3.3 \times 10^{-12}$ (Atkinson et al., 1997)	$2.3 \times 10^{-10}$ (Aschmann and Atkinson, 1995)	$6.8 \times 10^{-15}$ (Barnes et al., 1989)
Toluene	$6.2 \times 10^{-12}$ (Atkinson, 1986)	$5.9 \times 10^{-11}$ (Shi and Bernhard, 1997)	$1.3 \times 10^{-14}$ (Bierbach et al., 1999)
n-Perfluorohexane	-	-	-

"The steady state of the radicals and atoms, formed by the photochemical processes and consumed by the HCs and their degradation products, delivers concentrations which inversely depend on the initial amount of the  $\text{HC}_i$  injected (if wall loss and reactions with  $\text{CH}_4$ ,  $\text{O}_3$ , and other constituents are neglected), forming a total reactivity of the system towards the respective radical ( $\sum_i k_{X,i} [\text{HC}]_i$ ;  $X = \text{Cl}, \text{Br}, \text{or OH}$ ). The total production,  $Q_X$ , during the time  $\tau$  can be calculated by equalizing the source and the sinks, assuming a photostationary, steady state ( $d[X]/dt = 0$ )

$$Q_X = \int_0^\tau \sum_i k_{X,i} [HC_i]_t [X]_t dt \quad (3)$$

Adopting the initial HC concentrations,  $[HC]_{i,0}$ , and the rate constants of their reactions with the radical X as a constant total reactivity of the chamber contents towards X over the time of the experiment allows us to calculate a maximal value of X. Such an approximation assumes that the reactivity of the reaction products is the same as the reactivity of the  $HC_i$ , which is only valid in the early stage of each experiment at low consumption of the hydrocarbons. By using actually measured, dilution corrected  $[HC]_i$  values and neglecting any X-reactivity of the products, a minimal value of  $Q_X$  can be calculated." (Wittmer *et al.*, 2014)

"The measurements of the particle size distributions (number density N [ $\text{cm}^{-3}$ ]) allow us to determine the available reaction surface area ( $A [\text{m}^2 \text{ m}^{-3}]$ ) and the particle volume ( $V_{\text{particle}} [\text{m}^3 \text{ m}^{-3}]$ ), that equals the liquid water content (LWC) plus the tare volume of ions ( $r_{\text{Cl}^-} = 181 \text{ pm}$ ,  $r_{\text{SO}_4^{2-}} = 184 \text{ pm}$ ,  $r_{\text{Na}^+} = 102 \text{ pm}$ ,  $r_{\text{K}^+} = 137 \text{ pm}$ ,  $r_{\text{Mg}^{2+}} = 72 \text{ pm}$ ,  $r_{\text{Ca}^{2+}} = 106 \text{ pm}$ ,  $r_{\text{Fe}^{3+}} = 49 \text{ pm}$ ) (Shannon, 1976) at the adjusted RH. The measured LWC was corrected by considering the main ions in a spherical shape. The contribution of deposited particles on the chamber walls to the activated Cl was considered by measuring the Cl activation of a totally wall-deposited aerosol load. The Cl production terms are normalized to obtain absolute production rates  $dQ_{\text{abs}}/dt$  and absolute total productions  $Q_{\text{abs}}$  per  $\text{cm}^2$  of the aerosol surface. Therefore, the production rate (atoms  $\text{cm}^{-3} \text{ s}^{-1}$ ) is multiplied by the chamber volume,  $V_{\text{chamber}}$ , to obtain the total number of atoms produced per s. The result is divided by the actual, active aerosol surface that we define as the sum of (i) the measured aerosol surface when the lights were turned on ( $A_{0, \text{light}}$ ) and its deposition rate,  $\exp(-t_{\text{light}}/\tau_s)$ , (ii) the active, deposited surface during the time of injection, and (iii) the active, deposited surface forming after the injection is finished (equation 3). Whereas (ii) is determined by assuming an approximately linear increase of the aerosol surface during injection and calculating the respective deposition until the injection is stopped ( $t_{\text{inj,end}}$ ), (iii) is based on the measured aerosol surface area directly after injection ( $A_{0, \text{inj}}$ ) and its deposition during the time  $t_{\text{inj}}$  that starts when the injection ends. Both terms are multiplied by factor of 0.2, which is the fraction of deposited surface area that contributes to the halogen activation." (adapted from Wittmer *et al.*, 2015)

$$\frac{dQ_{\text{abs}}}{dt_{\text{light}}} = \frac{\frac{dQ_X}{dt_{\text{light}}} \times V_{\text{Chamber}}}{A_{0, \text{light}} \times \exp(-\frac{t_{\text{light}}}{\tau_s}) + 0.2 \times \left( \int_{t_{\text{inj,start}}}^{t_{\text{inj,end}}} \left( \frac{\Delta A_{0, \text{inj}} \times t}{\Delta t_{\text{inj,end}}} \right) dt + A_{0, \text{inj}} \times (1 - \exp(-\frac{t_{\text{inj}}}{\tau_s})) \right)} \quad (4)$$

## 2.3 Sample preparation

Several artificial seawater stock solution were prepared according to Table 1 with various Fe(III) content and with a  $\text{Cl}^-/\text{Br}^-$  ratio of 997. In order to investigate the influence of the inorganic constituents a NaCl-FeCl<sub>3</sub> mixture was additionally prepared. The stock solutions (except for NaCl) were diluted 1:28 to obtain  $\text{Cl}^-$  concentrations ranging from 15 to 35 mmol/L. These initial concentrations provide optimal aerosol size distributions with an adequate residence time within the charged smog chamber. The effect of various gas species was tested by adding O<sub>3</sub> from a ozonizer (Sorbios GSG 12) with electrical discharge applied on pure oxygen (Rießner Gase, >99.995%), NO<sub>2</sub> from a gas cylinder (Rießner Gase 104 vpm NO<sub>2</sub> with a purity of 98 % in synthetic air), or SO<sub>2</sub> from a gas cylinder (Rießner Gase, 0.99% SO<sub>2</sub> with a purity of 99.98% in N<sub>2</sub> with a purity of 99.999%).

## 2.4 Aerosol production and measurement

The prepared solutions were nebulized with an ultrasonic nebulizer (Quick Ohm QUV-HEV FT25/16-A, 35 W, 1.63 MHz) generating droplets in the  $\mu\text{m}$  range that quickly come into equilibrium with the surrounding and evaporate to a saturated sea salt solution with most abundant particles between 350-460 nm depending on the concentrations in the nebulized solution. A starting RH of  $\geq 40\%$  was adjusted before injecting the aerosols to avoid a crystallization of the particles. The injection takes typically 30-50 min. To avoid a dripping of the condensed droplets into the chamber, a heated transfer tube (made of copper) was constructed. More details on the properties of artificial sea salts in our smog chamber can be found in *Siekmann, 2008*.

After every experiment the chamber was cleaned by deionized water (Seralpur pro 90 cn,  $<0.055 \mu\text{s cm}^{-1}$ ) or the whole Teflon film was exchanged. Every new chamber was irradiated at least 4 h by the solar simulator and an additional UV lamp (Phillips TUV 55W,  $\lambda = 253.7 \text{ nm}$ ) with a load of 1000 ppb  $\text{O}_3$  at 50-80% RH to minimize the outgassing of the film. (*Kelly, 1982*)

During the experiment the aerosol size distributions and concentrations were monitored by an electrostatic classifier (TSI, 3071) in combination with a bipolar neutralizer ( $^{85}\text{Kr}$ ) and a condensation nucleus counter (TSI, 3020). Scanning and data evaluation was performed by a custom written software (*Balzer, 2012*).

The evaluation software is given in the Appendix 6.2. Typical resulting size distributions are shown in Figure 4.

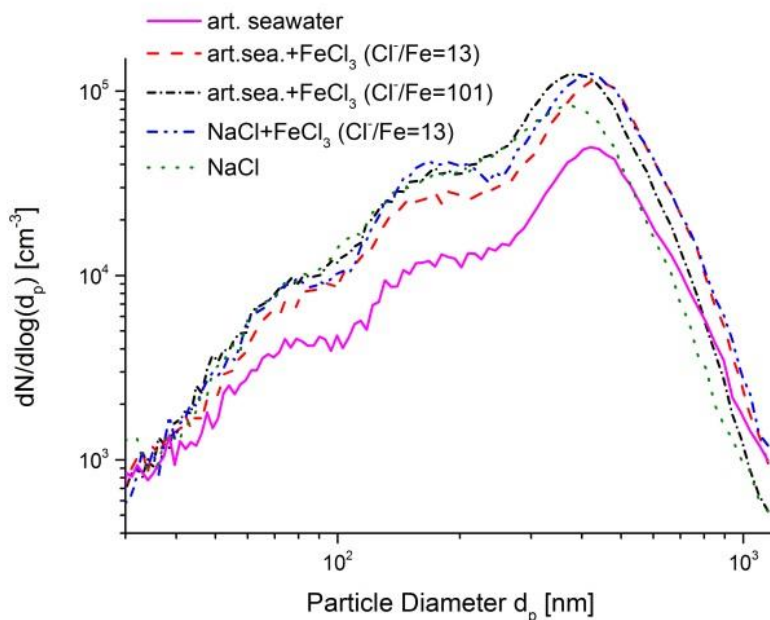


**Figure 4:** Typical initial (multiple-charge corrected) size distributions for aerosols generated by the nebulizer (30 - 45 min injection time) from various diluted stock solutions. Adapted from *Wittmer et al., 2015*.

## 2.5 Chamber wall effects

“Due to flashovers in the classifier throughout some experiments caused by the high RH, only the measurements at the beginning of those experiments were evaluable. Therefore, the measurements after injection and when the lights were turned on were used to calculate the dilution-corrected loss

by deposition based on the mean, dilution-corrected lifetimes  $\tau_{N,S}$  ( $N$  = particle number,  $s$  = total aerosol surface area) over the experiments without flashovers and neglecting the loss by coagulation. The deposition velocity depends on the salt concentration in the nebulized solution and thus on the mean particle diameter after injection. For instance, the artificial sea-salt solution and the pure NaCl solution gave lifetimes of  $\tau_N = 24\ 800$  s ( $\tau_S = 30\ 100$  s) and  $\tau_N = 25\ 000$  s ( $\tau_S = 31\ 100$  s). For the higher concentrated Fe(III)-doped artificial seawater (29–35 mmol Cl<sup>-</sup> L<sup>-1</sup>), the most abundant particle diameters were between 430 and 460 nm, resulting in a faster sedimentation with  $\tau_N = 4590 \pm 240$  s and  $\tau_S = 6070 \pm 520$  s compared to  $\tau_N = 6845$  s and  $\tau_S = 8820$  s for the lower concentrated pure NaCl+FeCl<sub>3</sub> solution (24 mmol Cl<sup>-</sup> L<sup>-1</sup>) with most abundant particle diameters between 390 and 420 nm. The respective contour plots are shown in Figure 5.

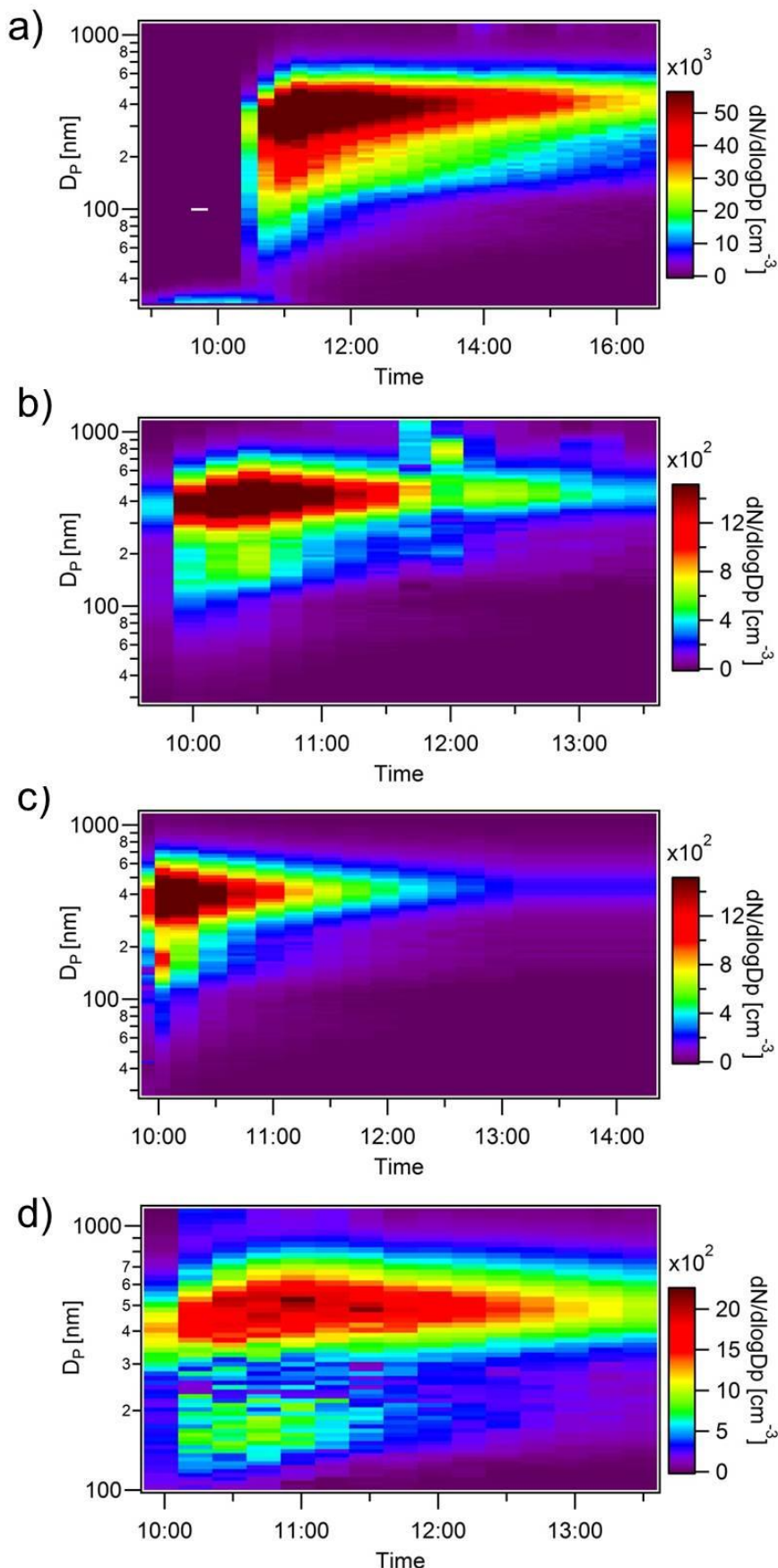


**Figure 5: Contour plots of selected experiments with nebulized a) NaCl (1 g/l), b) NaCl+FeCl<sub>3</sub> ( $\sim 18$  mmol L $^{-1}$  Cl $^-$ , Cl $^-$ /Fe(III) = 13), c) artificial seawater + FeCl<sub>3</sub> ( $\sim 29$  mmol L $^{-1}$  Cl $^-$ , Cl $^-$ /Fe(III) = 101) and d) artificial seawater + FeCl<sub>3</sub> ( $\sim 37$  mmol L $^{-1}$  Cl $^-$ , Cl $^-$ /Fe(III) = 13); adapted from Wittmer *et al.*, 2015.**

To quantify the particle deposition and its contribution to the active surface area (and thus to the Cl activation), a test measurement was performed to determine the fraction of Cl release by the active wall surface compared to the active aerosol surface: The iron doped artificial seawater sample ( $\text{Cl}^-/\text{Fe(III)} = 13$ ) was injected and allowed to deposit totally for 17 h (< 0.005 % of the surface area should have remained suspended) while keeping the RH at 80 %. Then the “aerosol-free” chamber was irradiated resulting in a Cl production that was  $20 \pm 4$  % compared to the actual production measured for the same sample in an aerosol experiment and was evaluated by taking the mean of the quotient of each total production (deposited and not deposited) normalized by the respective, initial LWC directly after injection. In equation (3), the contribution of deposited, active aerosol surface area is accounted for by adding 20 % of the deposited surface area since the time of injection to the surface area when the lights were turned on (corrected for deposition). The smaller active fraction when deposited on the wall can be explained by a physical surface reduction during the adhesion process of the droplets (possibly coagulating to larger droplets on the hydrophobic surface), by an inhomogeneous irradiation of the chamber walls (especially the large fraction of wall surface perpendicular to the solar simulator), but also by a drying effect due to the heating of the Teflon walls during irradiation. This demonstrates the contribution of active, deposited surface on the wall to the total active surface area during the experiment with Fe(III)-doped, pH adjusted ( $\text{pH} = 2.1\text{-}2.3$ ), artificial seawater ( $\text{Cl}^-/\text{Fe(III)} = 101$ ). The figure additionally includes  $dQ_{\text{abs}}/dt$  and  $Q_{\text{abs}}$  which are discussed in section 3.” (Wittmer *et al.*, 2015)

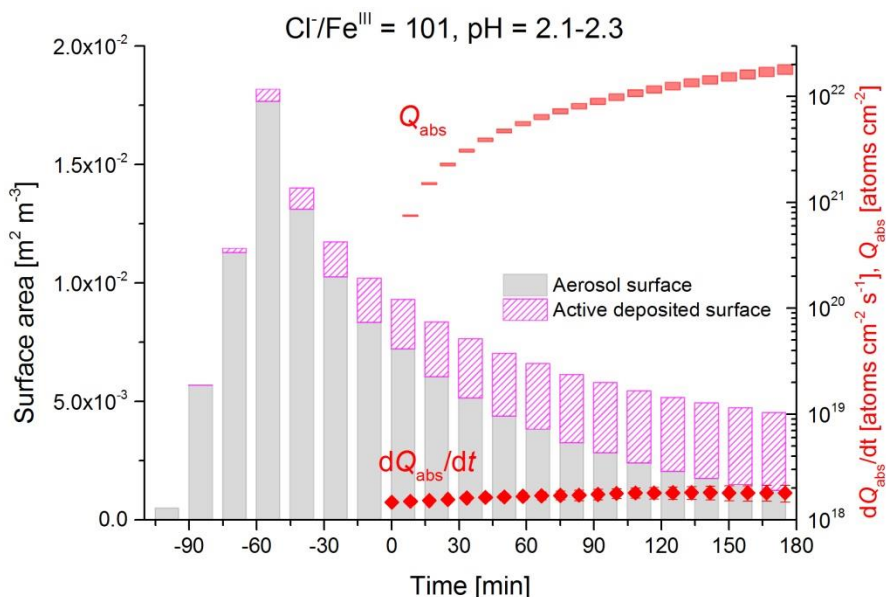


**Figure 6: Time profile of the sum of the total measured aerosol surface area and the active deposited surface during the experiment with Fe(III)-doped, pH-adjusted ( $\text{pH} = 2.1\text{-}2.3$ ) artificial seawater ( $\text{Cl}^-/\text{Fe(III)} = 101$ ) and the corresponding absolute gaseous mean Cl production rate ( $dQ_{\text{abs}}/dt$ ) [ $\text{atoms cm}^{-2} \text{ s}^{-1}$ ] and time integrated total Cl production  $Q_{\text{abs}}$  [ $\text{atoms cm}^{-2}$ ] per  $\text{cm}^2$  of active aerosol surface. Adapted from Wittmer *et al.*, 2015.**

### 3 Results

#### 3.1 Iron-free NaCl aerosol

The nebulizer was filled with 50 ml of a 1 g/l NaCl solution (p.a. Aldrich). In this experiment injection was performed with a Teflon tube which turned out to be inappropriate due to the condensation of the droplets within the tube and dripping of solution into the chamber. The injection time was 50 min. The time profile of the total aerosol concentration and the total aerosol surface is shown in Figure 7.

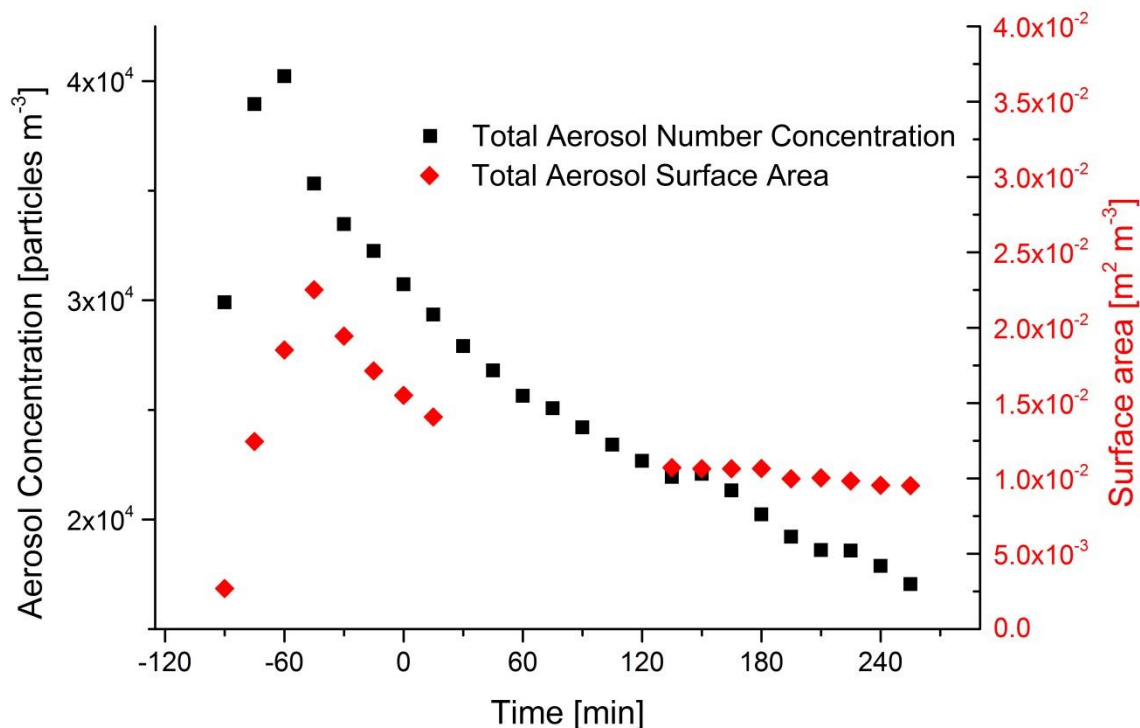


Figure 7: Time profiles of the total measured aerosol number concentration and the surface area for the experiment with NaCl aerosols. The aerosol was injected from -100 min to -50 min. At t = 0 the lights were turned on.

The following amount of hydrocarbons was injected

- 50 µl DMP
- 0.2 µl PFH (inert standard)
- 0.2 µl DMB
- 0.2 µl TMP
- 0.2 µl Tol

The dilution corrected time profiles of the injected hydrocarbons are shown in Figure 8 (left).

While toluene shows a significant decrease, the alkanes have been only slightly reduced, which is an indication of low chlorine atoms concentration. The quasi-stationary concentrations of OH and Cl radicals (Figure 8, right) were derived from the functions fitted (shown in Table 3) to the measurement data. The concentration of OH radicals has the typical value of about  $(3\text{-}5) \times 10^6 \text{ cm}^{-3}$ . Chlorine atoms had a concentration of  $(2\text{-}6) \times 10^4 \text{ cm}^{-3}$ , which is only slightly above the detection limit.

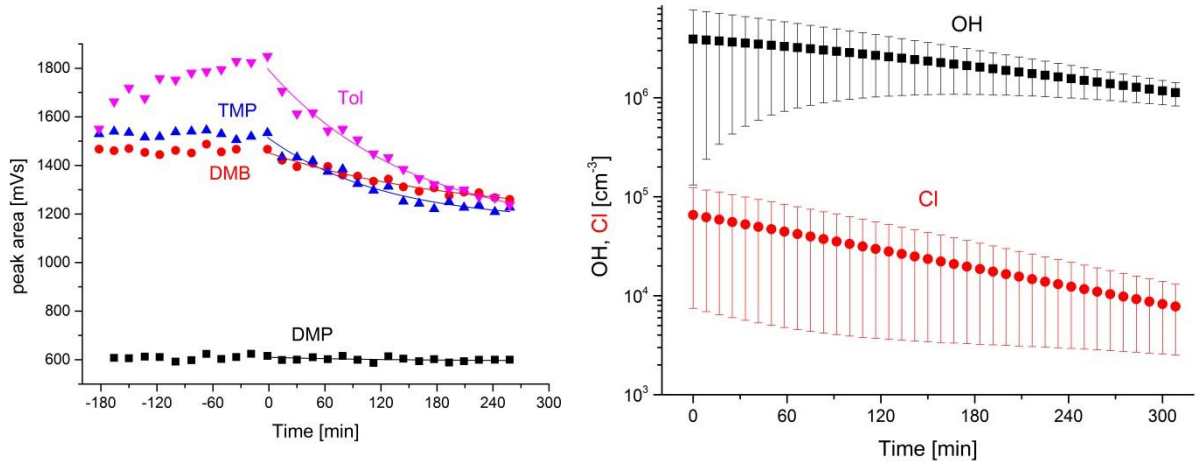


**Figure 8:** HC measurements in the NaCl aerosol experiment including the applied fitting functions (left) and the hence calculated concentrations of OH and Cl radicals (right). The irradiation started at the time 0.

**Table 3:** Fitting functions for the NaCl experiment from Figure 8 to derive the concentrations of OH und Cl

Hydrocarbon	Fitting function /mVs
2,2-Dimethylpropane (DMP)	$595 + 15e^{-t/8000s}$
2,2-Dimethylbutane (DMB)	$1195 + 257e^{-t/11763s}$
2,2,4-Trimethylpentane (TMP)	$116 + 345e^{-t/7451s}$
Toluene	$1124 + 668e^{-t/9096s}$

### 3.2 Iron-free artificial sea salt aerosol

The nebulizer was filled with ~50 ml of an iron-free artificial seawater solution (see Table 1) that was 1:28 diluted to ~18 mmol L<sup>-1</sup>. In this experiment injection was performed with a T-piece construction to avoid dripping of condensed solution. However it turned out to be not practical. The injection time was 66 min. The time profile of the total aerosol concentration and the total aerosol surface is shown in Figure 9. The jumps in the profile are caused by flashovers in the classifier. They are favored at high masses (high voltages) and therefore have a higher impact on the surface area than on the number concentration.

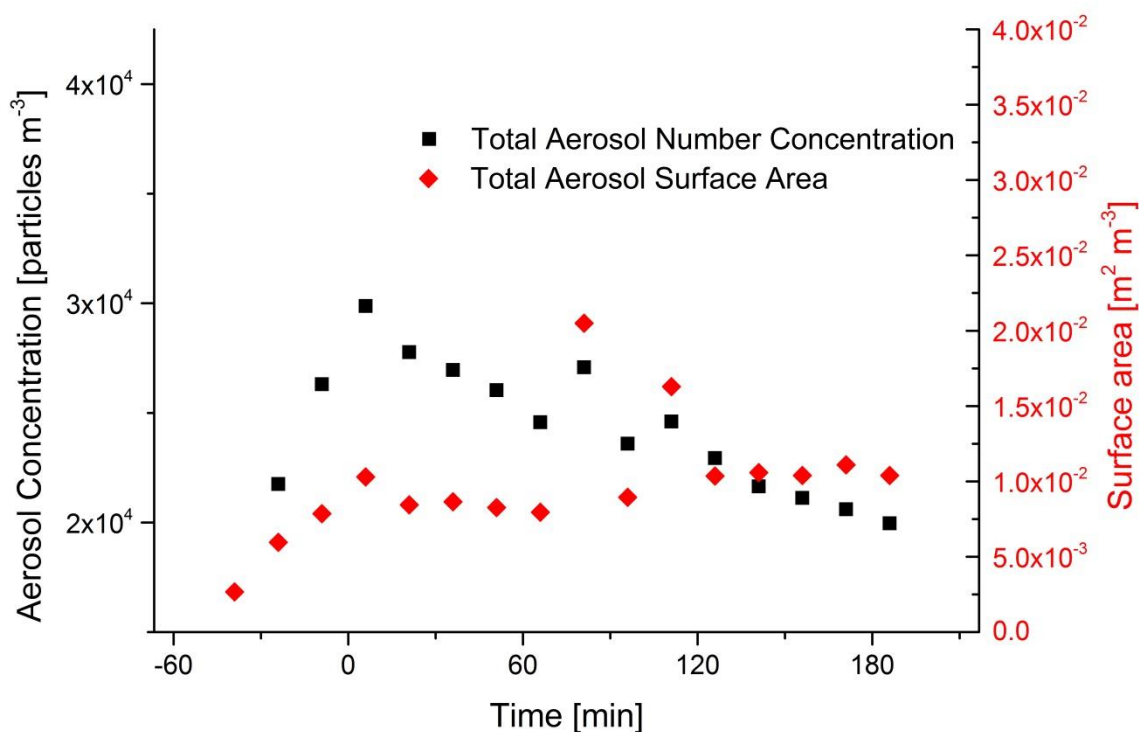
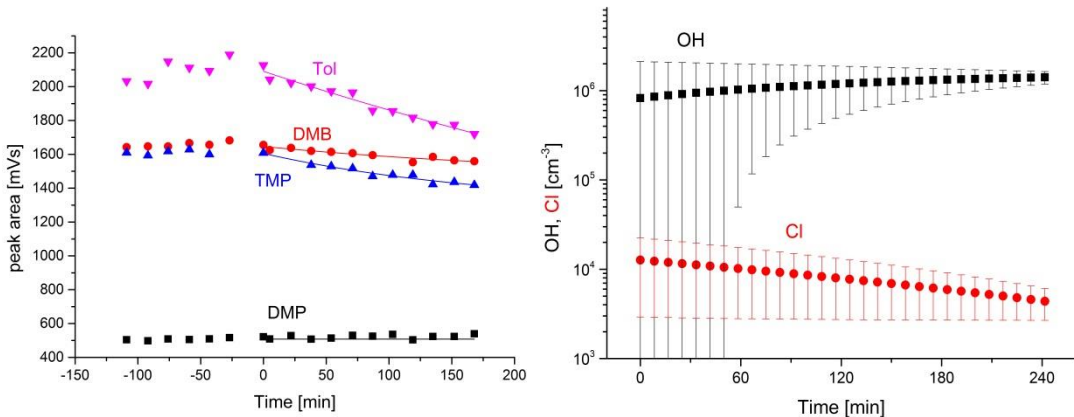


Figure 9: Time profiles of the total measured aerosol number concentration and the surface area for the experiment with artificial sea salt aerosols. At t= 0 the injection of the aerosol starts. At t= 90 min the lights were turned on.

The following amount of hydrocarbons was injected

- 50 µl DMP
- 0.2 µl PFH (inert standard)
- 0.2 µl DMB
- 0.2 µl TMP
- 0.2 µl Tol

The dilution corrected time profiles of the injected hydrocarbons are shown in Figure 10 (left).



**Figure 10:** HC measurements in the artificial sea salt aerosol experiment including the applied fitting functions (left) and the hence calculated concentrations of OH and Cl radicals (right). The irradiation started at the time 0.

Comparable to the NaCl experiment toluene shows a significant decrease and the alkanes have been only slightly reduced which is again an indication of low Cl concentrations. The quasi-stationary concentrations of OH and Cl radicals (Figure 10, right) were derived from the functions fitted (shown in Table 4) to the measurement data. The concentration of OH radicals has the typical value of about  $\sim 10^6 \text{ cm}^{-3}$ . Chlorine atoms had a concentration of  $\sim 10^4 \text{ cm}^{-3}$ , which is only slightly above the detection limit. The evaluation also included Br atoms that were below the detection limit and therefore are not shown in the plot.

**Table 4:** Fitting functions for the artificial sea salt experiment from Figure 10 to derive the concentrations of OH und Cl

Hydrocarbon	Fitting function /mVs
2,2-Dimethylpropane (DMP)	$500 + 8e^{-t/20000s}$
2,2-Dimethylbutane (DMB)	$1285 + 359e^{-t/38409s}$
2,2,4-Trimethylpentane (TMP)	$1236 + 367e^{-t/15267s}$
Toluene	$379 + 1712e^{-t/41847s}$

### 3.3 Iron-free artificial sea salt aerosol+ 20 ppb NO<sub>x</sub>

The nebulizer was filled with ~50 ml of an iron-free artificial seawater solution (see Table 1) that was 1:28 diluted to ~18 mmol L<sup>-1</sup>. In this experiment, injection was performed through a heated copper tube as described in section 2. The injection time was 60 min. The time profile of the total aerosol concentration and the total aerosol surface is shown in Figure 11. The plot ends at 90 min since the flashovers in the classifier disturbed the subsequent measurements.

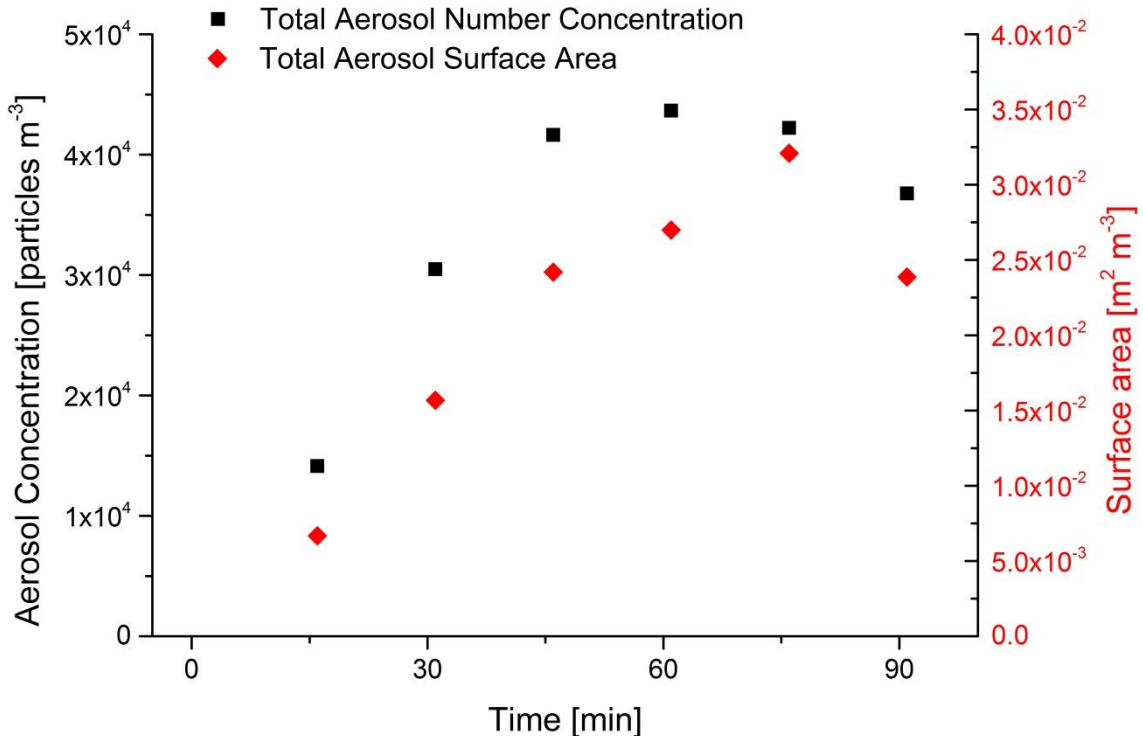


**Figure 11:** Time profiles of the total measured aerosol number concentration and the surface area for the experiment with artificial sea salt aerosols + NO<sub>x</sub> addition. At t= 0 the injection starts. At t= 140 min the lights were turned on.

The following amount of hydrocarbons was injected

- 80 µl DMP
- 0.2 µl PFH (inert standard)
- 0.2 µl DMB
- 0.2 µl TMP
- 0.2 µl Tol

The dilution corrected time profiles of the injected hydrocarbons are shown in Figure 12 (left).

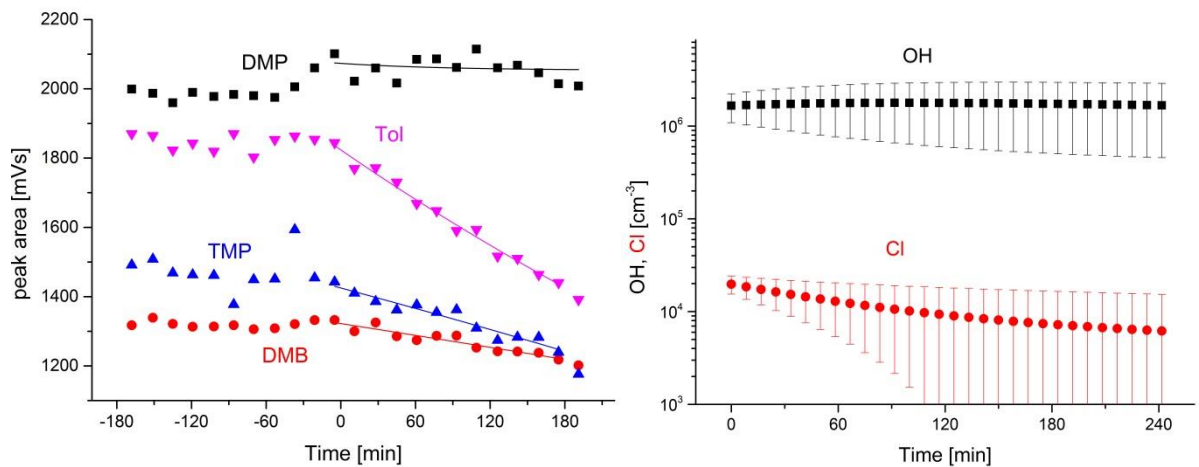


**Figure 12:** HC measurements in the artificial sea salt aerosol experiment with NO<sub>x</sub> addition (20 ppb) including the applied fit functions (left) and the hence calculated concentrations of OH and Cl radicals (right). The irradiation started at the time 0.

Comparable to the NaCl and artificial sea salt experiments toluene shows a significant decrease and the alkanes have been only slightly reduced whereas DMP does not significantly decrease. This is again an indication of low Cl concentrations. The quasi-stationary concentrations of OH and Cl radicals (Figure 12, right) were derived from the functions fitted (shown in Table 5) to the measurement data. The concentration of OH radicals has the typical value of about  $\sim 10^6$  cm<sup>-3</sup>. Chlorine atoms had a concentration of  $\sim 5 \cdot 10^5$  cm<sup>-3</sup>. The evaluation also included Br atoms that are at  $\sim 10^{10}$  cm<sup>-3</sup>.

**Table 5:** Fitting functions for the artificial seawater experiment with 20 ppb NO<sub>2</sub> addition from Figure 12 to derive the concentrations of OH und Cl

Hydrocarbon	Fitting function /mVs
2,2-Dimethylpropane (DMP)	$2054 + 20e^{-t/5000s}$
2,2-Dimethylbutane (DMB)	$903 + 545e^{-t/4839238409s}$
2,2,4-Trimethylpentane (TMP)	$1562e^{-t/79506s}$
Toluene	$-110 + 2106e^{-t/46681s}$

Figure 13 shows the time profiles of the monitored species and parameters during the experiment. During aerosol injection the RH increased up to 90 % what is the reason for the beginning of flashovers in the classifier. Moreover, the injection caused an NO<sub>x</sub> and NO increase of 5 and 2 ppb respectively. After injecting 20 ppb NO<sub>2</sub> and a waiting period of 60 min the light was turned on and caused a fast formation of NO and O<sub>3</sub> until the photostationary state is reached (Leighton ratio). The re-oxidation of NO to NO<sub>2</sub> and OH via HO<sub>2</sub> (formed by the depletion of the injected HC<sub>i</sub>) leads to a further O<sub>3</sub> formation that exceeds the NO<sub>x</sub> concentration due to the relatively large amount of HCs (~30 ppb).

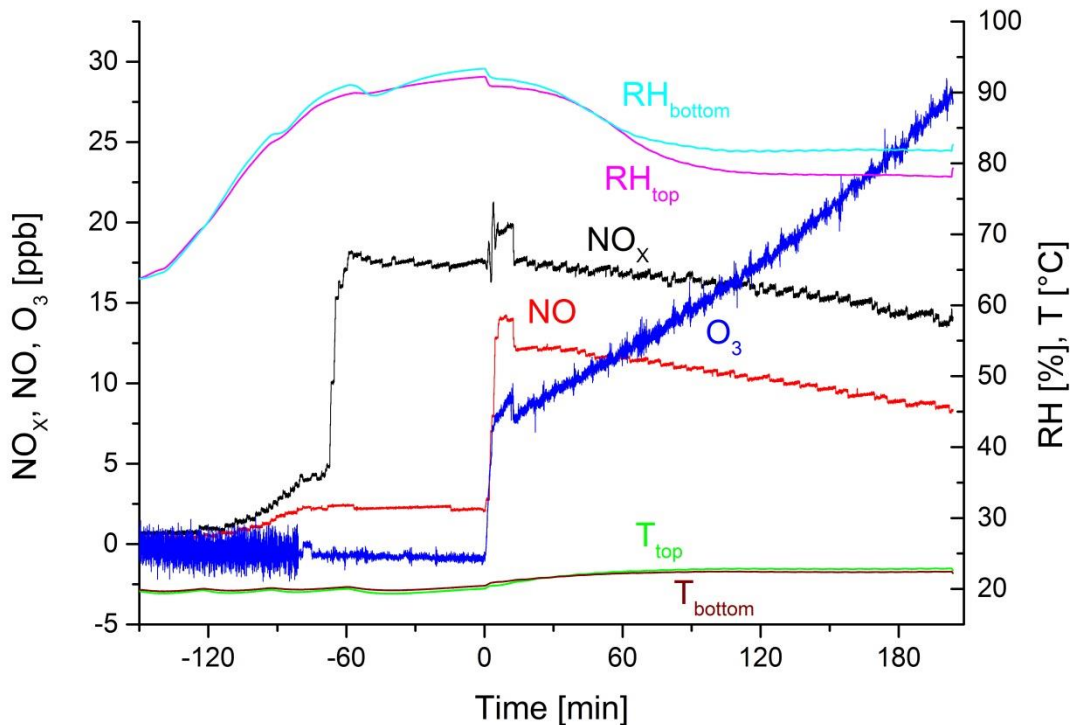


**Figure 13:** Time profiles of  $\text{NO}_x$ ,  $\text{NO}$ ,  $\text{O}_3$ , RH and T for the experiment with artificial sea salt aerosols +  $\text{NO}_x$  addition. The irradiation started at the time 0. The box-shaped artefact in the  $\text{NO}_x$ ,  $\text{NO}$  and  $\text{O}_3$  profile after turning the light on is probably an effect of chamber mixing since the same sampling tube is used.

### 3.4 Iron-free artificial sea salt aerosol+ 700 ppb $\text{O}_3$

The nebulizer was filled with  $\sim 50$  ml of an iron-free artificial seawater solution (see Table 1) that was 1:28 diluted to  $\sim 18 \text{ mmol L}^{-1}$ . In this experiment injection was performed with a heated copper tube as described in section 2. The injection time was 67 min. The time profile of the total aerosol concentration and the total aerosol surface is shown in Figure 14.

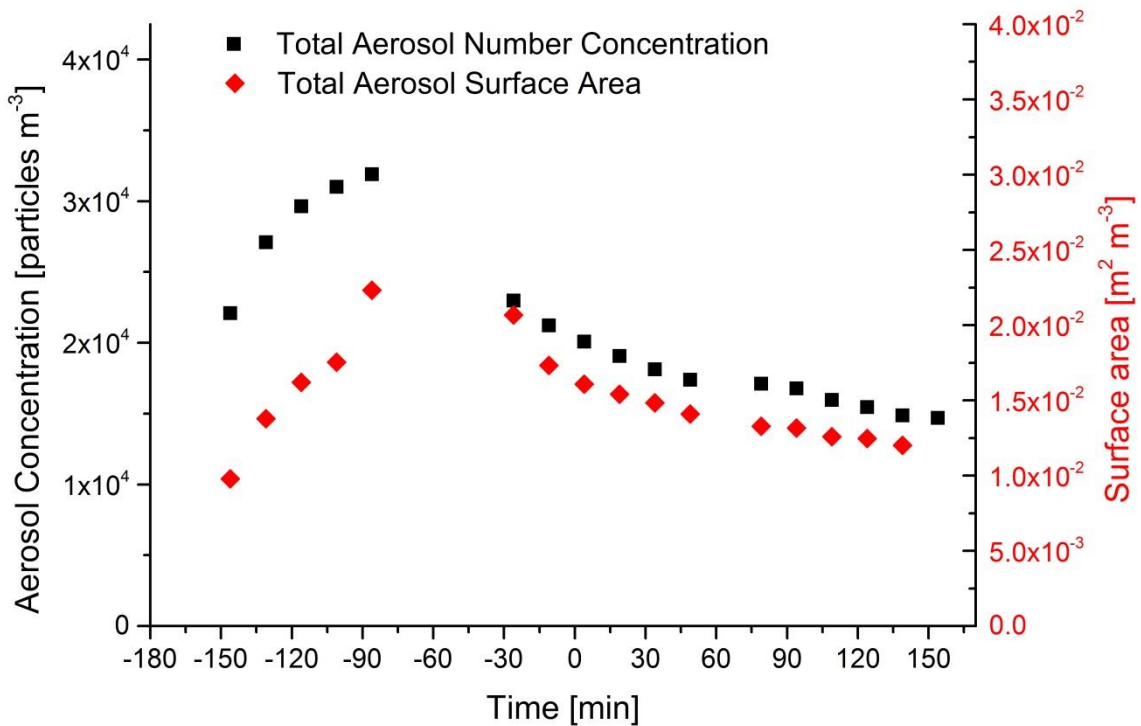
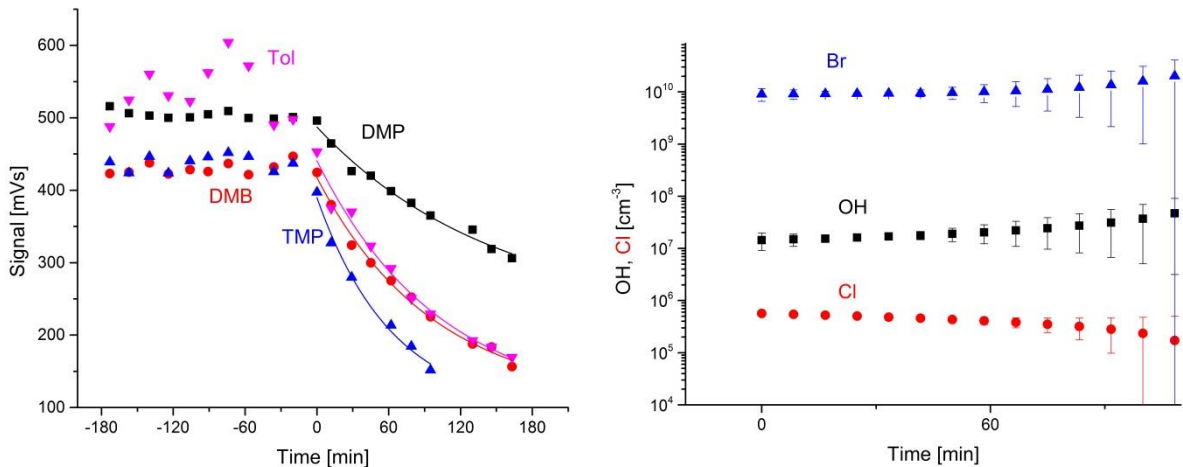


Figure 14: Time profiles of the total measured aerosol number concentration and the surface area for the experiment with artificial sea salt aerosols + O<sub>3</sub> addition. At t= -150 the aerosol injection starts. At t= 0 min the lights were turned on.

The following amount of hydrocarbons was injected

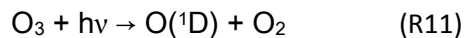
- 50 µl DMP
- 0.2 µl PFH (inert standard)
- 0.2 µl DMB
- 0.2 µl TMP
- 0.2 µl Tol

The dilution corrected time profiles of the injected hydrocarbons are shown in Figure 15 (left). The quasi-stationary concentrations of OH, Cl and Br radicals (Figure 15, right) were derived from the functions fitted (shown in Table 6) to the measurement data. The concentration of OH radicals has an elevated level of about >10<sup>7</sup> cm<sup>-3</sup>. Chlorine atoms had a concentration of ~10<sup>4</sup> cm<sup>-3</sup>, which is only slightly above the detection limit. The evaluation also included Br atoms that were ~10<sup>10</sup> cm<sup>-3</sup>.



**Figure 15:** HC measurements in the artificial sea salt aerosol experiment with O<sub>3</sub> addition (700 ppb) including the applied fit functions (left) and the hence calculated concentrations of OH and Cl radicals (right). The irradiation started at the time 0.

In this experiment a fast depletion of all HCs is observed. This is caused by elevated O<sub>3</sub> and thus OH concentrations formed via:



On the other hand higher Cl concentrations are observed compared to the zero air experiments (Figure 15). The enhanced Cl production in the iron-free experiments indicates that we observe an O<sub>3</sub> induced Cl and Br production. Several mechanisms come into consideration for the observed effects. At these O<sub>3</sub> levels, a main mechanism (that is responsible for the high Cl and Br production and the fast O<sub>3</sub> depletion) is the so called “Bromine Explosion” (Hausmann and Platt, 1994; Wennberg, 1999) and the associated formation of OCIO and ClO (Buxmann et al., 2012). Knipping et al., 2000 report a direct uptake of OH and subsequent Cl<sub>2</sub> release from NaCl aerosols. Furthermore, NO<sub>x</sub> (3-5 ppb are present after aerosol injection) forms N<sub>2</sub>O<sub>5</sub> during the dark phase, indicated by the loss of NO<sub>x</sub> when O<sub>3</sub> is injected and thus leads to HNO<sub>3</sub> formation in the aqueous phase causing an acid depletion with subsequent HCl release (Martens et al., 1973; de Haan and Finlayson-Pitts, 1997; Saul et al., 2006). Moreover, the uptake of N<sub>2</sub>O<sub>5</sub> activates X<sup>-</sup> by releasing XNO<sub>2</sub> (Behnke et al., 1997; Thornton et al., 2010; Bleicher et al., 2014) or even X<sub>2</sub> at acidic pH (<2) (Roberts et al., 2008), which is realistic for the iron doped sea-salt aerosol.

**Table 6: Fitting functions for the artificial sea salt experiment + 700 ppb O<sub>3</sub> from Figure 15 to derive the concentrations of OH und Cl**

Hydrocarbon	Fitting function /mVs
2,2-Dimethylpropane (DMP)	$224 + 263e^{-t/8950s}$
2,2-Dimethylbutane (DMB)	$129 + 290e^{-t/5151s}$
2,2,4-Trimethylpentane (TMP)	$95 + 295e^{-t/3776s}$
Toluene	$-95 + 346e^{-t/6243s}$

Figure 16 shows the time profiles of the monitored species and parameters during the experiment. During aerosol injection, the RH increased up to 90 %, causing flashovers in the classifier. Moreover, the injection caused an NO<sub>x</sub> and NO increase of 3 and 2 ppb respectively. After injecting 800 ppb O<sub>3</sub> and a waiting period of 40 min the light was turned. The O<sub>3</sub> injection leads to a rapid depletion of NO<sub>x</sub> by forming N<sub>2</sub>O<sub>5</sub> which is taken up by the aerosol.

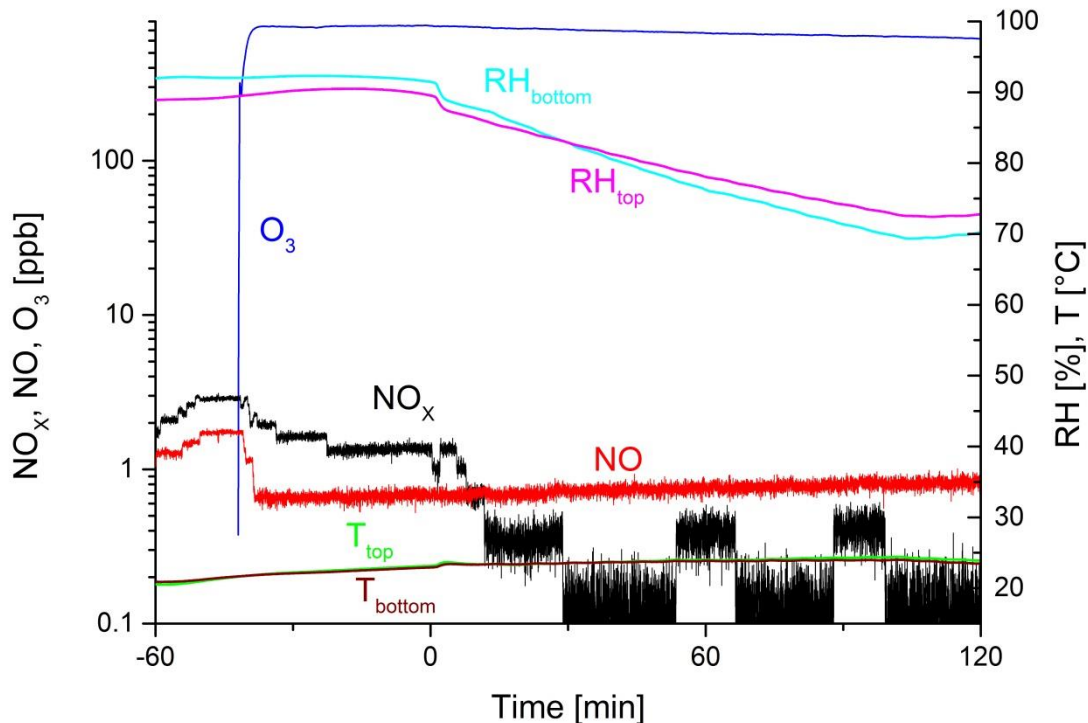


**Figure 16: Time profiles of NO<sub>x</sub>, NO, O<sub>3</sub>, RH and T for the experiment with artificial sea salt aerosols + O<sub>3</sub> addition. The irradiation started at the time t= 0. At t= -150 the aerosol was injected. At t= 110 min the humidification was increased to prevent a RH drop below 70.**

### 3.5 Iron-free artificial sea salt aerosol + 30 ppb SO<sub>2</sub>

The nebulizer was filled with ~50 ml of an iron-free artificial seawater solution (see Table 1) that was 1:28 diluted to ~18 mmol L<sup>-1</sup>. The injection time was 71 min. The time profile of the total aerosol concentration and the total aerosol surface cannot be shown since due to the flashovers only 2 measurements of the aerosol size distribution are available.

The following amount of hydrocarbons was injected

- 60 µl DMP
- 0.22 µl PFH (inert standard)
- 0.22 µl DMB
- 0.22 µl TMP
- 0.22 µl Tol

The dilution corrected time profiles of the injected hydrocarbons are shown in Figure 17.

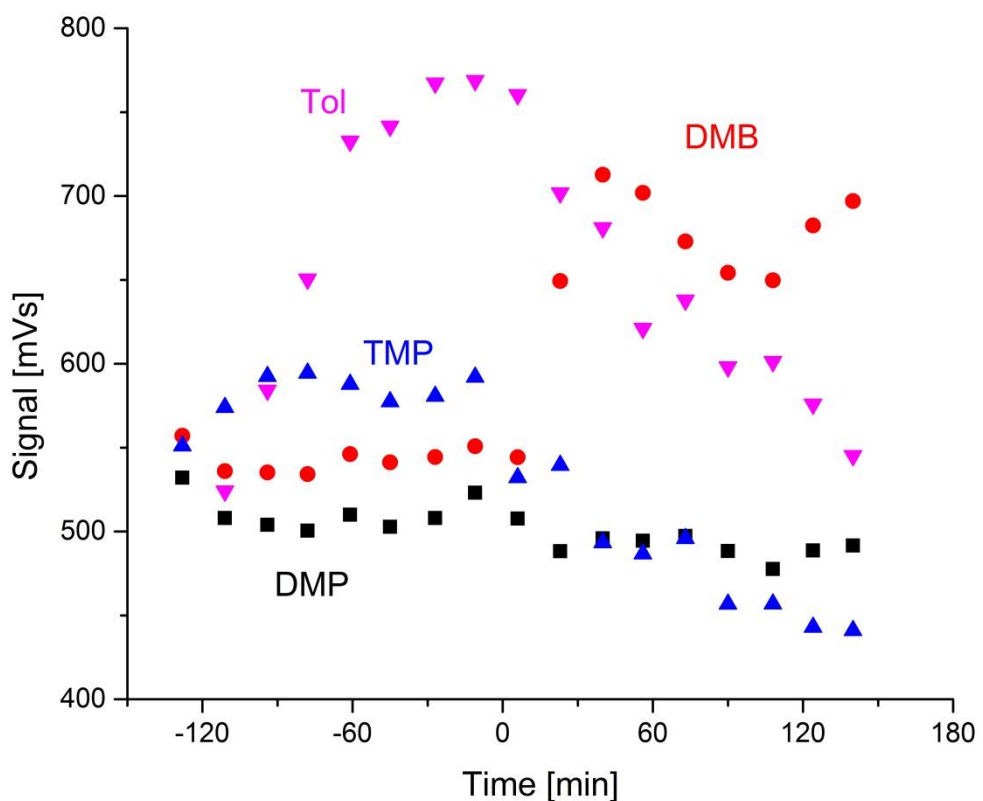


Figure 17: HC measurements in the artificial sea salt aerosol + 30 ppb SO<sub>2</sub>. The irradiation started at the time 0.

Comparable to the NaCl and artificial seawater experiment toluene shows a significant decrease and the alkanes have been only slightly reduced, prohibiting a further evaluation of Cl and OH concentrations.

### 3.6 Iron-doped artificial sea salt aerosol (molar $\text{Cl}^-/\text{Fe(III)}$ )=955)

The nebulizer was filled with ~50 ml of an iron-doped artificial seawater solution (see Table 1). 0.0277g  $\text{FeCl}_3$  (Merck) were dissolved in 200 ml of the artificial seawater stock solution and afterwards 1:28 diluted to ~28 mmol L<sup>-1</sup>. The injection time was 60 min. The time profile of the total aerosol concentration and the total aerosol surface cannot be shown since due to the flashovers only 2 measurements of the aerosol size distribution are available.

The following amount of hydrocarbons was injected

- 80  $\mu\text{l}$  DMP
- 0.4  $\mu\text{l}$  PFH (inert standard)
- 0.4  $\mu\text{l}$  DMB
- 0.4  $\mu\text{l}$  TMP
- 0.4  $\mu\text{l}$  Tol

The dilution corrected time profiles of the injected hydrocarbons are shown in Figure 18.

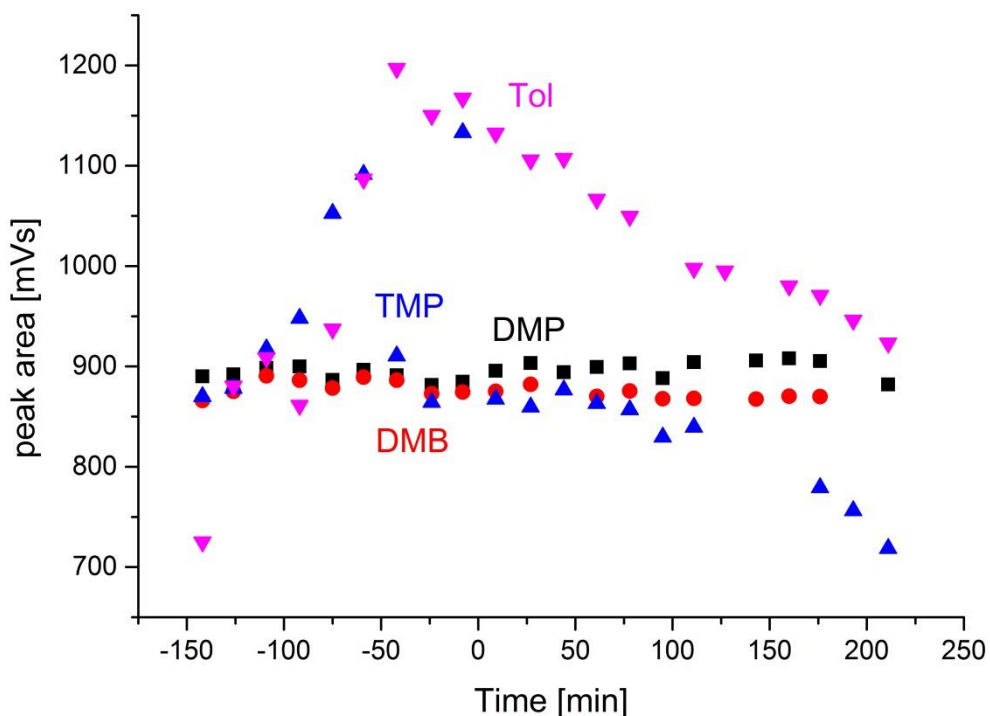
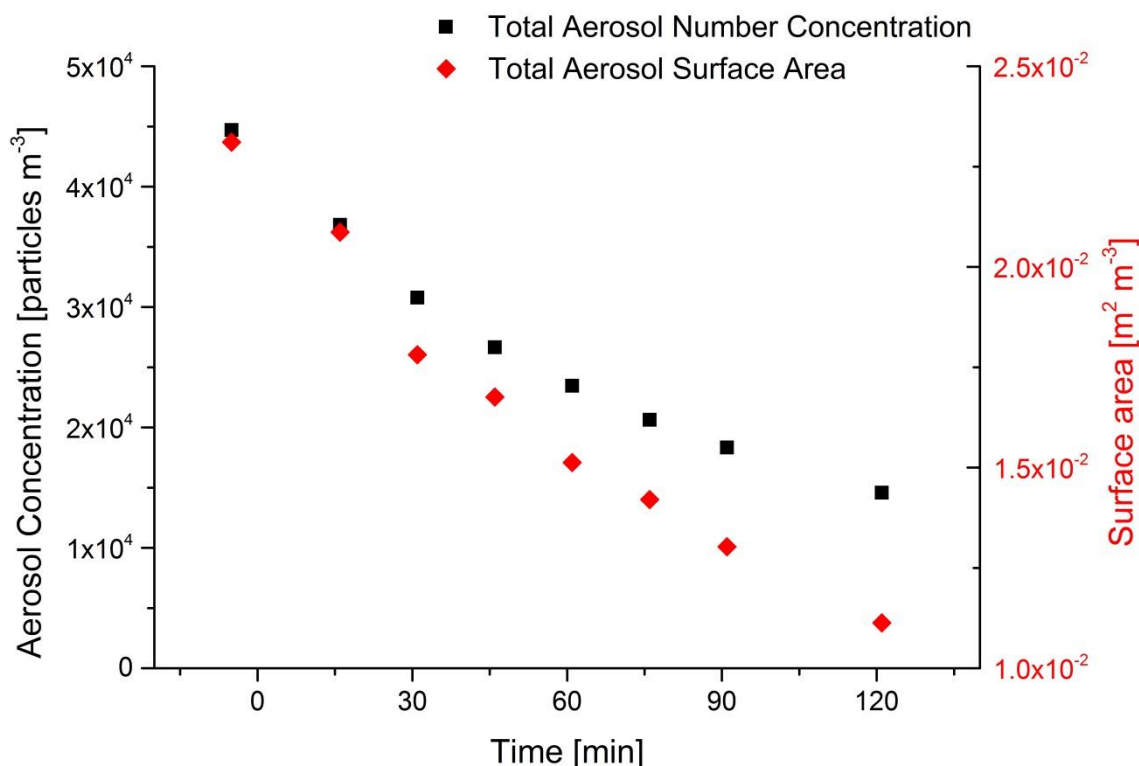


Figure 18: HC measurements in the iron doped artificial sea salt aerosol experiment ( $\text{Cl}^-/\text{Fe(III)} = 955$ ). The irradiation started at the time 0.

Comparable to the NaCl and artificial seawater experiment only toluene shows a significant decrease (based on the sensitivity towards OH) and the alkanes have been only slightly reduced, prohibiting a further evaluation of Cl and OH concentrations since no significant fit function can be applied for DMB and TMP.

### 3.7 Iron-doped artificial sea salt aerosol (molar Cl<sup>-</sup>/Fe(III)=101)

The nebulizer was filled with ~50 ml of an iron-doped artificial seawater solution (see Table 1). 0.1360g FeCl<sub>3</sub> (Merck) were dissolved in 100ml of the artificial seawater stock solution and afterwards 1:28 diluted to ~29 mmol L<sup>-1</sup>. The injection time was 43 min. The time profile of the total aerosol concentration and the total aerosol surface is shown in Figure 19.



**Figure 19:** Time profiles of the total measured aerosol number concentration and the surface area for the experiment with iron-doped artificial sea salt aerosol (Cl<sup>-</sup>/Fe(III)=101). At t= 0 the irradiation starts. At t= -80 min the injection starts. Because the particle counter needed technical service the aerosol measurements started

The following amount of hydrocarbons was injected

- 80 µl DMP
- 0.3 µl PFH (inert standard)
- 0.3 µl DMB
- 0.3 µl TMP
- 0.3 µl Tol

The dilution corrected time profiles of the injected hydrocarbons are shown in Figure 20 (left). The quasi-stationary concentrations of OH and Cl radicals (Figure 20, right) were derived from the functions fitted (shown in Table 7) to the measurement data. The concentration of OH radicals is between 10<sup>6</sup> and 10<sup>7</sup> cm<sup>-3</sup>. Chlorine atoms had an initial concentration of ~10<sup>5</sup> cm<sup>-3</sup>, and fastly decreased to 10<sup>4</sup> cm<sup>-3</sup> within the first 120 min. The evaluation also included Br atoms that were in the range of 10<sup>9</sup> - 10<sup>10</sup> cm<sup>-3</sup>.

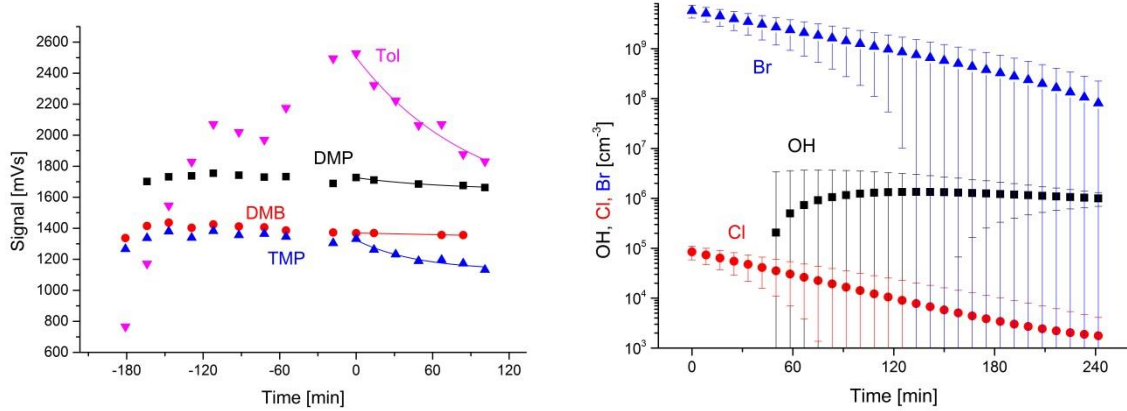


**Figure 20:** HC measurements in the iron-doped artificial sea salt aerosol ( $\text{Cl}^-/\text{Fe(III)}=101$ ) experiment including the applied fit functions (left) and the hence calculated concentrations of OH, Br and Cl radicals (right). The irradiation started at the time 0.

**Table 7:** Fitting functions for the iron-doped artificial sea salt aerosol ( $\text{Cl}^-/\text{Fe(III)}=101$ ) experiment from Figure 20 to derive the concentrations of OH und Cl

Hydrocarbon	Fitting function /mVs
2,2-Dimethylpropane (DMP)	$1647 + 79e^{-t/4148s}$
2,2-Dimethylbutane (DMB)	$1370e^{-t/472698s}$
2,2,4-Trimethylpentane (TMP)	$1127 + 197e^{-t/2895s}$
Toluene	$1504 + 998e^{-t/5577s}$

### 3.8 Iron-doped artificial sea salt aerosol (molar Cl<sup>-</sup>/Fe(III)=53)

The nebulizer was filled with ~50 ml of an iron-doped artificial seawater solution (see Table 1). 0.2675g FeCl<sub>3</sub> (Riedel-de Haën, sublimate, ≥ 99 %) were dissolved in 100ml of the artificial seawater stock solution and afterwards 1:28 diluted to ~30 mmol L<sup>-1</sup>. The injection time was 36 min. The time profile of the total aerosol concentration and the total aerosol surface is shown in Figure 21.

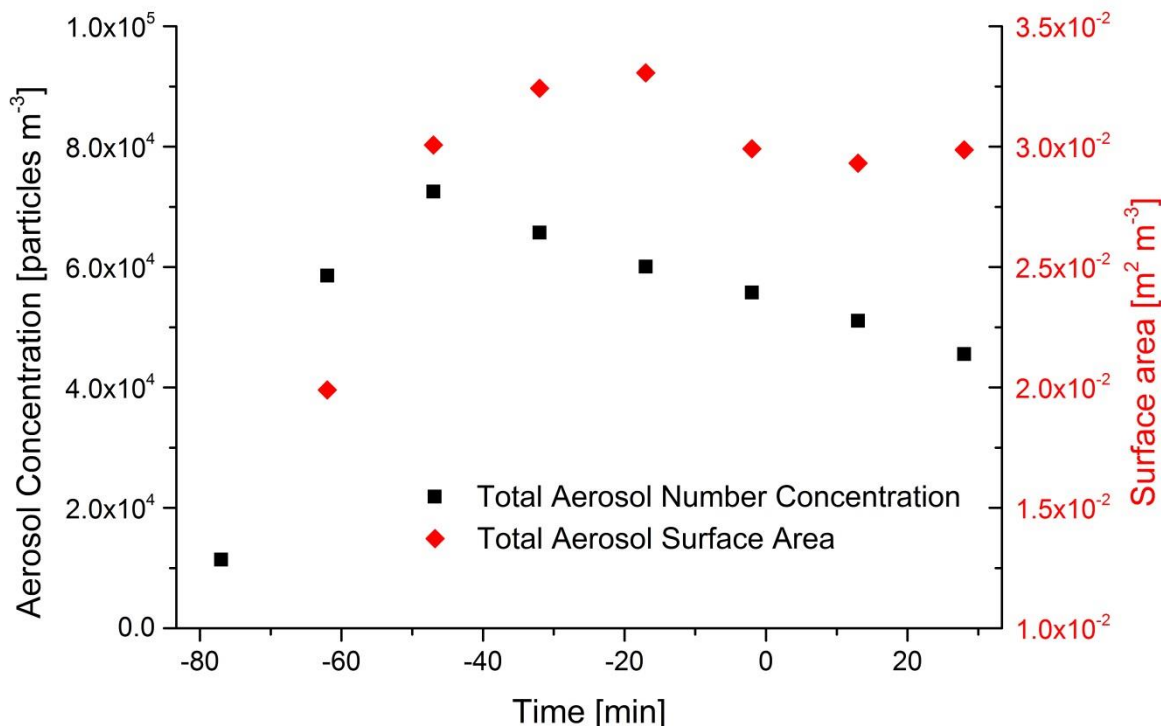
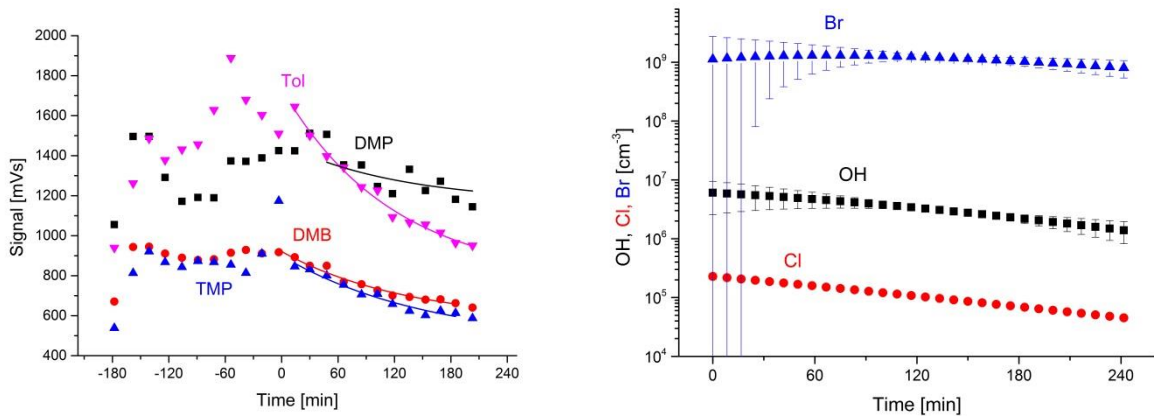


Figure 21: Time profiles of the total measured aerosol number concentration and the surface area for the experiment with iron-doped artificial sea salt aerosol (Cl<sup>-</sup>/Fe(III)=53). At t= 0 min the irradiation starts. At t= -60 min the injection starts.

The following amount of hydrocarbons was injected

- 50 µl DMP
- 0.2 µl PFH (inert standard)
- 0.2 µl DMB
- 0.2 µl TMP
- 0.2 µl Tol

The dilution corrected time profiles of the injected hydrocarbons are shown in Figure 22 (left). The quasi-stationary concentrations of OH and Cl radicals (Figure 22, right) were derived from the functions fitted (shown in Table 8) to the measurement data. The concentration of OH radicals is between 10<sup>6</sup> and 10<sup>7</sup> cm<sup>-3</sup>. Chlorine atoms had a more stable concentration (10<sup>5</sup> – 10<sup>6</sup> cm<sup>-3</sup>) than in the previous experiment with Cl<sup>-</sup>/Fe(III) =101. The evaluation also included Br atoms that were ~10<sup>9</sup> cm<sup>-3</sup>.



**Figure 22:** HC measurements in the iron-doped artificial sea salt aerosol ( $\text{Cl}^-/\text{Fe(III)}=51$ ) experiment including the applied fit functions (left) and the hence calculated concentrations of OH, Br and Cl radicals (right). The irradiation started at the time 0.

**Table 8:** Fitting functions for the iron-doped artificial sea salt aerosol ( $\text{Cl}^-/\text{Fe(III)}=51$ ) experiment from Figure 22 to derive the concentrations of OH und Cl

Hydrocarbon	Fitting function / mVs
2,2-Dimethylpropane (DMP)	$1165 + 297e^{-t/7508s}$
2,2-Dimethylbutane (DMB)	$570 + 350e^{-t/8051s}$
2,2,4-Trimethylpentane (TMP)	$475 + 425e^{-t/8919s}$
Toluene	$774 + 961e^{-t/7123s}$

### 3.9 Iron-doped artificial sea salt aerosol (molar Cl<sup>-</sup>/Fe(III)=13)

The nebulizer was filled with ~50 ml of an iron-doped artificial seawater solution (see Table 1). 1.3043g FeCl<sub>3</sub> (Riedel-de Haën, sublimate, ≥ 99 %) were dissolved in 100ml of the artificial seawater stock solution and afterwards 1:28 diluted to ~37 mmol L<sup>-1</sup>. The injection time was 46 min. The time profile of the total aerosol concentration and the total aerosol surface cannot be shown since due to the flashovers only 3 measurements of the aerosol size distribution are available that show a particle number concentration of ~61 000 particles m<sup>-3</sup> and an aerosol surface of ~0.0324 m<sup>2</sup> m<sup>-3</sup> directly after injection.

The following amount of hydrocarbons was injected

- 50 µl DMP
- 0.2 µl PFH (inert standard)
- 0.2 µl DMB
- 0.2 µl TMP
- 0.2 µl Tol

The dilution corrected time profiles of the injected hydrocarbons are shown in Figure 23 (left). The quasi-stationary concentrations of radicals (Figure 23, right) were derived from the functions fitted (shown in Table 9) to the measurement data. The concentrations of Br and OH radicals are not evaluable due to the dominating depletion of the HCs through Cl atoms. Cl atoms were very high concentrated with a more or less stable quasi-stationary concentration of ~1.3·10<sup>6</sup> cm<sup>-3</sup>.

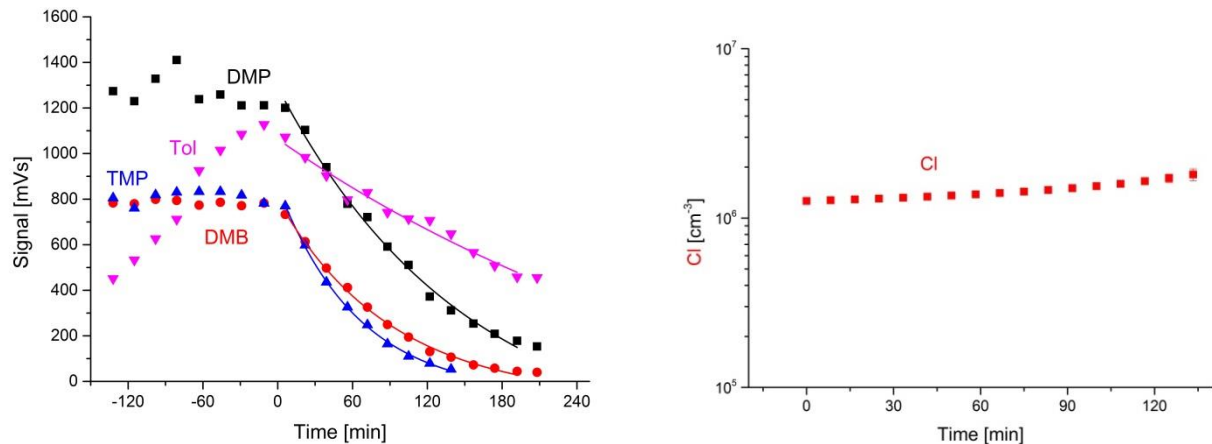


Figure 23: HC measurements in the iron-doped artificial sea salt aerosol (Cl<sup>-</sup>/Fe(III)=13) experiment including the applied fit functions (left) and the hence calculated concentrations of Cl radicals (right). The irradiation started at the time t= 0. The Cl error bars are too small to be visible.

**Table 9: Fitting functions for the iron-doped artificial sea salt aerosol ( $\text{Cl}^-/\text{Fe(III)}=13$ ) experiment from Figure 23 to derive the concentrations of Cl**

Hydrocarbon	Fitting function /mVs
2,2-Dimethylpropane (DMP)	$-208 + 1506e^{-t/8246s}$
2,2-Dimethylbutane (DMB)	$-56 + 859e^{-t/5179s}$
2,2,4-Trimethylpentane (TMP)	$-60 + 915e^{-t/3864s}$
Toluene	$-306 + 1373e^{-t/20885s}$

### 3.10 Iron-doped NaCl aerosol (molar $\text{Cl}^-/\text{Fe(III)}=13$ )

The nebulizer was filled with ~50 ml of an iron-doped artificial seawater solution (see Table 1). 0.278g  $\text{FeCl}_3$  (Riedel-de Haën, sublimate, ≥ 99 %) were dissolved in 1L of a 1 g/L NaCl solution (~18 mmol  $\text{L}^{-1}$   $\text{Cl}^-$ ). The injection time was 45 min. The time profile of the total aerosol concentration and the total aerosol surface is shown in Figure 24.

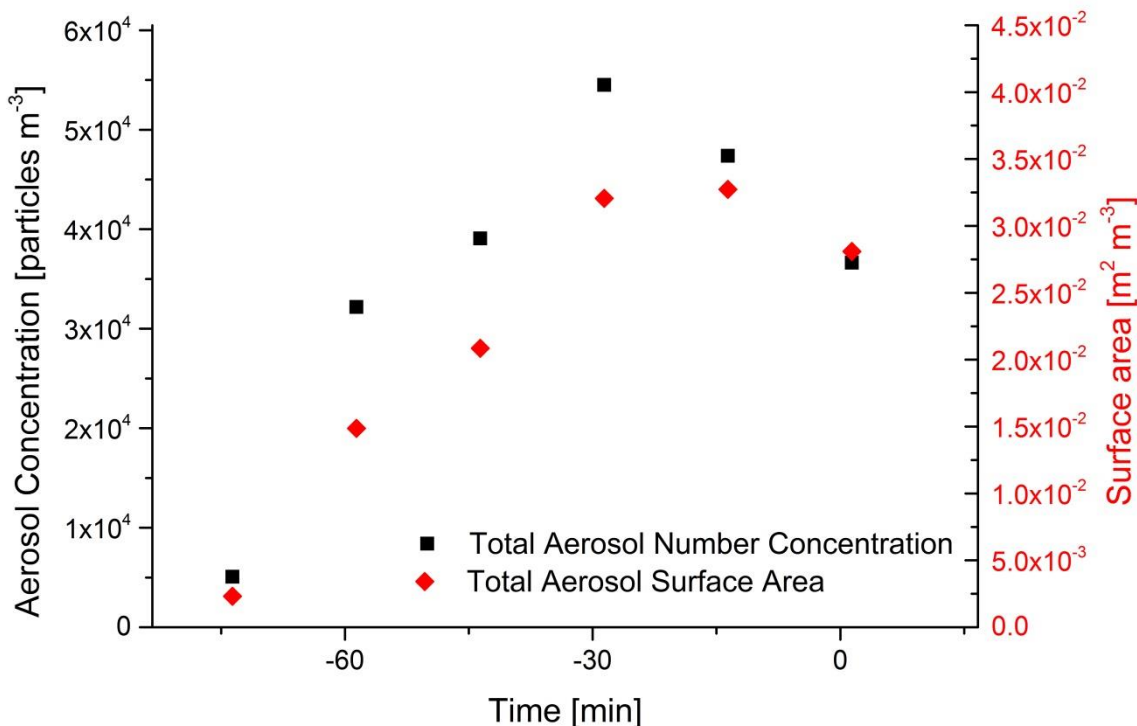


**Figure 24: Time profiles of the total measured aerosol number concentration and the surface area for the experiment with iron-doped NaCl aerosol ( $\text{Cl}^-/\text{Fe(III)}=13$ ). At  $t=0$  the irradiation starts. At  $t=-60$  min the injection starts.**

The following amount of hydrocarbons was injected

- 50  $\mu\text{l}$  DMP
- 0.2  $\mu\text{l}$  PFH (inert standard)
- 0.2  $\mu\text{l}$  DMB
- 0.2  $\mu\text{l}$  TMP
- 0.2  $\mu\text{l}$  Tol

The dilution corrected time profiles of the injected hydrocarbons are shown in Figure 25 (left). The quasi-stationary concentrations of radicals (Figure 25, right) were derived from the functions fitted (shown in Table 10) to the measurement data. The concentrations of Br and OH radicals are error-prone due to the dominating depletion of the HCs through Cl atoms. Cl atoms were very high concentrated with a more or less stable quasi-stationary concentration of  $\sim 1.7 \cdot 10^6 \text{ cm}^{-3}$ .

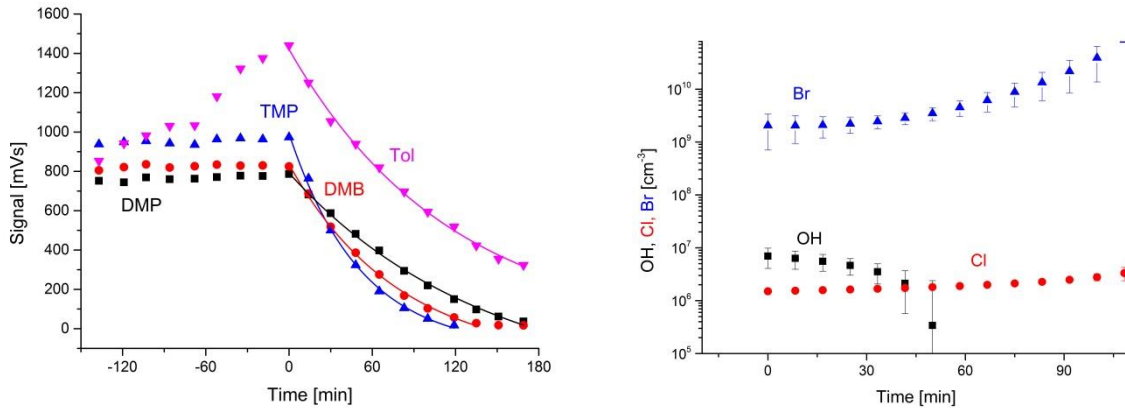


**Figure 25:** HC measurements in the iron-doped NaCl aerosol ( $\text{Cl}^-/\text{Fe(III)}=13$ ) experiment including the applied fit functions (left) and the hence calculated concentrations of Cl, OH, Br radicals (right). The irradiation started at the time 0.

**Table 10:** Fitting functions for the iron-doped NaCl aerosol ( $\text{Cl}^-/\text{Fe(III)}=13$ ) experiment from Figure 25 to derive the concentrations of Cl, OH, Br

Hydrocarbon	Fitting function /mVs
2,2-Dimethylpropane (DMP)	$-316 + 1107e^{-t/8458s}$
2,2-Dimethylbutane (DMB)	$-88 + 933e^{-t/4062s}$
2,2,4-Trimethylpentane (TMP)	$-105 + 1096e^{-t/3077s}$
Toluene	$19 + 1404e^{-t/6680s}$

### 3.11 Iron-doped artificial sea salt aerosol (molar Cl<sup>-</sup>/Fe(III)=13) + 620 ppb O<sub>3</sub>

The nebulizer was filled with ~50 ml of an iron-doped artificial seawater solution (see Table 1). 1.3043g FeCl<sub>3</sub> (Riedel-de Haën, sublimate, ≥ 99 %) were dissolved in 100ml of the artificial seawater stock solution and afterwards 1:28 diluted to ~37 mmol L<sup>-1</sup>. The injection time was 51 min. The time profile of the total aerosol concentration and the total aerosol surface is shown in Figure 26.

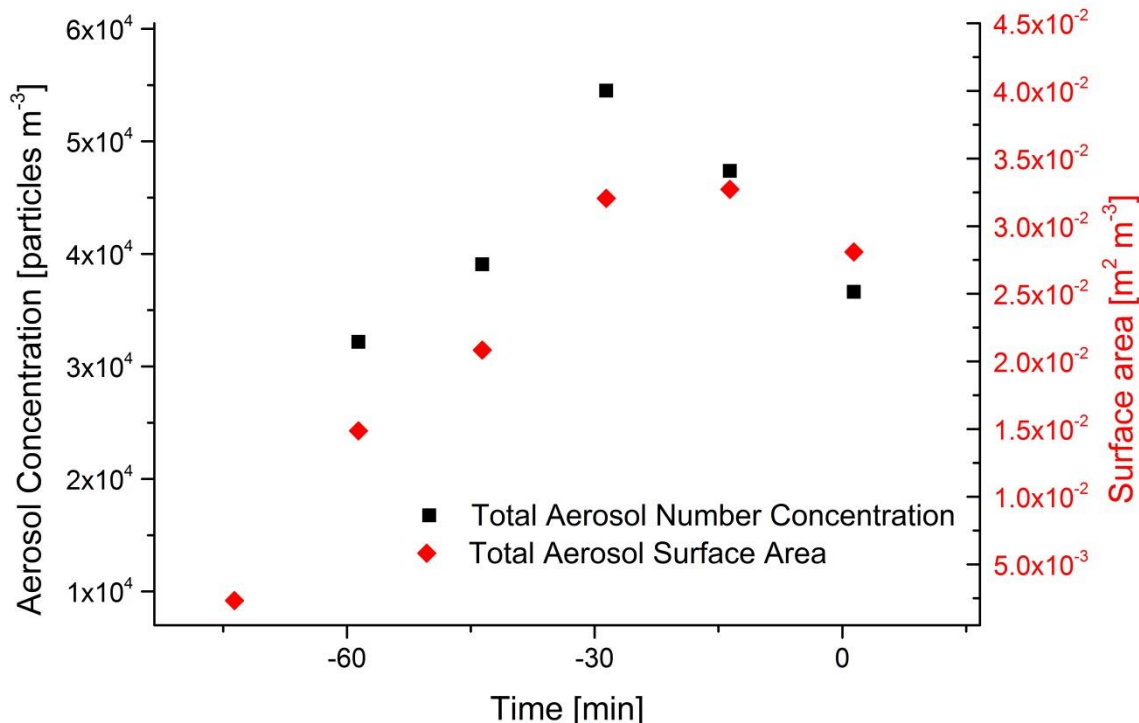


Figure 26: Time profiles of the total measured aerosol number concentration and the surface area for the experiment with iron-doped artificial sea salt aerosol (Cl<sup>-</sup>/Fe(III)=13)+O<sub>3</sub>. At t= 0 the irradiation starts. At t= -66 min the aerosol injection starts.

The following amount of hydrocarbons was injected

- 70 µl DMP
- 0.3 µl PFH (inert standard)
- 0.3 µl DMB
- 0.3 µl TMP
- 0.3 µl Tol

The dilution corrected time profiles of the injected hydrocarbons are shown in Figure 27 (left). The quasi-stationary concentrations of radicals (Figure 27, right) were derived from the functions fitted (shown in Table 11) to the measurement data. The concentrations of Br and OH radicals are error-prone due to the dominating depletion of the HCs through Cl atoms. Anyway, an elevated concentration of Br atoms ( $\sim 1.3 \cdot 10^{10} \text{ cm}^{-3}$ ) was detected compared to the experiment without O<sub>3</sub>. Cl atoms were very high concentrated with a more or less stable quasi-stationary concentration of  $\sim 4 \cdot 10^6 \text{ cm}^{-3}$ . At these O<sub>3</sub> levels, the halogen activation mechanisms as discussed in section 3.4 are

responsible for the additional increase of Cl and Br atoms compared to the pure iron-induced activation.

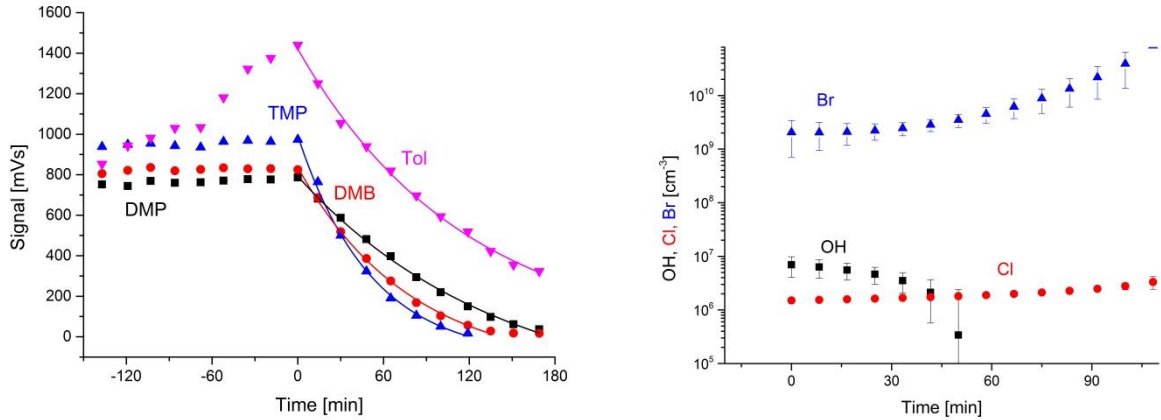


**Figure 27:** HC measurements in the iron-doped artificial sea salt aerosol ( $\text{Cl}^-/\text{Fe(III)}=13$ ) + 620 ppb  $\text{O}_3$  experiment including the applied fit functions (left) and the hence calculated concentrations of Cl, Br, OH radicals (right). The irradiation started at the time 0.

**Table 11:** Fitting functions for the iron-doped NaCl aerosol ( $\text{Cl}^-/\text{Fe(III)}=13$ ) experiment from Figure 27 to derive the concentrations of Cl, OH, Br

Hydrocarbon	Fitting function /mVs
2,2-Dimethylpropane (DMP)	$-116 + 1624e^{-t/2775s}$
2,2-Dimethylbutane (DMB)	$-53 + 1672e^{-t/1568s}$
2,2,4-Trimethylpentane (TMP)	$-49 + 1783e^{-t/1161s}$
Toluene	$263 + 2313e^{-t/2502s}$

Figure 28 shows the time profiles of the monitored species and parameters during the experiment. During aerosol injection the RH increased up to 80 %. Moreover, the injection caused an  $\text{NO}_x$  and NO increase of 3 and 1 ppb respectively. After injecting 620 ppb  $\text{O}_3$  and a waiting period of 13 min the light was turned. The  $\text{O}_3$  injection leads to a rapid depletion of  $\text{NO}_x$  by forming  $\text{N}_2\text{O}_5$  which is taken up

by the aerosol.

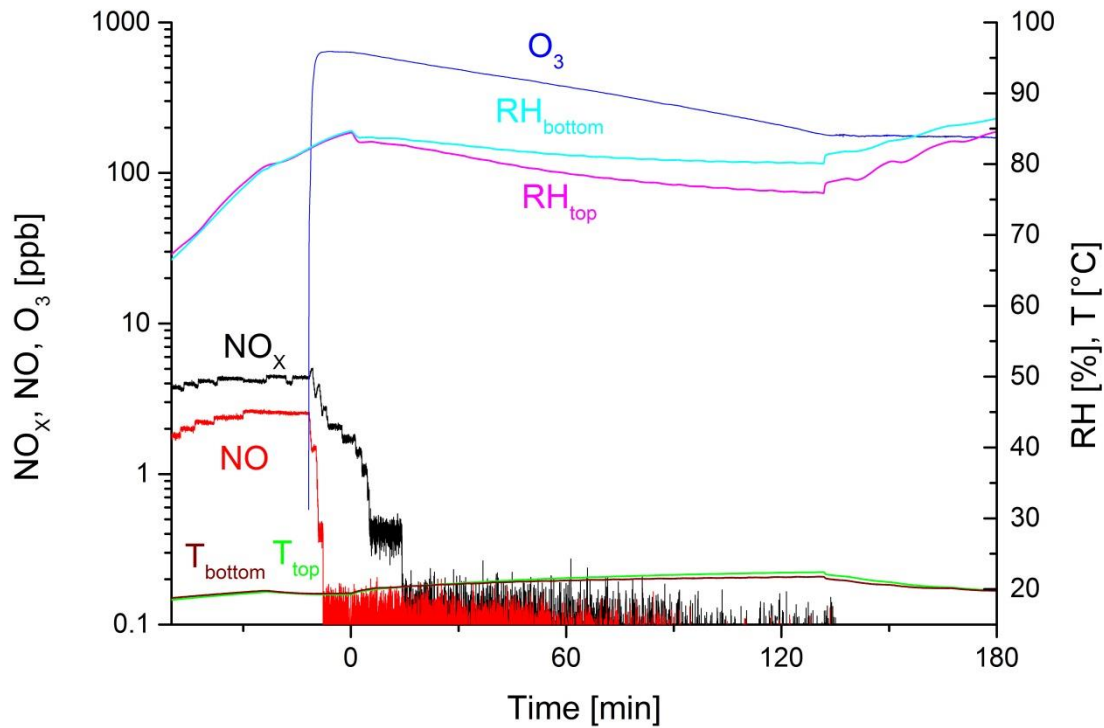


**Figure 28: Time profiles of  $\text{NO}_x$ ,  $\text{NO}$ ,  $\text{O}_3$ , RH and T for the experiment with iron-doped artificial sea salt aerosols +  $\text{O}_3$  addition. The irradiation started at the time  $t = 0$ . The  $\text{O}_3$  injection leads to a rapid depletion of  $\text{NO}_x$  by forming  $\text{N}_2\text{O}_5$  which is taken up by the aerosol. After 130 min the light was turned off and the dilution flux was increased.**

### 3.12 Iron-doped artificial sea salt aerosol (molar $\text{Cl}^-/\text{Fe(III)}=13$ ) + 20 ppb $\text{NO}_2$

The nebulizer was filled with ~50 ml of an iron-doped artificial seawater solution (see Table 1). 1.3043g  $\text{FeCl}_3$  (Riedel-de Haën, sublimate,  $\geq 99\%$ ) were dissolved in 100ml of the artificial seawater stock solution and afterwards 1:28 diluted to  $\sim 37 \text{ mmol L}^{-1}$ . The injection time was 61 min. The time profile of the total aerosol concentration and the total aerosol surface is shown in Figure 29.

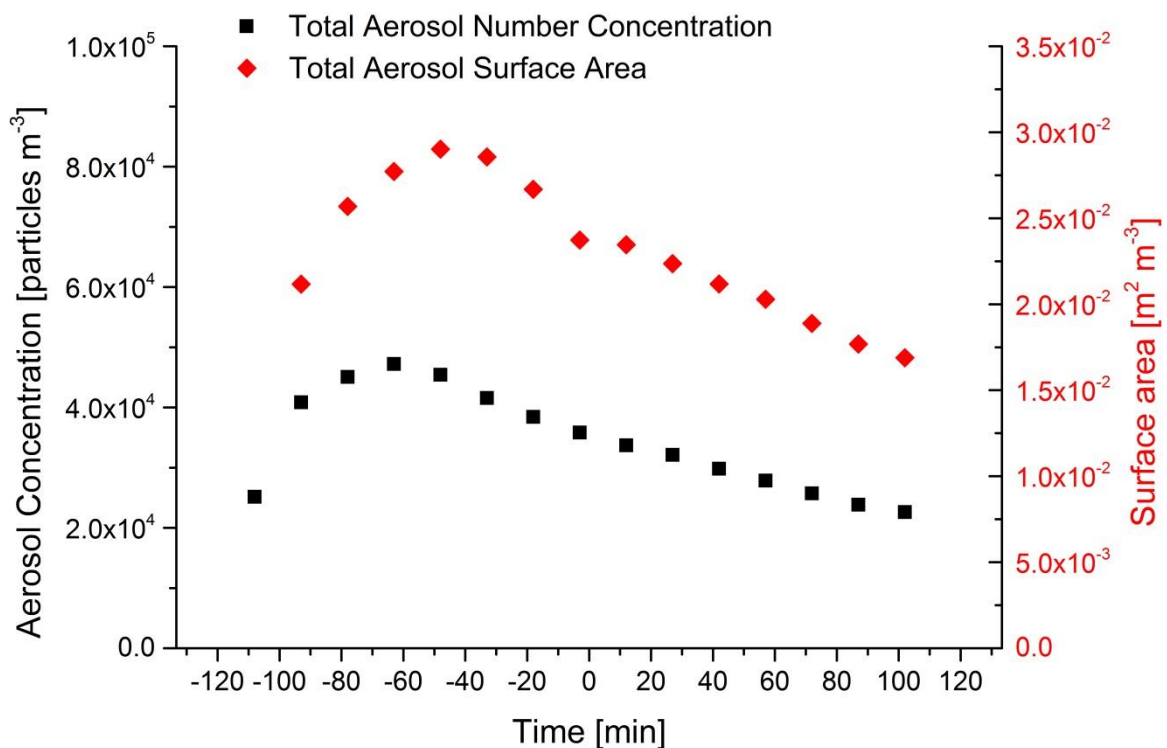
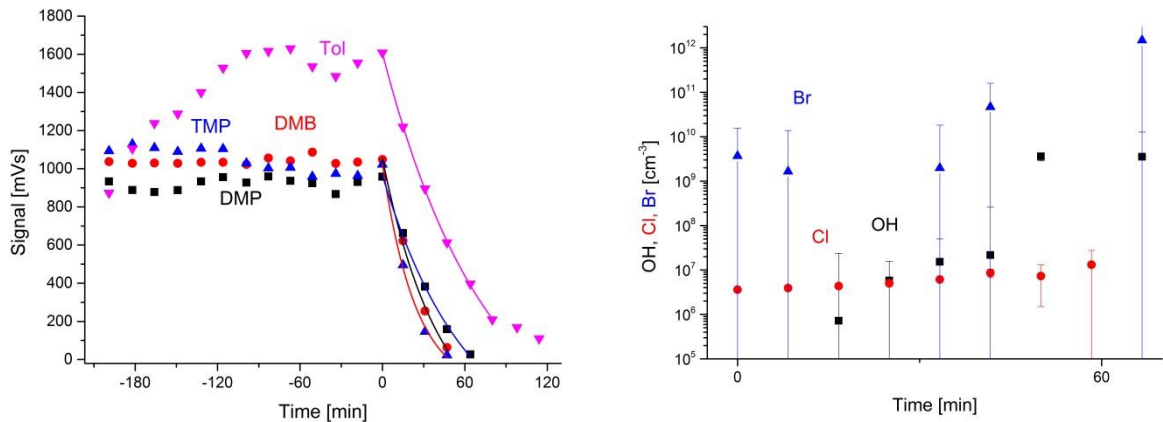


Figure 29: Time profiles of the total measured aerosol number concentration and the surface area for the experiment with iron-doped artificial sea salt aerosol ( $\text{Cl}^-/\text{Fe(III)}=13$ )+ $\text{NO}_2$ . At  $t=0$  the irradiation starts. At  $t=-120$  min the aerosol injection starts.

The following amount of hydrocarbons was injected

- 50  $\mu\text{l}$  DMP
- 0.2  $\mu\text{l}$  PFH (inert standard)
- 0.2  $\mu\text{l}$  DMB
- 0.2  $\mu\text{l}$  TMP
- 0.2  $\mu\text{l}$  Tol

The dilution corrected time profiles of the injected hydrocarbons are shown in Figure 30 (left). The quasi-stationary concentrations of radicals (Figure 30, right) were derived from the functions fitted (shown in Table 12) to the measurement data. The concentrations of Br and OH radicals are error-prone due to the dominating depletion of the HCs through Cl atoms. The mean Cl concentration during the first hour was  $\sim 6.5 \cdot 10^6 \text{ cm}^{-3}$ . At these  $\text{NO}_2$  levels, the halogen activation mechanisms as discussed in section 3.3 and 3.4 are responsible for the additional increase of Cl and Br atoms compared to the pure iron-induced Cl activation.



**Figure 30:** HC measurements in the iron-doped artificial sea salt aerosol ( $\text{Cl}^-/\text{Fe(III)}=13$ ) + 20 ppb  $\text{NO}_2$  experiment including the applied fit functions (left) and the hence calculated concentrations of Cl, Br and OH radicals (right). The irradiation started at the time 0.

**Table 12:** Fitting functions for the iron-doped artificial sea salt aerosol ( $\text{Cl}^-/\text{Fe(III)}=13$ ) + 20 ppb  $\text{NO}_2$  experiment from Figure 30 to derive the concentrations of Cl, OH, Br

Hydrocarbon	Fitting function /mVs
2,2-Dimethylpropane (DMP)	$-499 + 1464e^{-t/3666s}$
2,2-Dimethylbutane (DMB)	$-414 + 1468e^{-t/2468s}$
2,2,4-Trimethylpentane (TMP)	$-159 + 1186e^{-t/1455s}$
Toluene	$-147 + 1772e^{-t/3321s}$

Figure 31 shows the time profiles of the monitored species and parameters during the experiment. During aerosol injection the RH increased up to 80 %. Moreover, the injection caused an  $\text{NO}_x$  and NO increase of 4 and 3 ppb respectively. After injecting 20 ppb  $\text{NO}_2$  and a waiting period of 55 min the light was turned. The presence of  $\text{NO}_2$  leads to a fast  $\text{O}_3$  formation when the light was turned on and induces additional halogen activation mechanisms as described before. The  $\text{NO}_x$  depletion when the light is turned on is explained by  $\text{N}_2\text{O}_5$  formation and uptake to the aerosol but also by  $\text{HNO}_3$  and  $\text{XNO}_3$  ( $\text{X}=\text{Br}, \text{Cl}$ ) formation (see section 4: Summary and Discussion, R17, R18). The  $\text{O}_3$  depletion, visible after  $\sim 45$  min, is caused by the depletion through Br and Cl (discussed in section 4, R16).

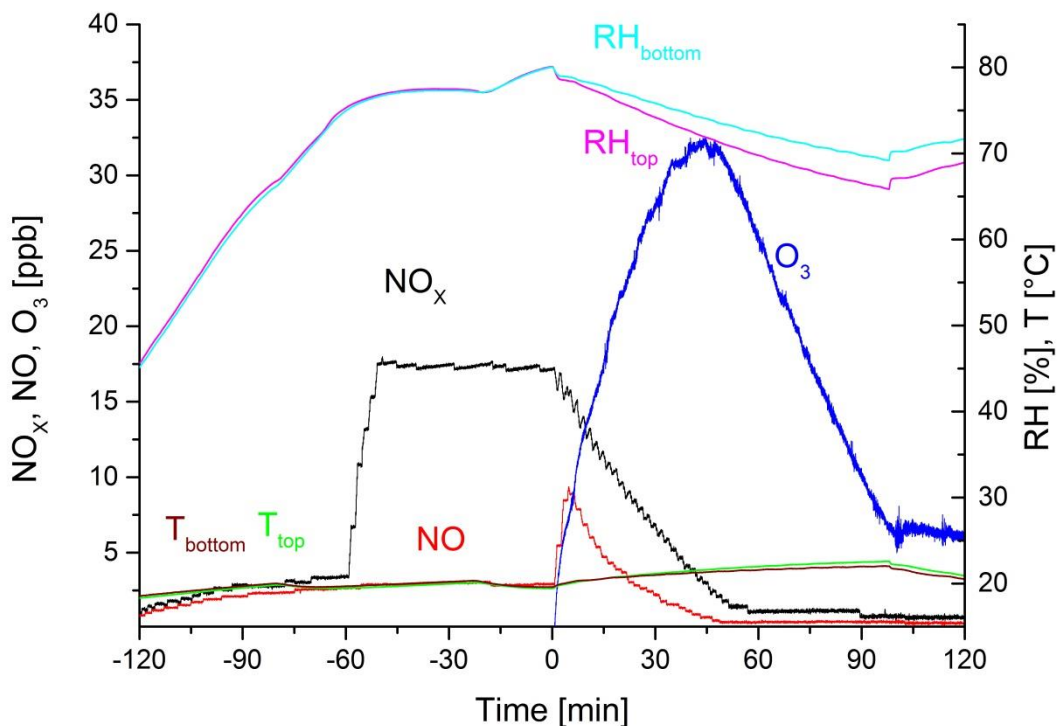


Figure 31: Time profiles of  $\text{NO}_x$ ,  $\text{NO}$ ,  $\text{O}_3$ , RH and T for the experiment with iron-doped artificial sea salt aerosols +  $\text{O}_3$  addition. The irradiation started at the time  $t = 0$  and stopped at  $t = 100$  min.

### 3.13 Iron-doped artificial sea salt aerosol (molar $\text{Cl}^-/\text{Fe(III)}=13$ ) + 20 ppb $\text{SO}_2$

The nebulizer was filled with ~50 ml of an iron-doped artificial seawater solution (see Table 1). 1.3043g  $\text{FeCl}_3$  (Riedel-de Haën, sublimate, ≥ 99 %) were dissolved in 100ml of the artificial seawater stock solution and afterwards 1:28 diluted to ~37 mmol  $\text{L}^{-1}$ . The injection time was 30 min. The time profile of the total aerosol concentration and the total aerosol surface is shown in Figure 32.

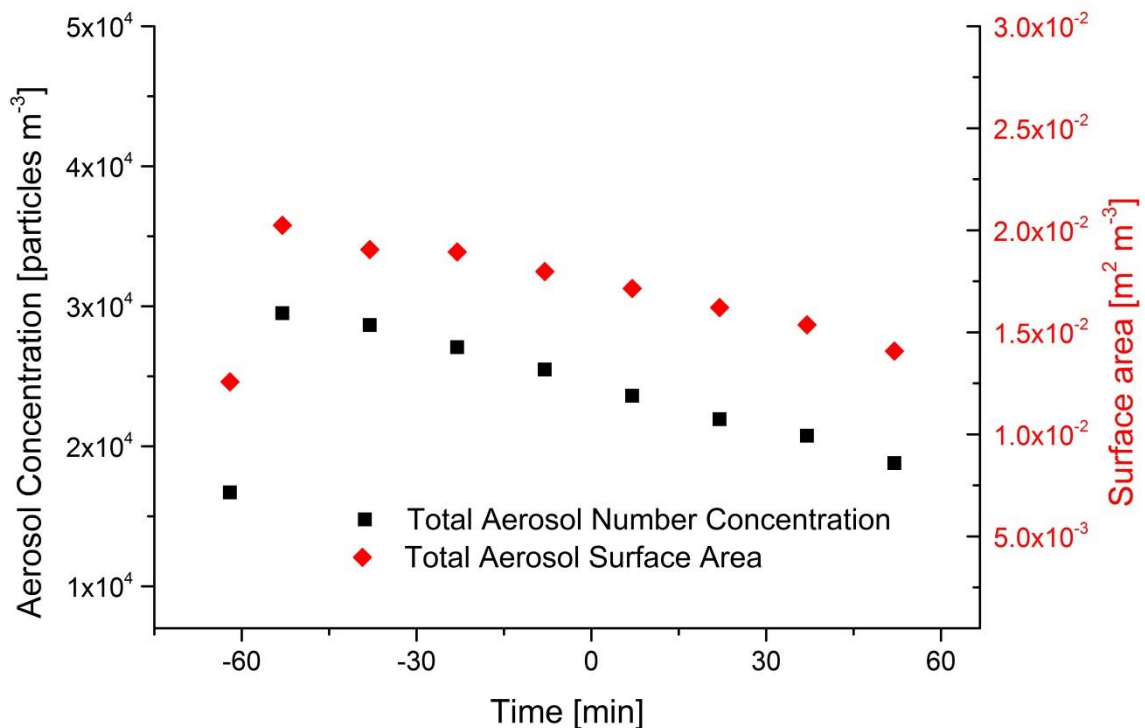
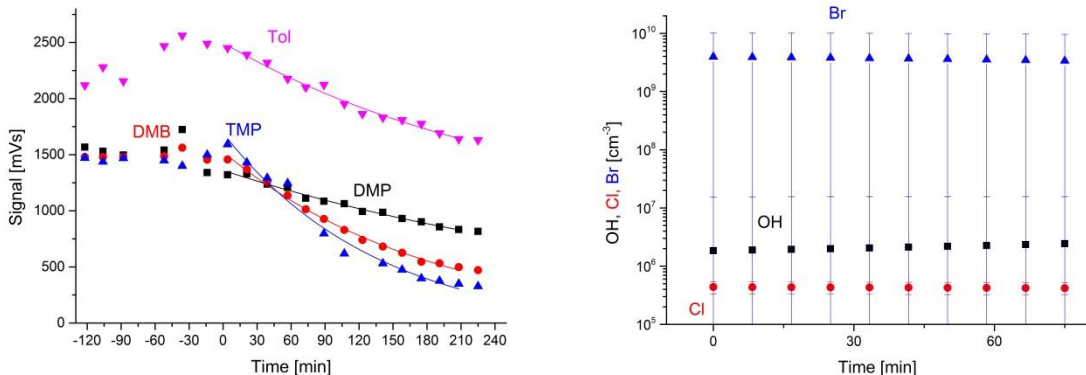


Figure 32: Time profiles of the total measured aerosol number concentration and the surface area for the experiment with iron-doped artificial sea salt aerosol ( $\text{Cl}^-/\text{Fe(III)}=13$ )+ $\text{SO}_2$ . At  $t= 0$  the irradiation starts. At  $t= -70$  min the aerosol injection starts.

The following amount of hydrocarbons was injected

- 50  $\mu\text{l}$  DMP
- 0.22  $\mu\text{l}$  PFH (inert standard)
- 0.22  $\mu\text{l}$  DMB
- 0.22  $\mu\text{l}$  TMP
- 0.22  $\mu\text{l}$  Tol

The dilution corrected time profiles of the injected hydrocarbons are shown in Figure 33 (left). The quasi-stationary concentrations of OH and Cl radicals (Figure 33, right) were derived from the functions fitted (shown in Table 13) to the measurement data. The concentration of OH radicals is between  $10^6$  and  $10^7 \text{ cm}^{-3}$ . The mean Cl concentration during the first hour was  $\sim 4.3 \cdot 10^5 \text{ cm}^{-3}$ . The evaluation also included Br atoms that were  $\sim 4 \cdot 10^9 \text{ cm}^{-3}$ .



**Figure 33:** HC measurements in the iron-doped artificial sea salt aerosol ( $\text{Cl}^-/\text{Fe(III)}=13$ ) + 20 ppb  $\text{SO}_2$  experiment including the applied fit functions (left) and the hence calculated concentrations of OH, Br and Cl radicals (right). The irradiation started at the time 0.

**Table 13:** Fitting functions for the iron-doped artificial sea salt aerosol ( $\text{Cl}^-/\text{Fe(III)}=13$ ) + 20 ppb  $\text{SO}_2$  experiment from Figure 33 to derive the concentrations of OH und Cl

Hydrocarbon	Fitting function /mVs
2,2-Dimethylpropane (DMP)	$253 + 1110e^{-t/19364s}$
2,2-Dimethylbutane (DMB)	$59 + 1472e^{-t/10062s}$
2,2,4-Trimethylpentane (TMP)	$101 + 1710e^{-t/6232s}$
Toluene	$935 + 1563e^{-t/15843s}$

### 3.14 Iron-doped artificial sea salt aerosol (molar $\text{Cl}^-/\text{Fe(III)}=13$ ) + 200 ppb $\text{SO}_2$

The nebulizer was filled with ~50 ml of an iron-doped artificial seawater solution (see Table 1). 1.3043g  $\text{FeCl}_3$  (Riedel-de Haën, sublimate, ≥ 99 %) were dissolved in 100ml of the artificial seawater stock solution and afterwards 1:28 diluted to ~37 mmol L<sup>-1</sup>. The injection time was 53 min. The time profile of the total aerosol concentration and the total aerosol surface cannot be shown since due to the flashovers only 3 measurements of the aerosol size distribution are available that show a particle number concentration of ~11 000 particles m<sup>-3</sup> and an aerosol surface of ~0.0931 m<sup>2</sup> m<sup>-3</sup> directly after injection.

The following amount of hydrocarbons was injected

- 80 µl DMP
- 0.3 µl PFH (inert standard)
- 0.3 µl DMB
- 0.3 µl TMP
- 0.3 µl Tol

The dilution corrected time profiles of the injected hydrocarbons are shown in Figure 34 (left). The

quasi-stationary concentrations of OH and Cl radicals (Figure 34, right) were derived from the functions fitted (shown in Table 14) to the measurement data. The concentration of OH radicals is between  $10^5$  and  $10^6 \text{ cm}^{-3}$ . The mean Cl concentration during the first hour was  $\sim 1.4 \cdot 10^5 \text{ cm}^{-3}$ . The evaluation also included Br atoms that were  $\sim 1 \cdot 10^9 \text{ cm}^{-3}$ .

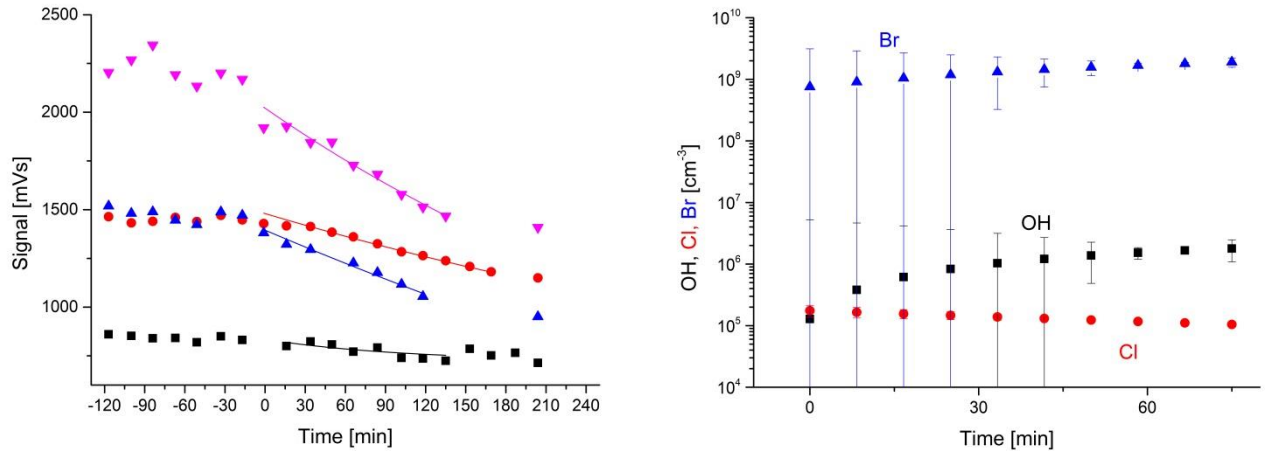


Figure 34: HC measurements in the iron-doped artificial sea salt aerosol ( $\text{Cl}^-/\text{Fe(III)}=13$ )+ 200 ppb  $\text{SO}_2$  experiment including the applied fit functions (left) and the hence calculated concentrations of OH, Br and Cl radicals (right). The irradiation started at the time 0.

Table 14: Fitting functions for the iron-doped artificial sea salt aerosol ( $\text{Cl}^-/\text{Fe(III)}=13$ )+ 200 ppb  $\text{SO}_2$  experiment from Figure 34 to derive the concentrations of OH und Cl

Hydrocarbon	Fitting function /mVs
2,2-Dimethylpropane (DMP)	$723 + 112e^{-t/6139s}$
2,2-Dimethylbutane (DMB)	$234 + 1246e^{-t/36720s}$
2,2,4-Trimethylpentane (TMP)	$-1255 + 2650e^{-t/54282s}$
Toluene	$2021e^{-t/25449s}$

### 3.15 Iron-doped artificial sea salt aerosol (molar Cl<sup>-</sup>/Fe(III)=101, acidified)

The nebulizer was filled with ~50 ml of an iron-doped artificial seawater solution (see Table 1). 0.1360g FeCl<sub>3</sub> (Merck) were dissolved in 100ml of the artificial seawater stock solution and afterwards 1:28 diluted to ~29 mmol L<sup>-1</sup>. After preparation, the pH was adjusted to 2.2 with 30 µl HCl solution (32%). The injection time was 45 min. The time profile of the total aerosol concentration and the total aerosol surface is shown in Figure 35.

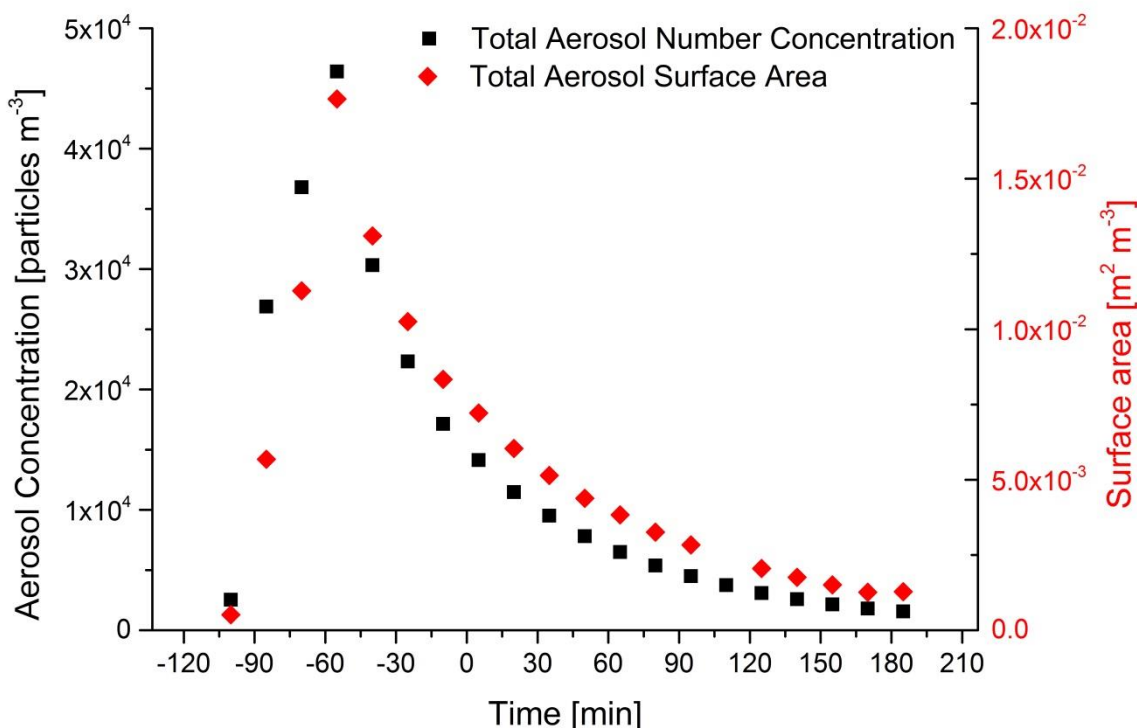
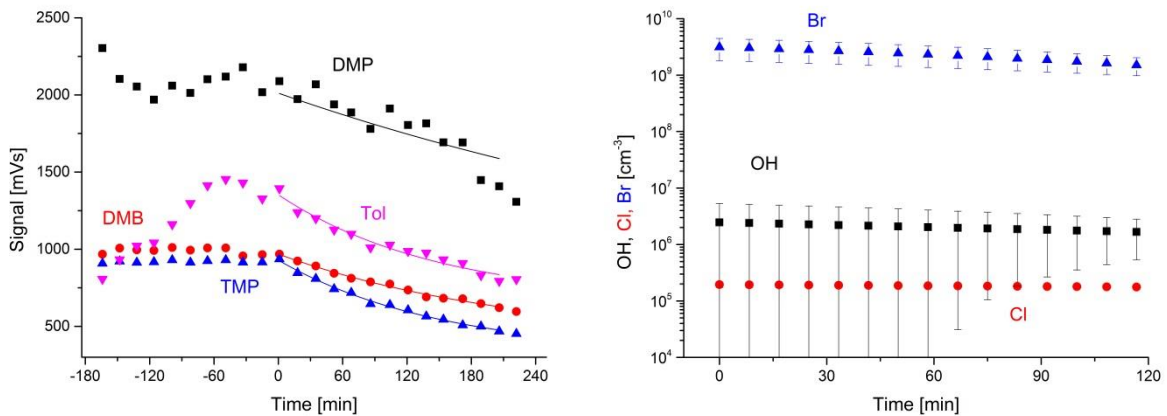


Figure 35: Time profiles of the total measured aerosol number concentration and the surface area for the experiment with iron-doped artificial sea salt aerosol and adjusted pH (Cl<sup>-</sup>/Fe(III)=101). At t= 0 the irradiation starts. At t= -105 min the aerosol injection starts.

The following amount of hydrocarbons was injected

- 70 µl DMP
- 0.2 µl PFH (inert standard)
- 0.2 µl DMB
- 0.2 µl TMP
- 0.2 µl Tol

The dilution corrected time profiles of the injected hydrocarbons are shown in Figure 36 (left). The quasi-stationary concentrations of OH and Cl radicals (Figure 36, right) were derived from the functions fitted (shown in Table 15) to the measurement data. The concentration of OH radicals is  $\sim 2.2 \cdot 10^6$  cm<sup>-3</sup>. The Cl atom concentration is relatively stable at  $\sim 1.9 \cdot 10^5$  cm<sup>-3</sup>. The evaluation also included Br atoms that were in the range of  $10^9$  -  $10^{10}$  cm<sup>-3</sup>.



**Figure 36:** HC measurements in the iron-doped artificial sea salt aerosol ( $\text{Cl}^-/\text{Fe(III)}=101$ , acidified) experiment including the applied fit functions (left) and the hence calculated concentrations of OH, Br and Cl radicals (right). The irradiation started at the time 0.

**Table 15:** Fitting functions for the iron-doped artificial sea salt aerosol ( $\text{Cl}^-/\text{Fe(III)}=101$ , acidified) experiment from Figure 36 to derive the concentrations of OH und Cl

Hydrocarbon	Fitting function /mVs
2,2-Dimethylpropane (DMP)	$574 + 1438e^{-t/35352s}$
2,2-Dimethylbutane (DMB)	$332 + 606e^{-t/15400s}$
2,2,4-Trimethylpentane (TMP)	$293 + 607e^{-t/9526s}$
Toluene	$642 + 671e^{-t/8955s}$

### 3.16 Iron-doped artificial sea salt aerosol (molar $\text{Cl}^-/\text{Fe(III)}=101$ ) + 20 ppb $\text{NO}_2$

The nebulizer was filled with ~50 ml of an iron-doped artificial seawater solution (see Table 1). 0.1360g  $\text{FeCl}_3$  (Merck) were dissolved in 100ml of the artificial seawater stock solution and afterwards 1:28 diluted to ~29 mmol L<sup>-1</sup>. The injection time was 32 min. The time profile of the total aerosol concentration and the total aerosol surface is shown in Figure 37.

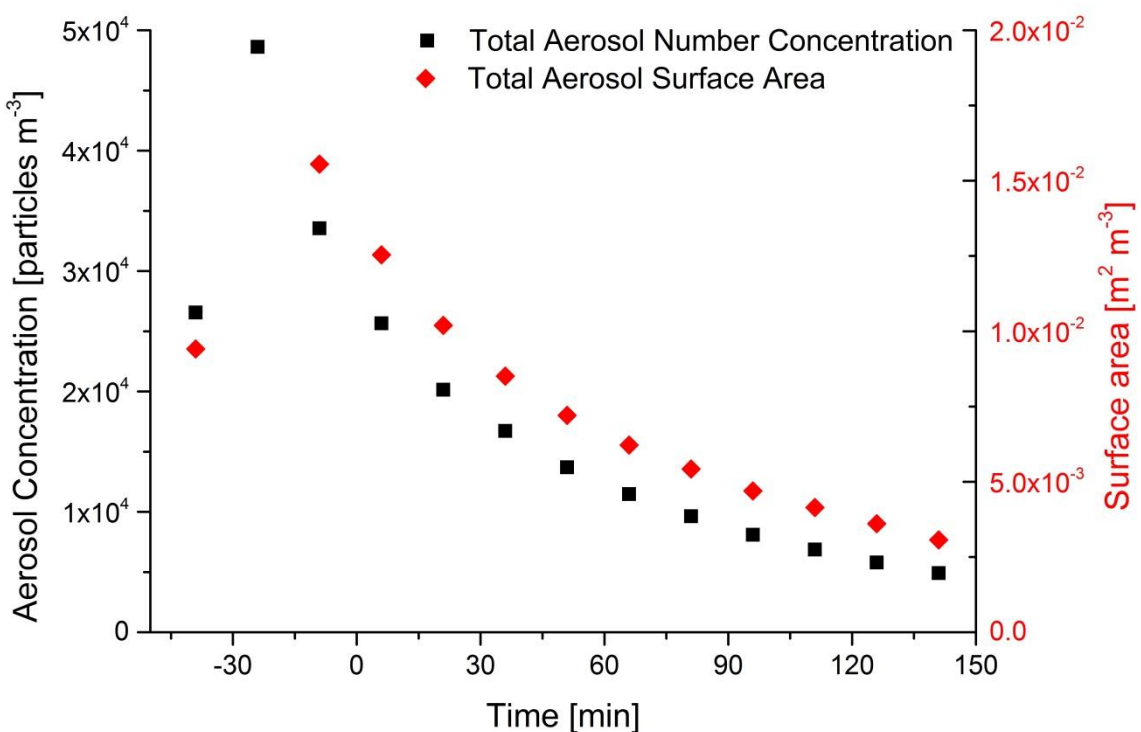
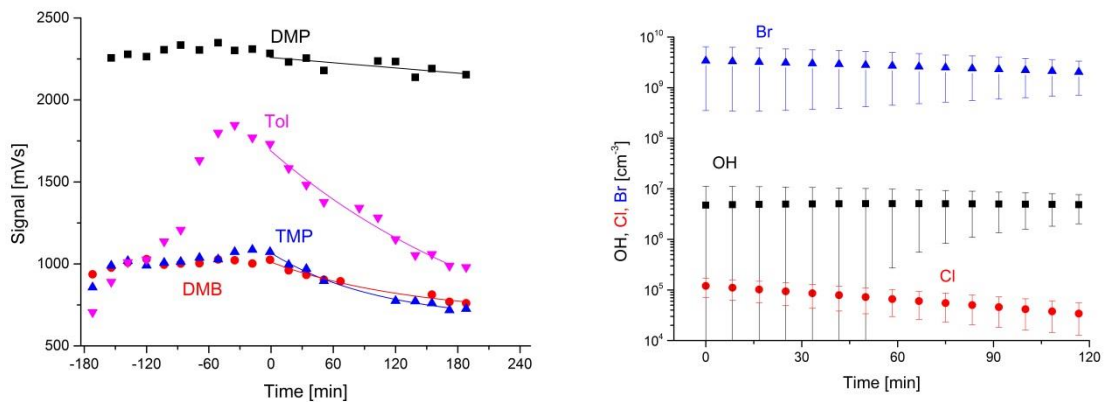


Figure 37: Time profiles of the total measured aerosol number concentration and the surface area for the experiment with iron-doped artificial sea salt aerosol ( $\text{Cl}^-/\text{Fe(III)}=101$ )+ $\text{NO}_2$ . At  $t=0$  the irradiation starts. At  $t=-50$  min the aerosol injection starts.

The following amount of hydrocarbons was injected

- 70  $\mu\text{l}$  DMP
- 0.2  $\mu\text{l}$  PFH (inert standard)
- 0.2  $\mu\text{l}$  DMB
- 0.2  $\mu\text{l}$  TMP
- 0.2  $\mu\text{l}$  Tol

The dilution corrected time profiles of the injected hydrocarbons are shown in Figure 38 (left). The quasi-stationary concentrations of radicals (Figure 38, right) were derived from the functions fitted (shown in Table 16) to the measurement data. The mean Cl concentration during the first hour was  $\sim 9.1 \cdot 10^5 \text{ cm}^{-3}$ . Mean Br and OH are  $\sim 3 \cdot 10^9 \text{ cm}^{-3}$  and  $\sim 5 \cdot 10^6 \text{ cm}^{-3}$ , respectively. At these  $\text{NO}_2$  levels, the halogen activation mechanisms as discussed in section 3.3 and 3.4 are responsible for the additional increase of Cl and Br atoms compared to the pure iron-induced Cl activation (see section 3.7).



**Figure 38:** HC measurements in the iron-doped artificial sea salt aerosol ( $\text{Cl}^-/\text{Fe(III)}=101$ ) + 20 ppb  $\text{NO}_2$  experiment including the applied fit functions (left) and the hence calculated concentrations of Cl radicals (right). The irradiation started at the time 0.

**Table 16:** Fitting functions for the iron-doped artificial sea salt aerosol ( $\text{Cl}^-/\text{Fe(III)}=101$ )+20 ppb  $\text{NO}_2$  experiment from Figure 38 to derive the concentrations of Cl, OH, Br

Hydrocarbon	Fitting function /mVs
2,2-Dimethylpropane (DMP)	$2164 + 111e^{-t/4767s}$
2,2-Dimethylbutane (DMB)	$689 + 321e^{-t/8059s}$
2,2,4-Trimethylpentane (TMP)	$658 + 410e^{-t/6112s}$
Toluene	$437 + 1255e^{-t/13060s}$

Figure 39 shows the time profiles of the monitored species and parameters during the experiment. During aerosol injection the RH increased up to 70 %. Moreover, the aerosol injection caused an  $\text{NO}_x$  and NO increase of 6 and 5 ppb respectively. After injecting 20 ppb  $\text{NO}_2$  and a waiting period of 49 min the light was turned. The presence of  $\text{NO}_2$  leads to a fast  $\text{O}_3$  formation when the light was turned on and induces additional halogen activation mechanisms as described before. The  $\text{NO}_x$  depletion is caused by  $\text{N}_2\text{O}_5$ ,  $\text{XNO}_3$  and  $\text{HNO}_3$  formation and uptake, as discussed for experiment 3.12 or in

section 4.

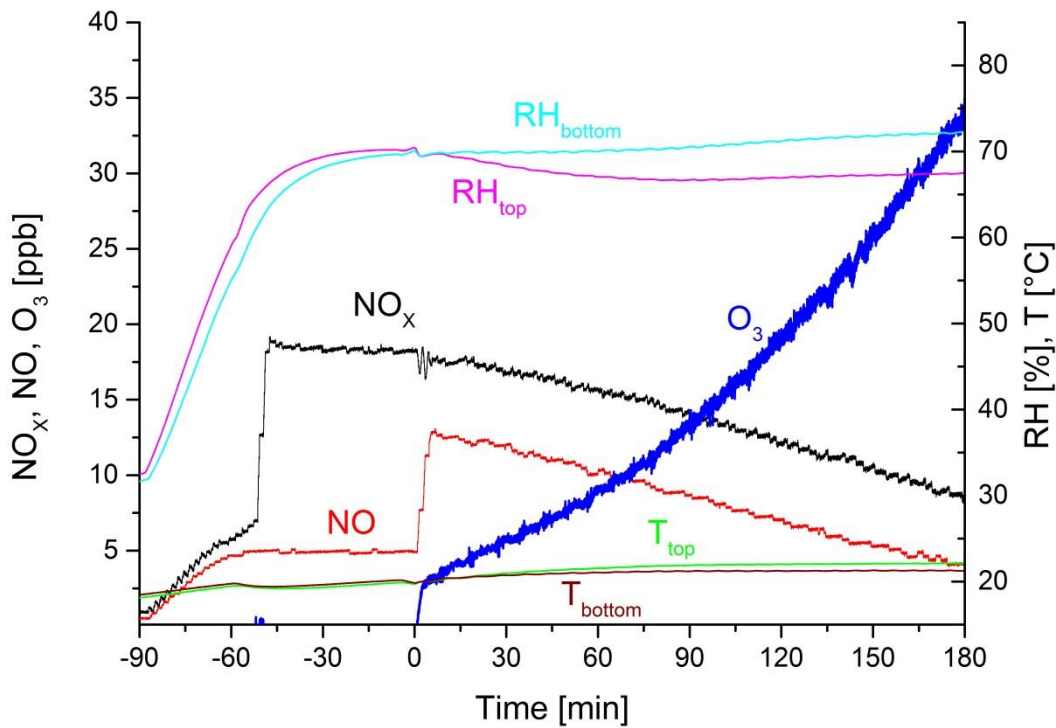


Figure 39: Time profiles of  $\text{NO}_x$ ,  $\text{NO}$ ,  $\text{O}_3$ , RH and T for the experiment with iron-doped artificial sea salt aerosols (molar  $\text{Cl}^-/\text{Fe(III)}=101$ ) + 20 ppb  $\text{NO}_2$  addition. The irradiation started at the time 0 and stopped at  $t= 195$  min. The aerosol injection caused an  $\text{NO}_x$  and  $\text{NO}$  increase of 6 and 5 ppb respectively

### 3.17 Iron-doped artificial sea salt aerosol (molar $\text{Cl}^-/\text{Fe(III)}=101$ , acidified) + 20 ppb $\text{NO}_2$

The nebulizer was filled with ~50 ml of an iron-doped artificial seawater solution (see Table 1). 0.1360g  $\text{FeCl}_3$  (Merck) were dissolved in 100ml of the artificial seawater stock solution and afterwards 1:28 diluted to ~29 mmol  $\text{L}^{-1}$ . After preparation, the pH was adjusted to 2.2 with 30  $\mu\text{l}$  HCl solution (32%). The injection time was 45 min. The time profile of the total aerosol concentration and the total aerosol surface is shown in Figure 40.

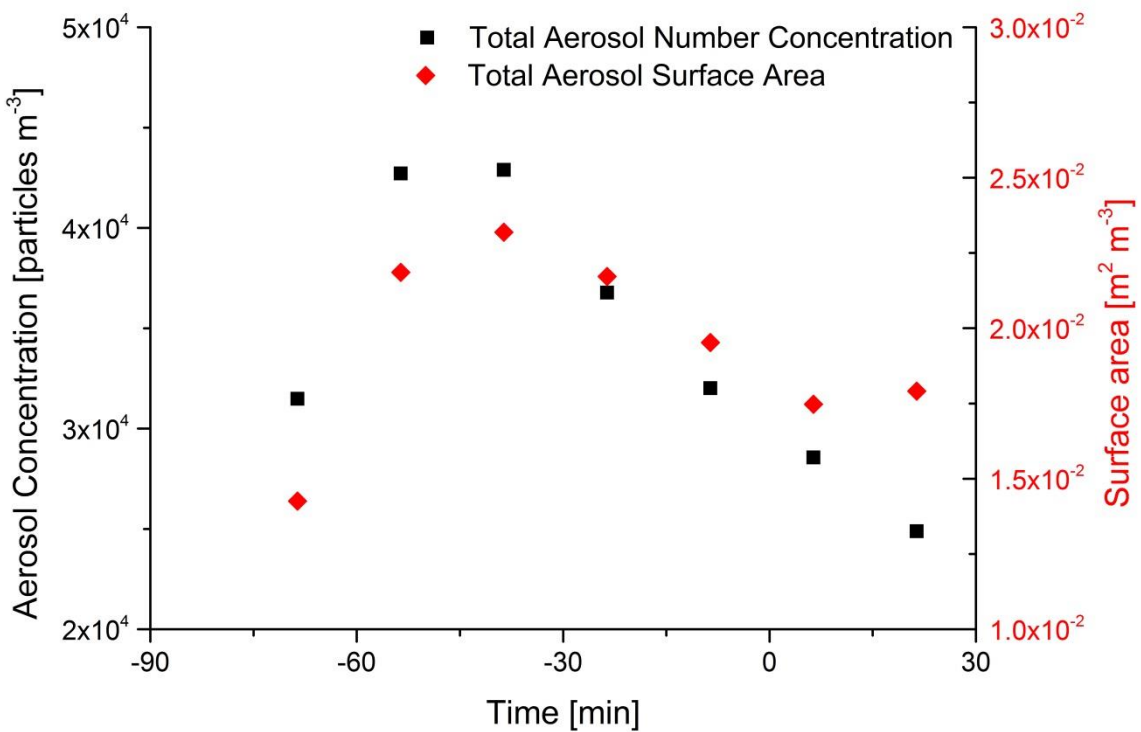
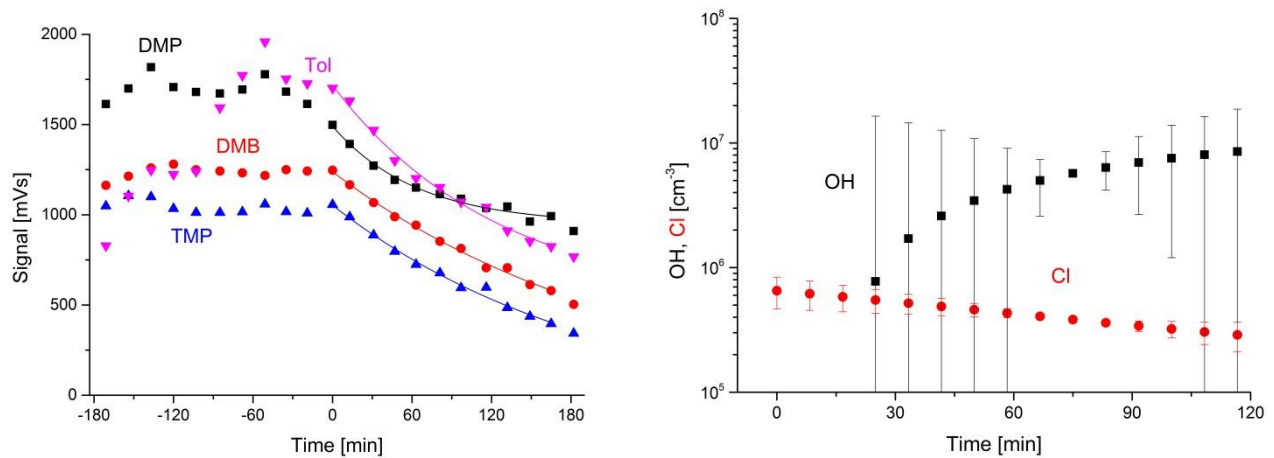


Figure 40: Time profiles of the total measured aerosol number concentration and the surface area for the experiment with iron-doped artificial sea salt aerosol ( $\text{Cl}^-/\text{Fe(III)}=101$ )+ $\text{NO}_2$ . At  $t=0$  the irradiation starts. At  $t=-70$  min the aerosol injection starts.

The following amount of hydrocarbons was injected

- 50  $\mu\text{l}$  DMP
- 0.2  $\mu\text{l}$  PFH (inert standard)
- 0.2  $\mu\text{l}$  DMB
- 0.2  $\mu\text{l}$  TMP
- 0.2  $\mu\text{l}$  Tol

The dilution corrected time profiles of the injected hydrocarbons are shown in Figure 41 (left). The quasi-stationary concentrations of radicals (Figure 41, right) were derived from the functions fitted (shown in Table 17) to the measurement data. The mean Cl concentration during the first hour was  $\sim 5.4 \cdot 10^5 \text{ cm}^{-3}$ . The mean OH is  $\sim 2.2 \cdot 10^6 \text{ cm}^{-3}$ . At these  $\text{NO}_2$  levels, the halogen activation mechanisms as discussed in section 3.3 and 3.4 are responsible for the additional increase of Cl and Br atoms compared to the pure iron-induced Cl activation (see section 3.7). Additionally, the low pH contributes to higher Cl concentrations (see Discussion).



**Figure 41:** HC measurements in the iron-doped artificial sea salt aerosol ( $\text{Cl}^-/\text{Fe(III)}=101$ , acidified) + 20 ppb  $\text{NO}_2$  experiment including the applied fit functions (left) and the hence calculated concentrations of Cl and OH radicals (right). The irradiation started at the time 0.

**Table 17: Fitting functions for the iron-doped artificial sea salt aerosol ( $\text{Cl}^-/\text{Fe(III)}=101$ )+20 ppb  $\text{NO}_2$  experiment from Figure 41 to derive the concentrations of Cl, OH, Br**

Hydrocarbon	Fitting function /mVs
2,2-Dimethylpropane (DMP)	$898 + 584e^{-t/4677s}$
2,2-Dimethylbutane (DMB)	$-275 + 1510e^{-t/17038s}$
2,2,4-Trimethylpentane (TMP)	$-206 + 1257e^{-t/13460s}$
Toluene	$462 + 1253e^{-t/7917s}$

Figure 42 shows the time profiles of the monitored species and parameters during the experiment. During aerosol injection the RH increased up to 70 %. Moreover, the injection caused an  $\text{NO}_x$  and NO increase of 3 and 2 ppb respectively. After injecting 20 ppb  $\text{NO}_2$  and a waiting period of 40 min the light was turned. The  $\text{O}_3$  concentration was not measured in this experiment since the ethylene gas was used up.

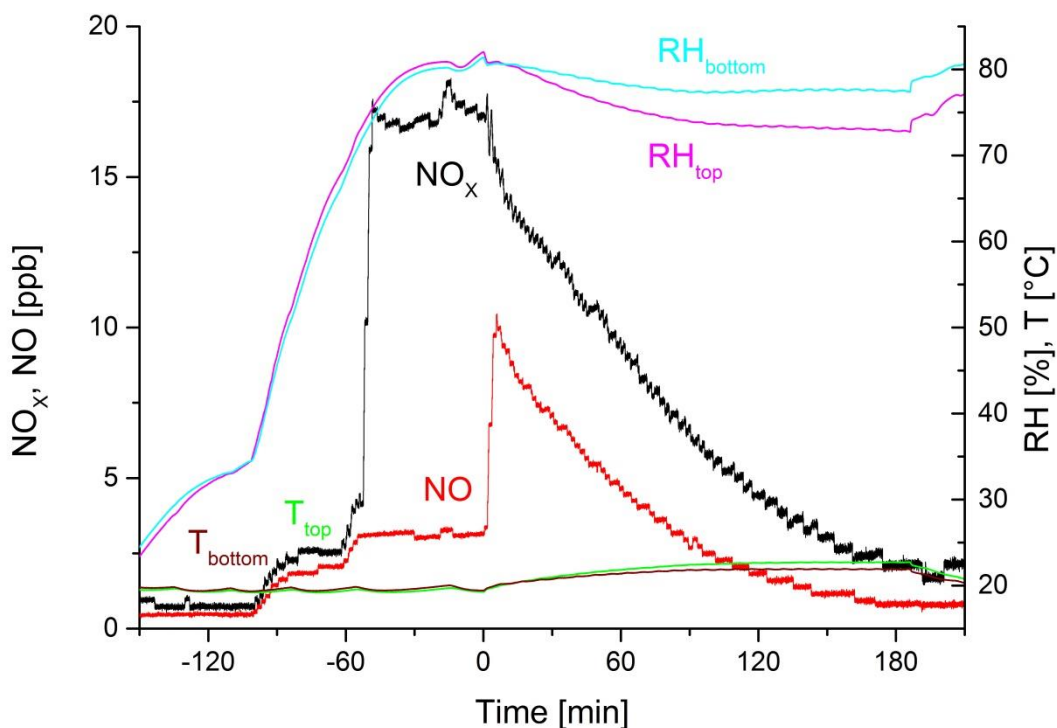


**Figure 42: Time profiles of  $\text{NO}_x$ ,  $\text{NO}$ , RH and  $T$  for the experiment with iron-doped artificial sea salt aerosols +  $\text{NO}_2$  addition. The irradiation started at the time  $t = 0$  and stopped at  $t = 190$  min. The  $\text{O}_3$  concentration was not measured in this experiment since the ethylene gas was used up.**

### 3.18 Sicotrans Orange doped artificial sea salt aerosol (molar $\text{Cl}^-/\text{Fe(III)}$ ~13)

The nebulizer was filled with ~50 ml of an artificial seawater solution (see Table 1) doped with Sicotrans Orange (BASF), where 5.044g Sicotrans Orange were stirred into 1 l of the artificial seawater stock solution with a scoop and afterwards 1:28 diluted to ~37 mmol L<sup>-1</sup>. The powder did not dissolve but rather formed a suspension with  $\text{Fe}_2\text{O}_3$  grains sinking to the bottom within 3-5 min. The injection time was 27 min. The time profile of the total aerosol concentration and the total aerosol surface is shown in Figure 43.

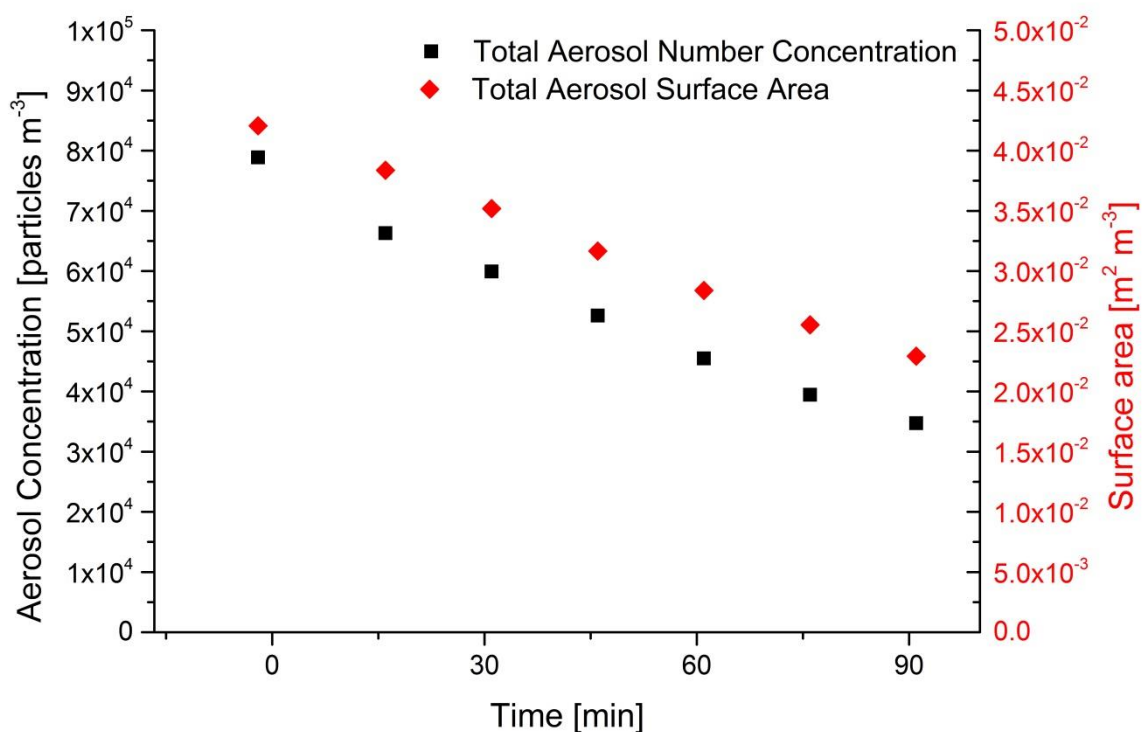


**Figure 43:** Time profiles of the total measured aerosol number concentration and the surface area for the experiment with artificial sea salt aerosol doped with Sicotrans Orange ( $\text{Cl}^-/\text{Fe(III)} \sim 13$ ). At  $t = 0$  the irradiation starts. At  $t = -90$  min the aerosol injection starts.

The following amount of hydrocarbons was injected

- 50  $\mu\text{l}$  DMP
- 0.12  $\mu\text{l}$  PFH (inert standard)
- 0.12  $\mu\text{l}$  DMB
- 0.12  $\mu\text{l}$  TMP
- 0.12  $\mu\text{l}$  Tol

The dilution corrected time profiles of the injected hydrocarbons are shown in Figure 44.

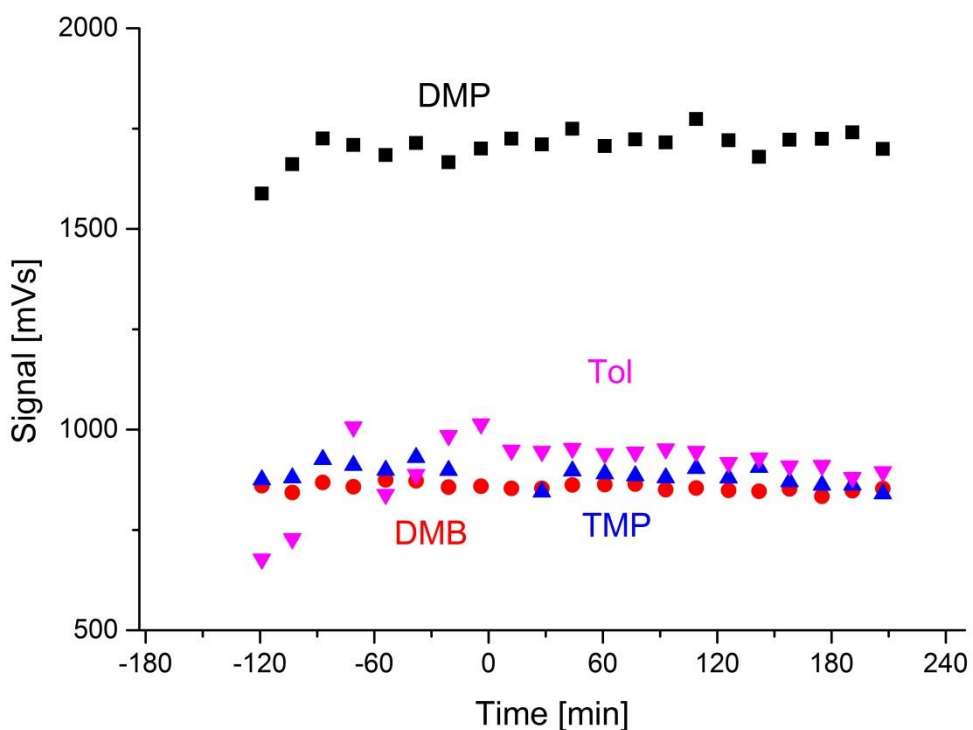


Figure 44: HC measurements during the experiment with artificial sea salt aerosol doped with Sicotrans Orange ( $\text{Cl}^-/\text{Fe(III)} \sim 13$ ). The irradiation started at the time 0.

Comparable to the blank analysis, taken over a period of 2 h, the HCs show no significant depletion upon irradiation, prohibiting a further evaluation of Cl and OH concentrations since no fit function can be applied.

### 3.19 Sicotrans Orange doped artificial sea salt aerosol (molar $\text{Cl}^-/\text{Fe(III)} \sim 13$ ), acidified

The nebulizer was filled with  $\sim 50$  ml of an artificial seawater solution (see Table 1) doped with Sicotrans Orange. 5.044g Sicotrans Orange (BASF) were stirred into 1 l of the artificial seawater stock solution and afterwards 1:28 diluted to  $\sim 37$  mmol L $^{-1}$ . The powder did not dissolve but rather formed a suspension. The pH was adjusted to 1-2 with 120  $\mu\text{l}$  HCl (32%). The injection time was 21 min. The time profile of the total aerosol concentration and the total aerosol surface is shown in Figure 45.

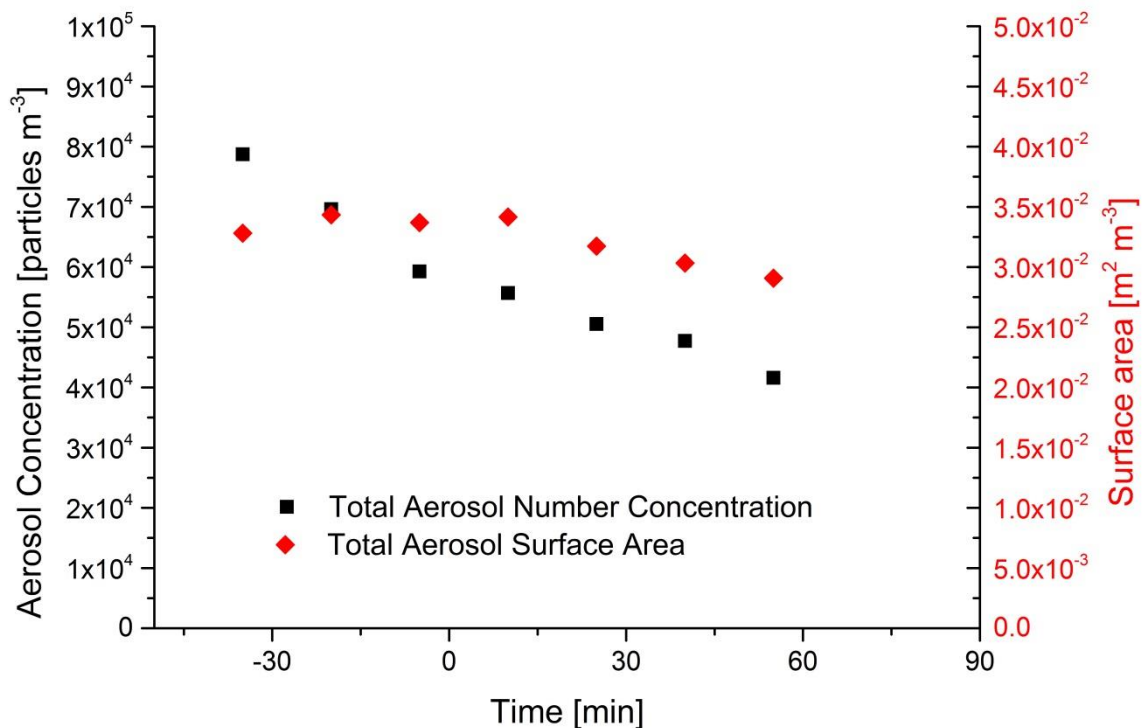
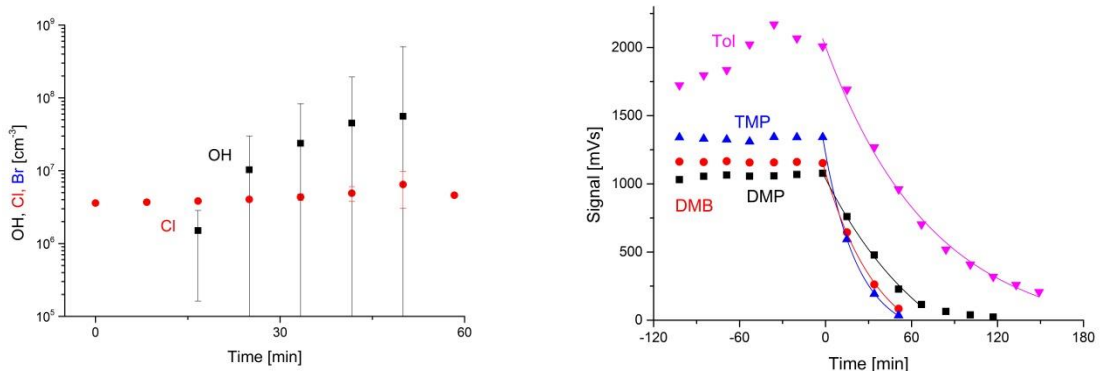


Figure 45: Time profiles of the total measured aerosol number concentration and the surface area for the experiment with artificial sea salt aerosol doped with Sicotrans Orange ( $\text{Cl}/\text{Fe(III)} \sim 13$ , acidified). At  $t = 0$  the irradiation starts. At  $t = -90$  min the aerosol injection starts.

The following amount of hydrocarbons was injected

- 50  $\mu\text{l}$  DMP
- 0.2  $\mu\text{l}$  PFH (inert standard)
- 0.2  $\mu\text{l}$  DMB
- 0.2  $\mu\text{l}$  TMP
- 0.2  $\mu\text{l}$  Tol

The dilution corrected time profiles of the injected hydrocarbons are shown in Figure 46 (left). The quasi-stationary concentrations of OH and Cl radicals (Figure 46, right) were derived from the functions fitted (shown in Table 18) to the measurement data. The concentrations of Br and OH radicals are error-prone due to the dominating depletion of the HCs by Cl atoms. Br atoms were not evaluable whereas OH radicals were in the range of  $10^6\text{-}10^7 \text{ cm}^{-3}$ . Cl atoms were very high concentrated with a more or less stable quasi-stationary concentration of  $\sim 4.4 \cdot 10^6 \text{ cm}^{-3}$ . The surprising high Cl concentration compared to the initial experiment with Sicotrans Orange can be explained by the pH adjustment. The pH between 1 and 2 in the solution causes also a very low pH in the generated aerosol and initiates dissolution processes of the iron oxide. Once dissolved in the aqueous phase, the low pH favors the formation of Fe-Cl complexes as a precursor of Cl production in the gas phase (see Introduction or e.g. Sholkovitz *et al.*, 2012).



**Figure 46:** HC measurements during the experiment with artificial sea salt aerosol doped with Sicotrans Orange ( $\text{Cl}^-/\text{Fe(III)} \sim 13$ , acidified) including the applied fit functions (left) and the hence calculated concentrations of OH and Cl radicals (right). The irradiation started at the time  $t=0$ .

**Table 18:** Fitting functions for the HC profiles of the experiment with artificial sea salt aerosol doped with Sicotrans Orange ( $\text{Cl}^-/\text{Fe(III)} \sim 13$ , acidified) from Figure 46 to derive the concentrations of OH und Cl

Hydrocarbon	Fitting function / mVs
2,2-Dimethylpropane (DMP)	$-90 + 1139e^{-t/2651s}$
2,2-Dimethylbutane (DMB)	$-265 + 1346e^{-t/2237s}$
2,2,4-Trimethylpentane (TMP)	$-124 + 1348e^{-t/1421s}$
Toluene	$-112 + 2118e^{-t/4445s}$

### 3.20 Sicotrans Orange doped artificial sea salt aerosol (molar $\text{Cl}^-/\text{Fe(III)} \sim 13$ ), 5 times frozen and thawed

The nebulizer was filled with ~50 ml of an artificial seawater solution (see Table 1) doped with Sicotrans Orange. 5.044g Sicotrans Orange (BASF) were stirred in 1 l of the artificial seawater stock solution and afterwards 1:28 diluted to ~37 mmol L<sup>-1</sup>. The powder did not dissolve but rather formed a suspension. The solution was 5 times frozen at -20°C for 1-3 hours and thawed at room temperature.

The aerosol injection time was 23 min. The time profile of the total aerosol concentration and the total aerosol surface is shown in Figure 47.

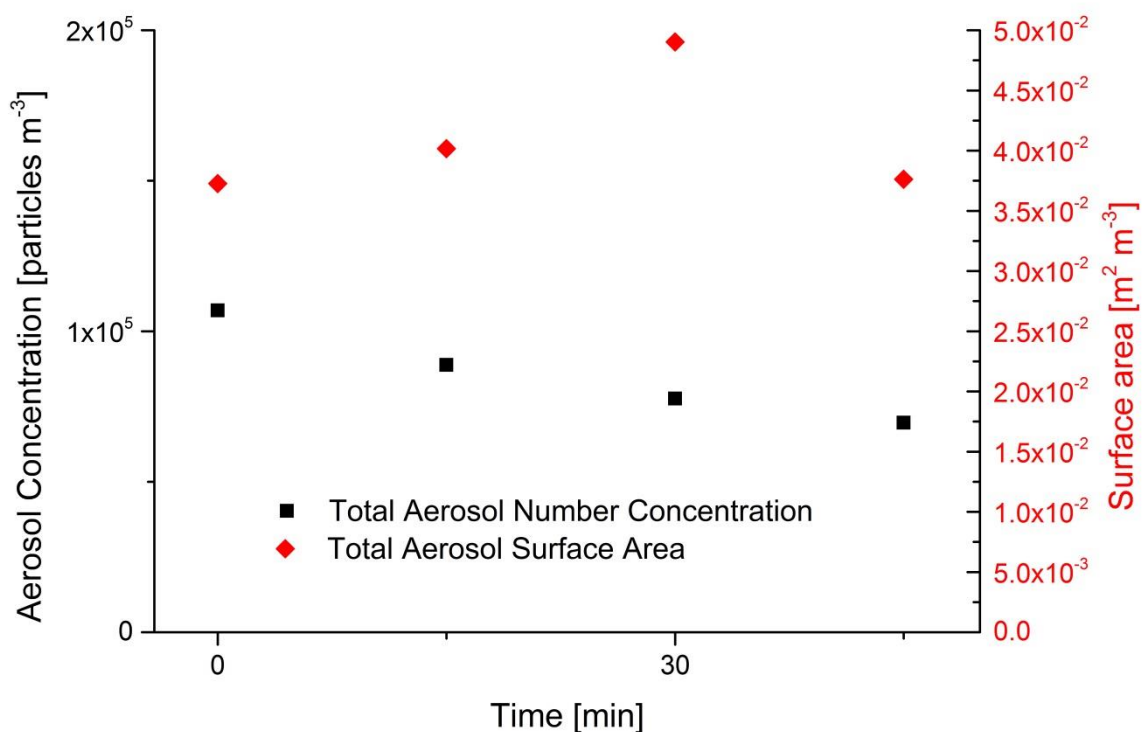


Figure 47: Time profiles of the total measured aerosol number concentration and the surface area for the experiment with artificial sea salt aerosol doped with Sicotrans Orange ( $\text{Cl}^-/\text{Fe(III)} \sim 13$ ), 5 times frozen and thawed. At  $t = 0$  the irradiation starts. At  $t = -75$  min the aerosol injection starts.

The following amount of hydrocarbons was injected

- 50  $\mu\text{l}$  DMP
- 0.2  $\mu\text{l}$  PFH (inert standard)
- 0.2  $\mu\text{l}$  DMB
- 0.2  $\mu\text{l}$  TMP
- 0.2  $\mu\text{l}$  Tol

The dilution corrected time profiles of the injected hydrocarbons are shown in Figure 48. The chamber is irradiated in two phases. The first (from  $t = -98$  min to  $t = -51$  min) to check for contamination and the second (from  $t = 0$  min to  $t = 130$  min) after the chamber was loaded with aerosol.

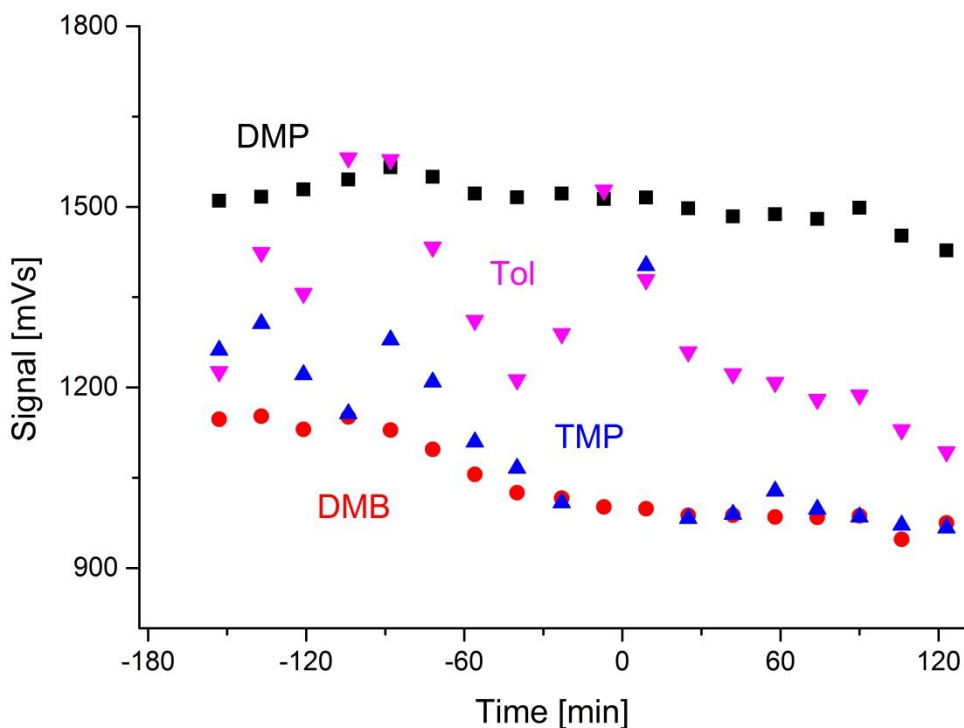


Figure 48: HC measurements during the experiment with artificial sea salt aerosol doped with Sicotrans Orange ( $\text{Cl}^-/\text{Fe(III)} \sim 13$ ), 5 times frozen and thawed. The first irradiation started at the time  $t = -98$  to  $t = -51$  to check for contamination of the previous experiment. The second irradiation phase was from  $t = 0$  to  $t = 130$  min. The aerosol was injected from  $t = -26$  min to  $t = -3$  min.

In comparison to the blank experiments, the HCs show no significant depletion upon starting the solar simulator, prohibiting a further evaluation of Cl and OH concentrations since no fit function can be applied. Even if a slight decrease in the HC time profiles is observed it is not significant enough to apply a fit function (y-axis suppresses 0). Moreover the slight decrease is most probably caused by contamination of experiment 3.19 since it is observable without aerosol injection during the first irradiation phase. This indicates that the freezing process does not significantly contribute to the iron oxide dissolution.

## 4 Summary and Discussion (most parts adapted from Wittmer et al., 2015)

Most parts of this summary and discussion section are word for word adapted from Wittmer et al. (2015). More details can be found therein. The experiments and the corresponding radical production rates and total productions are summarized in Table 19. As expected, the Cl production increases with increasing Fe(III) fraction in the aerosol. “A slightly higher Cl production of the pure NaCl-Fe(III) mixture was observed, that was probably caused by the speciation chemistry (as photolabile Fe(III)-Cl complexes can form easier in the absence of competing ions). Considering the diluted stock solutions, the pH was between 1.9 and 2.2 for both experiments. The buffer effect of the added bicarbonate ( $0.2 \text{ g L}^{-1}$ ) in the artificial sea water is very low, considering the high amount of  $\text{FeCl}_3$  added ( $13 \text{ g L}^{-1}$ ). Though the radical clock method is also able to quantify Br and OH, the depletion of hydrocarbons was dominated by Cl with its much higher reaction rate constants (Table 2) which prohibits significant detections of Br and OH (in most cases) that were close to the detection limit ( $\text{Br} \sim 10^9 \text{ molecules cm}^{-3}$ ;  $\text{OH} \sim 10^6 \text{ molecules cm}^{-3}$ ). The Cl production rates and the corresponding total production are shown in Figure 49.

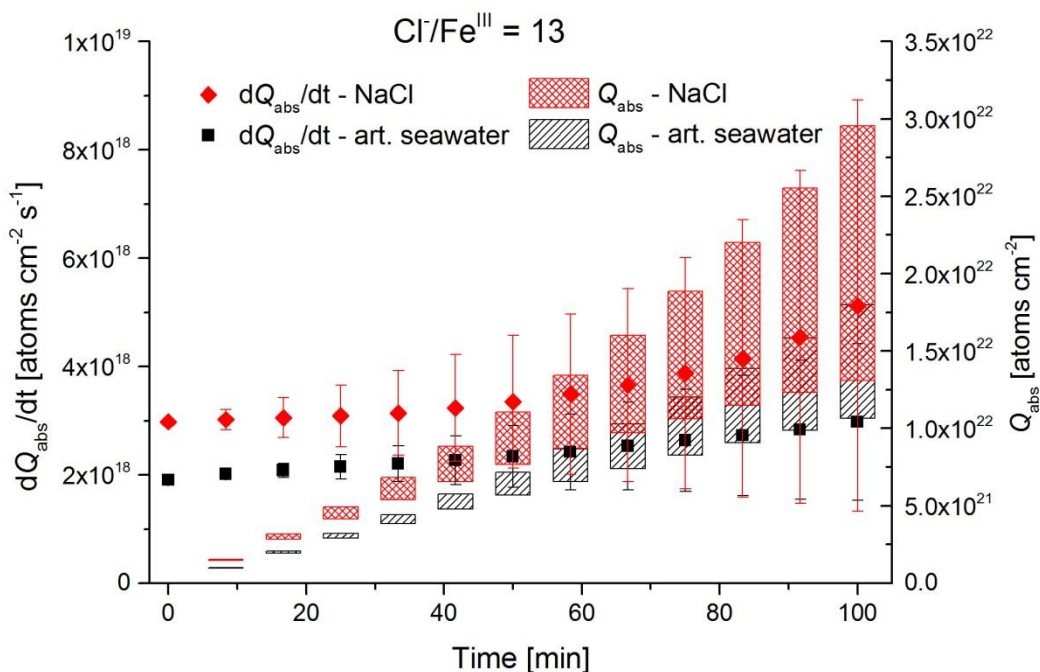
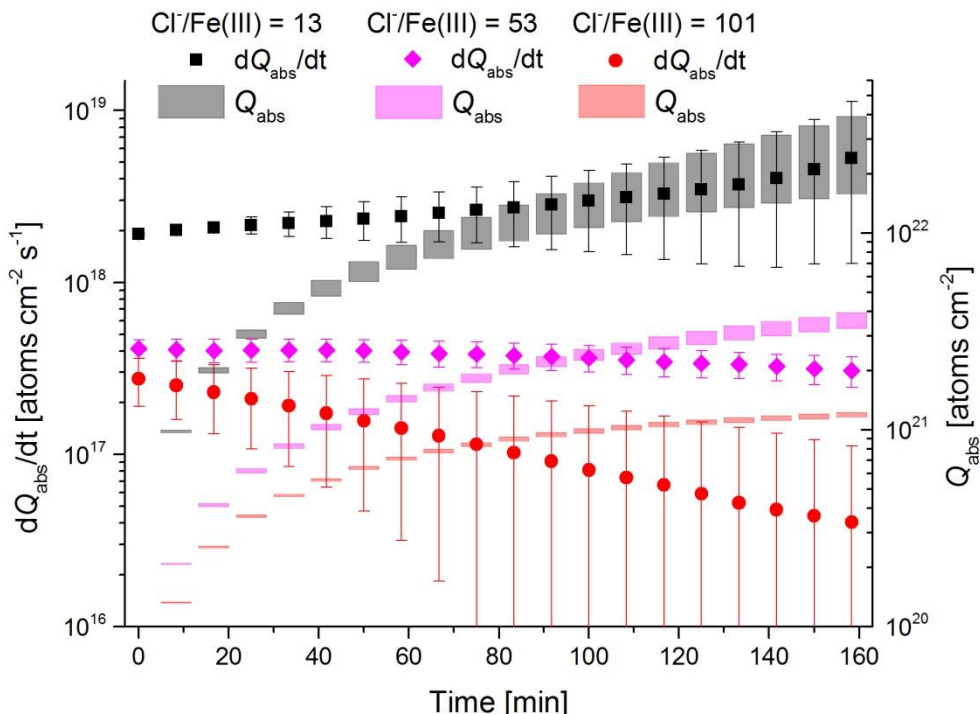


Figure 49. Absolute gaseous mean Cl production rate ( $dQ_{\text{abs}}/dt$ ) [ $\text{atoms cm}^{-2} \text{s}^{-1}$ ] and time integrated total minimum and maximum Cl production  $Q_{\text{abs}}$  [ $\text{atoms cm}^{-2}$ ] per  $\text{cm}^2$  of aerosol surface during the experiments with Fe(III)-doped artificial seawater and NaCl with  $\text{Cl}^-/\text{Fe}^{\text{III}} = 13$  respectively. The error bars for  $dQ_{\text{abs}}/dt$  include the minimum and maximum production rates and the respective statistical uncertainty. Adapted from Wittmer et al., 2015.

In order to determine the dependence of the chlorine activation on the  $\text{Cl}^-/\text{Fe}(\text{III})$  ratio in the aerosol, a series of experiments with a  $\text{Cl}^-/\text{Fe}(\text{III})$  ratio of 13 (i), 53 (ii), 101 (iii), 955 (iv), and a blank without added iron (v) was conducted. Whereas no significant Cl concentration was detected for run (iv) and (v), (iii) resulted in a total Cl production of  $(0.9-1.0) \cdot 10^{21} \text{ atoms cm}^{-2}$ , run (ii) of  $(2.3-2.6) \cdot 10^{21} \text{ atoms cm}^{-2}$  and run (i) of  $(1.1-1.8) \cdot 10^{22} \text{ atoms cm}^{-2}$  in the first 100 min (Figure 50). This demonstrates a continuous increase in produced Cl with increasing fraction of Fe(III) in the salt. A 1.9 times higher

fraction of Fe(III) results in a 2-3 times higher Cl production (comparing (iii) and (ii)), and 4.1 times more Fe(III) results in a 5-7 times higher Cl production (comparing (ii) and (i)). The higher amount of added  $\text{FeCl}_3$  cannot only explain the disproportionately higher Cl activation. In fact, the shift in the pH by adding 10 times more  $\text{FeCl}_3$  ( $\text{pH } 4 \rightarrow 2$ ) is in addition responsible for a higher fraction of photo-sensitive Fe(III)-Cl complexes. A slight decrease was observed for (iii) indicating an exhaustion of the Cl source, whereas samples (i) and (ii) result in a stable Cl production rate.

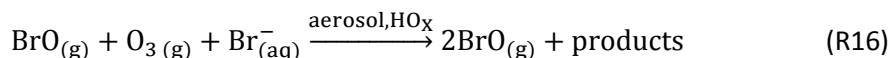


**Figure 50.** Absolute gaseous mean Cl production rate ( $dQ_{\text{abs}}/dt$ ) [ $\text{atoms cm}^{-2} \text{s}^{-1}$ ] and time integrated total minimum and maximum Cl production  $Q_{\text{abs}}$  [ $\text{atoms cm}^{-2}$ ] per  $\text{cm}^2$  of aerosol surface during the experiments with Fe(III)-doped artificial seawater at various Fe(III) concentrations:  $\text{Cl}'/\text{Fe(III)} = 13$  (black), 53 (magenta), 101 (red). Adapted from Wittmer *et al.*, 2015.

The presence of  $\text{NO}_2$  (~20 ppb) or  $\text{O}_3$  (630 ppb) in the gas phase additionally increased the Fe(III)-induced chloride activation to  $\sim 7 \cdot 10^{18}$  atoms  $\text{cm}^{-2} \text{s}^{-1}$  and  $\sim 9 \cdot 10^{18}$  atoms  $\text{cm}^{-2} \text{s}^{-1}$ , respectively. The Cl production significantly increased when  $\text{O}_3$  or/and Fe(III) were involved, whereas the blank experiment with iron free artificial sea salt and 20 ppb  $\text{NO}_2$  only resulted very low Cl production rates. “This indicates that the formation of  $\text{XNO}_3$  ( $\text{X} = \text{Cl}, \text{Br}$ ) via  $\text{XO}$  (R13, R14), or  $\text{HNO}_3$  via  $\text{OH}$  (R15) and the subsequent uptake on the aerosol may be relevant for the increase of the Fe(III)-induced chloride activation when  $\text{NO}_2$  is involved and the observed loss of  $\text{NO}_x$  (Finlayson-Pitts, 2003).

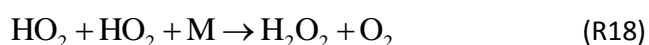


The uptake of  $\text{HNO}_3$  leads to an acidification of the aerosol and contributes to the re-oxidation of Fe(II) to Fe(III) via photolysis and  $\text{OH}^-$  formation in the aqueous phase (*Vione et al.*, 2005) and thus is potentially responsible for the enhanced gaseous Cl production, according to the mechanisms described in section 1. After acidification, the uptake of  $\text{HNO}_3$  leads to acid displacement with a subsequent release of HCl, (*Martens et al.*, 1973; *Haan and Finlayson-Pitts*, 1997; *Saul et al.*, 2006) whose reaction with OH is supposed to be a main Cl-atom source in the marine troposphere (*Behnke et al.*, 1995). In general, a low pH eases the release of HCl and other gaseous Cl precursors. (*Brimblecombe and Clegg*, 1988; *Keene et al.*, 1998; *Keene and Savoie*, 1998; *Bleicher et al.*, 2014) E.g. Keene and Savoie determined a gaseous HCl mixing ratio in the range of 0.1 ppb, and Keene et al. modeled HCl outgassing of 1 ppb  $\text{d}^{-1}$  for acidified sea salt (pH 3). Transferred to our conditions with typical OH concentrations of  $10^6$ - $10^7$  molecules  $\text{cm}^{-3}$  and a much higher LWC, this leads to gaseous Cl production rates in the range of  $10^9$  –  $10^{10}$  atoms  $\text{cm}^{-3} \text{ h}^{-1}$  and thus potentially contributes less than 10% to the observed Cl production. This accounts also for the HCl formation caused by the hydrogen abstraction during the consumption of the injected  $\text{HC}_i$  by Cl atoms. Furthermore, *Zetzsch and Behnke*, 1993 investigated the photochemical Cl production rates from 200-500 ppb  $\text{O}_3$  and 300 ppb HCl in the presence of NaCl,  $\text{Fe}_2\text{O}_3$  and  $\text{SiO}_2$  aerosol. They concluded that the heterogeneous  $\text{Cl}^-$  activation exceeds the Cl source by the gas-phase reaction of OH and HCl by far. Several effects were observed in the experiment where 620 ppb  $\text{O}_3$  was added (Figure 28). The Cl production rate and total Cl production are clearly above the values obtained in zero air and are similar to the  $\text{NO}_x$  experiment. On the other hand, the reactivity of  $\text{O}_3$  towards Cl ( $\sim 180 \text{ s}^{-1}$ ) is comparable to the total reactivity of the injected  $\text{HC}_i$  ( $\sim 200 \text{ s}^{-1}$ ) and not considered in the calculation of the total production Q, as it does not represent a final sink but rather initiates a reaction cycle via  $\text{HO}_2$  and HOCl where finally  $\text{Cl}_2$  is produced (*Pechtl and Glasow*, 2007; *Faxon and Allen*, 2013). In addition, *Sadanaga et al.*, 2001 observed enhanced  $\text{O}_3$  uptake rates in the presence of water-soluble Fe(III) in synthetic sea salt without irradiation. During the short dark period, an  $\text{O}_3$  depletion was hardly detectable, whereas we observed a  $\sim 4$  times lower  $\text{O}_3$  lifetime for the experiment with added Fe(III) ( $\sim 10^4 \text{ s}$ ) compared the pure artificial sea salt sample ( $\sim 4 \cdot 10^4$ ). This difference possibly explains the much higher Cl and Br production, at the same level of quasi-stationary OH concentrations ( $\sim 10^7$  molecules  $\text{cm}^{-3}$ ) for both experiments. Concerning the Br production, the quasi-stationary Br concentration was again on the order of  $10^9$  atoms  $\text{cm}^{-3}$  (close to the detection limit) and resulted in  $Q_{\text{abs}}$  values of  $(1-3) \cdot 10^{21}$  atoms  $\text{cm}^{-2} \text{ h}^{-1}$  for the iron-free and  $(3-8) \cdot 10^{21}$  atoms  $\text{cm}^{-2} \text{ h}^{-1}$  for the iron-doped sea salt. The enhanced Cl production in the iron-free experiments indicates that we observed an  $\text{O}_3$  induced Cl and Br production, that increases with decreasing pH (addition of Fe(III)) and contributes markedly to the enhanced iron-induced activation. Several mechanisms come into consideration for the observed effects. At these  $\text{O}_3$  levels, a main mechanism (that is responsible for the high Cl and Br production and the fast  $\text{O}_3$  depletion) is the so called “Bromine Explosion” (*Hausmann and Platt*, 1994) with the net reaction:



and the associated formation of OCIO and ClO (*Buxmann et al.*, 2012). However, it does not sufficiently explain the increase in production rates from  $\sim 2 \cdot 10^{18}$  atoms  $\text{cm}^{-2} \text{ s}^{-1}$  to  $\sim 10^{19}$  atoms  $\text{cm}^{-2} \text{ s}^{-1}$  with  $\text{O}_3$  addition when Fe(III) is involved, as the pH (when <5) is supposed to have no large effect on the mechanism (*Fickert et al.*, 1999), and the additional Cl production rate (when estimated from the iron-free experiment) is  $\sim 10^{18}$  atoms  $\text{cm}^{-2} \text{ s}^{-1}$ .

A further approach is the enhanced formation of  $\text{H}_2\text{O}_2$  in the gas phase (R17, R18),



that enters the aqueous phase rapidly and oxidizes Fe(II) back to Fe(III) and is able to form HOCl<sup>-</sup> or HOBr<sup>-</sup> which further dissociate and finally form Cl<sub>2</sub> or Br<sub>2</sub> (Oum et al., 1998).

*Knipping et al.*, 2000 even report a direct uptake of OH and subsequent Cl<sub>2</sub> release from NaCl aerosols. Furthermore, NO<sub>x</sub> (3-5 ppb are present after aerosol injection) forms N<sub>2</sub>O<sub>5</sub> during the dark phase, indicated by the loss of NO<sub>x</sub> when O<sub>3</sub> is injected (Figure 16 and 28), and thus leads to HNO<sub>3</sub> formation in the aqueous phase with similar consequences as described above. Moreover, the uptake of N<sub>2</sub>O<sub>5</sub> activates X<sup>-</sup> by releasing XNO<sub>2</sub> (*Finlayson-Pitts et al.*, 1989; *Behnke et al.*, 1997; *Thornton et al.*, 2010; *Bleicher et al.*, 2014) or even X<sub>2</sub> at acidic pH (<2), (*Roberts et al.*, 2008) which is realistic for the iron doped sea-salt aerosol.

In contrast to the reinforcing effects of NO<sub>x</sub> and O<sub>3</sub>, the situation changes with SO<sub>2</sub>. Two experiments were conducted with SO<sub>2</sub> concentrations of ~20 and ~200 ppb and a waiting period of 45 min before turning the solar simulator on. Similar to the impact of sulfate in a salt pan (*Wittmer et al.*, 2014), SO<sub>2</sub> inhibited the Cl production, as slightly lower dQ<sub>abs</sub>/dt and Q<sub>abs</sub> were observed. Several studies already examined the role and the uptake of SO<sub>2</sub> in combination with Fe(III) and Fe(II) for seawater. E.g. *Hoppel et al.*, 2001 report an uptake of 0.21-1.2 mmol L<sup>-1</sup> of nebulized seawater, which is in a similar range as the sulfate concentration of 1 mmol L<sup>-1</sup> in the artificial seawater stock solution (that is nebulized in our case). However, we used a 29 times diluted stock solution to obtain size distributions with a maximum diameter of 400-450 nm. Additionally, the dissolution of SO<sub>2</sub> depends on further dissociation reactions in the aqueous phase that depend on pH, temperature and ion content (*Gebel et al.*, 2000). Therefore, the uptake rate of Hoppel et al. is only transferable with caution, but considering the less concentrated stock solution it should only be a small amount of SO<sub>2</sub> that dissolves in the aqueous phase of the aerosol, mainly in the form of bisulfite (HSO<sub>3</sub><sup>-</sup>) regarding the pH range (2-6) of our samples. Especially at a low pH, where a high portion of dissolved Fe<sup>3+</sup> is available, the oxidation of sulfite to sulfate is catalyzed by Fe<sup>3+</sup> (*Zhang and Millero*, 1991; *Novič et al.*, 1996; *Manoj et al.*, 2008). Moreover, a significant oxidation path is the reaction of sulfite with HOCl and HOBr, both of which can intervene in the autocatalytic halogen release. Although sulfate can strongly inhibit the halogen activation, the impact of the freshly dissolved and oxidized SO<sub>2</sub> is probably very low with respect to the amount of sulfur that is already present in the artificial sea salt (*Troy and Margerum*, 1991; *Vogt et al.*, 1996). A further influence of SO<sub>2</sub> is observed, concerning the quasi-stationary OH concentrations that are close to the detection limit of 10<sup>6</sup> molecules cm<sup>-3</sup> for both experiments, due to the oxidation of SO<sub>2</sub> in the gas phase (SO<sub>2</sub>+OH→HOSO<sub>2</sub>; k = 1.3·10<sup>-12</sup> cm<sup>3</sup> molecules<sup>-1</sup>s<sup>-1</sup>) (*Atkinson et al.*, 2004) that competes with the Cl production via HCl + OH (k = 7.8·10<sup>-13</sup> cm<sup>3</sup> molecules<sup>-1</sup>s<sup>-1</sup>) (*Atkinson et al.*, 2007). Therefore, a slightly lower Cl production is observed for the SO<sub>2</sub> experiments. In the extreme case of 200 ppb, the Cl production decreases to ~70 % of the SO<sub>2</sub>-free experiment.

**Table 19. Molar Cl<sup>-</sup>/Fe(III) ratio, pH of the diluted, nebulized stock solution, gas phase composition within the smog chamber, total initial reactivity of the HCs in the chamber against Cl and Br, total aerosol surface measured directly after injection, quasi-stationary Cl<sub>qs</sub>, Br<sub>qs</sub>, and OH<sub>qs</sub> concentrations during irradiation during the 1<sup>st</sup> hour, and resulting total Cl and Br production per cm<sup>2</sup> aerosol surface. Adapted and modified from Wittmer et al., 2015.**

Cl <sup>-</sup> /Fe <sup>3+</sup>	pH of diluted stock solution	Gas phase	Initial Cl / OH / Br reactivity (s <sup>-1</sup> )	Initial aerosol surface area (10 <sup>-2</sup> ·m <sup>2</sup> m <sup>-3</sup> )	Cl <sub>qs</sub> / OH <sub>qs</sub> / Br <sub>qs</sub> concentration (10 <sup>5</sup> / 10 <sup>6</sup> / 10 <sup>9</sup> radicals cm <sup>-3</sup> ) <sup>E</sup>	Cl / Br production (10 <sup>21</sup> atoms cm <sup>-2</sup> h <sup>-1</sup> )	Q <sub>abs</sub>		
∞ <sup>A</sup>	4.7-5.0	Zero air	182 / 4.5 / 0.0074	1.0	~0.1 <sup>F</sup>	~1 <sup>F</sup>	~1 <sup>F</sup>	~0.3–0.4 <sup>F</sup>	n.d. <sup>G</sup>
∞ <sup>B</sup>	4.8-5.1	Zero air	163 / 3.9 / 0.0063	2.3	~0.4	5.1	<1 <sup>G</sup>	~0.6	n.d. <sup>G</sup>
∞ <sup>A</sup>	4.7-5.0	20 ppb NO <sub>x</sub>	209 / 4.2 / 0.0080	2.4	~0.1 <sup>F</sup>	2	1.2	n.d. <sup>G</sup>	0.6–0.7
∞ <sup>A</sup>	4.7-5.0	700 ppb O <sub>3</sub>	137 / 1.3 / 0.0053	2.2	4.9	17	9.4	3.1–4.9	1.6–2.8
955 <sup>C</sup>	4.5-4.8	Zero air	126 / 2.6 / 0.0039	1.2	~0.1 <sup>F</sup>	2.3	~1 <sup>F</sup>	~0.3–0.4 <sup>F</sup>	n.d. <sup>G</sup>
101 <sup>C</sup>	3.9-4.2	Zero air	201 / 4.3 / 0.0077	2.5	0.5	1.2	3.8	0.7–0.8	1.8–2.0
101 <sup>C,D</sup>	2.1-2.3	Zero air	177 / 3.3 / 0.0046	1.8	1.9	2.2	2.7	5.3–5.8	1.8–2.2
101 <sup>C</sup>	3.9-4.2	20 ppb NO <sub>x</sub>	196 / 3.9 / 0.0057	2.3	9.1	5	3	3.0–3.3	2.6–3.2
101 <sup>C,D</sup>	2.1-2.3	20 ppb NO <sub>x</sub>	169 / 3.6 / 0.0053	2.3	5.4	3	<1 <sup>G</sup>	6.8–7.9	n.d. <sup>G</sup>
51 <sup>C</sup>	3.3-3.6	Zero air	152 / 3.3 / 0.0052	3.2	1.9	5.4	1.2	1.4–1.5	~0.3
13 <sup>B</sup>	1.9-2.2	Zero air	118 / 2.9	2.4	16.7	4.8	<1 <sup>G</sup>	8.7–13	n.d. <sup>G</sup>
13 <sup>C</sup>	1.9-2.2	Zero air	125 / 2.4 / 0.0036	3.0	13.1	<1 <sup>G</sup>	<1 <sup>G</sup>	6.6–8.7	n.d. <sup>G</sup>
13 <sup>C</sup>	1.9-2.2	20 ppb NO <sub>x</sub>	139 / 3.2 / 0.0051	3.1	65.1	<1 <sup>G</sup>	<1 <sup>G</sup>	16–52	n.d. <sup>G</sup>
13 <sup>C</sup>	1.9-2.2	620 ppb O <sub>3</sub>	218 / 5.2 / 0.0085	3.4	40	13	13	18–45	3.0–8.1
13 <sup>C</sup>	1.9-2.2	~ 20 ppb SO <sub>2</sub>	204 / 4.9 / 0.0078	1.9	4.3	2.1	3.7	6.0–6.7	2.0–2.2
13 <sup>C</sup>	1.9-2.2	> 200 ppb SO <sub>2</sub>	178 / 4.4 / 0.0063	1.0	1.4	1.3	1.2	4.0–4.5	1.4–1.6
~13 <sup>H</sup>	5-6	Zero air	146 / 3.4 / 0.0034	4.2	<1 <sup>G</sup>	<1 <sup>G</sup>	<1 <sup>G</sup>	n.d. <sup>G</sup>	n.d. <sup>G</sup>
~13 <sup>I</sup>	5-6	Zero air	168 / 3.7 / 0.0068	3.3	<1 <sup>G</sup>	<1 <sup>G</sup>	<1 <sup>G</sup>	n.d. <sup>G</sup>	n.d. <sup>G</sup>
~13 <sup>I</sup>	1-2	Zero air	168 / 3.7 / 0.0069	3.3	44	<1 <sup>G</sup>	<1 <sup>G</sup>	13–45	0.6–0.7

<sup>A</sup>Fe(III)-free artificial seawater stock solution, <sup>B</sup>NaCl stock solution, <sup>C</sup>Artificial seawater stock solution, <sup>D</sup>pH adjusted to 2.1-2.3, <sup>E</sup>mean steady state concentrations during the 1<sup>st</sup> hour, <sup>F</sup>close to the detection limit, <sup>G</sup>below the detection limit, <sup>H</sup>artificial seawater stock solution with Sicotrans Orange (BASF), <sup>I</sup>artificial seawater stock solution with Sicotrans Orange (BASF), 5 times frozen and unfrozen

To estimate the effect of the aerosol pH on the Cl production, the pH of the diluted stock solution ( $\text{Cl}^-/\text{Fe(III)} = 101$ ) was adjusted to pH 2.1-2.3 by gently adding 32% HCl. The results demonstrated the immense effect of the pH (section 3.15). In comparison to the not adjusted sample (pH 3.9-4.2), the mean absolute production rate during the first 120 min increased by more than an order of magnitude from  $1.6 \cdot 10^{17}$  to  $1.8 \cdot 10^{18}$  atoms  $\text{cm}^{-2} \text{ s}^{-1}$  and led to an 8 times higher total Cl production per hour. There are multiple reasons responsible for this effect. As evaluated in several studies for Fe(III) doped salts, the speciation chemistry of Fe(III) strongly depends on the pH and ionic strength (Nadtochenko and Kiwi, 1998b; Lim et al., 2006; Wittmer et al., 2014). Figure 52a, b show the portions of Fe(III) complexes from total Fe(III) as a function of the pH, calculated by an equilibrium model in PHREEQC (Parkhurst and Appelo, 1999). According to Wittmer et al. the model is based on the MINTEQ database (Allison et al., 1991), and the activity coefficients are corrected by the Pitzer ion interaction approach (Pitzer, 1973) with the parameters listed in Tosca et al., 2005. The main equilibrium constants involving Fe(III) are listed in Table 20. For some ions (e.g. F<sup>-</sup>), there are no Pitzer parameters available, and the extended Debye-Hueckel equation (Hückel, 1925; Truesdell and Jones, 1973) was applied to calculate the respective activity coefficients. To get an insight into the processes during nebulization and evaporation, the speciation was calculated for the diluted stock solution (Figure 52a), filled into the nebulizer, as well as for the final aerosol (Figure 52b), assuming a saturation in Cl<sup>-</sup> (6.1 mol L<sup>-1</sup>) and unchanged molar ratios towards the other constituents. This assumption is extremely simplified based on the complexity of a multicomponent salt system (Tang et al., 1997) and implies a similar hydration and solubility behavior of NaCl and artificial sea-salt but accounts for the fact that Na<sup>+</sup> and Cl<sup>-</sup> represent by far the main ions. E.g. McCaffrey et al., 1987 measured similar Cl<sup>-</sup> saturation concentrations in evaporating seawater, whereas the concentration may change with increasing Fe(III) content.

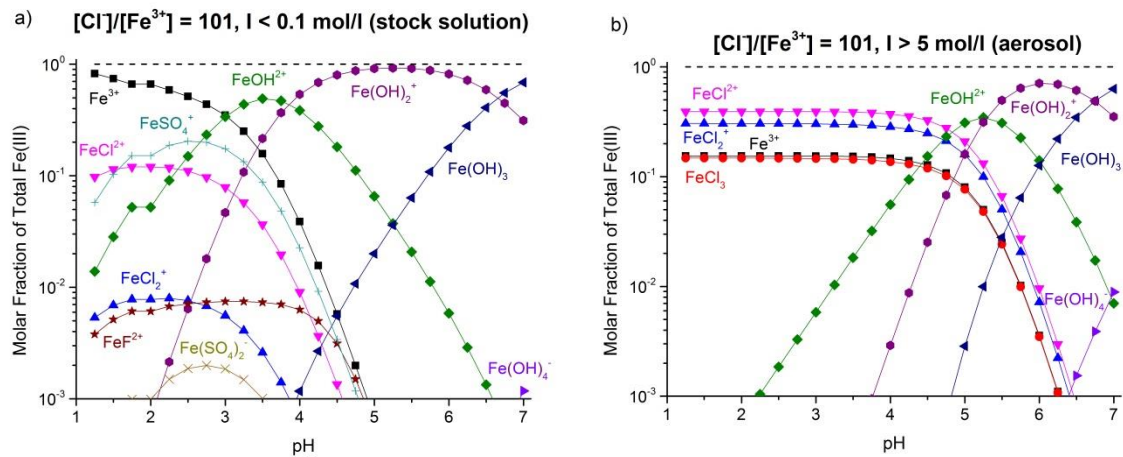


**Figure 51. Molar fraction of the formed Fe(III) species, relative to the total Fe(III) content in Fe(III)-doped artificial seawater ( $\text{Cl}^-/\text{Fe(III)} = 101$ ) as a function of the pH (according to the PHREEQC model) of the low concentrated diluted stock solution before nebulizing (a) and of the final, highly concentrated aqueous phase of the aerosol (b). The dashed line indicates a molar fraction of 1 (100%). Adapted from Wittmer et al., 2015.**

Even though high fractions of Fe<sup>3+</sup> ions and Fe(III)-hydroxy complexes are present in the stock solution, the decisive photolabile Fe(III)-Cl complexes start to form in a considerable fraction at pH 1-4.5 with increasing ionic strength (solvent concentrations). The pH of 4.5 is a turning point for the aerosol speciation where Fe(III)-hydroxy complexes are mainly present. Since Fe(III)-Cl complexes have a fraction of less than 5 % in the stock solution at the given pH of 3.9-4.2 (and it will take some time until the speciation equilibrium is

reached during the transition from the low concentrated stock solution to the high-concentrated liquid aerosol), the smaller amount of Fe(III)-Cl complexes could explain the lower gaseous Cl production for the untreated sample. This situation changes when the pH is adjusted to 1.9-2.2 already in the diluted stock solution. At such low pH values, Fe(III)-Cl complexes are formed much easier. Furthermore, the solubility of Fe(III) increases with decreasing pH, while more dissolved Fe(III) becomes available on an absolute scale (Millero *et al.*, 1995; Millero, 1998; Liu and Millero, 2002). Furthermore, the formation of the highly soluble hypochlorous acid (HOCl, Henry's law constant at 298 K:  $2.6 - 9.3 \cdot 10^2$  M atm<sup>-1</sup>; Sander, 1999) dominates at a pH between 4 and 7 over Cl<sub>2</sub>, that is favored at a pH lower than 4 and is much easier released to the gas phase (Henry's law constant:  $6.2 - 9.1 \cdot 10^{-2}$  M atm<sup>-1</sup>; Sander, 1999). Similar observations were also made by Lim *et al.*, 2006 who ascribed the decreasing Cl<sub>2</sub> source with decreasing pH to the speciation chemistry and solubility of the various chlorine species.

**Table 20: Main equilibrium constants ( $\log_{10} K$ ) for the formation of low molecular weight Fe(III) complexes with several ligands at zero ionic strength and 298 K. Adapted from Wittmer *et al.*, 2015.**

Equilibrium Constants	$\log_{10} K$
Water	
$\text{Fe}^{3+} + \text{H}_2\text{O} \rightleftharpoons \text{FeOH}^{2+} + \text{H}^+$	-2.19 ( <i>Baes and Mesmer, 1976</i> )
$\text{Fe}^{3+} + 2\text{H}_2\text{O} \rightleftharpoons \text{Fe(OH)}_2^+ + 2\text{H}^+$	-5.67 ( <i>Baes and Mesmer, 1976</i> )
$\text{Fe}^{3+} + 3\text{H}_2\text{O} \rightleftharpoons \text{Fe(OH)}_3 + 3\text{H}^+$	-12.0 ( <i>Baes and Mesmer, 1976</i> )
$\text{Fe}^{3+} + 4\text{H}_2\text{O} \rightleftharpoons \text{Fe(OH)}_4^- + 4\text{H}^+$	-21.6 ( <i>Baes and Mesmer, 1976</i> )
Chloride	
$\text{Fe}^{3+} + \text{Cl}^- \rightleftharpoons \text{FeCl}^{2+}$	1.48 ( <i>Kester et al., 1975</i> )
$\text{Fe}^{3+} + 2\text{Cl}^- \rightleftharpoons \text{FeCl}_2^+$	2.13 ( <i>Martell and Smith, 1976</i> )
$\text{Fe}^{3+} + 3\text{Cl}^- \rightleftharpoons \text{FeCl}_3$	1.13 ( <i>Yatsimirskii and Vasil'ev, 1960</i> )
Bromide	
$\text{Fe}^{3+} + \text{Br}^- \rightleftharpoons \text{FeBr}^{2+}$	0.61 ( <i>Lister and Rivington, 1955</i> )
$\text{Fe}^{3+} + 2\text{Br}^- \rightleftharpoons \text{FeBr}_2^+$	0.2 ( <i>Lister and Rivington, 1955</i> )
Fluoride	
$\text{Fe}^{3+} + \text{F}^- \rightleftharpoons \text{FeF}^{2+}$	6.2 ( <i>Nordstrom and Jenne, 1977</i> )
$\text{Fe}^{3+} + 2\text{F}^- \rightleftharpoons \text{FeF}_2^+$	10.8 ( <i>Nordstrom and Jenne, 1977</i> )
$\text{Fe}^{3+} + 3\text{F}^- \rightleftharpoons \text{FeF}_3$	14 ( <i>Nordstrom and Jenne, 1977</i> )
Sulfate	
$\text{Fe}^{3+} + \text{SO}_4^{2-} \rightleftharpoons \text{FeSO}_4^+$	3.92 ( <i>de Laat et al., 2004</i> )
$\text{Fe}^{3+} + 2\text{SO}_4^{2-} \rightleftharpoons \text{Fe}(\text{SO}_4)_2^-$	5.42 ( <i>de Laat et al., 2004</i> )

## Fraction of active iron

Multiplying the initial  $LWC_0$  (in  $\text{dm}^3 \text{ cm}^{-3}$ ) with the assumed saturation concentration of  $\text{Cl}^-$  ( $6.1 \text{ mol L}^{-1}$ ) in the produced aerosols and with the Avogadro constant ( $N_A = 6 \cdot 10^{23} \text{ mol}^{-1}$ ) and dividing by the molar  $\text{Cl}^-/\text{Fe(III)}$  ratio ( $r_{\text{Cl}/\text{Fe}}$ ) in the stock solutions, results in the concentration of Fe(III) in the chamber. The ratio to the minimum concentration of produced Cl atoms during the 1<sup>st</sup> hour of the experiments ( $Q_{\min}$ ) provides an estimation of the minimum fraction of active iron  $\lambda_{\text{Fe}}$  involved in the Cl production

$$\lambda_{\text{Fe}} = \frac{Q_{\min} \times r_{\text{Cl}/\text{Fe}}}{LWC_0 \times 6.1 \times N_A} \quad (9)$$

assuming that each Fe(III) produces  $\frac{1}{2}$   $\text{Cl}_2$  by excluding recycling effects and secondary activation mechanisms. The contribution of the tare volume of the ions to the measured LWC is  $0.11 \text{ m}^3 \text{ m}^{-3}$  (considered in the calculation), whereas the influence of  $\text{Fe}^{3+}$  ions on the LWC is negligible. Due to the strong assumption and unknown uncertainties ( $r_{\text{Cl}/\text{Fe}}$  in the aerosol can differ from the bulk, or the concentration of  $\text{Cl}^-$  can vary depending on the composition and thus deliquescence of the aerosol)  $\lambda_{\text{Fe}}$  represents a rather qualitative value for relative comparisons between the experiments. Figure 53 shows the results for all investigated Fe(III) containing samples, combined with the measured total minimum and maximum Cl production  $Q_{\text{abs}}$  during the first hour. Again, the increase in  $Q_{\text{abs}}$  for the artificial seawater samples with increasing Fe(III) concentration ( $\text{Cl}/\text{Fe(III)} = 13, 53, 101$ ) is highlighted, although  $\lambda_{\text{Fe}}$  is comparable (which indicates that similar Cl activation mechanisms are going on). This is also the case for the pure NaCl + Fe(III) sample where  $Q_{\text{abs}}$  and  $\lambda_{\text{Fe}}$  are higher, caused by absence of competing ligands for Fe(III) and thus a higher fraction of photolabile Fe(III)-Cl complexes.

The presence of 20 ppb  $\text{NO}_x$  in the gas phase led to a considerable increase of a factor 3-7 for  $Q_{\text{abs}}$  from the  $\text{Cl}/\text{Fe(III)} = 101$  and the  $\text{Cl}/\text{Fe(III)} = 13$  sample. Coexistent is the increase of  $\lambda_{\text{Fe}}$  which only pretends that Fe(III) is involved (even more than 100 %) but actually represents the additional Cl-activation mechanisms induced by  $\text{NO}_x$  as discussed in section 3. The same applies for the experiment with 620 ppb  $\text{O}_3$ . Decreasing the pH enhanced the activity of Fe(III), and more than 100% of Fe(III) seemed to be involved, which either is a consequence of recycling effects (re-oxidation of Fe(II)) that was formed by photolysis of Fe(III) complexes), or is caused by the uncertainty of  $\lambda_{\text{Fe}}$ . For the low-pH sample as well as for the untreated samples ( $\text{Cl}/\text{Fe(III)} = 13$  and 101), an increase in  $Q_{\text{abs}}$  and  $\lambda_{\text{Fe}}$  was observed with addition of 20 ppb  $\text{NO}_x$  which clearly demonstrates the  $\text{NO}_x$ -induced activation of chloride. The effect is not so pronounced at low aerosol pH.

$\text{SO}_2$  was able to slightly inhibit the Cl production. In particular high  $\text{SO}_2$  mixing ratios decreased the  $Q_{\text{abs}}$  and thus the fraction of active iron. One can compare  $\lambda_{\text{Fe}}$  to the salt-pan measurements, where a portion of 0.05-0.07% of active Fe(III) was determined (Wittmer *et al.*, 2014). Considering the salt pan containing 0.5 g  $\text{FeCl}_3 \cdot 6 \text{ H}_2\text{O}$  and 99.5 g NaCl results in a total molar Fe(III) content of  $1.8 \cdot 10^{-3}$ . This is quite high compared to the aerosol experiments with only  $\sim 3 \cdot 10^{-6} \text{ mol Fe(III)}$  at a LWC of  $\sim 2.7 \cdot 10^{-9}$  but total Cl sources comparable to the salt-pan experiments. These large differences prove the small active surface area of the salt pans compared to the homogeneously distributed and irradiated aerosol in the chamber.

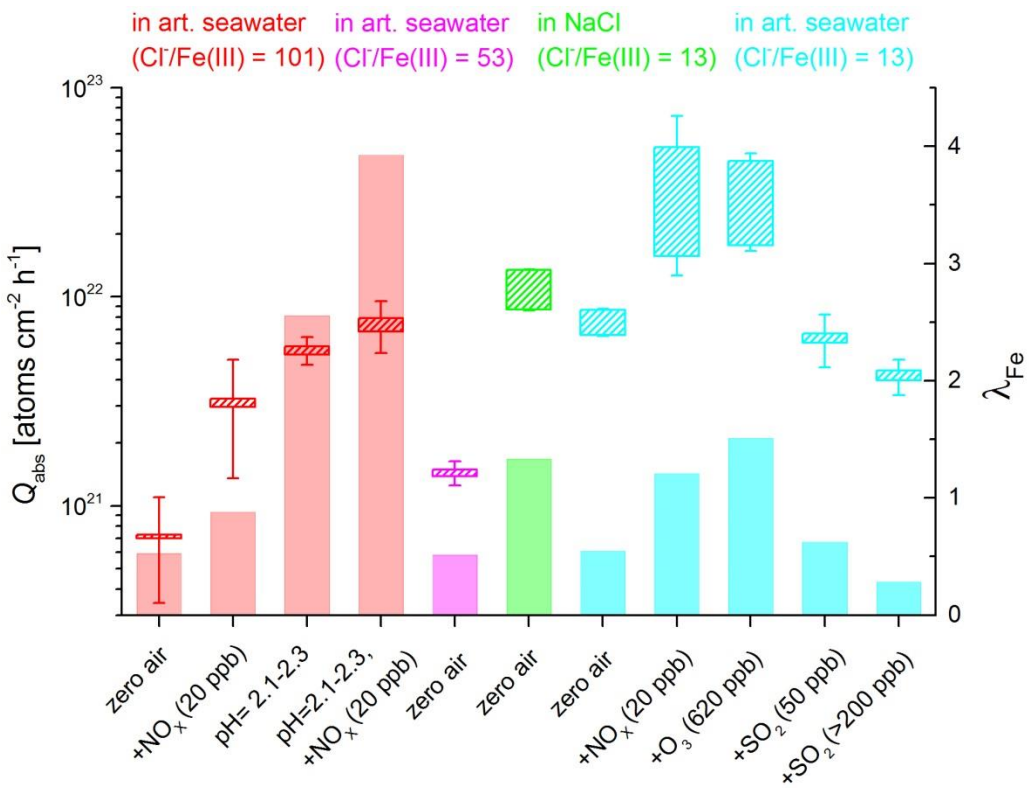


Figure 51. Overview of the minimum and maximum absolute Cl production  $Q_{\text{abs}}$  [ $\text{atoms cm}^{-2} \text{h}^{-1}$ ] over the first hour and the corresponding fraction of active Fe(III) ( $\lambda_{\text{Fe}}$ ) for each experiment with Fe(III) containing samples and various air contaminants ( $\text{NO}_x$ ,  $\text{O}_3$ ,  $\text{SO}_2$ ). Adapted from Wittmer *et al.*, 2015.

### Environmental Significance

The ratio of the concentrations of added pollutants and the generated aerosol concentrations ( $2\text{-}6 \text{ mg m}^{-3}$ ) are roughly in accordance with the conditions for sea-salt aerosol over the ocean. Although the smog chamber helps to understand the mechanisms, it is difficult to transfer the results to large scale atmospheric processes since the aerosol surface to volume ratio in the smog chamber is several orders of magnitude higher than in the atmosphere.

We investigated a very simplified system with no organic contaminants in the salt and under hydrocarbon-free conditions. Note that Fe complexes with oxygen-containing organics (such as phenolic compounds) can significantly increase the solubility in seawater (Kuma *et al.*, 1996). On the other hand, complexation can strongly inhibit the iron induced chlorine activation (Wittmer *et al.*, 2014), until the phenolic constituents are oxidized by OH and Cl from the photo-Fenton mechanism to the less inhibiting but solubility-promoting oxalate. Oxalate is a relatively stable intermediate of the oxidation of organics to  $\text{CO}_2$  and is supposed to inhibit the halogen activation by complexation with Fe(III) (Wittmer *et al.*, 2014) and by reaction with  $\text{Br}_2$  (Behnke *et al.*, 1999). Simultaneously, Fe(III) complex photolysis is an important additional sink for tartronate, pyruvate and oxalate, with a complex photolysis contribution to overall degradation of 46, 40, and 99% (Styler and Donaldson, 2012; Weller *et al.*, 2014). The soluble fraction of iron over the ocean ranges from 0-95 % as the bulk marine aerosol type reflects a mixing of multiple aerosol types and the solubility varies with the origin of iron, the aerosol size and composition (Siefert *et al.*, 1998; Baker *et al.*, 2006; Sholkovitz *et al.*, 2012). Moreover, the solubility increases due to the photoreduction of Fe(III) that is

responsible for a Fe(II) fraction in the aerosol of up to 50 % in remote marine areas (*Zhuang et al.*, 1992). An additional crucial factor for the role of Fe(III) photochemistry is the aerosol pH which may vary from 1-9, mainly depending on the origin and age of the aerosol and the corresponding aging processes (*Keene et al.*, 1998; *Keene and Savoie*, 1998).

Accounting for these effects in order to quantify the iron-induced Cl production in the troposphere, a sophisticated large scale model would be required. Based on a mean molar  $\text{Cl}^-/\text{Fe}$  ratio of 100-200 in the marine aerosol (Central Atlantic) (*Warneck*, 1999), on the thereof lower fraction of dissolved Fe(III), that can form photolabile complexes, and on the 20-200 times larger aerosol surface area in the chamber compared to the Atlantic aerosol (*O'Dowd et al.*, 2001), the mean natural contribution of Fe(III) induced Cl activation cannot compete with alternative mechanisms on a global scale (*Mahowald et al.*, 2009). This is also indicated by the low Cl (below the detection limit) in our experiment with  $\text{Cl}^-/\text{Fe(III)} = 997$ ). On the other hand, it may become important on a local scale with a larger Fe(III) burden exposed to saline media, e.g. ship plumes or other iron-containing combustion aerosols (*Ito*, 2013) or where soil dust comes into contact with sea salt but also in brine-containing soils (or salt lakes, such as the Dead Sea or Australian salt lakes (*Krause et al.*, 2013). Furthermore, iron-doped sea salt aerosols have been proposed as a method for climate engineering, aiming at an enhancement of the  $\text{CH}_4$  depletion by higher Cl levels in the marine boundary layer and at a simultaneously fertilization of the oceans (*Oeste*, 2004a; *Meyer-Oeste*, 2010). Our results represent a basis for a further model evaluation of the feasibility of such a project concerning the direct Fe(III) intrusion into sea salt. The main restrictions for a direct application of our results to the MBL are the short experimental run-time of 4h, the much higher aerosol surface to air volume ratio in the chamber compared to the MBL, the lower aerosol lifetime in the chamber (2-3 h) compared to comparable aerosols in the free troposphere (days-weeks, *Mahowald et al.*, 2005; *Wang et al.*, 2015) and the organic-free aerosol in a zero air environment. Furthermore, the evaluation of such a project needs the inclusion of tropospheric mixing dynamics and vertical  $\text{CH}_4$  profiles since the iron-containing aerosols are emitted locally.

Applying these results to the natural role of Fe(III) in the glacial-interglacial changes of atomic Cl concentrations and thus carbon isotope ratios (*Levine et al.*, 2011), one may discuss changes in the atmospheric soluble iron content (mineral dust content). *Levine et al.*, 2011, ascribe up to 10 % of the glacial-interglacial change in the isotopic composition of  $\text{CH}_4$  to the atomic Cl reaction. The changes are ascribed to circulation-driven changes in the strength of the Cl sink, changes in the lifetime of sea-salt aerosols (due to changes in precipitation), changes in the acidity of the atmosphere (e.g. due to changes in dimethyl sulphide (DMS) production), changes in the intensity of radiation required to photolyse  $\text{BrCl}$  and  $\text{Cl}_2$  (e.g. due to changes in stratospheric  $\text{O}_3$ ) accompanied by changes in the amount of  $\text{CH}_4$  removed by OH (*Levine et al.*, 2011). The “iron hypothesis” (*Martin*, 1990), that it may have caused the  $\text{CO}_2$  variations due to ocean fertilization, became support by sediment core analysis (e.g. *Martínez-García et al.*, 2011; *Martínez-García et al.*, 2014). The reasons for the parallel  $\text{CH}_4$  variations are still under discussion. Here it remains unclear, how much of the  $\text{CH}_4$  changes were source driven or sink driven (*Petit et al.*, 1999). To date, the intrusion of soluble iron is estimated to range from 0.1 to 0.25 Mt (*Johnson and Meskhidze*, 2013; *Myriokefalakis et al.*, 2015).

A potential alternative way to produce large amounts of atomic Cl in the gas phase is the direct pyrogenic emission of iron-oxide aerosol, e.g. from ships, aircrafts or power plants (*Oeste*, 2004b, *Meyer-Oeste*, 2010). The soot particles may absorb HCl (*Zhang and Iwasaka*, 2001; *Oeste*, 2004a; *Sullivan et al.*, 2007; *Tobo et al.*, 2009; *Meyer-Oeste*, 2010) that is present in the MBL (100-300 ppt, *Graedel and Keene*, W. C., 1996). Under these conditions, the particles are supposed to activate  $\text{Cl}^-$  coming from HCl emitted from the natural seasalt (*Oeste*, 2004b). The efficiency of such a Cl production is not investigated yet but it might be comparable to the results with acidified pyrogenic iron oxide Sicotrans Orange mix with sea salt at low pH.

Sicotrans is a likewise pyrogenic iron oxide pigment sold by BASF. Sicotrans Orange L 2416 is a mixture of iron(III) oxide and iron oxide hydrate (BASF Technical Information EVP 008605 e, November 2005). Sicotrans pigments have rod-like particles with a diameters in the range of 0,01 $\mu$ m and length of about 0,1 $\mu$ m (BASF data sheet Sicotrans Yellow 1916 MB/P 087 d.e. Oktober 2000, an iron oxide hydrate and BASF data sheet Sicotrans Red L 2817/L 2818 MB/P 088 d.e. Oktober 2000, an iron(III)oxide). The comparison must be considered with caution due to various particle production mechanisms (combustion and nebulization) and resulting particle size distributions and properties. Emitted Sicotrans Orange aerosol particles had been adjusted to pH 2 and dispersed/covered by sea salt as Cl<sup>-</sup> source and particle diameters between 0,35 - 0,46 $\mu$ m while the ISA oxid is emitted undiluted, keeps in flue gas and atmosphere contact, has particle diameters <0,1  $\mu$ m and is restricted to the gaseous HCl source. Pyrogenic iron oxide particles may have a larger specific surface area, a longer lifetime and a better availability of iron.

In general, an acidic environment seems to intensify the Fe(III)-induced Cl activation as proven for trace pollutants such as NO<sub>2</sub> (after oxidation to HNO<sub>3</sub>) or direct acidification (by oxalic acid, HCl or H<sub>2</sub>SO<sub>4</sub>). On the other hand, SO<sub>2</sub> slightly inhibits the activation mechanism, so it is difficult to draw a conclusion on the effect of other exhaust gases or trace gases resulting from the ocean fertilization (e.g. dimethyl sulphide).

### Acknowledgment

We wish to thank Franz D. Oeste, gM-Ingenieurbüro Kirchhain, Germany, for advice, Agnes Bednorz, Uli Krüger and Andrej Einhorn for technical support. This work was supported by Ries Consulting GmbH&Co Betriebs KG, Hosenfeld.

# References

- Alappattu, D.; Subrahmanyam, D. B.; Kunhikrishnan, P. K.; Somayaji, K. M.; Bhat, G. S.; Venkatesan, R.; Dutt, C. B. S.; Singh, A. B.; Soni, V. K.; Tripathi, A. S. On the marine atmospheric boundary layer characteristics over Bay of Bengal and Arabian Sea during the Integrated Campaign for Aerosols, gases and Radiation Budget (ICARB), *J Earth Syst Sci*, **2008**, 117, 281-291, doi:10.1007/s12040-008-0031-0.
- Allison, J. D.; Brown, D. S.; Kevin, J. MINTEQA2/PRODEFA2, A Geochemical Assessment Model for Environmental Systems: Version 3.0 User's Manual: Environmental Research Laboratory, Office of Research and Development, US Environmental Protection Agency, Athens, Georgia, USA, **1991**.
- Amphlett, J. and Whittle, E. Bromination of Fluoroalkanes. Part 4. Kinetics of Thermal Bromination of Fluoroform and Pentafluoroethane, *Trans. Faraday Soc.*, **1968**, 64, 2130, doi:10.1039/tf9686402130.
- Andreae, M. O.; Elbert, W.; Gabriel, R.; Johnson, D. W.; Osborne, S.; Wood, R. Soluble ion chemistry of the atmospheric aerosol and SO<sub>2</sub> concentrations over the eastern North Atlantic during ACE-2, *Tellus B*, **2000**, 52, 1066–1087, doi:10.1034/j.1600-0889.2000.00105.x.
- Aschmann, S. M. and Atkinson, R. Rate Constants for the Gas-Phase Reactions of Alkanes with Cl Atoms at 296 ± 2 K, *Int. J. Chem. Kinet.*, **1995**, 27, 613–622, doi:10.1002/kin.550270611.
- Atkinson, R. Kinetics and Mechanisms of the Gas-Phase Reactions of the Hydroxyl Radical with Organic Compounds under Atmospheric Conditions, *Chem. Rev.*, **1986**, 86, 69–201, doi:10.1021/cr00071a004.
- Atkinson, R. and Aschmann, S. M. Kinetics of the Gas Phase Reaction of Cl Atoms with a Series of Organics at 296 ± 2 K and Atmospheric Pressure, *Int. J. Chem. Kinet.*, **1985**, 17, 33–41, doi:10.1002/kin.550170105.
- Atkinson, R.; Baulch, D. L.; Cox, R. A.; Crowley, J. N.; Hampson, R. F.; Hynes, R. G.; Jenkin, M. E.; Rossi, M. J.; Troe, J. Evaluated kinetic and photochemical data for atmospheric chemistry: Volume I - gas phase reactions of O<sub>x</sub>, HO<sub>x</sub>, NO<sub>x</sub> and SO<sub>x</sub> species, *Atmos. Chem. Phys.*, **2004**, 4, 1461–1738, doi:10.5194/acp-4-1461-2004.
- Atkinson, R.; Baulch, D. L.; Cox, R. A.; Crowley, J. N.; Hampson, R. F.; Hynes, R. G.; Jenkin, M. E.; Rossi, M. J.; Troe, J. Evaluated kinetic and photochemical data for atmospheric chemistry: Volume III – gas phase reactions of inorganic halogens, *Atmos. Chem. Phys.*, **2007**, 7, 981–1191, doi:10.5194/acp-7-981-2007.
- Atkinson, R.; Baulch, D. L.; Cox, R. A.; Hampson, R. F.; Kerr, J. A.; Rossi, M. J.; Troe, J. Evaluated Kinetic, Photochemical and Heterogeneous Data for Atmospheric Chemistry: Supplement V.

IUPAC Subcommittee on Gas Kinetic Data Evaluation for Atmospheric Chemistry, *J. Phys. Chem. Ref. Data*, **1997**, 26, 521–1011, doi:10.1063/1.556011.

Baes, C. F.; Mesmer, R. E. *The Hydrolysis of Cations*. New York: Wiley, **1976**.

Baker, A. R. and Croot, P. L. Atmospheric and marine controls on aerosol iron solubility in seawater, *Marine Chemistry*, **2010**, 120, 4–13, doi:10.1016/j.marchem.2008.09.003.

Baker, A. R.; Jickells, T. D.; Witt, M.; Linge, K. L. Trends in the solubility of iron, aluminium, manganese and phosphorus in aerosol collected over the Atlantic Ocean, *Marine Chem.*, **2006**, 98, 43–58, doi:10.1016/j.marchem.2005.06.004.

Balzer, N. *Kinetische Untersuchungen der Halogen-Aktivierung einer simulierten Salzpfanne in einer Smogkammer*, Universität Bayreuth, Forschungsstelle für atmosphärische Chemie, Diss, **2012**, 5.

Barnes, I.; Bastian, V.; Becker, K. H.; Overath, R.; Tong, Z. Rate Constants for the Reactions of Br Atoms with a Series of Alkanes, Alkenes, and Alkynes in the Presence of O<sub>2</sub>, *Int. J. Chem. Kinet.*, **1989**, 21, 499–517, doi:10.1002/kin.550210703.

BASF Technical Information EVP 008605 e, November **2005**

BASF data sheet Sicotrans Yellow 1916 MB/P 087 d.e. Oktober **2000**

BASF data sheet Sicotrans Red L 2817/L 2818 MB/P 088 d.e. Oktober **2000**

Baulch, D. L.; Duxbury, J.; Grant, S. J.; Montague, D. C. Evaluated Kinetic Data for High Temperature Reactions. Volume 4. Homogeneous Gas Phase Reactions of Halogen-and Cyanide-Containing Species, *J. Phys. Chem. Ref. Data*, **1981**, 723.

Behnke, W.; Elend, M.; Krüger, U.; Zetzsch, C. The Influence of NaBr/NaCl Ratio on the Br<sup>–</sup> Catalysed Production of Halogenated Radicals, *J. Atmos. Chem.*, **1999**, 34, 87-99, doi:10.1023/A:1006297819663.

Behnke, W.; George, C.; Scheer, V.; Zetzsch, C. Production and Decay of ClNO<sub>2</sub> from the Reaction of Gaseous N<sub>2</sub>O<sub>5</sub> with NaCl Solution: Bulk and Aerosol Experiments, *J. Geophys. Res. D*, **1997**, 102, 3795–3804, doi:10.1029/96JD03057.

Behnke, W.; Scheer, V.; Zetzsch, C., **1995**. Production of a photolytic precursor of atomic Cl from aerosols and Cl<sup>–</sup> in the presence of O<sub>3</sub>. In: Anders Grimvall und EdW.B de Leer (Hg.): Naturally-produced organohalogens, Bd. 1: Springer Netherlands (Environment & Chemistry), 375-384. doi: [http://dx.doi.org/10.1007/978-94-011-0061-8\\_35](http://dx.doi.org/10.1007/978-94-011-0061-8_35).

Bierbach, A.; Barnes, I.; Becker, K. H. Rate Constants of the Br<sup>–</sup> Initiated Gas-Phase Oxidation of a Series of Alcohols, Furans and Benzenes at 300±2 K, *Atmos. Environ.*, **1999**, 33, 2981–2992, doi:10.1016/S1352-2310(99)00084-9.

Blain, S.; Quéguiner, B.; Armand, L.; Belviso, S.; Bombled, B.; Bopp, L.; Bowie, A.; Brunet, C.; Brussaard, C.; Carlotti, F.; Christaki, U.; Corbière, A.; Durand, I.; Ebersbach, F.; Fuda, J.-L.; Garcia, N.; Gerringa, L.; Griffiths, B.; Guigue, C.; Guillerm, C.; Jacquet, S.; Jeandel, C.; Laan, P.; Lefèvre, D.; Lo Monaco, C.; Malits, A.; Mosseri, J.; Obernosterer, I.; Park, Y.-H.; Picheral, M.; Pondaven, P.; Remenyi, T.; Sandroni, V.; Sarthou, G.; Savoye, N.; Scouarnec, L.; Souhaut, M.; Thuiller, D.; Timmermans, K.; Trull, T.; Uitz, J.; van Beek, P.; Veldhuis, M.; Vincent, D.; Viollier, E.; Vong, L.; Wagener, T. Effect of natural iron fertilization on carbon sequestration in the Southern Ocean, *Nature*, **2007**, 446, 1070–1074, doi:10.1038/nature05700.

Bleicher, S., **2012**. Zur Halogenaktivierung im Aerosol und in Salzpfannen. Halogen activation in aerosol and salt pans. doi: <http://nbn-resolving.de/urn/resolver.pl?urn:nbn:de:bvb:703-opus4-13701>.

Bleicher, S.; Buxmann, J. C.; Sander, R.; Riedel, T. P.; Thornton, J. A.; Platt, U.; Zetzsch, C. The Influence of Nitrogen Oxides on the Activation of Bromide and Chloride in Salt Aerosol, *Atmos. Chem. Phys. Discuss.*, **2014**, 14, 10135–10166, doi:10.5194/acpd-14-10135-2014.

Brimblecombe, P. and Clegg, S. L. The solubility and behaviour of acid gases in the marine aerosol, *J. Atmos. Chem.*, **1988**, 7, 1–18, doi:10.1007/BF00048251.

Bryukov, M. G.; Slagle, I. R.; Knyazev, V. D. Kinetics of Reactions of Cl Atoms with Methane and Chlorinated Methanes, *J. Phys. Chem. A*, **2002**, 106, 10532–10542, doi:10.1021/jp0257909.

Buxmann, J.; Balzer, N.; Bleicher, S.; Platt, U.; Zetzsch, C. Observations of Bromine Explosions in Smog Chamber Experiments above a Model Salt Pan, *Int. J. Chem. Kinet.*, **2012**, 44, 312–326, doi:10.1002/kin.20714.

de Laat, J.; Le, T. G.; Legube, B. A Comparative Study of the Effects of Chloride, Sulfate and Nitrate Ions on the Rates of Decomposition of  $\text{H}_2\text{O}_2$  and Organic Compounds by Fe(II)/ $\text{H}_2\text{O}_2$  and Fe(III)/ $\text{H}_2\text{O}_2$ , *Chemosphere*, **2004**, 55, 715–723, doi:10.1016/j.chemosphere.2003.11.021.

Duggen, S.; Croot, P.; Schacht, U.; Hoffmann, L. Subduction zone volcanic ash can fertilize the surface ocean and stimulate phytoplankton growth: Evidence from biogeochemical experiments and satellite data, *Geophys. Res. Lett.*, **2007**, 34, doi:10.1029/2006GL027522.

Eder, J. M. Über die Zersetzung des Eisenchlorides und einiger Organischer Ferridsalze im Lichte, *Monatshefte für Chemie*, **1880**, 1, 755–762, doi:10.1007/BF01517103.

Faxon, C. B. and Allen, D. T. Chlorine chemistry in urban atmospheres: A review, *Environ. Chem.*, **2013**, 10, 221, doi:10.1071/EN13026.

Fickert, S.; Adams, J. W.; Crowley, J. N. Activation of  $\text{Br}_2$  and  $\text{BrCl}$  via Uptake of HOBr onto Aqueous Salt Solutions, *J. Geophys. Res. D*, **1999**, 104, 23719–23727, doi:10.1029/1999JD900359.

- Finlayson-Pitts, B. J. The Tropospheric Chemistry of Sea Salt: a Molecular-Level View of the Chemistry of NaCl and NaBr, *Chem. Rev.*, **2003**, 103, 4801–4822.
- Finlayson-Pitts, B. J.; Ezell, M. J.; Pitts, J. N. Formation of Chemically Active Chlorine Compounds by Reactions of Atmospheric NaCl Particles with Gaseous N<sub>2</sub>O<sub>5</sub> and ClONO<sub>2</sub>, *Nature*, **1989**, 337, 241–244, doi:10.1038/337241a0.
- Gebel, M. E.; Finlayson-Pitts, B. J.; Ganske, J. A. The uptake of SO<sub>2</sub> on synthetic sea salt and some of its components, *Geophys. Res. Lett.*, **2000**, 27, 887–890, doi:10.1029/1999GL011152.
- Graedel, T. E. and Keene, W. C. The Budget and Cycle of Earth's Natural Chlorine, *Pure and Applied Chemistry*, **1996**, 68, doi:10.1351/pac199668091689.
- Gunn, R. and Woessner, R. H. Measurements of the systematic electrification of aerosols, *Journal of Colloid Science*, **1956**, 11, 254–259, doi:10.1016/0095-8522(56)90050-2.
- Haan, D. de and Finlayson-Pitts, B. J. Knudsen cell studies of the reaction of gaseous nitric acid with synthetic sea salt at 298 K, *J. Phys. Chem. A*, **1997**, 101, 9993–9999, doi:10.1021/jp972450s.
- Hausmann, M. and Platt, U. Spectroscopic measurement of bromine oxide and ozone in the high Arctic during Polar Sunrise Experiment 1992, *J. Geophys. Res.*, **1994**, 99, 25399, doi:10.1029/94JD01314.
- Hoppel, W.; Pasternack, L.; Caffrey, P.; Frick, G.; Fitzgerald, J.; Hegg, D.; Gao, S.; Ambrusko, J.; Albrechcinski, T. Sulfur dioxide uptake and oxidation in sea-salt aerosol, *J. Geophys. Res.*, **2001**, 106, 27575, doi:10.1029/2000JD900843.
- Hückel, E. Zur Theorie konzentrierterer wässriger Lösungen starker Elektrolyte, *Phys. Z.*, **1925**, 26, 93–147.
- Ito, A. Global Modeling Study of Potentially Bioavailable Iron Input from Shipboard Aerosol Sources to the Ocean, *Global Biogeochem. Cycles*, **2013**, 27, 1–10, doi:10.1029/2012GB004378.
- Jenkin, M. E.; Saunders, S. M.; Pilling, M. J. The Tropospheric Degradation of Volatile Organic Compounds: A Protocol for Mechanism Development, *Atmos. Environ.*, **1997**, 31, 81–104, doi:10.1016/S1352-2310(96)00105-7.
- Jickells, T. D. and Spokes, L. J. Atmospheric iron inputs to the oceans, *IUPAC series on analytical and physical chemistry of environmental systems*, **2001**, 7, 85–122.
- Johnson, M. S. and Meskhidze, N. Atmospheric dissolved iron deposition to the global oceans: effects of oxalate-promoted Fe dissolution, photochemical redox cycling, and dust mineralogy, *Geosci. Model Dev.*, **2013**, 6, 1137–1155, doi:10.5194/gmd-6-1137-2013.
- Keene, W. C.; Sander, R.; Pszenny, A. A.; Vogt, R.; Crutzen, P. J.; Galloway, J. N. Aerosol pH in the marine boundary layer, *J. Aerosol Sci.*, **1998**, 29, 339–356, doi:10.1016/S0021-8502(97)10011-8.

- Keene, W. C. and Savoie, D. L. The pH of deliquesced sea-salt aerosol in polluted marine air, *Geophys. Res. Lett.*, **1998**, 25, 2181–2184, doi:10.1029/98GL01591.
- Kelly, N. A. Characterization of fluorocarbon-film bags as smog chambers, *Environ. Sci. Technol.*, **1982**, 16, 763–770, doi:10.1021/es00105a007.
- Kester, D. R.; Byrne, R. H.; Liang, Y.-J., **1975**. Redox Reactions and Solution Complexes of Iron in Marine Systems. In: *Marine chemistry in the Coastal Environment*, Church, T. M. (Editor): Am. Chem. Soc., Washington (18), 56–79.
- Kester, D. R.; Duedall, I. W.; Connors, D. N.; Pytkowicz, R. M. Preparation of artificial seawater, *Limnol. Oceangr.*, **1967**, 12, 176–179, doi:10.4319/lo.1967.12.1.0176.
- Kiwi, J.; Lopez, A.; Nadtochenko, V. Mechanism and Kinetics of the OH-Radical Intervention during Fenton Oxidation in the Presence of a Significant Amount of Radical Scavenger ( $\text{Cl}^-$ ), *Environ. Sci. Technol.*, **2000**, 34, 2162–2168, doi:10.1021/es991406i.
- Knipping, E. M.; Lakin, M. J.; Foster, K. L.; Jungwirth, D.; Gerber, R.; Dabdub, D.; Finlayson-Pitts, B. J. Experiments and Simulations of Ion-Enhanced Interfacial Chemistry on Aqueous NaCl Aerosols, *Science*, **2000**, 288, 301–306, doi:10.1126/science.288.5464.301.
- Knutson, E. O. and Whitby, K. T. Aerosol classification by electric mobility: apparatus, theory, and applications, *Journal of Aerosol Science*, **1975**, 6, 443–451, doi:10.1016/0021-8502(75)90060-9.
- Krause, T.; Tubbesing, C.; Benzing, K.; Schöler, H. F. Model Reactions and Natural Occurrence of Furans from Hypersaline Environments, *Biogeosciences Discuss.*, **2013**, 10, 17439–17468, doi:10.5194/bgd-10-17439-2013.
- Kuma, K.; Nishioka, J.; Matsunaga, K. Controls on iron (III) hydroxide solubility in seawater: the influence of pH and natural organic chelators, *Limnol. Oceangr.*, **1996**, 41, 396–407.
- Langmann, B.; Zakšek, K.; Hort, M.; Duggen, S. Volcanic ash as fertiliser for the surface ocean, *Atmos. Chem. Phys.*, **2010**, 10, 3891–3899, doi:10.5194/acp-10-3891-2010.
- Lee, D.; Moller, J.; Read, A.; Lewis, C.; Mendes, L.; Carpenter, J. Year-round measurements of nitrogen oxides and ozone in the tropical North Atlantic marine boundary layer, *J. Geophys. Res.*, **2009**, 114, D21302, doi:10.1029/2009JD011878.
- Levine, J. G.; Wolff, E. W.; Jones, A. E.; Sime, L. C. The Role of Atomic Chlorine in Glacial-Interglacial Changes in the Carbon-13 Content of Atmospheric Methane, *Geophys. Res. Lett.*, **2011**, 38, L04801, doi:10.1029/2010GL046122.
- Lim, M.; Chiang, K.; Amal, R. Photochemical Synthesis of Chlorine Gas from Iron(III) and Chloride Solution, *J. Photochem. Photobiol., A*, **2006**, 183, 126–132, doi:10.1016/j.jphotochem.2006.03.005.

Lindenthal, A.; Langmann, B.; Paetsch, J.; Lorkowski, I.; Hort, M. The ocean response to volcanic iron fertilisation after the eruption of Kasatochi volcano: a regional scale biogeochemical ocean model study, *Biogeosciences Discuss.*, **2012**, 9, 9233–9257, doi:10.5194/bgd-9-9233-2012.

Lister, M. W. and Rivington, D. E. Some Ferric Halide Complexes, and Ternary Complexes with Thiocyanate Ions, *Can. J. Chem.*, **1955**, 33, 1603–1613, doi:10.1139/v55-194.

Liu, B. and Pui, D. On the performance of the electrical aerosol analyzer, *Journal of Aerosol Science*, **1975**, 6, 249–264, doi:10.1016/0021-8502(75)90093-2.

Liu, X. and Millero, F. J. The solubility of iron in seawater, *Marine Chem.*, **2002**, 77, 43–54, doi:10.1016/S0304-4203(01)00074-3.

Luria, M.; Van Valin, C. C.; Gunter, R. L.; Wellman, D. L.; Keene, W. C.; Galloway, J. N.; Sievering, H.; Boatman, J. F. Sulfur dioxide over the western North Atlantic Ocean during GCE/CASE/WATOX, *Global Biogeochem. Cycles*, **1990**, 4, 381–393, doi:10.1029/GB004i004p00381.

Machulek, A.; Vautier-Giongo, C.; Moraes, J. E. F.; Nascimento, C. A. O.; Quina, F. H. Laser Flash Photolysis Study of the Photocatalytic Step of the Photo-Fenton Reaction in Saline Solution, *Photochem. Photobiol. Sci.*, **2006**, 82, 208–212, doi:10.1562/2005-05-28-RA-548.

Madronich, S.; Velders, G. J.; Daniel, J.; Lal, M.; McCulloch, A.; Slaper, H. Halocarbon scenarios for the future ozone layer and related consequences, *Scientific assessment of ozone depletion*, **1998**, 998, 11.1-11.38.

Mahowald, N. M.; Baker, A. R.; Bergametti, G.; Brooks, N.; Duce, R. A.; Jickells, T. D.; Kubilay, N.; Prospero, J. M.; Tegen, I. Atmospheric global dust cycle and iron inputs to the ocean, *Global Biogeochem. Cycles*, **2005**, 19, n/a, doi:10.1029/2004GB002402.

Mahowald, N. M.; Engelstaedter, S.; Luo, C.; Sealy, A.; Artaxo, P.; Benitez-Nelson, C.; Bonnet, S.; Chen, Y.; Chuang, P. Y.; Cohen, D. D. Atmospheric Iron Deposition: Global Distribution, Variability, and Human Perturbations, *Ann. Rev. Mar. Sci.*, **2009**, 1, 245–278.

Manoj, S.; Mudgal, P.; Gupta, K. Kinetics of iron(III)-catalyzed autoxidation of sulfur(IV) in acetate buffered medium, *Transition Met. Chem.*, **2008**, 33, 311-316, doi:10.1007/s11243-007-9045-8.

Martell, A. E.; Smith, R. M. Critical Stability Constants. Volume 4. Inorganic Complexes: Plenum, New York, **1976**.

Martens, C. S.; Wesolowski, J. J.; Harriss, R. C.; Kaifer, R. Chlorine loss from Puerto Rican and San Francisco Bay area marine aerosols, *J. Geophys. Res.*, **1973**, 78, 8778–8792, doi:10.1029/JC078i036p08778.

Martin, J. H. Glacial-Interglacial CO<sub>2</sub> Change: The Iron Hypothesis, *Paleoceanography*, **1990**, 5, 1–13, doi:10.1029/PA005i001p00001.

- Martin, J. H.; Fitzwater, S. E.; Gordon, R. M. Iron deficiency limits phytoplankton growth in Antarctic waters, *Global Biogeochem. Cycles*, **1990**, 4, 5–12, doi:10.1029/GB004i001p00005.
- Martínez-García, A.; Rosell-Melé, A.; Jaccard, S. L.; Geibert, W.; Sigman, D. M.; Haug, G. H. Southern Ocean dust-climate coupling over the past four million years, *Nature*, **2011**, 476, 312–315, doi:10.1038/nature10310.
- Martínez-García, A.; Sigman, D. M.; Ren, H.; Anderson, R. F.; Straub, M.; Hodell, D. A.; Jaccard, S. L.; Eglinton, T. I.; Haug, G. H. Iron fertilization of the subantarctic ocean during the last ice age, *Science*, **2014**, 343, 1347–1350, doi:10.1126/science.1246848.
- McCaffrey, M.; B. Lazar; H. D. Ho. The evaporation path of seawater and the coprecipitation of Br<sup>-</sup> and K<sup>+</sup> with halite, *SEPM JSR*, **1987**, Vol. 57, doi:10.1306/212F8CAB-2B24-11D7-8648000102C1865D.
- Meyer-Oeste, F. D., **2010**. Method for cooling the troposphere am 6/8/2010. Anmeldenr: Publication Number: WO 2010/075856 A2. Veröffentlichungsnr: Publication Number: WO 2010/075856 A2.
- Millero, F. J. Solubility of Fe(III) in seawater, *Earth Planet. Sc. Lett.*, **1998**, 154, 323–329, doi:10.1016/S0012-821X(97)00179-9.
- Millero, F. J.; Gonzalez-Davila, M.; Santana-Casiano, J. M. Reduction of Fe(III) with Sulfite in Natural Waters, *J. Geophys. Res. D*, **1995**, 100, 7235–7244, doi:10.1029/94JD03111.
- Myriokefalitakis, S.; Daskalakis, N.; Mihalopoulos, N.; Baker, A. R.; Nenes, A.; Kanakidou, M. Changes in dissolved iron deposition to the oceans driven by human activity: a 3-D global modelling study, *Biogeosciences Discuss*, **2015**, 12, 3943–3990, doi:10.5194/bgd-12-3943-2015.
- Nadtochenko, V. and Kiwi, J. Primary Photochemical Reactions in the Photo-Fenton System with Ferric Chloride. 1. A Case Study of Xylidine Oxidation as a Model Compound, *Environ. Sci. Technol.*, **1998a**, 32, 3273–3281, doi:10.1021/es970962e.
- Nadtochenko, V. A. and Kiwi, J. Photolysis of FeOH<sup>2+</sup> and FeCl<sup>2+</sup> in Aqueous Solution. Photodissociation Kinetics and Quantum Yields, *Inorg. Chem.*, **1998b**, 37, 5233–5238, doi:10.1021/ic9804723.
- Nordstrom, D. K. and Jenne, E. A. Fluorite solubility equilibria in selected geothermal waters, *Geochimica et Cosmochimica Acta*, **1977**, 41, 175–188, doi:10.1016/0016-7037(77)90224-1.
- Novič, M.; Grgić, I.; Poje, M.; Hudnik, V. Iron-catalyzed oxidation of s(IV) species by oxygen in aqueous solution: Influence of pH on the redox cycling of iron, *Atmos. Environ.*, **1996**, 30, 4191–4196, doi:10.1016/1352-2310(96)00137-9.
- O'Dowd, C. D.; Becker, E.; Kulmala, M. Mid-latitude North-Atlantic aerosol characteristics in clean and polluted air, *Atmos. Res.*, **2001**, 58, 167–185, doi:10.1016/S0169-8095(01)00098-9.

Oeste, F. D., **2003**. Tropospheric volume elements enriched with vital elements and/or protective substances am 2/20/2003. Anmeldenr: Publication Number: WO 03/013698 A2.

Veröffentlichungsnr: Publication Number: WO 03/013698 A2.

Oeste, F. D. Climate cooling by interaction of artificial Loess haze with sea salt haze induced by iron or titanium doped ship- and aircraft fuel (international patents applied), *Schriftenreihe der Deutschen Geologischen Gesellschaft Heft 4: GeoLeipzig*, **2004a**.

Oeste, F. D. Geo-engineering and hazard warning by atmospheric dispersion of aerosol particles with a desirable impact on climate and traceable gases and hazard indicators (Poster presentation), *Society of environmental Toxicology and Chemistry (SETAC) Europe, 14th Annual meeting April 16-22, Prague, Czech Republic*, **2004b**.

Oum, K. W.; Lakin, M. J.; DeHaan, D. O.; Brauers, T.; Finlayson-Pitts, B. J. Formation of Molecular Chlorine from the Photolysis of Ozone and Aqueous Sea-Salt Particles, *Science*, **1998**, 279, 74–76, doi:10.1126/science.279.5347.74.

Parkhurst, D. L. and Appelo, C. A. User's Guide to PHREEQC (Version 2): A Computer Program for Speciation, Batch-Reaction, One-Dimensional Transport, and Inverse Geochemical Calculations, **1999**.

Pechtl, S. and Glasow, R. von. Reactive chlorine in the marine boundary layer in the outflow of polluted continental air: A model study, *Geophys. Res. Lett.*, **2007**, 34, doi:10.1029/2007GL029761.

Petit, J. R.; Jouzel, J.; Raynaud, D.; Barkov, N. I.; Barnola, J.-M.; Basile, I.; Bender, M.; Chappellaz, J.; Davis, M.; Delaygue, G.; Delmotte, M.; Kotlyakov, V. M.; Legrand, M.; Lipenkov, V. Y.; Lorius, C.; PEPin, L.; Ritz, C.; Saltzman, E.; Stievenard, M. Climate and atmospheric history of the past 420,000 years from the Vostok ice core, Antarctica, *Nature*, **1999**, 399, 429–436, doi:10.1038/20859.

Pitzer, K. S. Thermodynamics of Electrolytes. I. Theoretical Basis and General Equations, *J. Phys. Chem.*, **1973**, 77, 268–277, doi:10.1021/j100621a026.

Pollard, R. T.; Salter, I.; Sanders, R. J.; Lucas, M. I.; Moore, C. M.; Mills, R. A.; Statham, P. J.; Allen, J. T.; Baker, A. R.; Bakker, Dorothee C. E.; Charette, M. A.; Fielding, S.; Fones, G. R.; French, M.; Hickman, A. E.; Holland, R. J.; Hughes, J. A.; Jickells, T. D.; Lampitt, R. S.; Morris, P. J.; Nedelec, F. H.; Nielsdottir, M.; Planquette, H.; Popova, E. E.; Poulton, A. J.; Read, J. F.; Seeyave, S.; Smith, T.; Stinchcombe, M.; Taylor, S.; Thomalla, S.; Venables, H. J.; Williamson, R.; Zubkov, M. V. Southern Ocean deep-water carbon export enhanced by natural iron fertilization, *Nature*, **2009**, 457, 577–580, doi:10.1038/nature07716.

Roberts, J. M.; Osthoff, H. D.; Brown, S. S.; Ravishankara, A. R.  $\text{N}_2\text{O}_5$  oxidizes chloride to  $\text{Cl}_2$  in acidic atmospheric aerosol, *Science*, **2008**, 321, 1059, doi:10.1126/science.1158777.

Rue, E. L. and Bruland, K. W. Complexation of Iron(III) by Natural Organic Ligands in the Central North Pacific as Determined by a new Competitive Ligand Equilibration/Adsorptive Cathodic

Stripping Voltammetric Method, *Mar. Chem.*, **1995**, 50, 117–138, doi:10.1016/0304-4203(95)00031-L.

Sadanaga, Y.; Hirokawa, J.; Akimoto, H. Formation of Molecular Chlorine in Dark Condition: Heterogeneous Reaction of Ozone with Sea Salt in the Presence of Ferric Ion, *Geophys. Res. Lett.*, **2001**, 28, 4433–4436, doi:10.1029/2001GL013722.

Sander, R. Compilation of Henry's Law Constants for Inorganic and Organic Species of Potential Importance in Environmental Chemistry, <http://www.henrys-law.org/henry.pdf>, **1999**, Version 3.

Saul, T. D.; Tolocka, M. P.; Johnston, M. V. Reactive uptake of nitric acid onto sodium chloride aerosols across a wide range of relative humidities, *J. Phys. Chem. A*, **2006**, 110, 7614–7620, doi:10.1021/jp060639a.

Shannon, R. D. Revised effective ionic radii and systematic studies of interatomic distances in halides and chalcogenides, *Acta Cryst. A (Acta Crystallographica Section A)*, **1976**, 32, 751–767, doi:10.1107/S0567739476001551.

Shi, J. and Bernhard, M. J. Kinetic Studies of Cl-Atom Reactions with Selected Aromatic Compounds using the Photochemical Reactor-FTIR Spectroscopy Technique, *Int. J. Chem. Kinet.*, **1997**, 29, 349–358, doi:10.1002/(SICI)1097-4601(1997)29:5<349::AID-KIN5>3.0.CO;2-U.

Sholkovitz, E. R.; Sedwick, P. N.; Church, T. M.; Baker, A. R.; Powell, C. F. Fractional solubility of aerosol iron: Synthesis of a global-scale data set, *Geochimica et Cosmochimica Acta*, **2012**, 89, 173–189, doi:10.1016/j.gca.2012.04.022.

Siefert, R. L.; Johansen, A. M.; Hoffmann, M. R.; Pehkonen, S. O. Measurements of trace metal (Fe, Cu, Mn, Cr) oxidation states in fog and stratus clouds, *J. Air Waste Manag. Assoc.*, **1998**, 48, 128–143, doi:10.1080/10473289.1998.10463659.

Siekmann, F. Freisetzung von photolabilen und reaktiven Halogenverbindungen aus salzhaltigen Aerosolen unter simulierten troposphärischen Reinluftbedingungen in einer Aerosol-Smogkammer, *Forschungsstelle für atmosphärische Chemie, Universität Bayreuth, Diss.*, **2008**, 3, 1.5-3.3.

Soto-Jiménez, M. F. and Páez-Osuna, F. Diagenetic processes on metals in hypersaline mudflat sediments from a subtropical saltmarsh (SE Gulf of California): Postdepositional mobility and geochemical fractions, *Applied Geochemistry*, **2008**, 23, 1202–1217, doi:10.1016/j.apgeochem.2007.11.011.

Spolaor, A.; Valletlonga, P.; Cozzi, G.; Gabrieli, J.; Varin, C.; Kehrwald, N.; Zennaro, P.; Boutron, C.; Barbante, C. Iron Speciation in Aerosol Dust Influences Iron Bioavailability over Glacial-Interglacial Timescales, *Geophys. Res. Lett.*, **2013**, 40, 1618–1623, doi:10.1002/grl.50296.

Styler, S. A. and Donaldson, D. J. Heterogeneous photochemistry of oxalic acid on Mauritanian sand and Icelandic volcanic ash, *Environmental science & technology*, **2012**, 46, 8756–8763, doi:10.1021/es300953t.

Sullivan, R. C.; Guazzotti, S. A.; Sodeman, D. A.; Tang, Y.; Carmichael, G. R.; Prather, K. A. Mineral dust is a sink for chlorine in the marine boundary layer, *Atmospheric Environment*, **2007**, 41, 7166–7179, doi:10.1016/j.atmosenv.2007.05.047.

Tang, I. N.; Tridico, A. C.; Fung, K. H. Thermodynamic and optical properties of sea salt aerosols, *J. Geophys. Res.*, **1997**, 102, 23269, doi:10.1029/97JD01806.

Thornton, J. A.; Kercher, J. P.; Riedel, T. P.; Wagner, N. L.; Cozic, J.; Holloway, J. S.; Dubé, W. P.; Wolfe, G. M.; Quinn, P. K.; Middlebrook, A. M. A Large Atomic Chlorine Source Inferred from Mid-Continental Reactive Nitrogen Chemistry, *Nature*, **2010**, 464, 271–274, doi:10.1038/nature08905.

Tobo, Y.; Zhang, D.; Nakata, N.; Yamada, M.; Ogata, H.; Hara, K.; Iwasaka, Y. Hygroscopic mineral dust particles as influenced by chlorine chemistry in the marine atmosphere, *Geophys. Res. Lett.*, **2009**, 36, L05817, doi:10.1029/2008GL036883.

Tosca, N. J.; McLennan, S. M.; Clark, B. C.; Grotzinger, J. P.; Hurowitz, J. A.; Knoll, A. H.; Schröder, C.; Squyres, S. W. Geochemical Modeling of Evaporation Processes on Mars: Insight from the Sedimentary Record at Meridiani Planum, *Earth Planet. Sci. Lett.*, **2005**, 240, 122–148, doi:10.1016/j.epsl.2005.09.042.

Troy, R. C. and Margerum, D. W. Non-metal redox kinetics: hypobromite and hypobromous acid reactions with iodide and with sulfite and the hydrolysis of bromosulfate, *Inorg. Chem.*, **1991**, 30, 3538–3543, doi:10.1021/ic00018a028.

Truesdell, A. H.; Jones, B. F. WATEQ, A Computer Program for Calculating Chemical Equilibria of Natural Waters: US Department of the Interior, Geological Survey, **1973**.

Vione, D.; Maurino, V.; Minero, C.; Calza, P.; Pelizzetti, E. Phenol Chlorination and Photochlorination in the Presence of Chloride Ions in Homogeneous Aqueous Solution, *Environ. Sci. Technol.*, **2005**, 39, 5066–5075, doi:10.1021/es0480567.

Vogt, R.; Crutzen, P. J.; Sander, R. A mechanism for halogen release from sea-salt aerosol in the remote marine boundary layer, *Nature*, **1996**, 383, 327–330, doi:10.1038/383327a0.

Wang, R.; Balkanski, Y.; Boucher, O.; Bopp, L.; Chappell, A.; Ciais, P.; Hauglustaine, D.; Peñuelas, J.; Tao, S. Sources, transport and deposition of iron in the global atmosphere, *Atmos. Chem. Phys. Discuss.*, **2015**, 15, 7645–7705, doi:10.5194/acpd-15-7645-2015.

Warneck, P. Chemistry of the natural atmosphere: Academic press, **1999**.

Weller, C.; Tilgner, A.; Bräuer, P.; Herrmann, H. Modeling the Impact of Iron–Carboxylate Photochemistry on Radical Budget and Carboxylate Degradation in Cloud Droplets and Particles, *Environ. Sci. Technol.*, **2014**, *48*, 5652–5659, doi:10.1021/es4056643.

Wennberg, P. Atmospheric chemistry: Bromine explosion, *Nature*, **1999**, *397*, 299–301, doi:10.1038/16805.

Westervelt; Moore, R. H.; Nenes, A.; Adams, P. J. Effect of primary organic sea spray emissions on cloud condensation nuclei concentrations, *Atmos. Chem. Phys.*, **2012**, *12*, 89–101, doi:10.5194/acp-12-89-2012.

Wiedensohler, A. An approximation of the bipolar charge distribution for particles in the submicron size range, *Journal of Aerosol Science*, **1988**, *19*, 387–389, doi:10.1016/0021-8502(88)90278-9.

Wittmer, J.; Bleicher, S.; Ofner, J.; Zetzsch, C. Iron(III)-induced activation of chloride from artificial sea salt aerosol, *Environ. Chem.*, **2015**, *12*, 461–475, doi: 10.1071/EN14279

Wittmer, J.; Bleicher, S.; Zetzsch, C. Iron(III)-induced activation of chloride and bromide from modeled saltpans, *J. Phys. Chem. A*, **2014**, doi:10.1021/jp508006s.

Yatsimirskii, K. B.; Vasil'ev, V. P. Instability Constants of Complex Compounds: Pergamon Press, Oxford, **1960**.

Zetzsch, C. and Behnke, W. Heterogeneous Photochemical Sources of Atomic Cl in the Troposphere, *Ber. der Bunsengesell. für physikal. Chemie*, **1992**, *96*, 488–493, doi:10.1002/bbpc.19920960351.

Zetzsch, C. and Behnke, W., **1993**. Heterogeneous Reactions of Chlorine Compounds. In: H. Niki und K.H Becker (Hg.): The Tropospheric Chemistry of Ozone in the Polar Regions, Bd. 7: Springer, Berlin Heidelberg (NATO ASI Series), 291–306. doi: [http://dx.doi.org/10.1007/978-3-642-78211-4\\_21](http://dx.doi.org/10.1007/978-3-642-78211-4_21).

Zhang, D. and Iwasaka, Y. Chlorine deposition on dust particles in marine atmosphere, *Geophys. Res. Lett.*, **2001**, *28*, 3613–3616, doi:10.1029/2001GL013333.

Zhang, J.-Z. and Millero, F. J. The rate of sulfite oxidation in seawater, *Geochim. Cosmochim. Ac.*, **1991**, *55*, 677–685, doi:10.1016/0016-7037(91)90333-Z.

Zhu, X.; Prospero, J. M.; Millero, F. J.; Savoie, D. L.; Brass, G. W. The Solubility of Ferric Ion in Marine Mineral Aerosol Solutions at Ambient Relative Humidities, *Mar. Chem.*, **1992**, *38*, 91–107, doi:10.1016/0304-4203(92)90069-M.

Zhuang, G.; Yi, Z.; Duce, R. A.; Brown, P. R. Chemistry of iron in marine aerosols, *Global Biogeochem. Cycles*, **1992**, *6*, 161–173, doi:10.1029/92GB00756.



## 6 Appendix

### 6.1a Mathematica script for OH/Cl-evaluation

(\*Temperature, T, and the activation energies units are in Kelvin, the time t is in seconds.\*)

(\*Zuordnung der, an die Messergebnisse angepassten, hier sigmoiden Funktionen\*)

$$\begin{aligned} \text{NeoP}[t] &:= 552 + (936 - 552) / (1 + (t / 39164)^{1.1535}) \\ \text{DMB}[t] &:= 322 + (437.6 - 322) / (1 + (t / 9815.8)^{1.66026}) \\ \text{TMP}[t] &:= 324.9 + (572 - 324.9) / (1 + (t / 12560)^{1.25525}) \\ \text{toluol}[t] &:= 357.5 + (714.5 - 357.5) / (1 + (t / 11515)^{0.75906}) \end{aligned}$$

(\*Aufstellung der Differentialgleichungen mit Gewichtung durch die Geschwindigkeitskonstanten. Da die angepassten Funktionen differenzierbar sind, ist dies im strengeren Sinn ein überbestimmtes lineares Gleichungssystem mit zwei Unbekannten.\*)

$$\begin{aligned} k1 &:= \text{NeoP}'[\tau] == -1.65 \cdot 10^{-12} \cdot (T / 298)^2 \cdot \exp(-1720 / T) \cdot \text{NeoP}[\tau] \cdot \text{OH} - 1.11 \cdot 10^{-10} \cdot \text{NeoP}[\tau] \cdot \text{Cl} \\ k2 &:= \text{DMB}'[\tau] == -3.37 \cdot 10^{-11} \cdot \exp(-809 / T) \cdot \text{DMB}[\tau] \cdot \text{OH} - 1.68 \cdot 10^{-10} \cdot \text{DMB}[\tau] \cdot \text{Cl} \\ k3 &:= \text{TMP}'[\tau] == -2.09 \cdot 10^{-12} \cdot \exp(-1160 / T) \cdot \text{TMP}[\tau] \cdot \text{OH} - 2.26 \cdot 10^{-10} \cdot \text{TMP}[\tau] \cdot \text{Cl} \\ k4 &:= \text{toluol}'[\tau] == -2.09 \cdot 10^{-12} \cdot \exp(322 / T) \cdot \text{toluol}[\tau] \cdot \text{OH} - 5.90 \cdot 10^{-11} \cdot \text{toluol}[\tau] \cdot \text{Cl} \end{aligned}$$

(\*Header\*)

array = {"Zeit\toh12\toh13\toh14\toh23\toh24\toh34\tMittelOH\tstdOH\tcl12\tcl13\tcl14\tcl23\tcl24\tcl34\tMittelCl\tstdCl"};

T=298; (\*Temperatur\*)

i=0;

While[i<38, (\*Zeitschritte\*)

τ=i 500; (\*Zeitauflösung\*)

e12:={Cl,OH}/.Solve[{k1,k2},{Cl,OH}]; (\*Paarweise Lösung des lin. Gleichungssystems\*)

e13:={Cl,OH}/.Solve[{k1,k3},{Cl,OH}]; (\*und Zuordnung zu den Vektoren e\*)

e14:={Cl,OH}/.Solve[{k1,k4},{Cl,OH}];

e23:={Cl,OH}/.Solve[{k2,k3},{Cl,OH}];

e24:={Cl,OH}/.Solve[{k2,k4},{Cl,OH}];

e34:={Cl,OH}/.Solve[{k3,k4},{Cl,OH}];

oh12=e12[[1,2]]; cl12=e12[[1,1]]; (\*Auflösung der Vektoren in zwei Skalare\*)

oh13=e13[[1,2]]; cl13=e13[[1,1]];

oh14=e14[[1,2]]; cl14=e14[[1,1]];

oh23=e23[[1,2]]; cl23=e23[[1,1]];

oh24=e24[[1,2]]; cl24=e24[[1,1]];

oh34=e34[[1,2]]; cl34=e34[[1,1]];

(\*Berechnung des Mittelwerts und der Standardabweichung, hier nur unter Berücksichtigung der Alkan-Toluol Lösungen\*)

Mittel=(e24+e14+e34)/3;

std=\[Sqrt](1/2((e24-Mittel)^2+(e14-Mittel)^2+(e34-Mittel)^2));

(\*Ausgabe aller Ergebnisse\*)

```

array=Append[array,{ τ,oh12,oh13,oh14,oh23,oh24,oh34,Mittel[[1,2]],std[[1,2]],
cl12,cl13,cl14,cl23,cl24,cl34,Mittel[[1,1]],std[[1,1]]}];

i++]
Export["C:\users\cer\desktop\OHCl.dat",array];

```

## 6.1b Mathematica script for OH/Cl/Br-evaluation

```

NeoP[t_]:=2108×exp(-t/110992)
DMB[t_]:=4206×exp(-t/68077)
TMP[t_]:= 528.3 + (6.64564 106 - 528.3)/(1 + exp((t + 61007.46)/8078.15))
toluol[t_]:= 60.49 + (2.6118 106 - 450.11)/(1 + exp((t + 31237.9)/5213.6))

k1:=NeoP'[τ]==-1.65 10-12 (T/298)2×exp(-1720/T)× NeoP[τ] OH - 1.11 10-10 NeoP [τ]Cl
k2:=DMB'[τ]==-3.37 10-11 ×exp(-809/T)DMB[τ] OH- 1.68 10-10 DMB[τ] Cl
k3:=TMP'[τ]==-2.09 10-12 ×exp(-1160/T)TMP [τ]OH-2.26 10-10 TMP[τ]Cl -6.8 10-15 TMP[τ] Br
k4:=toluol'[τ]==-2.09 10-12 ×exp(322/T)toluol[τ] OH - 5.90 10-11 toluol[τ] Cl-1.3 10-14 toluol[τ] Br

array={"Zeit\toh123\toh134\toh234\tMittelOH\tstdOH\tcl123\tcl134\tcl234\tMittelcl\tstdcl\tbr123\tbr134
\tbr234\tMittelbr\tstdbr"};
T=298;
i=0;
While[i<30,
τ=i 500;
e123:={Cl,OH,Br}/.Solve[{k1,k2,k3},{Cl,OH,Br}];
e134:={Cl,OH,Br}/.Solve[{k1,k3,k4},{Cl,OH,Br}];
e234:={Cl,OH,Br}/.Solve[{k2,k3,k4},{Cl,OH,Br}];

oh123=e123[[1,2]];
oh134=e134[[1,2]];
oh234=e234[[1,2]];

cl123=e123[[1,1]];
cl134=e134[[1,1]];
cl234=e234[[1,1]];

br123=e123[[1,3]];
br134=e134[[1,3]];
br234=e234[[1,3]];

Mittel=(e123+e134)/2;

std=\[Sqrt](1/1(((e123-Mittel)2+(e134-Mittel)2)));
array=Append[array,{[],oh123,oh134,oh234, Mittel[[1,2]],std[[1,2]],
cl123,cl134,cl234,Mittel[[1,1]],std[[1,1]],br123,br134,br234,Mittel[[1,3]],std[[1,3]]}];

i++]
Export["C:\Users\cer\Desktop\OHCl.dat",array];

```

## 6.2a Classifier operating software

```
10 !---- CLASSIFIER STEUERPROGRAMM -----
20 !
30 !----- SCAN - MODE -----
40 !
50 OPTION BASE 1
60 DIM Version$[50]
70 !
80 Version$=" VECTRA-VERSION August 2009"
90 !
100 !
110 !
120 !---- OHNE MOB_DAT - ARRAY -----
130 ! 8
140 !---- U-in,U_out über PCL812-D/A-A/D-Karte -----
150 !
160 !
170 !
180 ! 8.10.91: MIT OFFSET-MESSUNG ,
190 ! 8.10.91: VERSCH.CL_ANZ FÜR D+A-MODE ,
200 ! 22.10.91: MIT TEMP.-MESS. CLASSIFIER
210 ! 2.12.91: MIT OFFSET D/A-WANDLER
220 ! 26. 2.92: NEUKAL. A/D-WANDLER
230 ! .12.94: AE16:NEU AUS PHYSIK,ZERO+SPAN
240 ! 5. 1.95: NEUE PT100-KAL.-DATEN
250 ! 6. 2.95: EINZEL-KAL. 8 KANAL-A/D
260 ! 21.11.97: CNC-TYLAN-STEUERUNG ÜBER D/A-KARTE
270 ! 18. 2.98: SLEEP-MODUS FÜR CNC-FLOW
280 !
290 ! 17. 1.05: NTC-MESSUNG MIT KEITHLEY195A
300 !
310 ! 6. 8.09: Lamda-Berechnung mit akt. Temperatur + Luftdruck (Zeile 1690)
320 !
330 COM /In/Zero(8),Span(8)
340 COM Dp(1000),Zp(1000),Dpo(1000),Dpu(1000)
350 COM Flag(1000),Vor_flag(1000),Sp(1000)
360 COM Dp_st,Punkte
370 COM Karte,Err,Messbereich
380 COM Z(1000),D(1000),U(1000),Faktor(1000),Cp(1000)
390 COM Time$(30)[20]
400 COM Zeit$[10],Ad$[200]
410 COM U_vor(50),Cmax(7),Cstep(7)
420 INTEGER DI(20),G1(1:256,1:2200),G2(1:256,1:2200),G3(1:256,1:2200)
430 INTEGER G4(1:256,1:2200),G5(1:256,1:2200),G6(1:256,1:2200),G7(1:256,1:2200),Gr(1:256,1:2200)
440 REAL Spannung
450 COM Keith$[15]
460 DIM Tt(16),Uin(8)
470 INTEGER Test(6),Kanal
480 DEG
490 !
500 !MASS STORAGE IS "C:\HPBASIC\CLASS\Seesalz"
510 !
520 First=0
530 !
540 !CONTROL CRT,10;0 ! Cursor aus
550 !
560 !
570 ALPHA HEIGHT 24
580 !
590 !
600 !-----
610 !
620 PRINTER IS 1
```

```

630 PRINT "----- ";Version$;" -----"
640 PRINT ""
650 !PRINT ""
660 PRINT "---- U_out, U_in, U_NTC über PCL812 D/A-A/D-Karte --"
670 !PRINT ""
680 PRINT ""
690 !LIST 260,290
700 !
710 !
720 Qa=.30    ! Aerosolfow in l/min
730 Qv=5.0    ! Verdünnungsflow in l/min
740 !
750 Karte=6
760 Messbereich=1
770 !
780 Off_anz=75
790 T_anz=100
800 Cnc_sleep$="N"
810 Cnc_wake_time=180
820 Cnc_flow_volth=.85   ! normaler Flow
830 Cnc_flow_voltl=.08   ! reduzierter Flow
840 Cnc_status$="W"      ! "W" für Wach, "S" für Schlaf
850 Cnc$="N"             ! "J" für CNC-File
860 Cnc_speich_stat=0
870 !
880 IF Cnc_sleep$="J" THEN GOSUB Cnc_wake_up
890 !
900 Raster=2^(1/12)
910 !Raster=2^(1/6)
920 !
930 U_max=10
940 Vor_punkte=10 ! Anz. Spannungen für Vorlauf
950 Diff=7
960 !
970 Sumvol$="J"
980 Dichte=1 ! .85
990 Sumvolfaktor=1.04 ! 257% bzw. 104% des Messbereichs , 2.57 fuer 2l/min, 1.04 fuer 5l/min
1000 !
1010 Gr_anz=7
1020 !
1030 Cmax(1)=1000
1040 Cstep(1)=100
1050 Cmax(2)=500
1060 Cstep(2)=100
1070 Cmax(3)=200
1080 Cstep(3)=20
1090 Cmax(4)=100
1100 Cstep(4)=10
1110 Cmax(5)=50
1120 Cstep(5)=5
1130 Cmax(6)=5000
1140 Cstep(6)=1000
1150 Cmax(7)=2000
1160 Cstep(7)=500
1170 Gr_nr=3
1180 !
1190 Cc_fit$="N"
1200 !
1210 Tylan=(Qv-.106)/1.136
1220 !
1230 PRINT " AEROSOLFLOW: ";Qa;"l/min  SHEATH-AIR: ";Qv;"l/min  SHEATH-AIR-TYLAN-SOLL: ";DROUND(Tylan,3);"V"
1240 PRINT ""
1250 !PRINT " Cc-FITFUNKTION VOM 5.7.90 , MAX. ABWEICHUNG 0.8% ( 16-1000 nm )"
1260 !
1270 !
1280 !

```

```

1290 Qa=Qa*1000/60 1300 Qv=Qv*1000/60
1310 !
1320 !
1330 Iz_cl=900 ! Intervallzeit Class. in sec
1340 !
1350 !----- Cl_anz für KEITHLEY : 2 l/min : Anz=11 Diff=7 od. Anz=15 Diff=5 -----
1360 ! " " " 5 " : Anz=17 Diff=4
1370 !----- Cl_anz für HPIB-BOX: 2 l/min : Anz=92 Diff=4 A-MODE
1380 !----- Cl_anz für HPIB-BOX: 2 l/min : Anz= Diff= D-MODE
1390 !
1400 Cl_anz1=75 ! Mess. pro Messpunkt (D-MODE)
1410 Cl_anz2=75 ! Mess. pro Messpunkt (A-MODE)
1420 !
1430 Cl_stab=3 ! Stabilisierungszeit vor 1.Mess.
1440 !
1450 Ez_cnc=400 ! " CNC in sec
1460 Iz_cnc=401 ! Intervallzeit CNC-Mess in sec
1470 Cnc_anz=75 ! Messabfragen pro Messung
1480 Cnc_stab=0 ! wie Cl_stab
1490 !
1500 Speich$="J"
1510 Auto$="N" ! Autom.Dauermessung
1520 !
1530 !
1540 !Zero ! Für 8-Kanal A/D-Wandler
1550 !Span ! " " 13.1.95
1560 !
1570 Uin_min=-.04
1580 Uin_max=10.05
1590 !
1600 !
1610 MAT Zero=(0) !(-.0432)
1620 Zero(2)=-.002
1630 !
1640 MAT Span=(1) !(1.026)
1650 !D_a_off=-.008 ! Für D/A-Wandler
1660 !
1670 !
1680 Richtung=0
1690 Messung=0
1700 Lam0=5.94E+1 ! mittl.freie Weglänge bei 1013mbar und 273K
1710 Luftdruck=970 ! mbar
1720 Tempera=298 ! K
1730 !
1740 Lam=Lam0*1013/Luftdruck*Tempera/273 ! nach Reist
1750 !
1760 !
1770 PRINT ""
1780 PRINT DATE$(TIMEDATE),TIME$(TIMEDATE)
1790 PRINT ""
1800 !
1810 !----- KEYS -----
1820 !
1830 Loop: !
1840 ON KEY (1) LABEL "NULLVOLT" GOSUB Nullvolt
1850 ON KEY (3) LABEL "MAXVOLT" GOSUB Maxvolt
1860 ON KEY (2) LABEL "PARAMET." GOTO Parameter
1870 GOTO Loop
1880 !
1890 !
1900 !
1910 Parameter: !
1920 Dp_st=500
1930 !INPUT "Bei welcher Part.grösse soll begonnen werden [nm] ?",Dp_st
1940 !
1950 Punkte=100

```

```

1960 !INPUT "Anzahl der Messpunkte?",Punkte
1970 !
1980 REDIM D(Punkte)
1990 REDIM Zp(Punkte)
2000 REDIM Cp(2*Punkte+Vor_punkte)
2010 REDIM U(2*Punkte+2*Vor_punkte)
2020 !
2030 MAT U=(0)
2040 MAT Cp=(0)
2050 MAT Dp=(0)
2060 !
2070 !
2080 GOTO 2200
2090 !
2100 !
2110 Zeit: !
2120 LINPUT "Datum (DD MMM YYYY) ?",Dat$ 2130 SET TIMEDATE DATE(Dat$)
2140 LINPUT "Zeit (HH:MM) ?",Zeit$
2150 SET TIME TIME(Zeit$)
2160 OFF KEY 3
2170 GOTO Loop
2180 !
2190 !-----
2200 !
2210 !
2220 !
2230 C_st=1+2.492*Lam/Dp_st+.84*Lam/Dp_st*EXP(-.43*Dp_st/Lam)
2240 Zp_st=1.6E-19*C_st*1.E+7/(3*PI*1.831E-4*Dp_st*1.E-7)
2250 !
2260 !
2270 Spannungsreihe: !
2280 !
2290 IMAGE "Dp:",DDDD.D," Zp:",D.DDDE," U:",DDDD.D," Z(I)/Z(1):",DDD.DDD," I:",DDD
2300 !
2310 !
2320 !
2330 FOR I=1 TO Punkte
2340 !
2350 Z(I)=Zp_st*Raster^(I-1)
2360 !
2370 Zps=Z(I)
2380 !
2390 IF Cc_fit$="J" THEN
2400   Ccc=.9156-5026*Zps-1.454E+5*Zps^2+5.447E+4*Zps^(1.630)+1570*Zps^(.7512)
2410   Dps=1.6E-19*Ccc*1.E+7/(3*PI*1.831E-4*Zps*1.E-7)
2420 ELSE
2430   CALL Dp(Zps,Dps,Lam)
2440 END IF
2450 !
2460 D(I)=Dps
2470 U(I)=Qv*2.64E-3/Z(I)
2480 Sp(I)=U(I)
2490 PRINT USING 2290;D(I),Z(I),U(I),Z(I)/Z(1),I
2500 NEXT I
2510 !
2520 !
2530 !
2540 !
2550 !-- SPANNUNGEN FÜR VORLAUF -----
2560 !
2570 FOR I=1 TO Vor_punkte
2580   U_vor(Vor_punkte+1-I)=U(1)*Raster^
2590 NEXT I
2600 !
2610 FOR I=1 TO Vor_punkte
2620   !PRINT I,INT(U_vor(I)),U_vor(I)/U(1)

```

```

2630 NEXT I
2640 !
2650 !-----
2660 !
2670 !
2680 ! ERZUGUNG DER SPANNUNGSREIHE EINSCHLIESS
2690 ! LICH VOR- UND NACHLAUF
2700 !
2710 !
2720 V=Vor_punkte
2730 P=Punkte
2740 !
2750 IMAGE DDD,XX,D,X,D,XX,DDDDD
2760 !
2770 FOR I=1 TO (P*2+V*2)
2780 !
2790 IF I<=V THEN
2800 Flag(I)=0
2810 Vor_flag(I)=1
2820 U(I)=U_vor(I)
2830 END IF
2840 !
2850 IF I>V AND I<=(V+P) THEN
2860 Flag(I)=1
2870 Vor_flag(I)=0
2880 U(I)=Sp(I-V)
2890 Dp(I)=D(I-V)
2900 END IF      2910 !
2920 IF I>(V+P) AND I<=(V+2*P) THEN
2930 Flag(I)=1
2940 Vor_flag(I)=0
2950 U(I)=Sp(V+2*P+1-I)
2960 Dp(I)=D(V+2*P+1-I)
2970 END IF      2980 !
2990 IF I>(V+2*P) THEN
3000 Flag(I)=1
3010 Vor_flag(I)=1
3020 U(I)=U_vor(2*V+2*P+1-I)
3030 END IF
3040 !
3050 !PRINT USING 2320;I,Flag(I),Vor_flag(I),U(I)
3060 !
3070 NEXT I
3080 !
3090 GOSUB Maxvolt
3100 !
3110 !-----
3120 !
3121 IF U(11)>10000 THEN
3122 BEEP
3123 BEEP
3125 CLEAR SCREEN
3126 PRINT "#####
3127 PRINT "OBACHT !! SPANNUNG > 10kV ";U(11)
3128 PRINT "#####
3129 BEEP
3130 BEEP
3131 PAUSE
3133 END IF
3134 !
3140 PRINT ""
3150 PRINT "'CONTINUE' wenn O.K.    Umax= ";INT(U(11));" V"
3160 PRINT ""
3170 !
3180 !-----
3190 !

```

```

3200 PAUSE
3210 !
3220 IF Speich$="J" THEN
3230 INPUT "Versuchsbezeichnung?",Vers$
3240 !INPUT "Anzahl der Messungen?",Anz 3250 Anz=1
3260 END IF
3270 !
3280 !
3290 PRINT ""
3300 PRINT ""
3310 PRINT "----- CLASSIFIER ----- ";Vers$; " --- ";DATE$(TIMEDATE)
3320 PRINT ""
3330 PRINT ""
3340 !
3350 !
3360 !
3370 !----- File anlegen -----
3380 IF Speich$="J" THEN
3390 CREATE BDAT Vers$&"C",INT(Anz*(2*P+V)/20)+2
3400 ASSIGN @F1 TO Vers$&"C"
3410 OUTPUT @F1;Vers$,DATE$(TIMEDATE),Punkte,Raster,Ez,Cl_anz,Vor_punkte,Qv,Qa
3420 OUTPUT @F1;D(*)
3430 OUTPUT @F1;Zp(*)
3440 END IF
3450 !
3460 !
3470 !-----
3480 !
3490 IF Speich$="J" AND Cnc$="J" THEN
3500 CREATE BDAT Vers$&"CN",3
3510 ASSIGN @F2 TO Vers$&"CN"
3520 END IF
3530 !
3540 !
3550 GOSUB Bas_graph
3560 !
3570 Gr_nr=1
3580 GLOAD G1(*)
3590 MAT Gr=G1
3600 !
3610 WINDOW Xmin,Xmax,0,Cmax(1)
3620 !
3630 !
3640 !
3650 !
3660 St: ! ----- CLASSIFIER-STEUERUNG -----
3670 !
3680 !
3690 Messung=Messung+1
3700 !
3701 Colorpen=Messung MOD 15
3702 IF Colorpen=0 THEN Colorpen=7
3703 !
3710 IF Speich$="N" THEN
3720 PRINT "-----!! SPEICHERN IST AUS !!-----"
3730 END IF
3740 !
3750 IF Auto$<>"J" THEN
3760 PRINT "' KEY 4' FÜR MESSUNG";Messung
3770 ELSE
3780 PRINT "---- AUTOM.MESSWIEDERHOLUNG ----"
3790 END IF
3800 !
3810 Loop1:
3820 LOOP
3830 IF Auto$="J" THEN

```

```

3840 IF Cnc_sleep$="J" THEN
3850   IF (TIMEDATE+Cnc_wake_time) MOD lz_cl<1 THEN GOSUB Cnc_wake_up
3860 END IF
3870 IF TIMEDATE MOD lz_cl<1 THEN Messbeginn
3880 DISP INT(lz_cl-(TIMEDATE MOD lz_cl))
3890 ELSE
3900 ON KEY 4 LABEL "MESSEN" GOTO Messbeginn
3910 END IF
3920 !
3930 ON KEY 2 LABEL "OFFS: ON" GOTO Offset
3931 IF Auto$="n" OR Auto$="N" THEN
3940 ON KEY 7 LABEL "Auto$:N" GOSUB Autoj
3941 ELSE
3942 ON KEY 7 LABEL " Auto$:J" GOSUB Auton
3943 END IF
3950 ON KEY 5 LABEL "TEMP: ON" GOTO Temp_sub
3960 ON KEY 8 LABEL "GRAPH<->" GOSUB Gr_wechsel
3970 IF Cnc_sleep$="J" THEN
3980 IF Cnc_status$="W" THEN
3990 ON KEY 6 LABEL "CNC-FLOWist HOCH" GOSUB Cnc_sleep
4000 ELSE
4010 ON KEY 6 LABEL "CNC-FLOWist LOW" GOSUB Cnc_wake_up
4020 END IF
4030 END IF
4040 END LOOP
4050 ! 4051 Autoj: !
4052 Auto$="J"
4053 RETURN
4054 !
4055 Auton: !
4056 Auto$="N"
4057 RETURN
4060 !
4070 Messbeginn:!-----
4080 !
4090 !
4100 Temp1=0
4110 !
4120 Sumvol=0
4130 !
4140 GOSUB Sub_temp
4150 !
4160 !PRINT USING 4330;Temp1
4170 !
4180 IMAGE (SDDD.DD,"^3C",XX)
4190 !
4200 !
4210 !
4220 !-- LESEN CNC-EXP. FUER CL_ANZ-ZUWEISUNG --
4230 !
4240 !
4250 Kanal=15
4260 GOSUB U_in
4270 IF Uin(3)>9.999 THEN Uin(3)=9.999
4280 IF Uin(3)<0 THEN Uin(3)=0
4290 Exp=INT(Uin(3)+.5)
4300 IF Exp>6 THEN Exp=6
4310 !
4320 IF Exp<=2 THEN
4330   Cl_anz=Cl_anz1
4340 ELSE
4350   Cl_anz=Cl_anz2
4360 END IF
4370 !
4371 ALPHA PEN Colorpen
4373 !

```

```

4380 !PRINT ""
4390 !PRINT "EXP:";Exp;" Cl_anz=";Cl_anz
4400 !PRINT ""
4410 !
4420 Step=1
4430 ! 4440 Start=1
4450 Ende=P*2+V*2
4460 !
4470 !
4480 Altkonz=0
4490 !
4500 GLOAD Gr(*)
4510 PRINT "MESSUNG :";Messung;" ";TIME$(TIMEDATE);" ";Vers$
4520 !
4530 Cp_max=0
4540 Dp_max=0
4550 !
4560 K=1
4570 !
4580 !-----
4590 !---- BEGINN DER MESSSCHLEIFE -----
4600 !-----
4610 !
4620 Nun=TIMEDATE
4630 !
4640 FOR I=Start TO Ende
4650 !
4660 ON KEY 8 LABEL "GRAPH<->" GOSUB Gr_wechsel
4670 !
4680 Spannung=U(I)/1000
4690 IF Spannung>U_max THEN Spannung=U_max
4700 CALL U_out(Spannung)
4710 !
4720 !
4730 Cl_mess: !-----
4740 !
4750 Cps=0
4760 !
4770 FOR J=1 TO Cl_anz
4780 !
4790 !
4800 DISABLE
4810 !
4820 Kanal=14
4830 GOSUB U_in
4840 Altkonz=Konz
4850 !IF Uin(2)>Uin_max THEN Uin(2)=Uin_max
4860 !IF Uin(2)<Uin_min THEN Uin(2)=Uin_min
4870 Konz=Uin(2)-Zero(2)
4880 !
4890 !
4900 !
4910 Kanal=15
4920 GOSUB U_in
4930 !
4940 ENABLE
4950 !
4960 IF Uin(3)>Uin_max THEN Uin(3)=Uin_max
4970 IF Uin(3)<Uin_min THEN Uin(3)=Uin_min
4980 Exp=INT(Uin(3)+.5)
4990 !
5000 Cp(K)=Konz*10^Exp
5010 !
5020 !IF Cp(K)<0 THEN Cp(K)=0
5030 !
5040 !LORG 8

```

```

5050 !MOVE Xmax,Cp(K)
5060 !LABEL "-"
5070 !PEN -1
5080 !MOVE Xmax,Cp(K)
5090 !LABEL "-"
5100 !PEN 1
5110 !
5120 !
5130 !----- COUNT-MODE Korrektur -----
5140 !
5150 IF Exp<=2 THEN
5160   Dkonz=Cp(K)
5170   FOR L=1 TO 4
5180     Dkonz=Cp(K)*EXP(Dkonz*5*3.5E-5)
5190   NEXT L
5200   Cp(K)=Dkonz
5210 END IF
5220 !
5230 !-----
5240 !
5250 Cps=Cps+Cp(K)
5260 !
5270 NEXT
5280 !
5290 Cp(K)=Cps/Cl_anz
5300 !
5310 IF Cp(K)>Cp_max THEN
5320   Cp_max=Cp(K)
5330   IF I>Diff THEN
5340     Dp_max=Dp(I-Diff)
5350   END IF
5360 END IF
5370 !
5380 !
5390 IMAGE 18A,XX,DDD,XX,SD.DDE V
5400 IMAGE 6A,DD,XX,DDDD,3A,XX,DDDD.D,3A,XX,SD.DDE,5A,XX,SD.DDE,X,10A,X,SD.DDE,18A
5410 !
5420 LORG 5
5430 !IF Messung MOD 2=0 THEN LINE TYPE 4
5440 !
5450 PEN Colorpen
5460 !
5470 IF (K-Diff)>1 AND (K-Diff)<=(2*P) THEN
5480   IF K>Punkte THEN
5490     LINE TYPE 4
5500   ELSE
5510     LINE TYPE 1
5520   END IF
5530 !
5540 MOVE LGT(Dp(I-1-Diff)),Cp(K-1)
5550 DRAW LGT(Dp(I-Diff)),Cp(K)
5560 !
5570 IF Sumvol$="J" THEN
5580   Dplgt=LGT(Dp(I-Diff))
5590   E1=(-42.3+58.2*Dplgt-13.7*Dplgt^2)/100
5600   Sumvoli=(Dp(I-Diff)/2000)^3*4/3*PI*Cp(K)/E1*Dichte/Sumvolfaktor/1000
5601   IF Sumvoli>=0 THEN
5610     Sumvol=Sumvol+Sumvoli
5611   END IF
5620   Sumvol_korr=Sumvol/(.95+7.5E-4*Dp_max)
5630 END IF
5640 END IF
5650 !
5651 ALPHA PEN INT(Messung MOD 8)
5660 IF Vor_flag(I)=1 THEN
5670   DISP USING 5390;"EINSCHWINGRAMPE ";I,Cp(K)

```

```

5680 ELSE
5690   DISP USING 5400;"Mess:";Messung,U(I)," V",Dp(I)," nm",Cp(K)," cm-3",Sumvol," mg/m3 ",Sumvol_korr," mg/m3 korrigiert"
5700 END IF
5710 !
5720 LINE TYPE 1
5730 PRINTER IS 1
5750 !
5760 !
5770 IF K=Punkte THEN
5780   Feuchte=0
5790   FOR M=1 TO 10
5800     Kanal=13
5810     GOSUB U_in
5820     IF Uin(1)>Uin_max THEN Uin(1)=Uin_max 1
5830     IF Uin(1)<Uin_min THEN Uin(1)=Uin_min 8
5840     Feuchte=Feuchte+(Uin(1)*Span(1)-Zero(1))*100
5850 NEXT M
5860 Feuchte=Feuchte/10
5870 PRINT "REL.FEUCHTE :";DROUND(Feuchte,4);"%"
5880 IF Sumvol$="J" THEN
5890   PRINT "geschaetzte Konzentration: ";DROUND(Sumvol,3);" mg/m3 ";"      ";DROUND(Sumvol_korr,3);" mg/m3 korrigiert"
5900   PRINT "Dp_max : ";DROUND(Dp_max,3);" nm    Cp_max : ";DROUND(Cp_max,3);" cm-3"
5910   Sumvol=0
5911   Sumvol_korr=0
5920   Cp_max=0
5930   Dp_max=0
5940 END IF
5950 END IF
5960 !
5970 IF Flag(I)=1 THEN K=K+1
5980 !
5990 NEXT I
6000 !
6010 K=K-1
6020 !
6030 REDIM Cp(K)
6040 !
6050 !
6060 !---- ENDE DER MESSSCHLEIFE -----
6070 !
6080 IF Sumvol$="J" THEN
6090   PRINT "geschaetzte Konzentration: ";DROUND(Sumvol,3);" mg/m3 ";"      ";DROUND(Sumvol_korr,3);" mg/m3 korrigiert"
6100   PRINT "Dp_max : ";DROUND(Dp_max,3);" nm    Cp_max : ";DROUND(Cp_max,3);" cm-3"
6110   Sumvol=0
6111   Sumvol_korr=0
6120 END IF
6130 !
6140 GOSUB Sub_temp
6150 !
6160 !
6170 !
6180 Delta_zeit=TIMEDATE-Nun
6190 PRINT "MESSZEIT :";Delta_zeit;" s"
6200 PRINT ""
6210 !
6220 Zeit$=TIME$(TIMEDATE)
6230 !
6240 IF Speich$="J" THEN
6250   BEEP 1200,.2
6260   BEEP 1000,.2
6270   BEEP 1200,.2
6280   OUTPUT @F1;Messung,Zeit$,Feuchte
6290   OUTPUT @F1;Temp1,Temp1,Temp1,Off,Res1,Res2,Res3
6300   OUTPUT @F1;Cp(*)

```

```

6310 END IF
6320 !
6330 IF Auto$="J" AND Cnc_sleep$="J" THEN GOSUB Cnc_sleep
6340 GSTORE Gr(*)
6350 !
6360 !CLEAR SCREEN
6370 !
6380 GOSUB St
6390 !
6400 !
6410 !----- GRAPHIK -----
6420 !
6430 !
6440 Bas_graph: !
6450 !
6460 !
6470 !
6480 DATA 20,30,50,70,100,200,300,500,700,1000,2000
6490 !
6500 DI_anz=11
6510 REDIM DI(DI_anz)
6520 !
6530 RESTORE 6480
6540 READ DI(*)
6550 !
6560 Xmax=LGT(D(1))
6570 Xmin=LGT(D(Punkte))
6580 !
6590 Jetzt=TIME(TIME$(TIMEDATE))
6600 CLEAR SCREEN
6610 GINIT
6611 PLOTTER IS CRT,"INTERNAL";COLOR MAP
6612 SET PEN 8 INTENSITY 0,1,.3
6613 !
6620 FOR L=1 TO Gr_anz
6630 Cp_max=Cmax(L)
6640 Cp_step=Cstep(L)
6650 GCLEAR
6660 VIEWPORT 20,90,60,98
6670 FRAME
6680 WINDOW Xmin,Xmax,0,Cp_max
6690 CSIZE 3,.
6700 CLIP OFF
6710 FOR J=1 TO DI_anz
6720 IF LGT(DI(J))<Xmin OR LGT(DI(J))>Xmax THEN 6810
6730 LDIR 0
6740 LORG 4
6750 MOVE LGT(DI(J)),0
6760 DRAW LGT(DI(J)),Cp_max/50
6770 LDIR 90
6780 LORG 8
6790 MOVE LGT(DI(J)),0
6800 LABEL DI(J)
6810 NEXT J
6820 !
6830 LDIR 0
6840 FOR J=0 TO Cp_max STEP Cp_step
6850 LORG 8
6860 MOVE Xmin,J
6870 LABEL J
6880 LORG 2
6890 MOVE Xmin,J
6900 DRAW (Xmax-Xmin)/40+Xmin,J
6910 NEXT J
6920 LORG 5
6930 SELECT L

```

```

6940 CASE 1
6950 GSTORE G1(*)
6960 CASE 2
6970 GSTORE G2(*)
6980 CASE 3
6990 GSTORE G3(*)
7000 CASE 4
7010 GSTORE G4(*)
7020 CASE 5
7030 GSTORE G5(*)
7040 CASE 6
7050 GSTORE G6(*)
7060 CASE 7
7070 GSTORE G7(*)
7080 END SELECT
7090 NEXT L
7100 !
7110 GCLEAR
7120 !
7130 RETURN
7140 !
7150 !
7160 !-----
7170 !
7180 !
7190 Gr_wechsel: !
7200 !
7210 SELECT Gr_nr
7220 CASE 1
7230 GSTORE G1(*)
7240 CASE 2
7250 GSTORE G2(*)
7260 CASE 3
7270 GSTORE G3(*)
7280 CASE 4
7290 GSTORE G4(*)
7300 CASE 5
7310 GSTORE G5(*)
7320 CASE 6
7330 GSTORE G6(*)
7340 CASE 7
7350 GSTORE G7(*)
7360 END SELECT
7370 !
7380 !
7390 !
7400 Gr_nr=(Gr_nr MOD Gr_anz)+1
7410 !
7420 SELECT Gr_nr
7430 CASE 1
7440 GLOAD G1(*)
7450 MAT Gr=G1
7460 Cp_max=Cmax(1)
7470 CASE 2
7480 GLOAD G2(*)
7490 MAT Gr=G2
7500 Cp_max=Cmax(2)
7510 CASE 3
7520 GLOAD G3(*)
7530 MAT Gr=G3
7540 Cp_max=Cmax(3)
7550 CASE 4
7560 GLOAD G4(*)
7570 MAT Gr=G4
7580 Cp_max=Cmax(4)
7590 CASE 5

```

```

7600 GLOAD G5(*)
7610 MAT Gr=G5
7620 Cp_max=Cmax(5)
7630 CASE 6
7640 GLOAD G6(*)
7650 MAT Gr=G6
7660 Cp_max=Cmax(6)
7670 CASE 7
7680 GLOAD G7(*)
7690 MAT Gr=G7
7700 Cp_max=Cmax(7)
7710 END SELECT
7720 WINDOW Xmin,Xmax,0,Cp_max
7730 RETURN
7740 !
7750 !
7760 !-----
7770 !
7780 !
7790 Offset: !
7800 !
7810 !
7820 PRINT "----- OFFSETMESSUNG CNC -----"
7830 !
7840 IF Cnc_sleep$="J" AND Cnc_status$="S" THEN GOSUB Cnc_wake_up
7850 OFF KEY 6
7860 !
7870 IF Speich$="J" AND Cnc$="J" THEN
7880 IF Cnc_speich_stat=0 THEN
7890 ON KEY 7 LABEL "SPEICH. CNC EIN" GOSUB Speich_cnc_ein
7900 ELSE
7910 ON KEY 7 LABEL "SPEICH. CNC AUS" GOSUB Speich_cnc_aus
7920 END IF
7930 END IF
7940 !
7950 Offs=0
7960 Rf=0
7970 !
7980 FOR J=1 TO Off_anz
7990 !
8000 ON KEY 2 LABEL "OFFS:OFF" GOTO Exit1
8010 !
8020 !
8030 !
8040 IF (Iz_cl-TIMEDATE MOD Iz_cl)<10 AND Auto$="J" THEN Exit1
8050 !
8060 !
8070 !
8080 Kanal=14
8090 GOSUB U_in
8100 !PRINT Uin(2)
8110 IF Uin(2)>Uin_max THEN Uin(2)=Uin_max
8120 IF Uin(2)<Uin_min THEN Uin(2)=Uin_min
8130 Altkonz=Konz
8140 Konz=Uin(2)
8150 !PRINT Konz
8160 !
8170 IF Sp_out=0 THEN DISP "---- OBACHT !! NULLVOLT ----- ";
8180 DISP INT(Iz_cl-(TIMEDATE MOD Iz_cl))
8190 !
8200 !
8210 Kanal=15
8220 GOSUB U_in
8230 IF Uin(3)>Uin_max THEN Uin(3)=Uin_max
8240 IF Uin(3)<Uin_min THEN Uin(3)=Uin_min
8250 !

```

```

8260 Exp=INT(Uin(3)+.5)
8270 !
8280 Of=Konz*10^Exp
8290 !
8300 !----- COUNT-MODE Korrektur -----
8310 !
8320 IF Exp<=2 THEN
8330   Dkonz=Of
8340   FOR L=1 TO 4
8350     Dkonz=Of*EXP(Dkonz*5*3.5E-5)
8360   NEXT L
8370   Of=Dkonz
8380 END IF
8390 !
8400 !
8410 Offs=Offs+Of
8420 !
8430 !
8440 !----- FEUCHTEMESSUNG -----
8450 !
8460 !
8470 Kanal=13
8480 GOSUB U_in
8490 !Uin(1)=VAL(Ad$[1,9])
8500 IF Uin(1)>Uin_max THEN Uin(1)=Uin_max
8510 IF Uin(1)<Uin_min THEN Uin(1)=Uin_min
8520 Rf=Rf+(Uin(1)*Span(1)-Zero(1))*100
8530 NEXT J
8540 !
8550 Off=Offs/Off_anz
8560 Rf=Rf/Off_anz
8570 !
8580 PRINT TIME$(TIMEDATE);
8590 !
8600 PRINT " OFFSET CNC :";DROUND(Off,4);" r.F.: ";DROUND(Rf,4);" %"
8610 !
8620 !
8630 IF Cnc_speich_stat=1 THEN
8640   OUTPUT @F2;TIME$(TIMEDATE),Off
8650 END IF
8660 GOTO 7860
8670 !
8680 Exit1: !
8690 !
8700 GOTO Loop1
8710 !
8720 !
8730 !-----
8740 !
8750 Cnc_wake_up: !
8760 DISABLE
8770 Spannung=Cnc_flow_volth
8780 CALL U_out(Spannung)
8790 !CALL U_out(Spannung)
8800 PRINT ""
8810 PRINT "CNC-FLOW: HOCH ";Cnc_flow_volth
8820 PRINT ""
8830 WAIT .7
8840 Cnc_status$="W"
8850 ENABLE
8860 RETURN
8870 !
8880 !-----
8890 !
8900 Cnc_sleep: !
8910 DISABLE

```

```

8920 Spannung=Cnc_flow_voltl
8930 CALL U_out(Spannung)
8940 !CALL U_out(Spannung)
8950 PRINT "CNC-FLOW: NIEDRIG ";Cnc_flow_voltl
8960 Cnc_status$="S"
8970 ENABLE
8980 RETURN
8990 !
9000 !-----
9010 !
9020 Speich_cnc_ein:!
9030 Cnc_speich_stat=1
9040 RETURN
9050 !
9060 Speich_cnc_aus:!
9070 Cnc_speich_stat=0
9080 RETURN
9090 !
9100 Maxvolt:!
9110 !
9120 Spannung=MAX(U(*))/1000
9130 IF Spannung>10 THEN Spannung=10
9140 Sp_out=Spannung
9150 CALL U_out(Spannung)
9160 RETURN
9170 !
9180 !
9190 !-----
9200 !
9210 !
9220 Nullvolt:!
9230 !
9240 Spannung=0
9250 !
9260 Sp_out=Spannung
9270 CALL U_out(Spannung)
9280 !
9290 !
9300 RETURN
9310 !
9320 !-----
9330 !
9340 !
9350 Temp_sub:!
9360 !
9370 GOSUB Sub_temp
9380 !
9390 ON KEY 5 LABEL "TEMP:OFF" GOTO Loop1
9400 GOTO Temp_sub
9410 !
9420 !
9430 Sub_temp:!-----
9440 !
9450 !
9460 DISP "---- TEMPERATURMESSUNG ----"
9470 !
9480 ENABLE
9490 !
9500 !
9510 !-- NTC-FAKTOREN ( Bereich: -24 bis +30°C ) : 12.1.05 -----
9520 !
9530 Ntc_off=62.46
9540 Ntc_span1=59.5
9550 Ntc_span2=5.876
9560 !
9570 !

```

```

9580 Mess: !
9590 !
9600 Temp1=0
9610 !
9620 -- Spannungsversorgung für NTC über D/A-PCL812-Karte 12.04.06 --
9630 !
9640 Spannung=5
9650 Sp_out=Spannung*409.5/1.015
9660 H_byte=INT(Sp_out DIV 256)
9670 L_byte=INT(Sp_out MOD 256)
9680 !PRINT "HByte:";H_byte;" LByte:";L_byte;" ";Spannung
9690 OUT (&H226),L_byte
9700 WAIT .1
9710 OUT (&H227),H_byte
9720 OUT (&H226),L_byte
9730 WAIT .1
9740 OUT (&H227),H_byte
9750 !
9760 T_anz=20
9770 FOR J=1 TO T_anz
9780 !
9790 Kanal=12
9800 OUT &H22A,Kanal ! Multiplexer-Kanal
9810 OUT &H229,0 ! Gaincontrol
9820 OUT &H22B,1 ! Modecontrol
9830 OUT &H22C,1 ! Trigger
9840 WHILE INP(&H225)>15 ! Konversion OK
9850 END WHILE
9860 !
9870 Hb=INP(&H225)
9880 WAIT .1
9890 Lb=INP(&H224)
9900 !
9910 U_ntc=((Hb-8)*256+Lb)/409.5*2
9920 !
9930 R_ntc=U_ntc/(5-U_ntc)*33 ! 33kOhm
9940 !
9950 IF R_ntc<=0 THEN R_ntc=1
9960 !
9970 Temp1=Temp1+(Ntc_off-Ntc_span1*LGT(R_ntc)+Ntc_span2*(LGT(R_ntc))^2)
9980 !
9990 DISP "---- TEMPERATURMESSUNG ----- ";T_anz-J,R_ntc
10000 !
10010 NEXT J
10020 !
10030 Temp1=Temp1/T_anz
10070 !
10071 PRINT USING 10072;Temp1
10072 IMAGE "TEMP: ",SDDD.DD, " °C"
10080 RETURN
10090 !
10100 !-----
10110 !
10120 U_in:!----- PCL812 A/D-Karte -----
10130 !
10140 !PRINT Kanal
10150 OUT &H22A,Kanal ! Multiplexer-Kanal
10160 OUT &H229,0 ! Gaincontrol
10170 OUT &H22B,1 ! Modecontrol
10180 OUT &H22C,1 ! Trigger
10190 WHILE INP(&H225)>15 ! Konversion OK
10200 END WHILE
10210 !
10220 Hb=INP(&H225)
10230 WAIT .01
10240 Lb=INP(&H224)

```

```

10250 !
10260 IF Kanal=15 THEN
10270 Uin(3)=((Hb-8)*256+Lb)/409.5*2 )
10280 !PRINT "Exp.:";Kanal,Hb,Lb,Uin(3)
10290 END IF
10300 !
10310 IF Kanal=14 THEN
10320 Uin(2)=((Hb-8)*256+Lb)/409.5*2
10330 !PRINT "Mantisse:";Kanal,Hb,Lb,Uin(2)
10340 END IF
10350 !
10360 IF Kanal=13 THEN
10370 Uin(1)=((Hb-8)*256+Lb)/409.5*2 )
10380 !PRINT "Exp.:";Kanal,Hb,Lb,Uin(3)
10390 END IF
10400 !
10410 RETURN
10420 !
10430 END
10440 !
10450 !
10460 !
10470 !*****!
10480 !
10490 !
10500 !
10510 !
10520 SUB U_out(Spannung)
10530 !
10540 Sp_out=Spannung*409.5/1.015
10550 H_byte=INT(Sp_out DIV 256)
10560 L_byte=INT(Sp_out MOD 256)
10570 !PRINT "HByte:";H_byte;" LByte:";L_byte;" ";Spannung
10580 OUT (&H224),L_byte
10590 WAIT .1
10600 OUT (&H225),H_byte
10610 OUT (&H224),L_byte
10620 WAIT .1
10630 OUT (&H225),H_byte
10640 !
10650 SUBEND
10660 !
10670 !-----
10680 !
10690 SUB Dp(Zps,Dps,Lam)
10700 !
10710 COM /Dp/Dp_start
10720 Dp:!
10730 !
10740 Zp=Zps
10750 Dp=1/Zp^.65/2 !STARTWERT
10760 !
10770 Dp_start=Dp
10780 Anz=1
10790 J=.1
10800 WHILE ABS(Zp-Zv)>1.E-9
10810 Fa=F
10820 IF Dp<1.E-2 THEN Dp=1.E-2
10830 C=1+2.492*Lam/Dp+.84*Lam/Dp*EXP(-.43*Dp/Lam)
10840 Zv=1.6E-19*C*.1.E+7/(3*PI*1.831E-4*Dp*.1.E-7)
10850 Delta=Zv-Zp
10860 IF Zv>Zp THEN
10870 F=1
10880 Dp=Dp+1/J
10890 ELSE
10900 F=0

```

```

10910 Dp=Dp-1/J
10920 END IF
10930 IF (Fa-F)<>0 THEN J=J*2
10940 !PRINT INT((Zp-Zv)*1.E+10),Dp,Anz,J
10950 Anz=Anz+1
10960 END WHILE
10970 !PRINT "Dp_start";Dp_start;" Dp:";Dp
10980 !
10990 Dps=Dp
11000
11010 DISP ""
11020 SUBEND
11030 !
11040 !

```

## 6.2b Classifier evaluation software

```

10 !
20 ! K
30 !---- CLASSIFIER - AUSWERTUNG November 2003 für HP-Vectra -----
40 !
50 !- VERSCHIEBEN ZWEIER MESSUNGEN GEGEN-
60 ! EINANDER / LADUNGSKORREKTUR
70 !
80 !-- NEUE VERSION : MIT VORLAUFPUNKTEN --
90 !
100 !10.10.90:BERECHNUNG TRANSFERFUNKTION
110 !29.11.90:PLOTTERAUSGABE MÜGLICH
120 !17.12.90:LISTING DER Cp's MÜGLICH
130 !22. 3.91:DATEN --> VAX
140 !28. 3.91:KORREKTUR GROSSER Dp's
150 !30. 4.91:AUTOM.AUSWERTUNG MÜGLICH
160 !17. 5.91:ZUS.DATEN FÜR VAX-FILE
170 !17. 5.91:AUTO_FIT MÜGLICH
180 !27. 5.91:KONZ.-KORR. VERD.-SYSTEM (5470)
190 !28. 5.91:MAT Fl_faktor MIT/OHNE VERD.
200 !29. 8.91:AUTO-FIT MIT VARIAB.KORR.-DATEN
210 !25.10.91:LAD.KORR. NACH WIEDENSOHLER
220 !XX.11.91:CLASS TEMP. MIT ABGESPEICHERT
230 !16.12.91:LAD.KORR. VOR FENST..KORR.
240 ! 9. 4.92:GRÖSSENFAKTOR BEI LAD.-KORR.
250 !10. 4.92: 23.4.92: 29.4.92:
260 !13. 8.92:AUTOM.DATENÜBERTR. -> VAX
270 ! 3. 9.92:2 VERSCH. MESSZEITEN TF1/TF2
280 ! 1.10.92:D_fak ist COMMON
290 ! 5.11.92:CMD,SMD,MMD - BERECHNUNG
300 !29. 3.93:EINLESEN VON BEKANNTEM KORR-DATEN
310 !18. 1.95:Fl_lad$ ist neu (Siehe 11450)
320 !24. 1.95:Lad_korr vor Fenster wahlweise
330 !26. 1.95:Schrittweite wählbar (Schr$)
340 ! 9. 2.95:Datums_flag:Mess.2.Tag für Vax
350 !
360 OPTION BASE 1
370 DIM D(300),X(40,300),Zp(300),Cc(300),DI(16)
380 DIM Xv(40,300),Yv(40,300),Ys(40,300),Sm(40)
390 DIM C(40,300),Y(40,300),F(300,6),Cv(40,300)
400 DIM Fc1(300,6),Fc2(300,6)
410 DIM Mess(40),Time$(40)[10],Tim$(40)[10]
420 DIM A_sum(40),V_sum(40),Time_sum(40),Rf(40)
430 DIM Kommentar$(40),Ko$(40)[20],Fil2$(40)
440 DIM Filename$(20),Spf_string$(500),Spf_string1$(200),Spf_string2$(200)
450 !
460 DIM Fit(5,500)
470 !
480 DIM Dpo(300),Dpu(300),Fl_faktor(2,300)

```

```

490 DIM C_korri$(40)[2]
500 DIM K_anzi(40),Korr_richtung(40)
510 DIM Temp(40,3),Offs(40)
520 DIM Offseti(40)
530 INTEGER Graph1(1:179,1:6309),Bas_graph(1:179,1:6309)
540 DIM Outp$[80]
550 INTEGER Temppp
560 DIM Dp_quer(40),Sigma_g(40),Cp_summe(40),Vol_summe(40)
570 DEG
580 !
590 !
600 Tf_kom: !
610 DATA "TF1 NaCl"
620 DATA "TF1 NaCl"
630 DATA "TF1 NaCl"
640 DATA "TF1 NaCl"
650 DATA ""
660 DATA "TF2 NaCl"
670 DATA "TF2 NaCl"
680 DATA "TF2 NaCl"
690 DATA "TF2 NaCl"
700 DATA "TF2 NaCl"
710 DATA "TF2 NaCl"
720 DATA "TF2 NaCl"
730 DATA "TF2 NaCl"
740 DATA "TF2 NaCl"
750 DATA "TF2 NaCl"
760 DATA "TF2 NaCl"
770 DATA "TF2 NaCl"
780 DATA "TF2 NaCl"
790 DATA "TF2 NaCl"
800 DATA "TF2 NaCl"
810 DATA "TF2 NaCl"
820 DATA "TF2 NaCl"
830 DATA "TF2 NaCl"
840 DATA "TF2 NaCl"
850 DATA "TF2 NaCl"
860 !
870 MAT Y=(0)
880 MAT A=(0)
890 MAT X=(0)
900 MAT A_sum=(0)
910 MAT V_sum=(0)
920 MAT C_korri$=("XX") !("N")
930 First_charge=0
940 D_fak=1
950 !

```

```

960 Diff=7
970 ! 2980 Bipol=1 ! =1:LAD.KORR NACH WIEDENSOHL.
990 ! ! <>1: STAND.LAD.KORR.
1000 Polar$="-" ! POLARITÄT DER CL.-ELEKTRODE
1010 !
1020 Lad_zuerst$="J" IN LADUNGSKORR. VOR FENSTER
1030 Schr$="Auto" ! Autom.Schrittweite
1040 !
1050 Cp_fak$="J" ! Korrektur TSI3020-Effizienz für Dp<37nm
1060 Fl_lad$="N"
1070 M1=1
1080 !
1090 Cmd$="N" ! BERECHNUNG CMD,SMD,MMD
1100 !
1110 Nachauswert$="N" !EINLESEN VON BEKANNTEN
1120 ! !KORR.-DATEN
1130 !
1140 !
1150 Auto$="N" !AUTOM.AUSW. Lim_u + Lim_o
1160 Auto_fit$="N" ! setzen
1170 Vol_print=1 ! 10 OD. 1(CRT) fuer Windows-HP-Basic
1180 !
1190 Lim_u=30
1200 Lim_o=1150
1210 !
1220 C_korr$="N" !KORR. FÜR RÜCKMESSUNG BEI
1230 K_anz=0 ! GR. PARTIKELN (S.4400)
1240 K_fak=1 ! KORR.-FAKTOR (S.4500)
1250 Korr_richtung=1 ! Rück -> Hin
1260 Korr_ok$="N" ! ÜBERNAHME EINZELN DEFI-
1270 ! ! NIERTER KORR.-DATEN
1280 !
1290 Verd$="N"
1300 Verd_faktor=1 ! 2 = 1:1
1310 Verd_pos$="V"
1320 Verd_korr$="N" ! KORR.-FUNKTION FÜR VERD.
1330 !
1340 !
1350 !
1360 !----- VERSUCHSDATEN -----
1370 !
1380 Vers$="catec200109C"
1390 !Filename$="catec200109C"
1400 Filename$=Vers$&"e"
1410 !
1420 Messzeit1=397 ! ZEIT FÜR 1 MESSUNG TF1
1430 Messzeit2=397 ! ZEIT FÜR 1 MESSUNG TF2
1440 !
1450 Filter_zeit1$="12:55"
1460 Filter_zeit2$="12:55"
1470 Dos_zeit$="11:26"
1480 !
1490 !
1500 Offset=0
1510 !
1520 !-----
1530 !
1540 !
1550 !
1560 Lam=68 !65.3 ! Mittl. freie Weglänge [nm]
1570 !
1580 Bas_flag=0 ! wird intern gesetzt
1590 Ladungs$="J" ! Ladungskorrektur
1600 Fl_norm$="J" ! Norm. über Transferfunktion
1610 !
1620 File$="N" ! Erz. Dp/Cp-Files

```

```

1630 !
1640 !----- EINSTELLBAR ÜBER 'KEYS' -----
1650 !
1660 Sum_gr$="N"
1670 Mittel$="N"
1680 Korr_1$="N"
1690 Korr_2$="N"
1700 Mehr_lad$="N" ! 3e+4e - Korrektur
1710 Summe$="N"
1720 Lkorr=2
1730 !
1740 !-----
1750 !
1760 !----- EINSTELLBAR ÜBER 'KEYS2' -----
1770 Sur1$="N"
1780 Vol1$="N"
1790 Kum$="N" ! Kumul. Anz.,Obfl.,Vol.
1800 Punkt$="N"
1810 Plotter=0 ! 0=CRT , 1=PLOTTER
1820 Pen=1
1830 Line=4
1840 !
1850 !-----
1860 !
1870 Sum_n=0
1880 !
1890 Feuchte=0 ! FÜR VAX-FILE
1900 Leer1=0 ! " "
1910 Leer2=0 ! " "
1920 !
1930 KBD CMODE ON
1940 !
1950 GOTO Versuch
1960 Keys: !
1970 !OFF KNOB
1980 !
1990 !
2000 IF Sur1$="N" AND Vol1$="N" THEN
2010 ON KEY 0 LABEL "ANZAHL" GOTO Sur1
2020 ELSE
2030 IF Sur1$="J" THEN
2040 ON KEY 0 LABEL "SURFACE" GOTO Vol1
2050 ELSE
2060 ON KEY 0 LABEL "VOLUME" GOTO Anz1
2070 END IF
2080 END IF
2090 ON KEY 3 LABEL "MESS WAHL" GOTO Messwahl
2100 ON KEY 1 LABEL "KORR - KEYS" GOTO Korr_keys
2110 ON KEY 5 LABEL "RECHNEN" GOTO Rechnung
2120 !
2130 ON KEY 2 LABEL "KEYS 2" GOTO Keys2
2140 !
2150 IF Summe$="J" THEN
2160 ON KEY 13 LABEL "SUMME= J" GOTO Summe1
2170 ELSE
2180 ON KEY 13 LABEL "SUMME= N" GOTO Summe2
2190 END IF
2200 !
2210 IF Mittel$="N" THEN
2220 ON KEY 4 LABEL "MITTEL= N" GOTO Mittel1
2230 ELSE
2240 ON KEY 4 LABEL "MITTEL= J" GOTO Mittel2
2250 END IF
2260 !
2270 IF Korr_1$="N" THEN
2280 ON KEY 6 LABEL " 1e = N" GOTO Kor1_1

```

```

2290 ELSE
2300 ON KEY 6 LABEL " 1e = J" GOTO Kor1_2
2310 END IF
2320 !
2330 !
2340 IF Korr_2$="N" THEN
2350 ON KEY 7 LABEL " 2e = N" GOTO Kor2_1
2360 ELSE
2370 ON KEY 7 LABEL " 2e = J" GOTO Kor2_2
2380 END IF
2390 !
2400 IF Mehr_lad$="N" THEN
2410 ON KEY 8 LABEL "3e+4e=N" GOTO Kor3_1
2420 ELSE
2430 ON KEY 8 LABEL "3e+4e=J" GOTO Kor3_2
2440 END IF
2450 !
2460 IF Sum_gr$="N" THEN
2470 ON KEY 9 LABEL "Sum_gr= N" GOTO Sum_gr1
2480 ELSE
2490 ON KEY 9 LABEL "Sum_gr= J" GOTO Sum_gr2
2500 END IF
2510 !
2520 !
2530 GOTO Keys
2540 !
2550 !
2560 Keys2: !-----
2570 !
2580 ON KEY 0 LABEL "AUTO- FIT" GOTO Auto_fit
2590 ON KEY 2 LABEL "NEU Ymx" GOTO Max_y
2600 ON KEY 3 LABEL "NEU Xmx" GOTO Max_x
2610 ON KEY 4 LABEL " KEYS 1" GOTO Keys
2620 ON KEY 5 LABEL "DIFF= "&VAL$(Diff) GOTO Diff
2630 ON KEY 7 LABEL "Fit" GOTO Fit
2640 !
2650 IF Kum$="J" THEN
2660 ON KEY 1 LABEL "KUM= J" GOTO Kum1
2670 ELSE
2680 ON KEY 1 LABEL "KUM= N" GOTO Kum2
2690 END IF
2700 !
2710 IF File$="N" THEN
2720 ON KEY 9 LABEL "FILE$= N" GOTO Fil1
2730 ELSE
2740 ON KEY 9 LABEL "FILE$= J" GOTO Fil2
2750 END IF
2760 !
2770 !
2780 ON KEY 6 LABEL "Lim_u_o" GOTO Knob
2790 !ON KEY 7 LABEL "LINE "&VAL$(Line) GOTO Line
2800 !ON KEY 8 LABEL "PEN "&VAL$(Pen) GOTO Pen
2810 ON KEY 8 LABEL "CHARGE" GOTO Charge
2820 !
2830 GOTO Keys2
2840 !
2850 !
2860 Korr_keys: !-----
2870 !
2880 IF C_korr$="J" THEN
2890 ON KEY 5 LABEL "Korr= J" GOTO Ckorr2
2900 END IF
2910 IF C_korr$="JJ" THEN
2920 ON KEY 5 LABEL "Korr=JJ" GOTO Ckorr3
2930 END IF
2940 IF C_korr$="N" THEN

```

```

2950 ON KEY 5 LABEL "Korr= N" GOTO Ckorr1
2960 END IF
2970 !
2980 ON KEY 6 LABEL "K_anz=&VAL$(K_anz) GOTO Kanz
2990 !
3000 IF Korr_richtung=1 THEN
3010 ON KEY 7 LABEL "Richt.= 1" GOTO Korrr1
3020 ELSE
3030 ON KEY 7 LABEL "Richt.= 2" GOTO Korrr2
3040 END IF
3050 !
3060 ON KEY 8 LABEL "Offs=&VAL$(Offset) GOTO Offset
3070 !
3080 ON KEY 1 LABEL " KEYS 1" GOTO Keys
3090 !
3100 ON KEY 3 LABEL "Korr. O.K." GOTO Korr_ok
3110 GOTO Korr_keys
3120 !
3130 !
3140 Mittel1: !
3150 Mittel$="J"
3160 GOTO Keys
3170 !
3180 Mittel2: !
3190 Mittel$="N"
3200 GOTO Keys
3210 !
3220 Kor1_1: Korr_1$="J"
3230 Ebene=1
3240 GOTO Keys
3250 !
3260 Kor1_2: Korr_1$="N"
3270 Ebene=1
3280 GOTO Keys
3290 !
3300 Kor2_1: Korr_2$="J"
3310 Ebene=1
3320 GOTO Keys
3330 !
3340 Kor2_2: Korr_2$="N"
3350 Ebene=1
3360 GOTO Keys
3370 !
3380 Kor3_1: Mehr_lad$="J"
3390 Ebene=1
3400 GOTO Keys
3410 !
3420 Kor3_2: Mehr_lad$="N"
3430 Ebene=1
3440 GOTO Keys
3450 !
3460 Sum_gr1: !
3470 Sum_gr$="J"
3480 GOTO Keys
3490 !
3500 Sum_gr2: !
3510 Sum_gr$="N"
3520 GOTO Keys
3530 !
3540 Sur1: !
3550 Sur1$="J"
3560 Vol1$="N"
3570 GOTO Keys
3580 !
3590 Vol1: !
3600 Vol1$="J"

```

```

3610 Sur1$="N"
3620 GOTO Keys
3630 !
3640 Anz1: !
3650 Vol1$="N"
3660 Sur1$="N"
3670 GOTO Keys
3680 !
3690 Kum1: !
3700 Kum$="N"
3710 GOTO Keys2
3720 !
3730 Kum2: !
3740 Kum$="J"
3750 GOTO Keys2
3760 !
3770 Fil1: !
3780 File$="J"
3790 GOTO Keys2
3800 !
3810 Fil2: !
3820 File$="N"
3830 GOTO Keys2
3840 !
3850 Line: !
3860 Line=(Line MOD 5)+1
3870 GOTO Keys2
3880 !
3890 Pen: !
3900 Pen=(Pen MOD 5)+1
3910 GOTO Keys2
3920 !
3930 Diff: !
3940 INPUT "Diff=",Diff
3950 GOTO Keys2
3960 !
3970 Punktnull: !
3980 !
3990 INPUT "WIEVIEL PUNKTE AUF NULL SETZEN ",Nulpkt
4000 !
4010 FOR I=1 TO Nulpkt
4020 C(M1,I)=0
4030 C(M1,(2*Punkte+Vor_punkte)-I)=0
4040 NEXT I
4050 GOTO Keys2
4060 !
4070 !
4080 !
4090 Rs232: !
4100 !
4110 Image11: IMAGE X,4D.D,XX,5D.D,+
4120 !
4130 ASSIGN @F9 TO 9
4140 CONTROL 9,4;3
4150 CONTROL 9,3;9600
4160 CONTROL 9,12;176 ! Handshake off
4170 PAUSE
4180 Fil$=Vers$&"_&VAL$(M1)&".HP"
4190 DISP Fil$
4200 OUTPUT @F9;Fil$
4210 WAIT .5
4220 FOR I=1 TO Punkte
4230 Fil2$=VAL$(DROUND(10^(X(M1,I)),4))&" "&VAL$(DROUND(Y(M1,I),5))
4240 OUTPUT @F9;Fil2$
4250 DISP Fil2$
4260 NEXT I

```

```

4270 DISP "ENDE"
4280 OUTPUT @F9;"ENDE"
4290 !
4300 GOTO Keys2
4310 !
4320 !
4330 Charge: !
4340 CALL Charge(Punkte,D(*),F(*),First_charge,D_fak,Polar$)
4350 MAT Fc1=F
4360 GOTO Keys2
4370 !
4380 Autovax: !
4390 !
4400 GRAPHICS OFF
4410 !
4420 M1=0
4430 Auto$="J"
4440 Vol_print=1
4450 Vol$="N"
4460 Sur$="N"
4470 Cmd$="N"
4480 Auto_fit$="N"
4490 Auto_vax$="J"
4500 !
4510 INPUT "VAX-Filename ( max.10 Zeichen :SEE0693AEW )",Vax_name$
4520 !
4530 PRINT "@HPAERO STARTEN, DANN 'CONTINUE' "
4540 PAUSE
4550 OFF KEY
4560 OFF KNOB
4570 !
4580 GOTO Messwahl
4581 !
4590 !
4600 Ckorr1: !
4610 C_korr$="J"
4620 GOTO Korr_keys
4630 !
4640 Ckorr2: !
4650 C_korr$="JJ"
4660 GOTO Korr_keys
4670 !
4680 Ckorr3: !
4690 C_korr$="N"
4700 GOTO Korr_keys
4710 !
4720 Kanz: !
4730 INPUT "K_anz",K_anz
4740 GOTO Korr_keys
4750 !
4760 Korrr1: !
4770 Korr_richtung=2
4780 GOTO Korr_keys
4790 !
4800 Korrr2: !
4810 Korr_richtung=1
4820 GOTO Korr_keys
4830 !
4840 Offset: !
4850 INPUT "Offset",Offset
4860 GOTO Korr_keys
4870 !
4880 Korr_ok: !
4890 C_korri$(M1)=C_korr$
4900 K_anzi(M1)=K_anz
4910 Korr_richtungi(M1)=Korr_richtung

```

```

4920 Offseti(M1)=Offset
4930 !
4940 PRINT "Messung:";M1;" Korr_richtungi:";Korr_richtungi(M1)
4950 PRINT "C_korri$:";C_korri$(M1);" K_anzi:";K_anzi(M1);" Offset:";Offseti(M1)
4960 GOTO Korr_keys
4970 !
4980 Max_y: !
4990 !
5000 INPUT "NEUES Y-MAX EINGEBEN ",Ymax
5010 GOTO Graphik
5020 !
5030 Max_x: !
5040 !
5050 INPUT "NEUES X-MIN EINGEBEN ",Xmin
5060 Xmin=LGT(Xmin)
5070 INPUT "NEUES X-MAX EINGEBEN ",Xmax
5080 Xmax=LGT(Xmax)
5090 Bas_flag=0
5100 GOTO Graphik
5110 !
5120 Rechnung: !
5130 !
5140 IF Ebene=2 THEN Ebene2
5150 GOTO Ebene1
5160 !
5170 Auto_fit: !
5180 !
5190 CLEAR SCREEN
5200 M1=0
5210 Cmd$="J"
5220 Mittel$="J"
5230 Kum$="N"
5240 Vol$="N"
5250 Sur$="N"
5260 Korr_ok$="J"
5270 Auto$="J"
5280 Auto_fit$="J"
5290 Vol_print=1
5300 !
5310 FOR I=1 TO Maxmess -
5320 PRINT C_korri$(I);";";
5330 NEXT I
5340 PRINT ""
5350 PRINT " M1 : ";M1;" CMD$ : ";Cmd$;" Lim_u : ";Lim_u;" Lim_o : ";Lim_o;" Korr_ok$ : ";Korr_ok$
5360 PRINT "Auto$ : ";Auto$;" Auto_fit$ : ";Auto_fit$;" Vol_print : ";Vol_print
5370 PRINT "Vol$ : ";Vol$;" Sur$ : ";Sur$;" Kum$ : ";Kum$
5380 PRINT ""
5390 PRINT "'Continue' für Auto_fit - Start"
5400 PAUSE
5410 GOTO Messwahl
5420 !
5430 !-----
5440 !
5450 !
5460 Versuch: !
5470 !
5480 ASSIGN @F1 TO Vers$
5490 ENTER @F1;Vers$,Date$
5500 ENTER @F1;Punkte,Raster,Ez,Cl_anz,Vor_punkte,Qv,Qa
5510 !
5520 !
5530 !
5540 PRINT Vers$,Date$
5550 PRINT "Punkte:";Punkte;" Raster:";Raster;" Ez:";Ez;" Cl_anz:";Cl_anz;" Vor_pkte:";Vor_punkte
5560 !
5570 REDIM D(Punkte)

```

```

5580 REDIM Zp(Punkte)
5590 !
5600 ENTER @F1;D(*)
5610 ENTER @F1;Zp(*)
5620 !
5630 Lim_o=D(1)
5640 Lim_u=D(Punkte)
5650 !
5660 !
5670 PRINT ""
5680 PRINT " I D(I) Zp(I) Zp(I)/Zp(1)"
5690 !
5700 IMAGE DDD,XX,DDDD.D,XX,D.DDE,XX,DDD.DD
5710 FOR I=1 TO Punkte
5720 L_d=Lam/D(I)
5730 Cc(I)=1+2.492*L_d+.84*L_d*EXP(-.43/L_d)
5740 Zp(I)=1.6E-12*Cc(I)/(3*PI*1.831E-11*D(I))
5750 PRINT USING 5700;I,D(I),Zp(I),Zp(I)/Zp(1)
5760 NEXT I
5770 !
5780 OFF ERROR
5790 CALL Charge(Punkte,D(*),F(*),First_charge,D_fak,Polar$)
5800 !
5810 MAT Fc1=F
5820 !
5830 !
5840 Transfer: ! -- BERECHNUNG TRANSFERFUNKTION --
5850 !
5860 DISP " BERECHNUNG DER TRANSFERFUNKTION "
5870 !
5880 REDIM Fl_faktor(2,Punkte)
5890 !
5900 FOR K=1 TO 1 ! TRANSFER MIT/OHNE VERD.
5910 IF K=2 THEN Qa=Qa/Verd_faktor
5920 PRINT "K :";K;" Qa:";Qa
5930 Mfliche=0
5940 PRINT ""
5950 !PRINT " Dp Dpu Dpo Fl_faktor"
5960 !
5970 FOR I=1 TO Punkte
5980 FOR J=1 TO 2
5990 Zpd(1)=Zp(I)*(1-Qa/Qv)
6000 Zpd(2)=Zp(I)*(1+Qa/Qv)
6010 !
6020 Ccc=.9156-5026*Zpd(J)-1.454E+5*Zpd(J)^2+5.447E+4*Zpd(J)^(1.630)+1570*Zpd(J)^(.7512)
6030 !
6040 Dpd=1.6E-19*Ccc*1.E+7/(3*PI*1.831E-4*Zpd(J)*1.E-7)
6050 !
6060 IF J=1 THEN Dpo(I)=Dpd
6070 IF J=2 THEN Dpu(I)=Dpd
6080 !
6090 NEXT J
6100 Fl_faktor(K,I)=(LOG(Dpo(I))-LOG(Dpu(I)))/2
6110 Mfliche=Mfliche+Fl_faktor(K,I)
6120 !PRINT USING 3160;D(I),Dpu(I),Dpo(I),Fl_faktor(I)
6130 !
6140 NEXT I
6150 IMAGE 3(DDD.D,XX),D.DDD
6160 !
6170 Gfliche=LOG((D(1)+Dpo(1))/2)-LOG((D(Punkte)+Dpu(Punkte))/2)
6180 !Gfliche=LOG(D(1))-LOG(D(Punkte))
6190 ! -
6200 Fliche=Mfliche/Gfliche
6210 !
6220 PRINT "ES WURDEN ";INT(Fliche*1000)/10;" % DES MESSBEREICHES ERFASST"
6230 !

```

```

6240 IMAGE DDD,X,DDD.D,XXX,#  

6250 !  

6260 !  

6270 Norm: !  

6280 !  

6290 DISP "NORMIERUNG" -  

6300 Fl_norm=Mfliche/Punkte  

6310 Fl_norm=Fl_norm*Gfliche/Mfliche  

6320 !  

6330 FOR I=1 TO Punkte  

6340 Fl_faktor(K,I)=1/(Fl_faktor(K,I)/(Fl_norm)) ! Darstellung wie üblich  

6350 !Fl_faktor(K,I)=1/Fl_faktor(K,I) ! dN / dlog(Dp)  

6360 NEXT I  

6370 Fl_sum=SUM(Fl_faktor)  

6380 !PRINT Fl_sum/Punkte,Fl_sum/Punkte*Fläche  

6390 !  

6400 DISP ""  

6410 NEXT K  

6420 !  

6430 ON ERROR GOTO Err  

6440 !  

6450 !  

6460 !  

6470 !  

6480 --- EINLESEN DER Cp's -----  

6490 FOR M=1 TO 40  

6500 PRINTER IS 1  

6510 ENTER @F1;Mess(M),Time$(M),Rf(M)  

6520 PRINT Mess(M),Time$(M),Rf(M)  

6530 ENTER @F1;Temp(M,1),Temp(M,1),Temp(M,1),Offs(M),Res1,Res2,Res3  

6540 PRINT Temp(M,1),Temppp,Temppp,Offs(M),Res1,Res2,Res3  

6550 FOR I=1 TO (Punkte*2+Vor_punkte)  

6560 ENTER @F1;C(M,I)  

6570 !PRINT C(M,I)  

6580 NEXT I  

6590 PRINT ""  

6600 NEXT M  

6610 !  

6620 Err:!  

6630 IF ERRN=59 THEN 6650  

6640 PRINT ERRM$  

6650 OFF ERROR  

6660 !  

6670 !  

6680 !  

6690 Maxmess=MAX(Mess(*))  

6700 !  

6710 RESTORE Tf_kom  

6720 FOR I=1 TO Maxmess  

6730 READ Ko$(I)  

6740 !PRINT Ko$(I)  

6750 NEXT I  

6760 !  

6770 Datums_flag=100  

6780 !  

6790 FOR I=2 TO Maxmess  

6800 IF TIME(Time$(I))<TIME(Time$(I-1)) THEN Datums_flag=I  

6810 NEXT I  

6820 !  

6830 !PRINT "Datums_flag:";Datums_flag  

6840 !  

6850 REDIM X(Maxmess+1,Punkte)  

6860 REDIM Xv(Maxmess+1,Punkte)  

6870 REDIM Y(Maxmess+1,Punkte)  

6880 REDIM Ys(Maxmess+1,Punkte)  

6890 ! -

```

```

6900 IF Nachauswert$="J" THEN
6910 CLEAR SCREEN
6920 FOR I=1 TO Maxmess
6930 PRINT "MESSUNG";I
6940 INPUT "Offseti",Offseti(I)
6950 INPUT "C_korri$(I)",C_korri$(I)
6960 INPUT "K_anzi",K_anzi(I)
6970 INPUT "Korr_richtungi",Korr_richtungi(I)
6980 NEXT I
6990 Korr_ok$="J"
7000 PRINT C_korri$(*)
7010 PRINT K_anzi(*)
7020 PRINT Korr_richtungi(*)
7030 PRINT Offseti(*)
7040 END IF
7050 !
7060 IF Ladungs$="J" THEN GOSUB Ladung
7070 !
7080 IF Auto$="J" THEN Messwahl
7090 !
7100 GOTO Keys
7110 !
7120 Messwahl: !-----
7130 !
7140 Ebene=1
7150 !
7160 PRINT "-----"
7170 PRINT ""
7180 IF Auto$="J" OR Auto_fit$="J" THEN
7190 M1=M1+1
7200 IF M1=(Maxmess+1) AND Auto_fit$="J" THEN Plot_sum
7210 !
7220 Offset=Offseti(M1)
7230 K_anz=K_anzi(M1)
7240 Korr_richtung=Korr_richtungi(M1)
7250 C_korr$=C_korri$(M1)
7260 !
7270 PRINT "Messung:";M1;" Korr_richtungi:";Korr_richtungi(M1)
7280 PRINT "C_korri$:";C_korri$(M1);"; K_anzi:";K_anzi(M1);"; Offset:";Offseti(M1)
7290 !
7300 GOTO 7550
7310 END IF
7320 !
7330 !
7340 !
7350 PRINT "MESSUNG1 (1-";Maxmess;"") EINGEBEN"
7360 INPUT M1
7370 !
7380 !
7390 IF Korr_ok$="J" THEN
7400 IF C_korri$(M1)="XX" THEN
7410 PRINT "---- KEINE VORDEF.KORR.-DATEN VORHANDEN ----"
7420 GOTO Keys
7430 ELSE
7440 Offset=Offseti(M1)
7450 K_anz=K_anzi(M1)
7460 Korr_richtung=Korr_richtungi(M1) -
7470 C_korr$=C_korri$(M1)
7480 PRINT "Messung:";M1;" Korr_richtungi:";Korr_richtungi(M1)
7490 PRINT "C_korri$:";C_korri$(M1);"; K_anzi:";K_anzi(M1);"; Offset:";Offseti(M1)
7500 !
7510 END IF
7520 END IF
7530 !
7540 !
7550 M1=M1

```

```

7560 M2=M1+1
7570 M12=M2
7580 !
7590 !
7600 Ebene1: !-----
7610 !
7620 !
7630 Neu_diff:!-----
7640 !
7650 DISP "EBENE1"
7660 !
7670 !-- NEUE ZUORDNUNG DER MESSWERTE -----
7680 !
7690 MAT Y=(0)
7700 MAT Yv=(0)
7710 !Bas_flag=0
7720 !
7730 FOR I=1 TO Punkte
7740 X(M1,I)=LGT(D(I))
7750 X(M2,I)=X(M1,I)
7760 Xmax=X(M1,1)
7770 Xmin=X(M1,Punkte)
7780 !
7790 Xv(M1,I)=X(M1,I)
7800 Xv(M2,I)=X(M1,I)
7810 !
7820 Cv(M1,I)=C(M1,I+Diff) ! SPLIT
7830 Cv(M2,I)=C(M1,I+Diff+Punkte) ! M1,M2
7840 !
7850 NEXT I
7860 !
7870 !
7880 !-- SPIEGELUNG DER MESSUNG M2 -----
7890 !
7900 !
7910 FOR I=1 TO Punkte
7920 Yv(M1,I)=Cv(M1,I)-Offset
7930 Yv(M2,I)=Cv(M2,Punkte+1-I)-Offset
7940 NEXT I
7950 !
7960 !
7970 !--- RÜCKMESSUNG O.K. ? -----
7980 !
7990 IF C_korr$="J" THEN
8000 IF Korr_richtung=1 THEN
8010 FOR I=1 TO K_anz
8020 !IF Yv(M2,I)>=K_fak*(Yv(M1,I)) THEN
8030 PRINT "KORREKTUR MESSPUNKT";I;".";INT(Yv(M2,I));" -->";INT(Yv(M1,I))
8040 Yv(M2,I)=Yv(M1,I)
8050 !END IF
8060 NEXT I
8070 ELSE
8080 FOR I=1 TO K_anz
8090 !IF Yv(M1,I)>=K_fak*(Yv(M2,I)) THEN
8100 PRINT "KORREKTUR MESSPUNKT";I;".";INT(Yv(M1,I));" -->";INT(Yv(M2,I))
8110 Yv(M1,I)=Yv(M2,I)
8120 !END IF
8130 NEXT I
8140 END IF
8150 END IF
8160 !
8170 IF C_korr$="JJ" THEN
8180 FOR I=1 TO K_anz
8190 Yv(M1,I)=0
8200 Yv(M2,I)=0
8210 NEXT I

```

```

8220 END IF
8230 !
8240 IF Lad_zuerst$="J" THEN
8250 IF Lkorr=2 THEN
8260 GOSUB Ladungskorr2
8270 ELSE
8280 GOSUB Ladungskorr
8290 END IF
8300 END IF
8310 !
8320 !
8330 !-- NORMIERUNG MIT TRANSFERFUNKTIONEN --
8340 !
8350 IF Fl_norm$="J" THEN
8360 IF Verd$="J" AND Verd_pos$="H" THEN
8370 FOR I=1 TO Punkte
8380 Yv(M1,I)=Yv(M1,I)*Fl_faktor(2,I)
8390 Yv(M2,I)=Yv(M2,I)*Fl_faktor(2,I)
8400 NEXT I
8410 ELSE
8420 FOR I=1 TO Punkte
8430 Yv(M1,I)=Yv(M1,I)*Fl_faktor(1,I)
8440 Yv(M2,I)=Yv(M2,I)*Fl_faktor(1,I)
8450 NEXT I
8460 END IF
8470 END IF
8480 !
8490 !
8500 !
8510 IF Lad_zuerst$="N" THEN
8520 IF Lkorr=2 THEN
8530 GOSUB Ladungskorr2
8540 ELSE
8550 GOSUB Ladungskorr
8560 END IF
8570 END IF
8580 !
8590 !--- KONZ.-KORREKTUR VERDÜNNUNGS-SYSTEM --
8600 !
8610 IF Verd$="J" AND Verd_pos$="H" AND Verd_korr$="J" THEN
8620 !
8630 PRINT "---- KONZ.-KORREKTUR VERD.-SYSTEM ----"
8640 FOR I=1 TO Punkte
8650 !PRINT I,Yv(M1,I),
8660 Yv(M1,I)=Yv(M1,I)*(1.107+1.7708E+6/(LOG(D(I))^11.545))
8670 !
8680 Yv(M2,I)=Yv(M2,I)*(1.107+1.7708E+6/(LOG(D(I))^11.545))
8690 !PRINT Yv(M1,I)
8700 NEXT I
8710 !
8720 Leer1=1
8730 !
8740 ELSE
8750 !
8760 Leer1=0
8770 !
8780 END IF
8790 !
8800 IF Verd$="J" AND Verd_korr$="J" THEN
8810 !
8820 PRINT "---- KONZ.-KORREKTUR VERD.-SYSTEM VORNE ----"
8830 FOR I=1 TO Punkte
8840 PRINT Yv(M1,I),
8850 Yv(M1,I)=Yv(M1,I)*Verd_faktor
8860 Yv(M2,I)=Yv(M2,I)*Verd_faktor
8870 PRINT Yv(M1,I)

```

```

8880 NEXT I
8890 END IF
8900 !
8910 !----- neu 26.8.2009: TSI3020-Effizienz-Korrektur -----
8920 !
8930 IF Cp_fak$="J" OR Cp_fak$="j" THEN
8940 !
8950 FOR J=M1 TO (M1+1)
8960 FOR I=1 TO Punkte
8970 IF X(J,I)<=1.568 THEN !Dp<=37nm
8980 Fak=100/(X(J,I)*127.1-98.9)
8990 Yv(J,I)=Yv(J,I)*Fak
9000 END IF
9010 NEXT I
9020 NEXT J
9030 !
9040 !
9050 END IF
9060 !
9070 !
9080 !----- MESSZEIT -----
9090 !
9100 IF M1<=M_anz_tf1 THEN
9110 Messzeit=Messzeit1
9120 ELSE
9130 Messzeit=Messzeit2
9140 END IF
9150 !
9160 D_zeit=Messzeit/2
9170 IF K_anz=Punkte THEN
9180 IF Korrrichtung=1 THEN
9190 D_zeit=Messzeit/4*3
9200 ELSE
9210 D_zeit=Messzeit/4
9220 END IF
9230 END IF
9240 !
9250 Tim$(M1)=TIME$(TIME(Time$(M1))-D_zeit)
9260 !
9270 !
9280 !---- FÜR VAX-FILE : -----
9290 !
9300 Zeit1=TIME(Tim$(M1))-TIME(Dos_zeit$)
9310 Zeit1=Zeit1/60
9320 !
9330 IF M1<=M_anz_tf1 THEN
9340 Zeit2=TIME(Filter_zeit1$)-TIME(Tim$(M1))
9350 ELSE
9360 Zeit2=TIME(Filter_zeit2$)-TIME(Tim$(M1))
9370 END IF
9380 !
9390 Zeit2=Zeit2/60
9400 !
9410 IF M1>=Datums_flag THEN
9420 !
9430 Zeit1=Zeit1+60*24
9440 Zeit2=Zeit2-60*24
9450 !
9460 END IF
9470 !
9480 !
9490 !-- GESAMTSUMME PARTIKEL -----
9500 !
9510 Sum_cp=0
9520 FOR I=1 TO Punkte
9530 Sum_cp=Sum_cp+(Yv(M1,I)+Yv(M2,I))/2 ! Darstellung wie üblich

```

```

9540 !Sum_cp=Sum_cp+(Yv(M1,I)+Yv(M2,I))/2*Fl_norm ! wenn bei Normierung dN / dlog(Dp) gewählt
9550 NEXT I
9560 !
9570 S_sum=S_sum+Sum_cp
9580 DISP "Cp_gesamt:";INT(Sum_cp);"cm^-3"
9590 !
9600 !
9610 Ebene=2
9620 !
9630 !-----
9640 !
9650 Ebene2: !-----
9660 !
9670 MAT Y=Yv
9680 !
9690 !
9700 !-- OBERFL.-UND VOL.-BERECHNUNG -----
9710 !
9720 Sur_vol2: !
9730 !
9740 Sd1=0
9750 Sd2=0
9760 Sd3=0
9770 Sd4=0
9780 S_n=0
9790 !
9800 FOR I=1 TO Punkte
9810 !
9820 IF Cmd$="J" THEN
9830 !
9840 Sd1=Sd1+(Yv(M1,I)+Yv(M2,I))/2*(10^(X(M1,I))/1000)
9850 Sd2=Sd2+(Yv(M1,I)+Yv(M2,I))/2*(10^(X(M1,I))/1000)^2
9860 Sd3=Sd3+(Yv(M1,I)+Yv(M2,I))/2*(10^(X(M1,I))/1000)^3
9870 Sd4=Sd4+(Yv(M1,I)+Yv(M2,I))/2*(10^(X(M1,I))/1000)^4
9880 S_n=S_n+(Yv(M1,I)+Yv(M2,I))/2
9890 !
9900 END IF
9910 !
9920 IF Sur1$="J" THEN
9930 Y(M1,I)=Yv(M1,I)*PI*(10^(X(M1,I))/1000)^2
9940 Y(M2,I)=Yv(M2,I)*PI*(10^(X(M2,I))/1000)^2
9950 END IF
9960 IF Vol1$="J" THEN
9970 Y(M1,I)=Yv(M1,I)*4*PI/3*(10^(X(M1,I))/2000)^3
9980 Y(M2,I)=Yv(M2,I)*4*PI/3*(10^(X(M2,I))/2000)^3
9990 END IF
10000 NEXT I
10010 !
10020 !
10030 IF Cmd$="J" THEN
10040 !
10050 PRINT USING 10060;" CMD :";1000*Sd1/S_n;" SMD :";1000*Sd3/Sd2;" MMD :";1000*Sd4/Sd3
10060 IMAGE 3(6A,DDDD,XX)
10070 !
10080 PRINT USING 10090;"DoaS:";1000*(Sd2/S_n)^.5;" DoaV:";1000*(Sd3/S_n)^(1/3)
10090 IMAGE 2(6A,DDDD,XX)
10100 !
10110 END IF
10120 !
10130 !
10140 !-----
10150 !
10160 Kumulieren:!
10170 Sy1=0
10180 Sy2=0
10190 IF Kum$="J" THEN

```

```

10200 FOR I=(Punkte-1) TO 1 STEP -1
10210   Sy1=Sy1+Y(M1,I)
10220   Y(M1,I)=Sy1
10230   Sy2=Sy2+Y(M2,I)
10240   Y(M2,I)=Sy2
10250 NEXT I
10260 END IF
10270 !
10280 !
10290 IF Summe$="J" THEN
10300   FOR I=1 TO Punkte
10310     Ys(1,I)=Ys(1,I)+Y(M1,I)
10320     Ys(2,I)=Ys(2,I)+Y(M2,I)
10330   NEXT I
10340   M1=M1+1
10350   IF M1>Maxmess THEN 10390 -
10360   IF Sm(M1)=0 THEN 10340
10370   M2=M2+1
10380 GOTO Ebene1
10390 !
10400 MAT Y=Ys
10410 MAT Y=Y/(Sum_n)
10420 MAT Ys=(0)
10430 !
10440 Sum_cp=S_sum/Sum_n
10450 M1=1
10460 M2=2
10470 FOR I=1 TO Punkte
10480   X(M1,I)=LGT(D(I))
10490   X(M2,I)=X(M1,I)
10500 NEXT I
10510 !
10520 END IF
10530 !
10540 !
10550 IF Mittel$="J" THEN
10560   FOR I=1 TO Punkte
10570     Y(M1,I)=(Y(M1,I)+Y(M2,I))/2
10580   NEXT I
10590 END IF
10600 !
10610 !
10620 IF Auto_vax$="J" AND Auto$="J" THEN Vax
10630 !
10640 GOTO Maxmin
10650 !
10660 !
10670 Summe1:!
10680 Summe$="N"
10690 Sum_n=0
10700 GOTO Keys
10710 !
10720 Summe2:!-----
10730 !
10740 GRAPHICS OFF
10750 CLEAR SCREEN
10760 !
10770 PRINT "ANZAHL DER AUFZUSUMMIERENDEN MESSUNGEN ?"
10780 INPUT Sum_n
10790 MAT Sm=(0)
10800 MAT Ys=(0)
10810 S_sum=0
10820 Summe$="J"
10830 FOR I=1 TO Sum_n
10840 INPUT "WELCHE MESSUNG",S
10850 Sm(S)=1

```

```

10860 IF I=1 THEN
10870   M1=S
10880   M2=M1+1
10890 END IF
10900 NEXT I
10910 GOTO Ebene1
10920 !
10930 !
10940 !
10950 Maxmin:!
10960 Ymax=MAX(Y(*))
10970 !
10980 !PRINT "Ymax:";Ymax;" Xmin:";Xmin;" Xmax:";Xmax
10990 !
11000 !
11010 Graphik:!
11020 !
11030 CLEAR SCREEN
11040 GRAPHICS ON
11050 VIEWPORT 25,90,45,85
11060 PEN 1
11070 IF Plotter=1 THEN
11080 PLOTTER IS 705,"HPGL"
11090 ELSE
11100 PLOTTER IS CRT,"INTERNAL"
11110 END IF
11120 !PRINT CHR$(12)
11130 IF Sum_gr$="N" OR Bas_flag=0 THEN
11140 GINIT
11150 GCLEAR
11160 LINE TYPE 1
11170 IF Plotter=1 THEN PLOTTER IS 705,"HPGL"
11180 VIEWPORT 25,90,45,85
11181 IF Ymax<1 THEN Ymax=1
11190 WINDOW Xmin,Xmax,0,Ymax
11200 FRAME
11210 END IF
11220 !
11230 CSIZE 2.5,.7
11240 IF Plotter=1 THEN PLOTTER IS 705,"HPGL"
11250 !
11260 CLIP OFF
11270 !
11280 IF Bas_flag=0 THEN
11290 !
11300 !
11310 DATA 20,30,40,50,60,80,100,150,200,300,400,500,600,800,1000,1200
11320 RESTORE 11310
11330 READ DI(*)
11340 !
11350 FOR I=1 TO 16
11360 IF LGT(DI(I))>Xmax OR LGT(DI(I))<Xmin THEN 11450
11370 LDIR 90
11380 LORG 8
11390 MOVE LGT(DI(I)),0
11400 LABEL DI(I)
11410 LDIR 0
11420 LORG 4
11430 MOVE LGT(DI(I)),0
11440 DRAW LGT(DI(I)),.04*Ymax
11450 NEXT I
11460 !
11470 LORG 9
11480 MOVE Xmax,-Ymax/3.5
11490 LABEL "Dp [nm] "
11500 LORG 5

```

```

11510 !
11520 LORG 1
11530 LDIR 90
11540 MOVE Xmin-(Xmax-Xmin)/5,0
11550 !
11560 LABEL " Cp / Kanal"
11570 LORG 5
11580 LDIR 0
11590 !
11600 Bas_flag=1
11610 IF Plotter=0 THEN
11620 GSTORE Bas_graph(*)
11630 END IF
11640 ELSE ! das heisst : Bas_flag=1
11650 IF Plotter=0 THEN
11660 GLOAD Bas_graph(*)
11670 END IF
11680 END IF ! END IF für Bas_flag
11690 !
11700 IF Sum_gr$="N" OR Bas_flag=0 THEN
11710 Y_step=10^(INT((LGT(Ymax)+.7))/10
11720 !
11730 FOR I=0 TO Ymax STEP Y_step
11740 LORG 2
11750 MOVE Xmin,I
11760 DRAW Xmin+.02*(Xmax-Xmin),I
11770 LORG 8
11780 MOVE Xmin,I
11790 LABEL I
11800 NEXT I
11810 END IF
11820 !
11830 IF Sum_gr$="J" THEN GLOAD Graph1(*)
11840 !
11850 !CLIP 30,130,37,112
11860 LORG 5
11870 !
11880 FOR I=2 TO Punkte
11890 PEN M1
11900 LINE TYPE 1
11910 !IF Y(M1,I-1)<>0 THEN PEN 1
11920 MOVE X(M1,I-1),Y(M1,I-1)
11930 DRAW X(M1,I),Y(M1,I)
11940 IF Punkt$="J" THEN -
11950 MOVE X(M1,I),Y(M1,I)
11960 LABEL "+"
11970 END IF
11980 NEXT I
11990 LINE TYPE Line
12000 IF Mittel$="J" THEN 12120
12010 FOR I=2 TO Punkte
12020 PEN M1
12030 !IF Y(M2,I-1)<>0 THEN PEN M1
12040 MOVE X(M2,I-1),Y(M2,I-1)
12050 DRAW X(M2,I),Y(M2,I)
12060 IF Punkt$="J" THEN -
12070 MOVE X(M2,I),Y(M2,I)
12080 LABEL "+"
12090 END IF
12100 NEXT I
12110 !
12120 LINE TYPE 1
12130 PEN 1
12140 !FRAME
12150 !
12160 IF File$="J" THEN

```

```

12170 INPUT "MESSUNG ABLEGEN?",Ma$
12180 IF Ma$="J" OR Ma$="j" THEN
12190 !INPUT "LAUFENDE NUMMER?",Nr$
12200 Nr$=VAL$(M1)
12210 CREATE Filename$&Nr$&".DAT",1
12220 ASSIGN @F2 TO Filename$&Nr$&".DAT";FORMAT ON
12230 Outp$=Vers$&" , "&Date$&" , "&Time$(M1)
12240 OUTPUT @F2;Outp$
12250 PRINT Outp$
12260 IF Vol1$="J" THEN OUTPUT @F2;"Volumen"
12270 IF Sur1$="J" THEN OUTPUT @F2;"Oberfläche"
12280 IF Sur1$="N" AND Vol1$="N" THEN OUTPUT @F2;"Anzahl"
12290 FOR I=1 TO Punkte
12300 Outp$=VAL$(DROUND(D(I),4))&" , "&VAL$(DROUND(Y(M1,I),4))
12310 OUTPUT @F2;Outp$
12320 PRINT Outp$
12330 NEXT I
12340 ASSIGN @F2 TO *
12350 END IF
12360 END IF
12370 !
12380 DISP Y(M1,1),Y(M1,Punkte)
12390 !
12400 Cp_summe(M1)=Sum_cp
12410 !
12420 IF Vol1$="J" AND Kum$="J" THEN
12430 Vol_summe(M1)=Y(M1,1)
12440 END IF
12450 !
12460 CSIZE 2,.7
12470 !
12480 IF Sum_gr$="N" THEN
12490 MOVE Xmin,1.20*Ymax
12500 LORG 3
12510 LABEL " ";Vers$;" ";M1;" Cps.:";INT(Sum_cp);"cm^3"
12520 MOVE Xmin,1.13*Ymax
12530 LORG 3
12540 LABEL " Vol:";Vol$;" Sur:";Sur1$;" Kum.:";Kum$;" Norm.:";Fl_norm$
12550 MOVE Xmin,Ymax
12560 LORG 1
12570 LABEL " 1e:";Korr_1$;" 2e:";Korr_2$;" 3e+4e:";Mehr_lad$;" ;Tim$(M1)
12580 END IF
12590 !
12600 VIEWPORT 25,90,45,95
12610 FRAME
12620 KEY LABELS OFF
12630 IF Plotter=0 THEN GSTORE Graph1(*)
12640 KEY LABELS ON
12650 ! -
12660 IF Auto$="J" THEN Cp_sum
12670 !
12680 GOTO Keys
12690 !
12700 !
12710 Ladung:!
12720 !--- BERECHNUNG DER LADUNGSVERTEILUNG ---
12730 !
12740 DISP "--- BERECHNUNG DER LADUNGSVERTEILUNG ---"
12750 !PRINT "Dp N=1 2 3 4 5"
12760 FOR I=1 TO Punkte
12770 FOR N=1 TO 8
12780 L(N)=EXP(-N^2*(4.8E-10)^2/(D(I)*1.E-7*1.38E-16*295))
12790 NEXT N
12800 !
12810 Sumx=0
12820 FOR N=1 TO 8

```

```

12830 Sumx=Sumx+2*L(N)
12840 NEXT N
12850 !
12860 !
12870 FOR N=1 TO 5 -
12880 F(I,N)=L(N)/(1+Sumx)
12890 NEXT N
12900 !
12910 !PRINT USING 9140;D(I),F(I,1),F(I,2),F(I,3),F(I,4),F(I,5)
12920 NEXT I
12930 !
12940 ! -
12950 IMAGE DDD.D,5(XX,D.DDDD)
12960 !
12970 DISP """
12980 !
12990 MAT Fc2=F
13000 PRINTER IS 1
13010 RETURN
13020 !
13030 !
13040 !
13050 Ladungskorr:!
13060 Ladungskorr2:!
13070 !
13080 IF Bipol=1 THEN
13090 MAT F=Fc1
13100 PRINT "MAT=1",Bipol
13110 ELSE
13120 MAT F=Fc2
13130 PRINT "MAT=2",Bipol
13140 END IF
13150 !
13160 !
13170 DIM Yyy(500,6)
13180 MAT Yyy=(0)
13190 !
13200 FOR I=1 TO Punkte
13210 Yyy(I,1)=Yv(M1,I)
13220 NEXT I
13230 !
13240 IF Schr$="Auto" THEN
13250 Schritt2=INT(LOG(2)/LOG(Raster)+.1)
13260 Schritt3=INT(LOG(3)/LOG(Raster)+.1)
13270 Schritt4=INT(LOG(4)/LOG(Raster)+.1)
13280 Schritt5=INT(LOG(5)/LOG(Raster)+.1)
13290 Schritt6=INT(LOG(6)/LOG(Raster)+.1)
13300 ELSE
13310 INPUT "Schritt2",Schritt2
13320 INPUT "Schritt3",Schritt3
13330 INPUT "Schritt4",Schritt4
13340 END IF
13350 !
13360 PRINT "SCHRITT2: ";Schritt2;" SCHRITT3: ";Schritt3;" SCHRITT4: ";Schritt4;" SCHRITT5: ";Schritt5;" SCHRITT6: ";Schritt6
13370 WAIT .3
13380 !
13390 IF Mehr_lad$="J" OR Korr_2$="J" THEN
13400 FOR M=M1 TO M1+1
13410 FOR I=1 TO Punkte
13420 !
13430 K2=Yv(M,I)*F(I,2)/F(I,1)
13440 K3=Yv(M,I)*F(I,3)/F(I,1)
13450 K4=Yv(M,I)*F(I,4)/F(I,1)
13460 K5=Yv(M,I)*F(I,5)/F(I,1)
13470 K6=Yv(M,I)*F(I,6)/F(I,1)
13480 !PRINT USING 13170;K2,K3,K4,K5,K6 -

```

```

13490 IMAGE 5(SDDD.DD,XXX)
13500 !
13510 !
13520 IF (I+Schritt2)>Punkte THEN 13590
13530 IF Fl_lad$="J" THEN
13540 Yv(M,I+Schritt2)=Yv(M,I+Schritt2)-K2*Fl_faktor(1,I+Schritt2)/Fl_faktor(1,I)
13550 ELSE
13560 Yv(M,I+Schritt2)=Yv(M,I+Schritt2)-K2
13570 END IF
13580 Yyy(I+Schritt2,2)=Yv(M,I+Schritt2)
13590 !
13600 IF Mehr_lad$="J" THEN
13610 IF (I+Schritt3)>Punkte THEN 13680
13620 IF Fl_lad$="J" THEN
13630 Yv(M,I+Schritt3)=Yv(M,I+Schritt3)-K3*Fl_faktor(1,I+Schritt3)/Fl_faktor(1,I)
13640 ELSE
13650 Yv(M,I+Schritt3)=Yv(M,I+Schritt3)-K3
13660 END IF
13670 Yyy(I+Schritt3,3)=Yv(M,I+Schritt3)
13680 !
13690 IF (I+Schritt4)>Punkte THEN 13760
13700 IF Fl_lad$="J" THEN
13710 Yv(M,I+Schritt4)=Yv(M,I+Schritt4)-K4*Fl_faktor(1,I+Schritt4)/Fl_faktor(1,I)
13720 ELSE
13730 Yv(M,I+Schritt4)=Yv(M,I+Schritt4)-K4
13740 END IF
13750 Yyy(I+Schritt4,4)=Yv(M,I+Schritt4)
13760 !
13770 IF (I+Schritt5)>Punkte THEN 13850
13780 IF Fl_lad$="J" THEN
13790 Yv(M,I+Schritt5)=Yv(M,I+Schritt5)-K5*Fl_faktor(1,I+Schritt5)/Fl_faktor(1,I)
13800 ELSE
13810 Yv(M,I+Schritt5)=Yv(M,I+Schritt5)-K5
13820 END IF
13830 Yyy(I+Schritt5,5)=Yv(M,I+Schritt5)
13840 !
13850 IF (I+Schritt6)>Punkte THEN 13930
13860 IF Fl_lad$="J" THEN
13870 Yv(M,I+Schritt6)=Yv(M,I+Schritt6)-K6*Fl_faktor(1,I+Schritt6)/Fl_faktor(1,I)
13880 ELSE
13890 Yv(M,I+Schritt6)=Yv(M,I+Schritt6)-K6
13900 END IF
13910 Yyy(I+Schritt6,6)=Yv(M,I+Schritt6)
13920 END IF
13930 !
13940 NEXT I
13950 NEXT M
13960 END IF
13970 !
13980 FOR I=1 TO Punkte
13990 !PRINT USING 13700;D(I),Yyy(I,1),Yyy(I,2),Yyy(I,3),Yyy(I,4),Yyy(I,5)
14000 NEXT I
14010 !
14020 IMAGE DDDD.D,6(XX,DDDD.D)
14030 FOR M=M1 TO M1+1
14040 FOR I=1 TO Punkte
14050 !
14060 !Korr_1e: !---- 1-fach Ladungskorrektur ----
14070 ! -
14080 IF Korr_1$<>"N" THEN
14090 IF Yv(M,I)<0 THEN Yv(M,I)=0
14100 Yv(M,I)=Yv(M,I)/F(I,1)
14110 ELSE
14120 Yv(M,I)=Yv(M,I)
14130 END IF
14140 !

```

```

14150 NEXT I
14160 NEXT M
14170 !
14180 RETURN
14190 !
14200 !
14210 !
14220 Knob:!-----
14230 !
14240 LINE TYPE 1
14250 Xpos=Punkte
14260 !
14270 !
14280 !
14290 Turn:!
14300 !
14310 LORG 5
14320 IF Xpos<1 THEN Xpos=1
14330 IF Xpos>Punkte THEN Xpos=Punkte
14340 !
14350 GLOAD Graph1(*)
14360 !
14370 !
14380 K_loop:!
14390 !
14400 ON KEY 9 LABEL " KEYS " GOTO Ex
14410 ON KEY 7 LABEL "LIMIT_U" GOTO Limu
14420 ON KEY 8 LABEL "LIMIT_O" GOTO Limo
14430 ON KEY 6 LABEL " FIT " GOTO Fit
14440 ON KEY 5 LABEL "CP_SUMME" GOTO Cp_sum
14450 GOTO K_loop
14460 !
14470 !
14480 Limu:!
14490 DISP "Lim_u mit Maus"
14500 TRACK CRT IS ON
14510 DIGITIZE Digx,Digy,Dig$
14520 Lim_u=10^Digx
14530 LORG 3
14540 MOVE Xmin,Ymax
14550 LABEL INT(Lim_u*10)/10
14560 DISP "Digx";Digx;" Lim_u";Lim_u
14570 GOTO K_loop
14580 !
14590 !
14600 Limo:!
14610 DISP "Lim_o mit Maus"
14620 TRACK CRT IS ON
14630 DIGITIZE Digx,Digy,Dig$
14640 Lim_o=10^Digx
14650 LORG 9
14660 MOVE Xmax,Ymax
14670 LABEL INT(Lim_o*10)/10;"nm"
14680 DISP "Digx";Digx;" Lim_o";Lim_o
14690 GOTO K_loop
14700 !
14710 Cp_sum:!
14720 !
14730 Cp_sum=0
14740 FOR I=1 TO Punkte
14750 IF (D(I)>=Lim_u) AND (D(I)<=Lim_o) THEN
14760   IF Mittel$="J" THEN
14770     Cp_sum=Cp_sum+Y(M1,I)
14780   ELSE
14790     Cp_sum=Cp_sum+Y(M1,I)/2+Y(M2,I)/2
14800 END IF

```

```

14810 END IF
14820 NEXT I
14830 !
14840 !
14850 DISP "Cp_s:";Cp_sum
14860 !
14870 IF Auto$="J" THEN
14880 PRINTER IS Vol_print
14890 PRINT "MESS:";M1;" ";Tim$(M1);" Sum_cp:";INT(Sum_cp);" R.F.:";DROUND(Rf(M1),4);" Temp.:";DROUND(Temp(M1,1),4);
14900 V_sum(M1)=Cp_sum
14910 A_sum(M1)=Sum_cp
14920 END IF
14930 IF Vol$="J" THEN
14940 PRINT "Summe Vol. (";INT(Lim_u);"-";INT(Lim_o);"nm ):";INT(Cp_sum*100)/100;"cm^-3"
14950 END IF
14960 !
14970 PRINT """
14980 !
14990 IF Cmd$="J" THEN
15000 !
15010 Cmd=1000*Sd1/S_n
15020 Smd=1000*Sd3/Sd2
15030 Mmd=1000*Sd4/Sd3
15040 ! -
15050 Doas=1000*(Sd2/S_n)^.5
15060 Doav=1000*(Sd3/S_n)^(1/3)
15070 !
15080 PRINT USING
15090;" CMD :" ;Cmd;" SMD :" ;Smd;" MMD :" ;Mmd;" DoaS;" Doas;" DoaV: " ;Doav 15090 IMAGE 5(6A,DDDD,XX)
15100 !
15110 END IF
15120 !
15130 !
15140 PRINTER IS 1
15150 !
15160 IF Auto_fit$="J" THEN Fit
15170 !
15180 IF Auto$="J" THEN GOTO Messwahl
15190 GOTO K_loop
15200 !
15210 Ex:!
15220 OFF KNOB
15230 GOTO Keys
15240 !
15250 !
15260 Plot_sum:!
15270 !
15280 J=0
15290 FOR I=1 TO Maxmess
15300 IF A_sum(I)>0 THEN
15310 J=J+1
15320 V_sum(J)=V_sum(I)
15330 A_sum(J)=A_sum(I)
15340 Time_sum(J)=TIME(Time$(I))
15350 END IF
15360 NEXT I
15370 !
15380 !
15390 !-----

```

```

15400 GOTO Spw
15410 !-----
15420 !
15430 REDIM Time_sum(J)
15440 REDIM V_sum(J)
15450 REDIM A_sum(J)
15460 !
15470 X_min=MIN(Time_sum(*))
15480 X_max=MAX(Time_sum(*)))
15490 Y_min=INT(LGT(MIN(V_sum(*))))
15500 Y_max=INT(1+LGT(MAX(V_sum(*))))
15510 !
15520 Decade=(Y_max-Ymin)-1
15530 !
15540 GRAPHICS ON
15550 GCLEAR
15560 VIEWPORT 25,90,45,85
15570 WINDOW X_min,X_max,Y_min,Y_max
15580 FRAME
15590 CLIP OFF
15600 !
15610 FOR I=2 TO J
15620 MOVE Time_sum(I-1),LGT(V_sum(I-1))
15630 DRAW Time_sum(I),LGT(V_sum(I))
15640 NEXT I
15650 !
15660 !
15670 !
15680 LINE TYPE 1
15690 FOR I=Y_min TO Y_max
15700 LORG 2
15710 MOVE X_min,I
15720 DRAW X_min+(X_max-X_min)/15,I
15730 LORG 8 15740 MOVE X_min,I
15750 LABEL "10"
15760 LORG 7
15770 MOVE X_min,I
15780 LABEL I
15790 NEXT I
15800 !
15810 !Y_min=INT(LGT(MIN(A_sum(*))))
15820 Y_max=INT(1+LGT(MAX(A_sum(*))))
15830 Y_min=Y_max-Decade
15840 !
15850 WINDOW X_min,X_max,Y_min,Y_max
15860 LINE TYPE 4
15870 !
15880 FOR I=2 TO J
15890 MOVE Time_sum(I-1),LGT(A_sum(I-1))
15900 DRAW Time_sum(I),LGT(A_sum(I))
15910 NEXT I
15920 !
15930 LINE TYPE 1
15940 FOR I=Y_min TO Y_max
15950 LORG 8
15960 MOVE X_max,I
15970 DRAW (X_max-(X_max-X_min)/15),I
15980 LORG 2
15990 MOVE X_max,I
16000 LABEL "10"
16010 LORG 1
16020 MOVE X_max,I
16030 LABEL ";"I
16040 NEXT I
16050 !

```

```

16060 LDIR 90
16070 FOR I=0 TO (24*3600.) STEP 1800
16080 IF I>=X_min AND I<=X_max THEN
16090   LORG 2
16100   MOVE I,Y_min
16110   LABEL "."
16120   LORG 8
16130   MOVE I,Y_min
16140   LABEL USING "5A";TIME$(I)&" "
16150 END IF
16160 NEXT I
16170 !
16180 Spw:!-----
16190 INPUT "SigmaPlot-File erzeugen?",Spf$
16200 !
16210 IF Spf$="J" OR Spf$="j" THEN
16220 !
16230 OFF ERROR
16240 !
16250 INPUT "erste Messung?",Spf_st
16260 INPUT "letzte Messung?",Spf_end
16270 Ts_null=Time_sum(Spf_st)/60
16280 ! -16290 Spf_file$=Vers$&".spf"
16300 CREATE Spf_file$,1
16310 ASSIGN @F7 TO Spf_file$;FORMAT ON
16320 !
16330 FOR I=Spf_st TO Spf_end
16340   Time_sum(I)=Time_sum(I)/60-Ts_null
16350   Spf_string1$=Time$(I)&" , "&VAL$(DROUND(Cp_summe(I),4))&" , "&VAL$(DROUND(Vol_summe(I),4))&" ,
16360   Spf_string2$=VAL$(DROUND(Time_sum(I),4))&" , "&VAL$(DROUND(Dp_quer(I),4))&" , "&VAL$(DROUND(Sigma_g(I),4))
16370   Spf_string$=Spf_string1$&Spf_string2$
16380   OUTPUT @F7;Spf_string$
16390 NEXT I
16400 !
16401 Auto$="N"
16402 Auto_fit$="N"
16403 !
16405 PRINT "Speichern O.K."
16410 ASSIGN @F7 TO *
16420 !
16430 END IF
16440 !
16450 !
16460 GOTO Keys
16470 !
16480 !
16490 List:!
16500 !
16510 Vax_dat$="N"
16520 !INPUT "DATENÜBERTRAGUNG --> VAX?",Vax_dat$
16530 !IF Vax_dat$="J" THEN GOTO Vax
16540 !
16550 PRINTER IS 701
16560 !
16570 PRINT " ;Vers$;" ;Date$;" Messung:";M1
16580 PRINT """
16590 PRINT " Norm.:";Fl_norm$;" 1e:";Korr_1$;" 2e:";Korr_2$;" 3e +4e:";Mehr_lad$
16600 !
16610 PRINT """
16620 PRINT " Oberfl.:";Sur1$;" Volumen:";Vol1$
16630 !
16640 PRINT """
16650 IF Mittel$="J" THEN PRINT " Mittelwert Hin- und Rückmessung"
16660 !
16670 PRINT """
16680 PRINT """

```

```

16690 PRINT "    Dp [ nm ]    Cp [ cm^-3 ] "
16700 !
16710 PRINT """
16720 !
16730 FOR I=Punkte TO 1 STEP -1
16740  PRINT USING 16790;10^(X(M1,I)),Y(M1,I)
16750  IF I MOD 5=0 THEN PRINT """
16760 NEXT I
16770 !
16780 PRINTER IS 1
16790 IMAGE XXXXX,DDDD.D,12X,DDDDD.D
16800 GOTO Keys
16810 !
16820 !
16830 !
16840 !
16850 !
16860 Fit!:-----
16870 !
16880 OFF KNOB
16890 ALPHA ON
16900 !
16910 MAT Yv=Y
16920 !
16930 Npt=0
16940 FOR I=Punkte TO 1 STEP -1
16950  IF Xv(M1,I)<=LGT(Lim_o) AND X(M1,I)>=LGT(Lim_u) THEN
16960    Npt=Npt+1
16970    X(M1,Npt)=10^Xv(M1,I)
16980    Y(M1,Npt)=Yv(M1,I)
16990    !PRINT X(M1,Npt),Y(M1,Npt)
17000 END IF
17010 NEXT I
17020 !
17030 Npts=Npt
17040 !REDIM X(2,Npt)
17050 !REDIM Y(2,Npt)
17060 !
17070 !
17080 !--- CLASSIFIER-AUSWERTUNG LOG-VERT. --
17090 !
17100 !
17110 !
17120 DIM A$(4)[84],Sigmay(100)
17130 COM Yfit(500),Deriv(10),A(10),Deltaa(10)
17140 COM Sigmaa(10),Zz(1,2),Lab(30)
17150 DIM Mode$(10)[25]
17160 DIM Yk(500),Y_vor(500),Cp_vor(500),Flag(500)
17170 DIM Kkz(30),Ct(30),Yd1(500),Yd2(500)
17180 !
17190 INTEGER Graph_1(1:256,1:192),Graph_2(1:256,1:192)
17200 INTEGER Graph_3(1:256,1:192),Graph_4(1:256,1:192)
17210 INTEGER Graph_5(1:256,1:192),Graph_6(1:256,1:192)
17220 !
17230 MAT Deltaa=(.00001)
17240 Flamda=.001
17250 Nterms=3
17260 Fit_flag=1
17270 Autoflag=0
17280 Ae_flag=0
17290 A(3)=1
17300 A(4)=300
17310 A(5)=2
17320 !
17330 !
17340 Speich$="N"

```

```

17350 Print_flag$="N"
17360 Funk_plot$="J"
17370 !
17380 !
17390 Yst=0
17400 Ynd=1
17410 !
17420 !
17430!Versuch: !
17440 !
17450 FOR I=1 TO 120
17460 Flag(I)=1
17470 NEXT I
17480 !
17490 !
17500 Ae_file=0
17510 !
17520 CLEAR SCREEN
17530 !
17540 !
17550 GRAPHICS OFF
17560 !
17570 !
17580 Sur_vol:!
17590 !
17600 !
17610 IF Print_flag$="J" THEN Listing
17620 !
17630 GOTO 17690
17640 Listing:-----
17650 List_flag=1
17660 PRINTER IS 701
17670 OFF KEY (9)
17680 !
17690 PRINT ""
17700 PRINT ""
17710 PRINT "-- CLASSIFIER ----- ";Vers$;" -- ";Messzeit$;" -----"
17720 PRINT ""
17730 !
17740 IF Mittel$="J" THEN
17750 PRINT "---- Mittelwerte der Messungen ";Mess_pl;"+";Mess_pl+1;" ---"
17760 ELSE
17770 PRINT "----- Messung ";Mess_pl;" -----"
17780 END IF
17790 !
17800 PRINT ""
17810 PRINT ""
17820 PRINT " Dp [nm] Cmess Ckorr (1e+2e) Summe [%]"
17830 PRINT ""
17840 !
17850 IMAGE XX,DDD.D,X,DDDDDDDD.D,XX,DDDDDDDD.D!,XXXXXXXX,DDD.DD
17860 !
17870 !
17880 Sum_ck=0
17890 FOR I=1 TO Npts
17900 IF Y(M1,I)<0 THEN Y(M1,I)=0 -
17910 Sum_ck=Sum_ck+Y(M1,I)
17920 NEXT I
17930 !
17940 Cks=0
17950 FOR I=1 TO Npts
17960 Cks=Cks+Y(M1,I)
17970 !PRINT USING 10210;X(M1,I),Cp(I),Y(M1,I)!,Cks/Sum_ck*100
17980 NEXT I
17990 PRINT ""
18000 PRINT ""

```

```

18010 PRINT "Partikelsumme :";Cks
18020 !
18030 PRINTER IS 1
18040 !
18050 IF List_flag=1 THEN
18060 List_flag=0
18070 END IF
18080 !
18090 !
18100 !-----
18110 Yt=MAX(Y(*))
18120 !
18130 !
18140 Kanal_listing:!
18150 IMAGE DDDD.D,"nm",#
18160 IMAGE DDDD.D," ",#
18170 IMAGE L
18180 PRINTER IS 1
18190 !
18200 !-----
18210 !
18220 D_vor:!
18230 !
18240 !---- ABSCHØTZUNG Dg , Sigma ----
18250 !
18260 Dgz=0
18270 Sum=0
18280 !
18290 FOR I=1 TO Npts
18300 Dgz=Dgz+Y(M1,I)*LOG(X(M1,I))
18310 Sum=Sum+Y(M1,I)
18320 IF Sum=0 THEN 18340
18330 !PRINT EXP(Dgz/Sum)
18340 NEXT I
18350 !
18360 Dgz=Dgz/Sum
18370 Dg=EXP(Dgz)
18380 A(1)=Dg
18390 !
18400 !
18410 Sumsig=0
18420 FOR I=1 TO Npts
18430 Sumsig=Sumsig+Y(M1,I)*(LOG(Dg)-LOG(X(M1,I)))^2
18440 NEXT I
18450 !
18460 Sigma=EXP((Sumsig/(Sum-1))^0.5)
18470 A(2)=Sigma
18480 !
18490 PRINT "ERSTABSCHØTZUNG: Dp=";A(1);" Sigma=";A(2)
18500 !
18510 !
18520 Deltaa(1)=2
18530 Deltaa(2)=.05
18540 Flamda=.001
18550 !
18560 F_d=1/(Dg*LOG(Sigma)*(2*PI)^0.5)
18570 !
18580 !
18590 !----- IMAX -----
18600 !
18610 Imax=1
18620 Ymax=0
18630 FOR I=2 TO Npts
18640 IF Y(M1,I)>Ymax THEN
18650 Ymax=Y(M1,I)
18660 Imax=I

```

```

18670 !PRINT "lmax:";lmax
18680 END IF
18690 NEXT I
18700 !
18710 !
18720 l=lmax
18730 A(4)=300
18740 A(5)=1.8
18750 A(6)=1
18760 A(3)=1
18770 Deltaa(4)=2
18780 !
18790 ! 018800 !-----
18810 !
18820 Loop=0
18830 !
18840 Key:!
18850 ON KEY (0) LABEL " PLOT " GOSUB Gr_lbl
18860 ON KEY (1) LABEL "LISTING" GOTO Listing
18870 ON KEY (2) LABEL "VERSUCH" GOTO Versuch
18880 ON KEY (3) LABEL " KEYS " GOTO Keys
18890 ON KEY (5) LABEL "LOCK_A()" GOTO Lock
18900 ON KEY (6) LABEL "CONT_FIT" GOTO Curfit
18910 ON KEY (7) LABEL "G_STORE" GOTO Gstore
18920 !ON KEY (6) LABEL " " GOTO Key
18930 ON KEY (9) LABEL "G_LOAD " GOTO Gload
18940 IF Loop=0 THEN Y_norm
18950 GOTO Key
18960 !
18970 Gr_lbl:!
18980 Gr_fl=1
18990 RETURN
19000 !
19010 Lock:!
19020 CLEAR SCREEN
19030 !
19040 PRINT "SOLL DER DURCHMESSER (1) ODER SIGMA (2) KONSTANT GEHALTEN WERDEN ?"
19050 !
19060 INPUT Lk
19070 !
19080 IF Lk=1 THEN
19090 INPUT "Dp [nm]",A(1)
19100 END IF
19110 IF Lk=2 THEN
19120 INPUT "Sigma (1.1 - 5)",A(2)
19130 END IF
19140 !
19150 !
19160 Y_norm:!
19170 !
19180 Loop=1
19190 Nfree=Npts-Nterms
19200 !
19210 Ymx=Y(M1,lmax)
19220 FOR I=1 TO Npts
19230 Y(M1,I)=Y(M1,I)/Ymx
19240 !PRINT "Y(M1,I);Y(M1,I)"
19250 NEXT I
19260 !
19270 PRINT "lmax: ";lmax;" Ywertmax: ";Ywertmax
19280 !
19290 IF Funk_plot$="N" THEN Grap
19300 !
19310 !
19320 FOR I=1 TO Npts
19330 GOSUB Functn

```

```

19340 Yfit(l)=Fu
19350 NEXT l
19360 !
19370 GOSUB Fchisq
19380 Chisqua=Chisq+1
19390 !
19400 !
19410 Ywertmax=1
19420 !
19430 !-----
19440 !
19450 Gr_fl=0
19460 !
19470 Curfit: !
19480 !
19490 Funk_flag=0
19500 !
19510 GOSUB Cf
19520 !
19530 !
19540 IF (Gr_fl=1) OR (Chisqua-Chisqr)<1.E-4 THEN GOTO Grap
19550 !
19560 PRINT "Chisq.:";INT(Chisqr*100000.)/100;" Delta:";Chisqua-Chisqr
19570 PRINT ""
19580 IF Nterms<4 THEN
19590 DISP "Dp ":";INT(A(1)*1000)/1000;" Sigma_g ":";INT(A(2)*1000)/1000
19600 ELSE
19610 DISP USING 19640;A(1),A(2),A(3),A(4),A(5),A(6)
19620 END IF
19630 Chisqua=Chisqr
19640 IMAGE 2(DDD.DD,X,D/DDDD,X,D.DDD,XXXX)
19650 !
19660 !
19670 GOTO Curfit
19680 !
19690 !
19700 Fit_flag=0
19710 !
19720 !
19730 Plot:!
19740 !
19750 A(1)=INT(A(1)*100)/100
19760 A(2)=INT(A(2)*100)/100
19770 !
19780 Dp_v=10^(LGT(A(1))+6.9*(LGT(A(2)))^2)
19790 Dp_s=10^(LGT(A(1))+4.6*(LGT(A(2)))^2)
19800 !
19810 !Mtzeit=(TIME(Messzeit$)-Nullzeit)/60
19820 !
19830 Cpmt=EXP(Ak(1)-Ak(2)*Mtzeit-Ak(3)*Mtzeit^2-Ak(4)*Mtzeit^.5)
19840 Cpmt=DROUND(Cpmt,4)
19850 !
19860 IF Speich$="J" THEN PRINTER IS 701
19870 !
19880 PRINT Vers$;" Mess:";Mess_pl;" ";Messzeit$;" Dp:";A(1);" Sig_g:";A(2);
19890 PRINT "Dp_v:";INT(Dp_v*100)/100;" Dp_s:";INT(Dp_s*100)/100;" Cp:";Cpmt
19900 !
19910 PRINTER IS 1
19920 !
19930 IF Ct(lmax)=0 THEN Ct(lmax)=1
19940 !
19950 !
19960 PRINT ""
19970 PRINT "Ymx/Ywertmax :";Ymx/Ywertmax
19980 PRINT ""
19990 PRINT "Ymx/Ywertmax/Ct(lmax) :";Ymx/Ywertmax/Ct(lmax)

```

```

20000 !
20010 IF Speich$="J" THEN
20020 !
20030 !***** SPEICHERN *****
20040 !
20050 ON ERROR GOTO Err_create
20060 !
20070 !
20080 IF Ae_file=0 THEN
20090 Ae_file=1
20100 CREATE BDAT Vers$&"AE",Maxmess
20110 ASSIGN @F2 TO Vers$&"AE"
20120 END IF
20130 !
20140 GOTO Speich_ae
20150 !
20160 !
20170 Err_create: !
20180 IF ERRN=80 THEN
20190 PRINT "FEHLER CREATE "
20200 GOTO 20100
20210 ELSE
20220 IF ERRN=54 THEN
20230 PRINT "FILENAME SCHON VERGEBEN ,LÖSCHEN ?"
20240 INPUT File_l$%
20250 IF File_l$%"J" THEN
20260 File_l$%"N" -
20270 PURGE Vers$&"AE"
20280 CREATE BDAT Vers$&"AE",Maxmess
20290 ASSIGN @F2 TO Vers$&"AE"
20300 GOTO Speich_ae
20310 ELSE
20320 PRINT "PAUSE-MODE"
20330 PAUSE
20340 END IF
20350 END IF
20360 PRINT "FEHLER FILENAME - PAUSE-MODE"
20370 PAUSE
20380 END IF
20390 !
20400 OFF ERROR
20410 !
20420 Speich_ae: !
20430 !
20440 ON ERROR GOTO Err_ass
20450 !
20460 !
20470 T=TIME(Messzeit$)
20480 Hrs=T DIV 3600
20490 Min=(T MOD 3600)/60
20500 T=INT(Hrs*100+Min)
20510 S=(Dp_s)^2*PI*Cpmt/1.E+6
20520 V=(Dp_v)^3*PI*Cpmt/6/1.E+9
20530 Snv=6^(2/3)*PI^(1/3)*(Dp_s/Dp_v)^2
20540 PRINT T,Cpmt,A(1),A(2),Dp_s,Dp_v,S,V,Snv
20550 OUTPUT @F2;T,Cpmt,A(1),A(2),Dp_s,Dp_v,S,V,Snv
20560 GOTO Grap
20570 !
20580 Err_ass: !
20590 PRINT "FEHLER ASSIGN - PAUSE-MODE"
20600 OFF ERROR
20610 PAUSE
20620 !
20630 !
20640 !
20650 END IF

```

```

20660 PRINTER IS 1
20670 !
20680 Grap:!-----
20690 !
20700 !
20710 DIM X1(500)
20720 DIM Y1(500)
20730 DIM Fehler(500)
20740 !REDIM X(Npts)
20750 !REDIM Y(Npts)
20760 OFF KEY (0)
20770 PRINTER IS 1
20780 CLEAR SCREEN
20790 GCLEAR
20800 GRAPHICS ON
20810 ALPHA OFF
20820 !MAT X1= X
20830 !MAT Y1= Y
20840 !MAT SORT X
20850 !MAT SORT Y
20860 VIEWPORT 25,90,45,85
20870 !
20880 Gr_fl=0
20890 !
20900 Xst=LOG(X(M1,1))
20910 Xnd=LOG(X(M1,Npts))
20920 !
20930 !
20940 Yst=0
20950 Ynd=1
20960 WINDOW Xst,Xnd,Yst,Ynd
20970 FRAME
20980 CLIP OFF
20990 !
21000 !----- ACHSENBESCHRIFTUNG -----
21010 !----- X-ACHSE -----
21020 !
21030 DATA 10,20,30,40,50,60,70,80,100,150,200,300,400,500,600,700,800,900,1000
21040 !
21050 RESTORE 21030
21060 !
21070 LORG 5
21080 CSIZE 3.5,1
21090 !
21100 FOR I=1 TO 19
21110 READ Lab(I)
21120 IF LOG(Lab(I))>Xnd OR LOG(Lab(I))<Xst THEN 21210
21130 LDIR 0
21140 LORG 5
21150 MOVE LOG(Lab(I)),0
21160 DRAW LOG(Lab(I)),.05
21170 LDIR 90
21180 LORG 8
21190 MOVE LOG(Lab(I)),0
21200 LABEL Lab(I)
21210 NEXT I
21220 !
21230 LDIR 0
21240 !
21250 !----- Y-ACHSE -----
21260 !
21270 FOR I=0 TO 1 STEP .2
21280 LORG 5
21290 MOVE Xst,I
21300 DRAW Xst+(Xnd-Xst)/50,I
21310 LORG 8

```

```

21320 MOVE Xst,I
21330 LABEL I*100
21340 NEXT I
21350 !
21360 MOVE Xst,.9
21370 LORG 8
21380 LABEL "[%] "
21390 !
21400 !----- PLOT - BESCHRIFTUNG -----
21410 !
21420 !
21430 CSIZE 3.5,.8
21440 LORG 2
21450 MOVE Xst,1.22
21460 !
21470 IF Mittel$<>"J" THEN
21480 !LABEL Vers$;" ";MI1
21490 ELSE
21500 !LABEL Vers$;"";MI1 I;"+";MI2
21510 END IF
21520 !
21530 !
21540 LORG 8
21550 MOVE Xnd,1.1
21560 LABEL Time$(MI1)
21570 !
21580 !
21590 LORG 2
21600 MOVE Xst,1.08
21610 !
21620 IF Fit_flag=1 AND Funk_plot$="J" THEN
21630 !LABEL "Dp:";INT(A(1)*10)/10;" Sigm_g:";INT(A(2)*100)/100
21640 !
21650 END IF
21660 !
21670 MOVE Xnd,.15
21680 LORG 9
21690 LABEL "[nm] "
21700 !
21710 !
21720 !-----
21730 GOTO 21870
21740 Rxx=0
21750 S=0
21760 FOR I=1 TO Npts
21770 Rx=Rx+X1(I)
21780 Rxx=Rxx+X1(I)^2
21790 S=S+(Y1(I)-FNFunctn(X1(*),I,A(*)))^2 '21800 Xx=Yk(I)-FNFunctn(X1(*),I,A(*))
21810 NEXT I
21820 !
21830 S=S/(Npts-2)
21840 Dd=Npts*Rxx-Rx^2
21850 Sa2=SQR(Npts*S/Dd)
21860 !
21870 FOR I=1 TO Npts
21880 MOVE LOG(X(M1,I)),Y(M1,I)
21890 LORG 5
21900 CSIZE 1.5,.8
21910 IF Flag(I)=1 THEN
21920 !LABEL "*"
21930 ELSE
21940 !LABEL ""
21950 END IF
21960 NEXT I
21970 !
21980 !

```

```

21990 MOVE LOG(X(M1,1)),0
22000 !
22010 !
22020 !---- FUNKTION ZEICHNEN -----
22030 !
22040 IF Funk_plot$<>"N" THEN
22050  Funk_flag=1
22060  FOR Xx=X(M1,1) TO X(M1,Npts) STEP ABS(X(M1,1)-X(M1,Npts))/800
22070  LINE TYPE 1
22080  I=1
22090  Zz(1,1)=Xx
22100  GOSUB Functn
22110  Ypl=Fu
22120  PLOT LOG(Xx),Ypl
22130  !PRINT Xx,Ypl
22140  LINE TYPE 1
22150  NEXT Xx
22160  Funk_flag=0
22170 END IF
22180 !
22190 !-----
22200 !
22210 !
22220 CSIZE 3.5,.8
22230 LORG 3
22240 MOVE Xst,1.35
22250 !LABEL "Fl:";Fak_korr$;" 3e:";Mehr_lad$;" Kk:";Konz_korr$;" Vol:";Vol$;" Sur:";Sur$
22260 !
22270 ALPHA ON
22280 !
22290 !
22300 !PRINT CHR$(12)
22310 PRINT """
22320 PRINT "Messung ";MI1
22330 !
22340 PRINTER IS Vol_print
22350 PRINT USING 22380;A(1),A(2),Chisqua
22360 PRINT """
22370 PRINTER IS 1
22380 IMAGE "Dp_quer: ",DDD.D,XX,"Sigma_g: ",D.DDD,XX,"Chisquare: ",D.DDDDD
22390 !
22400 Dp_quer(MI1)=A(1)
22410 Sigma_g(MI1)=A(2)
22420 !
22430 PAUSE
22440 IF Auto_fit$="J" THEN Messwahl
22450 VIEWPORT 25,90,45,85
22460 FRAME
22470 !
22480 GOTO Keys
22490 !
22500 !
22510 Gstore:!
22520 !
22530 !
22540 PLOTTER IS CRT,"INTERNAL"
22550 !
22560 Store_key:!
22570 ON KEY (0) LABEL "GRAPH_1" GOTO Sto1
22580 ON KEY (1) LABEL "GRAPH_2" GOTO Sto2
22590 ON KEY (2) LABEL "GRAPH_3" GOTO Sto3
22600 ON KEY (3) LABEL "GRAPH_4" GOTO Sto4
22610 ON KEY (4) LABEL "GRAPH_5" GOTO Sto5
22620 ON KEY (5) LABEL "GRAPH_6" GOTO Sto6
22630 !
22640 GOTO Store_key

```

```

22650 !
22660 Sto1:!
22670 GSTORE Graph_1(*)
22680 Gflag1=1
22690 GOTO Key
22700 !
22710 Sto2:!
22720 GSTORE Graph_2(*)
22730 Gflag2=1
22740 GOTO Key
22750 !
22760 Sto3:!
22770 GSTORE Graph_3(*)
22780 Gflag3=1
22790 GOTO Key
22800 !
22810 Sto4:!
22820 GSTORE Graph_4(*)
22830 Gflag4=1
22840 GOTO Key
22850 !
22860 Sto5:!
22870 GSTORE Graph_5(*)
22880 Gflag5=1
22890 GOTO Key
22900 !
22910 Sto6:!
22920 GSTORE Graph_6(*)
22930 Gflag6=1
22940 GOTO Key
22950 !
22960 !
22970 !----- LOAD GRAPHICS -----
22980 !
22990 Gload:!
23000 !
23010 PLOTTER IS CRT,"INTERNAL"
23020 GRAPHICS ON
23030 ALPHA OFF
23040 !
23050 Gkeys:!
23060 OFF KEY {8}
23070 !
23080 !
23090 Load_key:!
23100 ON KEY (0) LABEL "GRAPH_1" GOTO Load1
23110 ON KEY (1) LABEL "GRAPH_2" GOTO Load2
23120 ON KEY (2) LABEL "GRAPH_3" GOTO Load3
23130 ON KEY (3) LABEL "GRAPH_4" GOTO Load4
23140 ON KEY (4) LABEL "GRAPH_5" GOTO Load5
23150 ON KEY (5) LABEL "GRAPH_6" GOTO Load6
23160 ON KEY (8) LABEL "AUTO_PL" GOTO Auto_pl
23170 ON KEY (9) LABEL "KEYS" GOTO Key
23180 !
23190 GOTO Load_key
23200 !
23210 Load1:!
23220 GLOAD Graph_1(*)
23230 GOTO Load_key
23240 !
23250 Load2:!
23260 GLOAD Graph_2(*)
23270 GOTO Load_key
23280 !
23290 Load3:!
23300 GLOAD Graph_3(*)

```

```

23310 GOTO Load_key
23320 !
23330 Load4:!
23340 GLOAD Graph_4(*)
23350 GOTO Load_key
23360 !
23370 Load5:!
23380 GLOAD Graph_5(*)
23390 GOTO Load_key
23400 !
23410 Load6:!
23420 GLOAD Graph_6(*)
23430 GOTO Load_key
23440 !
23450 Auto_pl:!
23460 !
23470 ON KEY (5) LABEL " WAIT+" GOTO Wait_plus
23480 ON KEY (6) LABEL " WAIT-" GOTO Wait_minus
23490 !
23500 IF Gflag1=1 THEN
23510 GLOAD Graph_1(*)
23520 WAIT Pl_wait
23530 END IF
23540 IF Gflag2=1 THEN
23550 GLOAD Graph_2(*)
23560 WAIT Pl_wait
23570 END IF
23580 IF Gflag3=1 THEN
23590 GLOAD Graph_3(*)
23600 WAIT Pl_wait
23610 END IF
23620 IF Gflag4=1 THEN
23630 GLOAD Graph_4(*)
23640 WAIT Pl_wait
23650 END IF
23660 IF Gflag5=1 THEN
23670 GLOAD Graph_5(*)
23680 WAIT Pl_wait
23690 END IF
23700 IF Gflag6=1 THEN
23710 GLOAD Graph_6(*)
23720 WAIT Pl_wait
23730 END IF
23740 !
23750 GOTO Auto_pl
23760 !
23770 !
23780 Wait_plus:!
23790 Pl_wait=Pl_wait*1.5
23800 GOTO Auto_pl
23810 !
23820 Wait_minus:!
23830 Pl_wait=Pl_wait/1.5
23840 IF Pl_wait<=.1 THEN Pl_wait=.10
23850 GOTO Auto_pl
23860 !
23870 !
23880 GOTO Key
23890 !
23900 !
23910 !
23920 !
23930 !
23940 ! 023950 !#####
23960 ! 023970 !#####
23980 !

```

```

23990 !
24000 !
24010 !
24020 !
24030 Fchisq!:!
24040 !
24050 Chisq=0 -
24060 IF Nfree>0 THEN GOTO M20
24070 Fchisq=0
24080 GOTO M40
24090 !
24100 M20: FOR I=1 TO Npts
24110 M30: Chisq=Chisq+(Y(M1,I)-Yfit(I))^2
24120 NEXT I
24130 Free=Nfree
24140 M40:!
24150 RETURN
24160 !
24170 !*****!
24180 !
24190 Cf:!
24200 Count=Count+1
24210 PRINT Count,
24220 !DEFAULT OFF
24230 DIM Weight(100)
24240 DIM Alpha(10,10)
24250 DIM Beta(10)
24260 !DIM Deriv(10)
24270 DIM Array(10,10) 24280 REDIM Array(Nterms,Nterms)
24290 DIM B(10)
24300 Nfree=Npts-Nterms
24310 !
24320 !
24330 L31: FOR J=1 TO Nterms
24340 Beta(J)=0
24350 FOR K=1 TO J
24360 Alpha(J,K)=0
24370 NEXT K
24380 NEXT J
24390 !
24400 L41: FOR I=1 TO Npts
24410 GOSUB Fderiv
24420 FOR J=1 TO Nterms
24430 GOSUB Functn
24440 Beta(J)=Beta(J)+(Y(M1,I)-Fu)*Deriv(J)
24450 FOR K=1 TO J
24460 Alpha(J,K)=Alpha(J,K)+Deriv(J)*Deriv(K)
24470 NEXT K
24480 NEXT J
24490 NEXT I
24500 !
24510 FOR J=1 TO Nterms
24520 FOR K=1 TO J
24530 Alpha(K,J)=Alpha(J,K)
24540 NEXT K
24550 NEXT J
24560 !
24570 FOR I=1 TO Npts
24580 GOSUB Functn
24590 Yfit(I)=Fu
24600 GOSUB Fchisq
24610 Chisq1=Chisq
24620 NEXT I
24630 !
24640 L71: FOR J=1 TO Nterms
24650 FOR K=1 TO Nterms

```

```

24660 Array(J,K)=Alpha(J,K)/SQR(Alpha(J,J)*Alpha(K,K))
24670 NEXT K
24680 Array(J,J)=1+Flamda
24690 NEXT J
24700 MAT Array=INV(Array)
24710 Det=1/DET(Array)
24720 FOR J=1 TO Nterms
24730 B(J)=A(J)
24740 FOR K=1 TO Nterms
24750 IF J=Lk THEN 24770 !-----
24760 B(J)=B(J)+Beta(K)*Array(J,K)/SQR(Alpha(J,J)*Alpha(K,K))
24770 NEXT K
24780 NEXT J
24790 !
24800 FOR I=1 TO Npts
24810 GOSUB Functn
24820 Yfit(I)=Fu
24830 NEXT I
24840 !
24850 GOSUB Fchisq
24860 Chisqr=Chisq
24870 IF Chisq1-Chisqr>=0 OR Flamda>1.E+20 THEN GOTO L101
24880 Flamda=10*Flamda
24890 GOTO L71
24900 !
24910 L101: FOR J=1 TO Nterms
24920 IF J=Lk THEN 24940
24930 A(J)=B(J)
24940 Sigmaa(J)=SQR(Array(J,J)/Alpha(J,J))
24950 NEXT J
24960 Flamda=Flamda/10
24970 !
24980 RETURN
24990 !
25000 !
25010 !*****
25020 !
25030 !
25040 Fderiv:!
25050 !
25060 FOR J=1 TO Nterms
25070 Aj=A(J)
25080 Delta=Deltaa(J)
25090 A(J)=Aj+Delta
25100 GOSUB Functn
25110 Yfit2=Fu
25120 A(J)=Aj-Delta
25130 GOSUB Functn %25140 Deriv(J)=(Yfit2-Fu)/(2*Delta)
25150 A(J)=Aj
25160 NEXT J
25170 !
25180 RETURN
25190 !
25200 !
25210 !*****
25220 !
25230 !
25240 Functn:!
25250 !
25260 IF Funk_flag=0 THEN Xx=X(M1,I)
25270!
25280!
25290 IF A(1)<5 THEN A(1)=5
25300 IF A(2)<1.02 THEN A(2)=1.02 -
25310 !IF A(1)>90 THEN A(1)=90
25320 IF A(2)>5 THEN A(2)=5

```

```

25330 !
25340 !IF A(3)<.7 THEN A(3)=.7
25350 IF A(3)>5 THEN A(3)=5
25360 !
25370 IF Nterms>3 THEN
25380 IF A(4)<150 THEN A(4)=150
25390 !IF A(4)>.8*A(1) THEN A(4)=.8*A(1)
25400 !
25410 IF A(5)>4 THEN A(5)=4
25420 IF A(5)<1.1 THEN A(5)=1.1
25430 !
25440 IF A(6)<=.1 THEN A(6)=.1 -
25450 IF A(6)>=3 THEN A(6)=3
25460 END IF
25470 !
25480 OFF ERROR
25490 ON ERROR GOTO 25610
25500 !
25510 !
25520 Fu=A(3)*EXP(-(LOG(Xx)-LOG(A(1)))^2/(2*(LOG(A(2)))^2))
25530 !
25540 !
25550 IF Nterms>3 THEN
25560 Fu=Fu+A(6)*EXP(-(LOG(Xx)-LOG(A(4)))^2/(2*(LOG(A(5)))^2))
25570 END IF
25580 !
25590 GOTO Weiter
25600 ! PRINT Xx,Fu
25610 Error:!
25620 !
25630 PRINT Xx,Fu
25640 IF Fu<1.E-30 THEN Fu=1.E-30
25650 OFF ERROR
25660 !
25670 Weiter:!
25680 !
25690 RETURN
25700 !
25710 !
25720 !
25730 END
25740 !
25750 SUB Charge(Punkte,D(*),F(*),First_charge,D_fak,Polar$)
25760 !
25770 DISP "CHARGE"
25780 !
25790 !- LADUNGSVERT. NACH FUCHS/WIEDENSOHLER -
25800 !
25810 !----- 25.10.91 -----
25820 !
25830 OPTION BASE 0
25840 !
25850 REAL A(4,6),S(250,6),Ff(6),Frac(12)
25860 !
25870 !D_fak=1
25880 !
25890 IF First_charge<>0 THEN
25900 PRINT "D_fak zur Zeit: ";D_fak
25910 INPUT "GRÖSSENFAKTOR EINGEBEN (St.=1)",D_fak
25920 !
25930 MAT D=D*(D_fak)
25940 END IF
25950 !
25960 First_charge=1
25970 !
25980 !

```

```

25990 E=1.6022E-19 ! in C -
26000 K=1.38066E-23 ! in J/K
26010 T=293
26020 Ep=8.85E-12 ! in C/(V*m)
26030 Z=.875 !Mobilitätsquotient +/- -ionen
26040 !
26050 IF Polar$= "+" THEN Z=1/Z
26060 !
26070 !
26080 Sec:!
26090 !
26100 FOR I=1 TO Punkte
26110 FOR N=3 TO 6
26120 !
26130 Dp=D(I)*1.E-9
26140 Edkt=Ep*Dp*K*T
26150 !
26160 !
26170 F1=E/((4*PI^2*Edkt)^.5)
26180 !
26190 F2=(N-2*PI*Edkt/(E^2)*LOG(Z))^2
26200 !
26210 F3=2*(2*PI*Edkt/(E^2))
26220 !
26230 F(I,N)=F1*EXP(-F2/F3)
26240 !PRINT D(I),N,F(I,N)
26250 NEXT N
26260 NEXT I
26270 !
26280 IMAGE "D:",DDDD," nm F(N): ",D.DDE," F(N): ",DDD.DD,"%"
26290 !
26300 !
26310 !
26320 !-----
26330 !
26340 Dp=Dp*1.E+9!wieder in nm
26350 !
26360 !
26370 DATA -13.63922, 10.96291, 1.43321
26380 DATA -3.25825, 0.99413, -0.09708
26390 !
26400 DATA 1.68332, -5.90214, 8.63996
26410 DATA -4.77820, 1.16592, -0.10716
26420 !
26430 DATA 1.99969, -0.10137, 0.30725
26440 DATA -0.33717, 0.10230, -0.010497
26450 !
26460 DATA 1.29248, -4.78374, 7.15638
26470 DATA -3.90964, 0.93238, -0.083543
26480 !
26490 DATA -6.9776, -3.4179, 13.108
26500 DATA -7.8917, 1.8967, -0.16632
26510 !
26520 !
26530 RESTORE 26370
26540 FOR J=0 TO 4
26550 FOR I=0 TO 5
26560 READ A(J,I)
26570 NEXT I
26580 PRINT ""
26590 NEXT J
26600 !
26610 !
26620 !
26630 FOR I=1 TO Punkte
26640 Dp=D(I)

```

```

26650 FOR J=0 TO 4
26660 S(I,J)=0
26670 FOR K=0 TO 5
26680 S(I,J)=S(I,J)+A(J,K)*(LGT(Dp))^K
26690 NEXT K
26700 !
26710 !
26720 !Fn=10^(S(J)-2) !-2 WEIL KOEFF. FÜR %
26730 !Ff(J)=Fn
26740 !F(I,J-2)=Fn
26750 NEXT J
26760 !
26770 IF Polar$= "+" THEN -
26780 F(I,1)=10^(S(I,1)-2) -
26790 F(I,2)=10^(S(I,0)-2)
26800 ELSE -
26810 F(I,1)=10^(S(I,3)-2) -
26820 F(I,2)=10^(S(I,4)-2)
26830 END IF
26840 !
26850 !PRINT "Dp:";D(I)
26860 !PRINT USING 26440;1,F(I,1),2,F(I,2),3,F(I,3),4,F(I,4),5,F(I,5),6,F(I,6)
26870 !
26880 NEXT I
26890 ! -
26900 IMAGE 6(SD,":",D.DDE,XX)
26910 !
26920 MAT D=D/(D_fak)
26930 !
26940 DISP "O.K."
26950 !
26960 SUBEND

```